



Assessment of mycolic acids as ligand for nanoencapsulated anti-tuberculosis drug targeting

Yolandy Lemmer

Submitted in partial fulfillment of the degree

Philosophiae Doctor Biochemistry

in the

Department of Biochemistry

Faculty of Natural and Agricultural Sciences

University of Pretoria

Pretoria

October 2010



Submission declaration:

I Yolandy Lemmer declare that the thesis which is herewith submitted to for the degree *Philosophiae Doctor* Biochemistry at the University of Pretoria, is my own work and has not previously been submitted by me for a degree at this or any other tertiary institution.

Plagiarism Declaration

UNIVERSITY OF PRETORIA
FACULTY OF NATURAL AND AGRICULTURAL SCIENCES
DEPARTMENT OF BIOCHEMISTRY

Full name _____ Student number: _____
Title of the work: _____

Declaration

1. I understand what plagiarism entails and am aware of the University's policy in this regard.
2. I declare that this _____ (e.g. essay, report, project, assignment, dissertation, thesis etc) is my own, original work. Where someone else's work was used (whether from a printed source, the internet or any other source) due acknowledgement was given and reference was made according to departmental requirements.
3. I did not make use of another student's previous work and submit it as my own.
4. I did not allow and will not allow anyone to copy my work with the intention of presenting it as his or her own work.

Signature _____ Date _____

Acknowledgements

I would like to thank the following individuals and organizations for their support towards the completion of my PhD degree.

Most importantly, our **Creator and King**, for the guidance and support in the good and trying times and never leaving my side.

Prof. J.A. Verschoor my promoter for all my post graduate studies, for his door always being open whether it is science related or not. For all the interesting discussions, valuable input, positive criticism and for guiding me in the writing of my thesis.

Dr. Hulda Swai my promoter at the CSIR, for allowing me to be part of her research group and giving me the opportunity to study abroad, as well as all the valuable life lessons I have learned during our motivating discussions.

Dr. Boitumelo Semete-Makokotlela my co-promoter at the CSIR, for assisting me in my experimental planning and helping me to make it work, as well as the excellent help and contribution in the writing of my thesis - without your help it would not have been successful.

Dr. Arwyn Tomos Jones my supervisor at Cardiff University, without whom I would have never successfully done all the *in vitro* studies.

Prof. Dave G. Fernig my supervisor at University of Liverpool, who assisted me in the biosensor experimental work.

Dr. Bienyameen Baker and the University of Stellenbosch for the use of their facilities.

Very special thanks to **Mrs. Sandra van Wyngaardt**, for going out of your way to help me in the lab even in the late hours of the night especially the bacterial experiments and most of all being my second mother.

The BIA group, for all the valuable suggestions and help in my work and always making me feel welcome.

All the individuals in the **TB research group** at the CSIR, for their help with experiments, suggestions and tolerating my inquisitiveness.

A special thanks to **Mr. Lonji Kalambo** for his excellent ideas and help in the particle synthesis. **Mrs. Laetitia Booysen** and **Mrs. Ilse Wepener** for assisting me in my cell culture work as well as being my friends. I would also like to thank **Miss Bathabile Ramalapa** for her technical assistance with the SEM analyses and **Mr. Wayne Barnes** for his technical assistance in the FACS experiments. To my friend and colleague **Mr. Chrisitan Stutzer** for all the good suggestions and revisions.

I would also like to thank, **NRF SA-UK Bilateral** fund for financial support, **CSIR** for the studentship and infrastructure, **DST** for supporting infrastructure and the **Marie Curie fellowship**.

My family and friends, for their moral support and always trying to understand. Special thanks to my **mother** and **father** for the moral support and encouragements. My twin sister **Xelia**, for always being there and being my best friend. Thank you to **Marshant** for being such a good listener and brother. Lastly, I would want to especially thank **Corné**, words cannot express the gratitude I have and how deeply I appreciate all that you have done, truly my better half.



Table of contents

Acknowledgements	iii
List of abbreviations	ix
List of figures.....	xiii
Summary	xv
Opsomming.....	xvi
Chapter 1: General introduction.....	1
1.1 Epidemiology of tuberculosis	1
1.1.2 MDR-TB in South Africa.....	2
1.2 TB treatment	3
1.3 Nanoparticles (NP) as drug delivery vehicles	5
1.3.1 Background	5
1.3.2 Physicochemical properties.....	6
1.3.3 Preparation and modification of polymeric nano carriers	8
1.3.4 Different types of nanodrug delivery systems.....	10
1.3.4.1 Liposomes	10
1.3.4.2 Dendrimers.....	11
1.3.4.3 Nanoemulsions.....	11
1.3.4.4 Niosomes.....	11
1.3.4.5 Solid lipid nanoparticles (SLN)	12
1.3.4.6 Polymeric micelles.....	12
1.3.4.7 Polymeric nanoparticles.....	12
1.3.4.7.1 Polylactic acid (PLA).....	14
1.3.3.7.2 Poly-ε- caprolactone (PCL)	14
1.3.4.7.3 Chitosan	15
1.3.4.7.4 Gelatin.....	15
1.3.4.7.5 Poly-alkyl-cyano-acrylate (PAC).....	15
1.3.4.7.6 Poly, DL, lactic-co-glycolic acid, (PLGA)	15
1.3.5 Applications of nanoparticles in therapeutic treatment.....	17

1.3.6 PLGA as preferred nanoencapsulation approach for anti-TB drugs	18
1.4 Targeting of nanoencapsulated anti-TB drugs to the sites of infection	19
1.4.1 Macrophage receptor(s) for entry of <i>M. tuberculosis</i>	20
1.4.2 Localized tissue markers of TB infection	20
1.4.3 Mycolic acid ligands for drug targeting	23
1.4.3.1 MA structure-function relationship.....	26
1.4.3.2 MA as virulence factors	29
1.4.3.3 Mycolic acids as surrogate marker antigen in TB	30
1.5 Aim of the project.....	30
Chapter 2: The cholesterol nature of MA as a tool for targeting	32
2.1 Introduction	32
2.2 Hypothesis	36
2.3 Aims of study.....	36
2.4 Materials	36
2.4.1 Consumables	36
2.4.2 Buffers	37
2.4.3 Instrumentation.....	38
2.5 Methods	38
2.5.1 Fluorescent labelling of mycolic acids.....	38
2.5.2 Biosensor experiments	40
2.5.2.1 Preparation of mycolic acids, labelled mycolic acids or cholesterol containing liposomes	40
2.5.2.2 Measuring the affinity between Amphotericin B and either mycolic acids, labelled mycolic acids or cholesterol.....	40
2.5.3 Enzyme-linked immunosorbent assay (ELISA) to test the antigenicity of MA derivatives	41
2.5.4 Enzyme-linked immunosorbent assay (ELISA) of synthetic MA	42
2.6 Results	43
2.6.1 Fluorescent labeling of MA.....	43
2.6.2 Comparative Amphotericin B recognition of MA, labelled MA or cholesterol	44

2.6.3 Effect of a modified carboxylic group of MA on antibody binding and recognition.....	45
2.6.4 Response of patient sera to natural and synthetic mycolic acids	47
2.7 Discussion.....	53
Chapter 3: Synthesis and characterization of mycolic acid containing nanoparticles .	56
3.1 Introduction	56
3.2 Hypothesis	58
3.3 Aims of study.....	58
3.4 Materials	58
3.4.1 Consumables	58
3.4.2 Buffers	61
3.4.3 Instrumentation.....	62
3.5 Methods	62
3.5.1 Preparation of INH containing nanoparticles with labelled MA.....	62
3.5.2 Nanoparticle characterization.....	63
3.5.2.1 Quantification of INH in nanoparticles.....	63
3.5.2.2 Quantification of MA in nanoparticles	64
3.5.3 <i>In vitro</i> cell viability assay	64
3.5.4 Uptake of nanoparticles by macrophages.....	65
3.5.4.1 Cell culture maintenance.....	66
3.5.4.2 Differentiating cells	66
3.5.4.3 Flow cytometry	66
3.5.5 Nanoparticle uptake and localization by confocal microscopy.....	67
3.5.5.1 Cell culture maintenance.....	67
3.5.5.2 Differentiating cells	68
3.5.5.3 Nanoparticle uptake in U937 and THP-1 macrophages	68
3.5.5.4 Nanoparticle, transferrin and dextran uptake in U937 and THP-1 macrophage cells.....	68
3.5.5.5 Nanoparticle treatment and fixation of macrophage cells	69
3.5.5.6 Immunofluorescence staining of U937 and THP-1 fixed macrophages	69



3.5.5.6.1 Immunostaining for α -tubulin	70
3.5.5.6.2. Rhodamine staining for actin	70
3.5.6 <i>In vitro</i> drug testing in <i>Mycobacterium tuberculosis</i> H37Rv infected THP-1 macrophages	71
3.5.6.1 Cell culture maintenance.....	71
3.5.6.2 Differentiating cells	71
3.5.6.3 Macrophage infection with <i>M.tb</i> H37Rv	72
3.5.6.4 Nanoparticle drug treatment	72
3.5.6.5 Harvesting TB bacilli from macrophages	72
3.6 Results	74
3.6.1 Characterization of MA / INH encapsulated particles	74
3.6.2 Quantification of MA containing nanoparticles.....	77
3.6.3 <i>In vitro</i> cell viability assay	78
3.6.4 Flow cytometric measurement of uptake of nanoparticles by macrophages	80
3.6.5 Cell culture	82
3.6.5.1 Nanoparticle uptake in U937 and THP-1 macrophages	83
3.6.5.2 Immunofluorescence staining of fixed macrophages	88
3.6.6 <i>In vitro</i> drug testing in <i>M.tb</i> H37Rv infected THP-1 macrophages	90
3.7 Discussion.....	94
Chapter 4: Conclusion.....	102
References.....	114
Appendix.....	129
Articles that this thesis contributed towards.....	129

List of abbreviations

AD/ADD	4-androstene-3,17-dione/1,4androstadiene-3,17-dione pathway
AIDS	acquired immune deficiency syndrome
5BMF	5-Bromomethylfluorescein
Ca ²⁺	calcium
Caco-2	human colorectal carcinoma cell line
CIP	coronin interactin protein
CSIR	Council for Scientific and Industrial Research
DCM	dichloromethane
dddH ₂ O	double distilled deionized water
DIM	Phthiocerol dimycocerosates
DOT	Directly Observed Treatment
EE	encapsulation efficiency
EEA1	Early endosomal antigen 1
EIPA	5-N-ethyl-N-isopropylamiloride
EO	ethylene oxide
EPR	enhanced permeation and retention
ER	endoplasmic reticulum
FACS	fluorescence activated cell sorting
FAS	fatty acid synthetases
FCS	foetal calf serum
Fe ₂ O ₃	ferrous oxide

GI	bacterial growth index
HASMC	human arterial smooth muscle cells
HIV	human immunodeficiency virus
HPLC	High Performance Liquid Chromatography
IFN- γ	interferon-gamma
Igr	intracellular growth
IL-12	interleukin 12
INH	isoniazid
LAM	lipoarabinomannan
LD	lipid droplet
LpdC	lipoamide dehydrogenase C
LXR	liver X receptor
MA	mycolic acids
ManLAM	mannose-capped lipoarabinomannan
MARCO	macrophage receptor with collagenous structure
<i>M. avium</i>	<i>Mycobacterium avium</i>
MDR-TB	multidrug resistant tuberculosis
<i>M. leprae</i>	<i>Mycobacterium leprae</i>
MOI	multiplicities of infection
MS	mass spectrometry
<i>M.tb</i>	<i>Mycobacterium tuberculosis</i>
mV	milli-volts
MW	molecular weight

nm	nanometer
NMR	nuclear magnetic resonance
NP	nanoparticles
PAC	poly-alkyl-cyano-acrylate
PAMP	pathogen associated molecular patterns
PBS	phosphate buffer saline
PCL	poly- ϵ -caprolactone
PDI	polydispersity index
PEG	polyethylene glycol
PFA	paraformaldehyde
PIM	phosphatidylinositol-mannoside
PI(3)P	phosphatidylinositol-3-phosphate
PI(3)K/Vps34	phosphoinositide 3- kinase
PLA	polylactic acid
PLGA	poly, DL, lactic-co-glycolic acid
PMA	phorbol 12-myristate 13-acetate
PO	propylene oxide
PVA	polyvinyl alcohol
RIF	rifampicin
RSA	Republic of South Africa
rpm	revolutions per minute
RT	room temperature
SapM	<i>M. tuberculosis</i> effector molecule

SEM	scanning electron microscopy
S1P	sphingosine-1-phosphate
SiO ₂	amorphous silica oxide
SLN	solid lipid nanoparticles
TACO	tryptophane aspartate containing coat protein
TB	tuberculosis
TDM	trehalose dimycolate
THP-1	myelomonocytic cell line
TLC	thin layer chromatography
TLR	toll-like receptors
TMM	trehalose monomycolate
TNF- α	tumour necrosis factor alpha
TraSH	transposon site hybridization
U937	histiocytic lymphoma
USFDA	United States food and drug administration
WHO	World Health Organisation
w/o	water in oil
w/o/w	water in oil in water
WST	tetrazolium salt
w/v	weight/volume
XDR-TB	extensively drug resistant tuberculosis
ZnO	zinc oxide

List of figures

Figure 1.1 Worldmap indicating TB incidence for 2007	2
Figure 1.2 Schematic illustration of different modifications and usages to formulate the nanodrug carrier	9
Figure 1.3 Schematic illustration of a variety of drug delivery systems.....	13
Figure 1.4 Different polymeric nanoparticles for the use of drug encapsulation.	14
Figure 1.5 PLGA nanoparticles are hydrolysed in an acidic environment to the monomers lactic and glycolic acid	17
Figure 1.6 Survival mechanisms of the mycobacteria, in the macrophage host.....	22
Figure 1.7 Schematic representation of a mycobacterial cell wall.	24
Figure 1.8 Structures of mycolic acids from <i>M.tb</i>	25
Figure 2.1 Reconstruction of the two dimensional TLC.....	44
Figure 2.2 Normalised AmB binding capacity on immobilized lipid antigens	45
Figure 2.3 Chemical structure of fluorescein labelled MA.....	46
Figure 2.4 Comparison of antibody recognition to MA, ME-MA and Fluorescein-MA.	47
Figure 2.5 ELISA signals of antibody binding in TB positive and TB negative pooled patient sera to synthetic MA.	48
Figure 2.6 ELISA antibody binding signals of TB positive and TB negative patient sera to synthetic methoxy mycolic acids.	50
Figure 2.7 ELISA antibody binding signals of TB positive and TB negative patient sera to synthetic hydroxyl mycolic acids.	51
Figure 2.8 ELISA antibody binding of TB positive and TB negative patient sera to synthetic keto mycolic acids.	52
Figure 2.9 ELISA antibody binding signals of TB positive and TB negative sera to synthetic alpha mycolic acids.	52
Figure 3.1 Representative SEM image of the surface of PLGA nanoparticles with Fluorescein labelled MA.....	76
Figure 3.2 Basic fuchsin that will associate with mycolic acids of <i>M.tb</i>	77
Figure 3.3 Standard curve obtained for MA and Fluorescein-MA by making use of the Carbol fuchsin dye.	78

Figure 3.4 Effects of PLGA, ferrous oxide, fumed silica, zinc oxide and MA containing particles on viability of the Caco-2 cell line after 24 hours as done by a WST assay. 79

Figure 3.5 Effects of PLGA and MA containing particles on viability of the U937 cell line after 24 hours as done by a MTT assay. 80

Figure 3.6 Flow cytometry of nanoparticle uptake in THP-1 cell culture at increasing concentrations of Fluorescein -MA and rhodamine containing nanoparticles. 82

Figure 3.7 Live cell images of Fluorescein-MA PLGA nanoparticles taken up by a) THP-1 and b) U937 macrophages..... 83

Figure 3.8 Bright field confocal images of cell morphology of THP-1 macrophages after uptake of nanoparticles A) Coumarin PLGA B) unlabeled PLGA nanoparticles. 84

Figure 3.9 Endocytic probes used for representation of endocytic pathways..... 85

Figure 3.10 Confocal images of intracellular processing of Fluorescein-MA using single sections through the macrophage cells of the pulse/chase experiments..... 86

Figure 3.11 Confocal imaging of possible colocalization of Fluorescein-MA PLGA 89

Figure 3.12 Actin involvement in the uptake of Fluorescein-MA PLGA 90

Figure 3.13 The effect of nano-encapsulation of INH on its efficiency to suppress growth of *M.tb* in infected THP-1 macrophages using BACTEC..... 92

Summary

South Africa currently has the highest incidence of TB per 100 000 people in the world. In 2007 alone 112 000 people died of TB in South Africa, of which 94 000 were co-infected with HIV. Although TB treatments exist, poor patient compliance and drug resistance are challenges to TB management programs worldwide. Here, this challenge was addressed by the development of a polymeric anti-TB nanodrug delivery system for anti-TB drugs that could enable entry, targeting and sustained release for longer periods, hence reducing the dose frequency and simultaneously improve patient compliance. The aim was to prepare functionalised polymeric nano drug delivery vehicles to target TB infected macrophage cells. Successful nano encapsulation of anti-TB drugs was achieved and uptake of the antibiotics in the cells, demonstrated. A possible targeting agent, mycolic acids (MA) from *M. tuberculosis* was explored. The MA incorporated into nanoparticles could possibly serve as a ligand for cholesterol-rich areas, due to the cholesterol nature of MA and the fact that MA is attracted to cholesterol. In another targeting scenario, MA incorporated into nanoparticles may interact with the anti-mycolic acid antibodies that are anticipated to be present in higher concentrations at the infected areas. The cholesterol nature of MA was confirmed and how it related to the fine structure of the MA. The prepared MA containing nanoparticles were shown *in vitro* to be taken up in macrophage cell lines, without the MA hindering the uptake of the particles. In terms of toxicity, nanoparticles with or without MA were found to be acceptable for use, although MA did affect the viability of the cells more than poly, DL, lactic-co-glycolic acid particles alone in *in vitro* studies. This paves the way for testing MA as a ligand to target anti-TB drugs to the sites of infection in human TB patients.

Opsomming

Suid Afrika het tans die hoogste insidensie van TB per 100 000 mense in die wêreld. In 2007 het 112 000 mense gesterf van TB in Suid Afrika waarvan 94 000 mense geko-infekteer was met MIV. Alhoewel TB behandeling bestaan, is daar 'n groot uitdaging vir TB programme in die wêreld as gevolg van swak pasiënt-voldoening asook middel weerstandigheid wat ontstaan. Hierdie uitdaging is aangespreek deur die ontwikkeling van 'n polimeriese anti-TB nanomiddel-aflerwing stelsel wat opneembaarheid kan verhoog asook stadige vrystelling van die middel kan bewerkstellig wat dan die dosis kan verlaag en pasiënt-voldoening kan bevorder. Die doel van die projek was om die anti-TB nanomiddel aflerwing stelsel te sintetiseer en dit na TB geïnfecteerde selle te teiken. Die nanopartikels was suksesvol gesintetiseer met geïnkorporeerde anti-TB middels wat in selle opgeneem was. 'n Moontlike teikenmiddel, mikoosure van die *M. tuberculosis* bakterieë is ondersoek. Die mikoosure kon geïnkorporeer word in die nanopartikels wat as 'n ligand sou kon dien vir die cholesterol- ryke areas as gevolg van die cholesterioëde aard van die mikoosure, asook die feit dat mikoosure aangetrek word deur cholesterol. 'n Ander moontlikheid is dat die mikoosure met anti-mikoosuur teenliggame kan reageer wat waarskynlik in hoër konsentrasies teenwoordig sal wees in die geïnfecteerde areas. Die cholesterioëde aard van die mikoosure was bevestig, asook hoe die struktuur van die mikoosure daarmee verband hou. Daar is aangetoon dat die mikoosuur-bevattende nanopartikels *in vitro* in selle opgeneem word sonder dat die mikoosure die opname belemmer het. In terme van toksisiteit was die nanopartikels met en sonder mikoosure bevind om geskik te wees vir gebruik, alhoewel die mikoosure die lewensvatbaarheid van die selle meer geaffekteer het as die poly, DL, lactic-co-glycolic acid-partikels alleen in *in vitro* studies. Die resultate maak die pad oop om mikoosure te toets as ligande om anti-TB middels te teiken na die geïnfecteerde loki van TB pasiënte.

Chapter 1: General introduction

1.1 Epidemiology of tuberculosis

Tuberculosis (TB) has returned to become one of the leading causes of preventable deaths in some 200 countries and territories, including South Africa [1]. Paleopathology studies showed that the *M.tb* complex was detected even in Egyptian mummies by making use of modern day DNA and HPLC analysis [2, 3]. The bacillus causing the actual disease, *Mycobacterium tuberculosis* (*M.tb*), was identified and described by the German physician Robert Koch in 1882 [4]. Prior to Robert Koch's work, the disease "consumption" was believed to have various sources depending on the affected community's folklore [5]. Early treatments focused on a healthy diet and the administration of expectorants and purgatives, with the first sanatorium opened in 1854 in Germany where good hygiene and fresh air were thought to stimulate the body's natural immune system. Consequently the success rate was much higher than any previous treatment and the system was adopted by other countries such as Britain. The further critical improvement of public health reduced the number of tuberculosis cases even before the introduction of antibiotics in the mid 20th century [6].

However, an increase in mortality rates from the 1980s changed this perception dramatically. It could be attributed to the breakdown in health services, the spread of HIV/AIDS and the emergence of multidrug-resistant TB (MDR-TB) [5]. Co-infection with the human immunodeficiency virus (HIV), a phenomenon that started in the 1980s and became eminent in the late 1990s, causes a severe burden on the individual's immune system making them susceptible to opportunistic infections, of which TB is the most prominent. The mortality rate for individuals which are co-infected with TB is very high [1]. MDR-TB is a dangerous form of drug-resistant TB, that comes about when the infecting bacillus develops resistance to at least INH and RIF, the two most often used first line anti-TB drugs.

As indicated in the global tuberculosis control report of 2009 from the world health organisation [1], South Africa currently has the highest incidence of TB per 100 000 (358 per 100 000) people in the world. In 2007 an estimated 112 000 people died of

TB in South Africa alone, of which 94 000 (72%) were co-infected with HIV [1]. In 2007, the prevalence of TB per 100,000 people was highest in sub-Saharan Africa, and was also relatively high in Asia [1] as illustrated in figure 1.1.

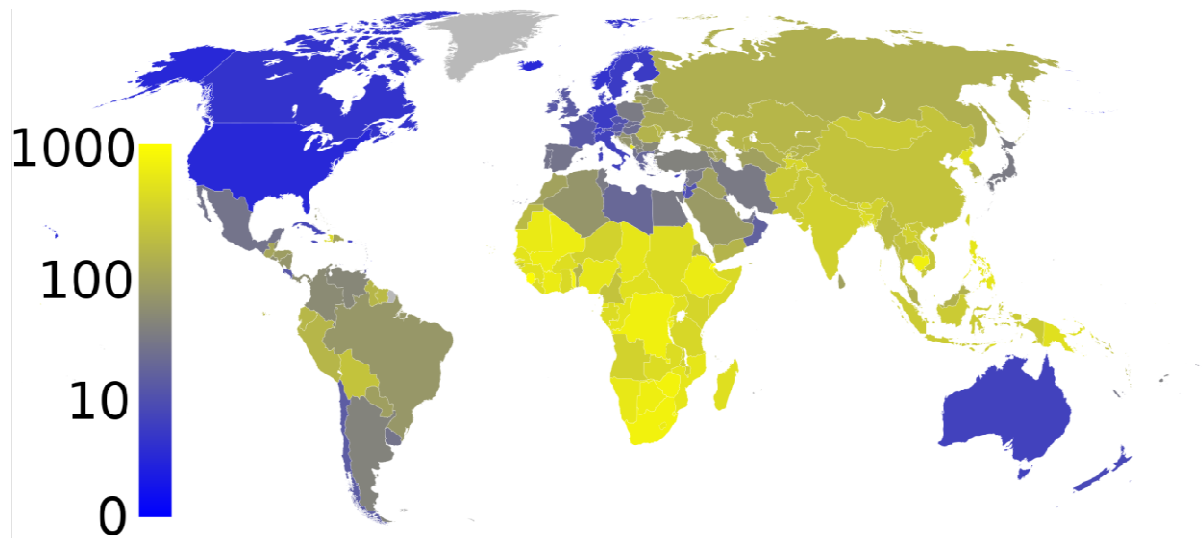


Figure 1.1 Worldmap indicating TB incidence for 2007 [1].

1.1.2 MDR-TB in South Africa

The serious threat of tuberculosis, especially MDR and extensively drug resistant (XDR) TB, is a great concern in Southern Africa particularly pertaining to individuals with HIV/AIDS. XDR-TB comes about when resistance to INH and RIF is compounded by an additional resistance to the second line drugs, including any fluoroquinolones and at least one of the three injectables (kanamycin, amikacin or capreomycin) [7].

The concern about XDR-TB was emphasized following a clinical study in 2006 at the Church of Scotland Hospital in KwaZulu-Natal, South Africa. Of the 536 TB patients hospitalized at the time, 221 were found to have MDR-TB, of which 53 were diagnosed with XDR-TB. Of these, 52 died within 25 days. At the time, it was thought that the co-infection of 44 of these patients with HIV was the reason behind their development of XDR-TB [8]. However, recent evidence presented by Dr. Tony Moll at the 2nd TB conference, 1-4 June 2010 in Durban South Africa, indicated that

the XDR-TB primarily originated in the hospital through inadequate infection control. XDR-TB developed in patients that never had TB or HIV infection before, but were hospitalized for other ailments in wards that held one or two undiagnosed XDR-TB patients. In another study done in a HIV co-infected population at a South African gold mine, it was found that existing TB control measures were insufficient to control the spread of drug resistant TB. Furthermore inappropriate therapy as well as a delay in diagnosis contributed to drug resistance and the transmission of the disease [9].

1.2 TB treatment

The era of antibiotics started when streptomycin was discovered in 1946 followed by the successful testing of isoniazid (INH) in 1952, which was shown to be the most important antibiotic in the standard treatment regime against TB. Other drugs were developed in the following years: pyrazinamide in 1954, ethambutol in 1962 and rifampicin (RIF) in 1963 [5].

The treatment of tuberculosis differs from that of other infectious diseases due to the long treatment time needed to cure the patient [10]. A characteristic difficulty of tuberculosis is the persistence of the pathogenic mycobacteria, regardless of prolonged antibiotic treatment. The micro-environment containing dormant bacteria could change over a period of time causing the bacteria to recommence growth, at which stage they are vulnerable to the standard drugs [11, 12]. Because some of the subpopulations of *M.tb* may not be eliminated effectively with standard antibiotics, prolonged periods of the treatments are required [13]. These heterogeneous subpopulations of the bacteria are able to survive within granulomatous lesions surrounded by foamy macrophages in a persistent or latent state, with lacking clinical symptoms [13, 14]. Most bactericidal drugs are only effective against actively growing bacilli and the extended treatment times are needed to then inhibit the regrowth of the bacteria [15]. The length of treatment depends on the presence of non-replicating bacteria and pathogens in a stationary phase present in old lesions of fibrotic tissue [16]. The implementation of a 6 month or longer treatment regime with antibiotics for cases of susceptible TB resulted in a remarkable reduction in the

number of deaths of tuberculosis cases per 100 000 population in the 1960s, such that TB was thought to be a curable disease that was easy to manage.

Antibiotics against TB can be classified into two lines of combination treatment, of which application of the more expensive and less efficient second line is dictated by the development of drug resistance to the first. The decision to commence with a treatment regime for TB is not taken lightly, due to the severe side effects that can occur. For example, first line drugs can cause, drug induced hepatitis, nausea, deafness and progressive loss of vision [10]. The first line of drugs includes INH, RIF, ethambutol, pyrazinamide and streptomycin used for the treatment of drug sensitive TB. There are currently 6 second line drugs used for the treatment of MDR-TB. However these drugs have more toxic side effects (e.g. cycloserine). Second line drugs are difficult to come by in developing countries (e.g. fluoroquinolones) or are less effective than first line drugs (e.g. *p*-aminosalicylic acid). XDR TB brought the concept of 'third line' drugs to the fore that may be used in such extreme cases as a last resort. These are drugs that are not listed by the WHO as second line drugs or of which the efficacies are not yet proven [17].

The current standard first line treatment regimen according to the South African tuberculosis control programme of 2004 consists out of an initial (or intensive) phase of 2 months consisting of 4 drugs INH, RIF, pyrazinamide, and ethambutol. Streptomycin is added to the regime when the person is re-treated for TB. A continuation phase of 4 months with INH and RIF follows after the intensive phase to effect sterilization, i.e. the complete elimination of the infecting mycobacteria [10]. Due to the duration of the treatment and the increased probability of non-compliance that this holds for the patient, drug resistance to any one drug can develop.

Most of the standard chemotherapy is not effective for individuals that have MDR-TB and there is practically no cure for XDR-TB. Drug resistant mycobacterial pathogens are increasingly detected in persons who have been previously treated for TB where a possible cause could be the failure to complete lengthy drug regimens and the pathogens becoming resistant to especially the two first line drugs, INH and RIF through mutations [16, 18-20]. The approach to control this disease now is either to discover new chemotherapies effective against *M.tb*, as well as to enhance the potential of existing drugs to treat MDR-TB [21].

Treating TB patients who are co-infected with HIV poses some major challenges. This includes drug-drug interactions between antiretroviral drugs (protease inhibitors and non-nucleoside reverse transcriptase inhibitors) and rifamycins, which could result in subtherapeutic concentrations of anti-retroviral drugs. When overlapping toxicities of the anti-retroviral and anti-tuberculosis drugs increase, discontinuation of the treatment may be required. Another complication is immunopathological reactions and clinical deterioration due to immune reconstitution inflammatory syndrome where a worsening or recurrence of TB occurs when antiretroviral treatment is commenced. It is suggested that antiretroviral therapy should be delayed until the intensive phase of anti-tuberculosis treatment is completed, but delayed antiretroviral therapy on the other hand also increases the risk of morbidity and mortality in patients in the advanced stages of HIV [20, 22].

If a new TB treatment is going to replace the already existing therapy then it should at least shorten the duration of treatment or reduce the number of dosages to be taken. Furthermore the new drug should improve the treatment of MDR-TB or provide effective treatment against latent TB infection [23]. A current approach to address the efficacy of drug treatment lies in the investigation of novel systems for drug delivery. One such approach that was investigated during the course of this thesis investigated the feasibility of using sustained release nanoparticles together with a targeting ligand to target TB infected cells.

1.3 Nanoparticles (NP) as drug delivery vehicles

1.3.1 Background

Improvement of anti-tuberculosis drugs has enjoyed a lot of attention in the past decade [16]. New approaches for TB drug treatment are becoming essential to combat this disease, especially for patients with co-infections and drug resistance. Various therapeutic compounds suffer from limitations which are primarily due to low solubility, short half life, rapid clearance from the biological system and considerable side effects. Some anti-tuberculosis agents such as RIF have several drawbacks with

poor aqueous solubility, low stability and poor bioavailability [16]. A way to address this issue lies in the development of nanotechnology based drug delivery systems.

Nanotechnology has many definitions but can mainly be summarised as “the design, characterization, production, and application of structures, devices, and systems by controlled manipulation of size and shape at the nanometer scale (atomic, molecular, and macromolecular scale) that produces structures, devices, and systems with at least one novel/superior characteristic or property [24].

Under this definition also falls the study of medicine in the nanometer scale. Nanomedicine could be defined as “the use of nanoscale or nanostructured materials in medicine that according to their structure have unique medical effects” [25].

Some of the earliest forms of nanodrug delivery vehicles were lipid vesicles i.e. liposomes described in 1960's by Bangham *et al.* [26]. Since then several organic and inorganic molecules were investigated for their use as vehicles in nanomedicines. The first example of a controlled release polymer was reported in 1976 [27]. Thereafter cell specific targeting of nanomedicines were investigated with vehicles such as liposomes in 1980 [28]. In later studies the use of polyethylene glycol (PEG) to increase blood circulation time for liposomes and polymers followed. The approval of doxorubicin liposomes for the treatment of AIDS associated Kaposi's sarcoma was achieved in 1995 [28]. From there onwards an array of nanomedicine devices were patented and described in literature with the majority aiming at improved drug solubility and addressing poor bioavailability [25]. In a study done by Wagner and colleagues in 2006 they identified 38 nanomedicine products on the market contributed to 75% of the total sales on drug delivery systems. However, none of the current nanomedicines approved for commercial use was for the treatment of TB [25].

Some of the physicochemical properties that make nanomedicine so appealing will be discussed in more detail.

1.3.2 Physicochemical properties

The advantage of nanomedicine lies in the size of the material/particles used, the ability to be able to control the release of the therapeutic agent and being able to cross biological barriers that hindered successful therapies in the past [29]. Further more, NPs can improve drug solubility and facilitate intracellular drug delivery as well as targeting drugs to the site of infection. The small size of the nano molecules can assist in the uptake and biodistribution of the particles in that they could more easily traverse capillaries and therefore penetrate deeper into the target areas, thus increasing accumulation and diffusion in the tissue as was shown by Rijcken *et al.* They also indicated that the size could influence the circulation half life. As the size decreases, the circulation time increases as the smaller particles are less prone to opsonisation, thereby reducing the required frequency of drug intake, increasing the efficacy of the dose and possibly even shortening the duration of treatment [30].

Passive or active targeting can be achieved with nanoparticulate drug delivery systems. Passive targeting is mostly achieved because of the small size and longer circulation time of the particles that facilitate accumulation at the pathological site, possibly due to locally increased capillary permeability [31]. With active targeting, the surface of the nanoparticle is modified with targeting molecules (homing devices) that interact with their ligands in the tissue and may provide a way for the drugs to reach the site of interest with high specificity [31].

The zeta potential or the surface charge of the particle is also a good indicator for the probability of particle uptake. Phagocytosis increases when a particle has a positive charge compared to being neutral or negative [30]. Additionally the stability of the nanoparticles in terms of aggregation in different media can be predicted with the known zeta potential. Neutral nanoparticles tend to aggregate, while charged nanoparticles repel one another [30, 32, 33].

In comparison to more bulky carriers smaller particles have a larger surface area per unit of mass, due to the increase in surface-to-volume ratio. This can influence the release kinetics of the particles. The controlled release of a therapeutic agent from a nanocarrier is a big gain from this technology. Nano encapsulated pharmaceuticals can be obtained by dissolving, entrapping, encapsulating or binding of the drug to the nanoparticle matrix.

The encapsulated or adsorbed drugs can be released from the nanoparticle carriers in a number of different ways. Desorption of the drug from the surface, diffusion through either the nanoparticle matrix or nanoparticle wall, erosion of the nanoparticle matrix and a combined erosion diffusion process [34, 35]. The rate of release of the drugs depends mostly on the degradation, solubility and diffusion of the composition of the matrix material. For example the molecular weight of the polymer determines the degradation rate of the material, where a higher molecular weight compound degrades slower than a compound with a lower molecular weight. Other advantages of nanoparticles include the chemical control of surface characteristics and the actual polymer composition to form different constituents of the polymer to suit the needs for the different routes of administration [36].

1.3.3 Preparation and modification of polymeric nano carriers

Different nanotechnologies are available that have been applied for medical purposes and drug development. Nanoparticle drug delivery systems can either be formulated with synthetic or natural compounds [35]. Formulation is one of the most important considerations for nanocomposite systems. Nanoparticle composition and morphology of the core and corona determine the type of nanoparticles produced [30]. The nature and density of the nanoparticle coatings, their size and dissolution properties are the primary factors that determine the efficacy of drug delivery.

Polymeric nanoscale vesicles can be chemically modified and manipulated to have different surface ligands and physical properties to contain a number of different therapeutic agents for various diseases, as illustrated in figure 1.2. Typically the materials for forming the nanoparticles have been prepared mainly by dispersion of the preformed polymers or polymerization of the monomers [34].

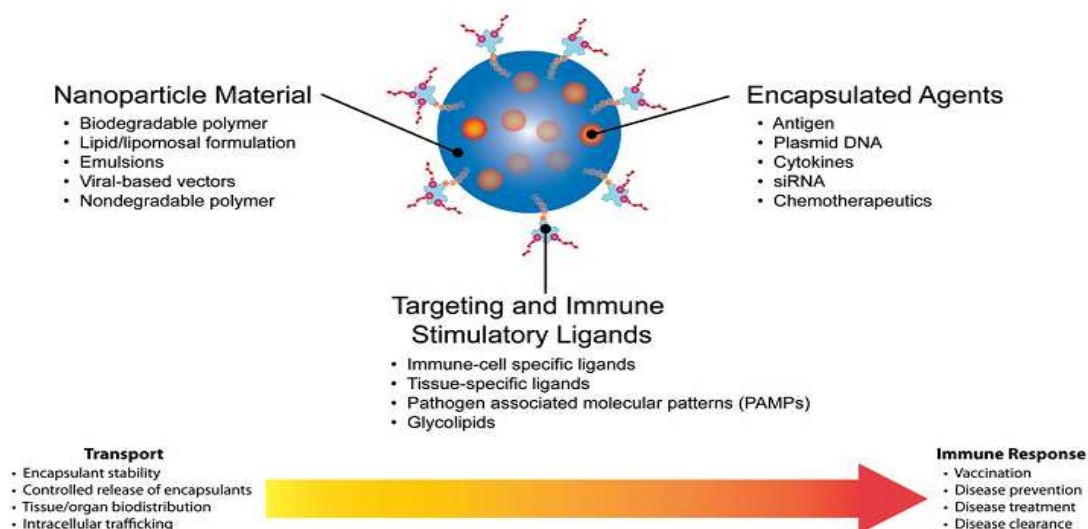


Figure 1.2 Schematic illustration of different modifications and usages to formulate the nanodrug carrier [37].

Nanoparticles can also be synthesized from different materials to control the rate of drug release, capacity for drug loading and intracellular trafficking of the particle. The material can be designed to protect and stabilize the particles in adverse physiological and external environments. Physical stability of the nanoparticulate system can be controlled to avoid aggregation and sedimentation over time that could create a potential safety concern [38]. Addition of ligands or modifications to the surface of the nanoparticles have been shown to achieve certain beneficial properties, like increasing retention time in blood by evading opsonisation and targeting to the site of infection to reduce the normal dosage required [35, 37]. Surface antigens such as peptides, nucleic acid aptamers and antibodies have been added to functionalize the surface of the particle and to target certain ligands in the biological environment [30, 39-41].

A major biological barrier in controlled drug delivery is the process of opsonisation, where opsonins such as antibodies or complement molecules bind to a foreign molecule to enhance the process of phagocytosis and therefore clearance of the particle by the immune system. Surface modification of the nanoparticles with ligands aiming at increasing the active life of the material was demonstrated with PEG or PEG containing copolymers. The PEG was grafted or adsorbed to the surface of the

nanoparticle to form a hydrophilic layer that increased the blood circulation time, possibly due to the hindrance of the adsorption of plasma proteins (or opsonins) onto the surface of the nanoparticle [30, 42, 43]. Pluronics, copolymer surfactants made from poly(ethylene oxides) and poly(propylene oxide) mixtures, were also used to increase circulation and were found to be less prone to phagocytosis and better able to accumulate within tumour cells by enhanced permeation and retention (EPR) through passive targeting [44]. Polaxamers, consisting of block copolymers of ethylene oxide (EO) and propylene oxide (PO), have also been used to coat nanoparticle surfaces to prolong circulation time and to reduce the uptake in the liver [31, 43]. Polysorbate 80 (Tween 80) coated nanoparticles are an example of molecules that enable the nanoparticles to cross the blood-brain barrier [45].

1.3.4 Different types of nanodrug delivery systems

A variety of drug delivery systems exist that can be used to improve the efficacy of a drug. Here, the focus will be on the different types of nanodrug carriers that are currently employed for therapeutics (Figure 1.3).

1.3.4.1 Liposomes

Liposomes (lipid vesicles) consist of a phospholipid bilayer with an aqueous core. They can be nano or micro sized. The large variety of phospholipids that can be used, allows for formulation of a range of biochemical and biophysical properties of liposomes [46] to incorporate hydrophobic agents within the membrane layer or entrap hydrophilic molecules in the aqueous core. Liposomes are taken up readily by phagocytic cells of the reticuloendothelial system making them ideal carriers for targeting macrophages, in particular when negatively charged phospholipids are included in the liposome formulation that enhance macrophage binding and uptake. Some limitations that this type of carrier pose is that they tend to be leaky, thus controlled release is not as effective, and also the liposomes is not very stable over time during storage [46, 47].

1.3.4.2 Dendrimers

Dendrimers are well defined hyperbranched macromolecules with a three dimensional structure usually with a size range of 1-100 nm. Dendritic polymers may be symmetrical, monodispersed branched structures or could be irregular, polydispersed assemblies of random hyperbranched polymers, thereby providing a number of options to select for incorporating therapeutic drugs. The end groups of the branched chains can be functionalized in order to bind molecules such as proteins and antibodies, these dendrimers could be challenging to synthesize to obtain the organised architecture required to form the specific dendrimer [48].

1.3.4.3 Nanoemulsions

Nanoemulsions are nanodispersions generated spontaneously and are formed from translucent oil in water dispersions. These emulsions are stable in suspensions due to their small droplet size [38]. Colloidal suspensions of high concentrations of pure drugs together with surfactants are called nanosuspensions. These suspensions are normally used for drugs that have a limited solubility in water and in oils [38]. The technique to form these suspensions is quite cost-effective, because poorly soluble drugs can be handled better, requiring simpler techniques such as high pressure homogenization, in the manufacturing process.

1.3.4.4 Niosomes

Niosomes, another type of nanodispersions are liposome-like vesicles produced from charged phospholipids and non-ionic surfactants. These molecules were developed as alternatives to overcome several limitations of liposomes. Niosomes can be used to host hydrophilic and hydrophobic drugs [16, 49].

1.3.4.5 Solid lipid nanoparticles (SLN)

SLN are formed from nanocrystalline suspensions of lipids prepared in water. It provides better encapsulation efficiency and stability than liposomes [16] and both hydrophilic and hydrophobic drugs can be incorporated [50]. The preparation method uses minimal amounts of organic solvents. In comparison, polymeric nanoparticles require high volumes of organic solvents in the manufacturing process that affect both the price and the quality control of the product [16].

1.3.4.6 Polymeric micelles

Polymeric micelles are formed by the self assembly of amphiphilic polymers in water. The hydrophilic portion of the molecules form the outer most layer of the micelle exposed to the aqueous environments where hydrophilic drugs could be added, whereas the micelles form a hydrophobic core where hydrophobic type drugs could be incorporated in order to facilitate solubility in the aqueous environment [16]. Extended drug release and circulation time are some of the advantages of the polymeric micelles [38].

1.3.4.7 Polymeric nanoparticles

Polymeric nanoparticles are formulated and synthesized according to the requirements needed for the specific type of therapy [35]. Biodegradable polymers are preferred materials as they have the additional advantage of biocompatibility with cells [51]. Upon synthesis of the nanoparticles, the drug molecules can either be entrapped inside or adsorbed onto the surface of the particle. The challenge of these type of particles are the use of solvents during the synthesis process [16, 34, 35].

A number of commonly applied polymers will be described in more detail.

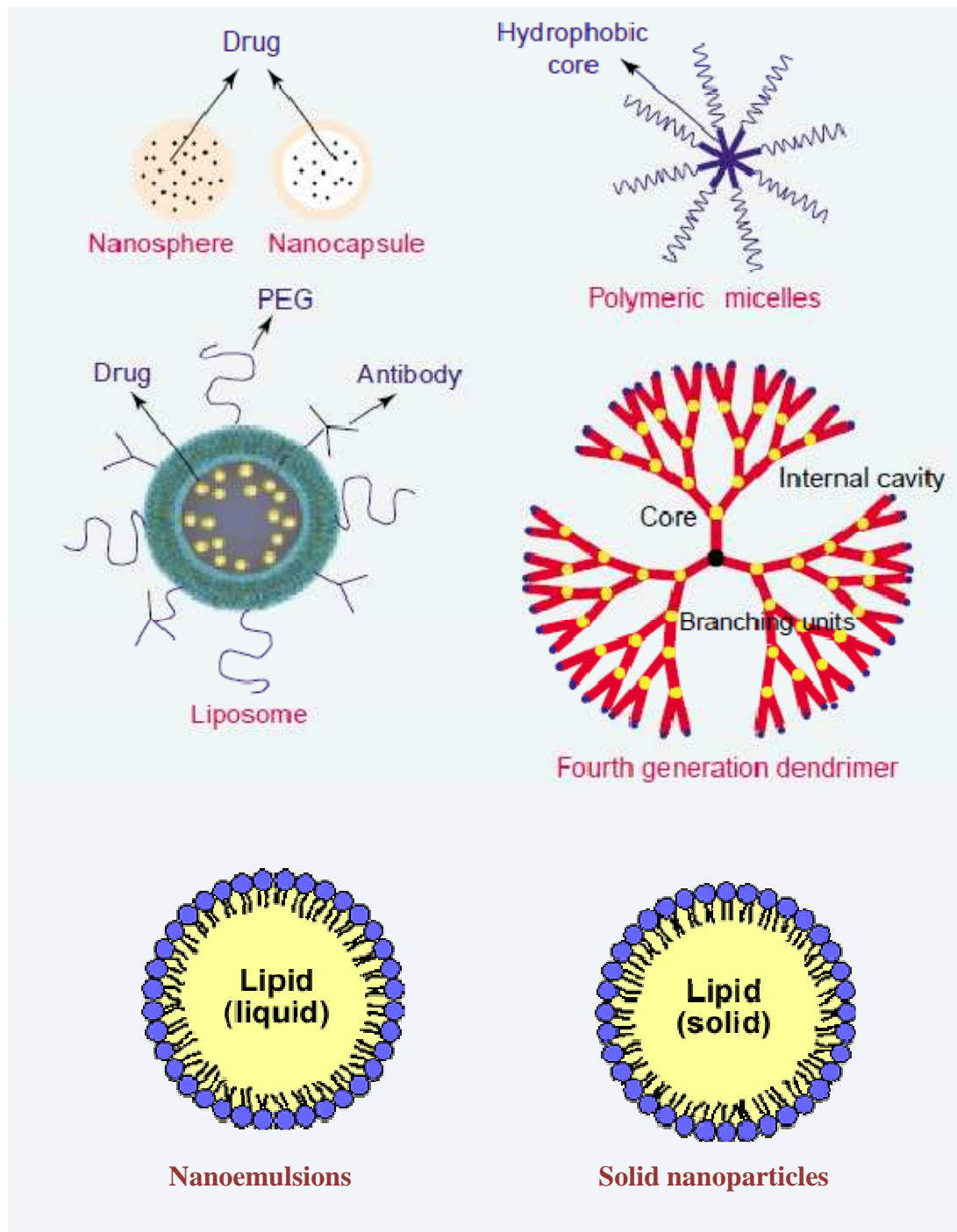


Figure 1.3 Schematic illustration of a variety of drug delivery systems (adapted from www.scf-online.com/english/25e/images25e/daniels1b25e.gif)[52].

1.3.4.7.1 Polylactic acid (PLA)

PLA, (Figure 1.4) is a polymer that is often used. It can be prepared with a salting out procedure, thereby avoiding the use of chlorinated solvents. With characteristics of good biocompatibility and biodegradability, PLA is often used to encapsulate proteins with minimal stress [35].

1.3.3.7.2 Poly-ε- caprolactone (PCL)

PCL, (Figure 1.4) is suitable for human use as it is degraded by hydrolysis of the ester linkages under physiological conditions. It is especially suited for long term implantable devices, due to the long degradation time of the polymer [35].

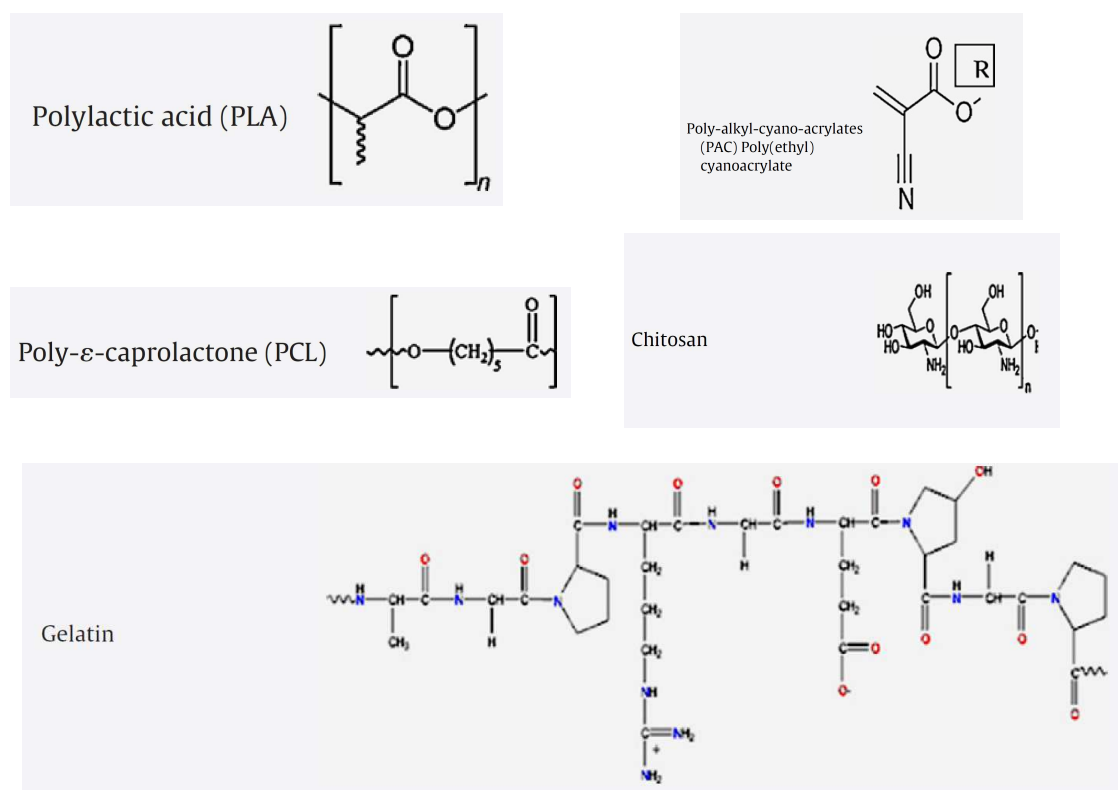


Figure 1.4 Different polymeric nanoparticles for the use of drug encapsulation [35].

1.3.4.7.3 Chitosan

Chitosan is a positively charged natural carbohydrate polymer derived from crustacean chitin (Figure 1.4). It is of interest for oral drug delivery, because it was shown that the cationic polymer was able to open tight junctions between epithelial cells making macromolecular uptake possible [53].

1.3.4.7.4 Gelatin

Gelatin is a polyampholyte with anionic, cationic and hydrophilic groups (Figure 1.4) that is extensively used in the food and medical industry. By varying the cross-linking degree of the polymer, the mechanical and thermal properties can be changed. Encapsulated agents are released from these particles via a diffusion controlled mechanism [35]. Gelatin has also been used to coat other polymers such as poly, DL, lactic-co-glycolic acid, (PLGA) to enhance fibronectin recognition and interaction [54].

1.3.4.7.5 Poly-alkyl-cyano-acrylate (PAC)

PAC (Figure 1.4) is degradable by esterases in biological environments, but produces some toxic products that can damage the central nervous system [35]. Compared to polymers such as PLGA and PLA, PAC degradation occurs over a few days rather than a few weeks. The use of different polymers for nanoencapsulation of drugs thus depends on the required rate of drug release.

1.3.4.7.6 Poly, DL, lactic-co-glycolic acid, (PLGA)

PLGA is a biodegradable polymer with very low toxicity. It undergoes hydrolysis in the body to form lactic acid and glycolic acid monomers that are metabolized via the

citric acid cycle as illustrated in figure 1.5 [43, 44, 51, 55]. PLGA has been approved by the United States food and drug administration (USFDA) for human and nanomedicine use [35]. Nanoparticles such as PLGA provide protection to poorly soluble and unstable agents in the body. They are also able to be internalised by cells and escape endosomes due to their small size [29, 34]. Different synthesis techniques have been used to form PLGA nanoparticles of which emulsion diffusion, solvent evaporation and nanoprecipitation are the most popular [35, 56]. PLGA nanoparticles are generally formulated by making use of solvent evaporation or displacement techniques [55].

For these types of techniques, reagents such as polyvinyl alcohol (PVA) have been most commonly used as the emulsifier assisting in the formation of smaller and more uniform particles. Other surfactants such as Pluronics have also been used. PVA enhances particle stability by forming a barrier to the diffusional release of incorporated compounds. Studies done by Sahoo *et al.* showed that different concentrations of PVA influence PLGA nanoparticle characteristics such as size and zeta potential as well as *in vitro* uptake [57] as more time is needed to break the polymer into soluble oligomers by hydrolysis [58]. Drug diffusion and matrix erosion are some of the methods that have been reported to cause the drug to be released from the polymer. Altering of the polymeric characteristics such as surface charge, molecular weight, hydrophobicity and number of monomers lead to varied release kinetics [32, 59, 60]. It has been shown that some nanoparticles (such as PLGA) escape the endo-lysosomes and enters the cytosolic compartment of the macrophage depending on the particle's characteristics [32, 51].

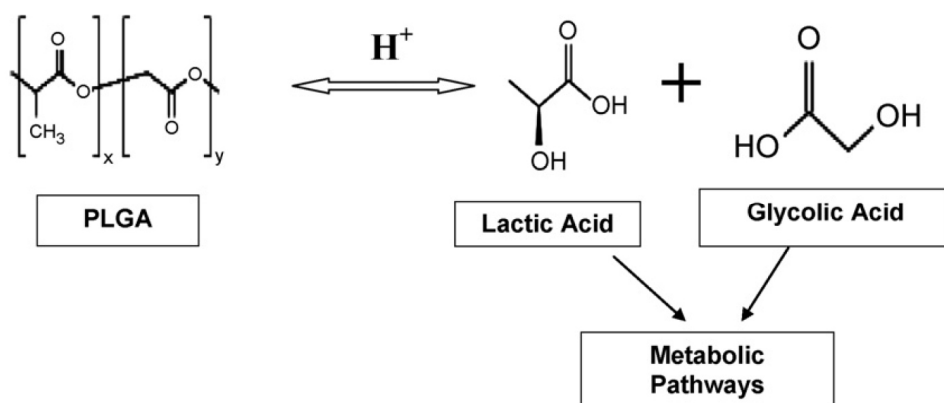


Figure 1.5 PLGA nanoparticles are hydrolysed in an acidic environment to the monomers lactic and glycolic acid [35].

1.3.5 Applications of nanoparticles in therapeutic treatment

Therapeutic compounds against several illnesses have been encapsulated to improve their efficiency. An example of PLA nanoparticles used in chemotherapy is the neuroleptic compound savoxepine, where the authors showed that the drug carrier extended the release of the drug for more than a week [42]. It has been shown by Thapa and co-workers that PLA containing alpha-galactosylceramide was selectively taken up by macrophages and dendritic cells [61]. The encapsulation of an anti-tumor agent, ftorafur, with PAC was shown to enhance the efficiency of the drug [62]. Encapsulation also improved the biological activity of anti-cancer agents such as paclitaxel and 9-nitrocamptothecin [56, 63]. Another interesting application for polymers, reported by Di Toro *et al.* was to apply PLGA and PLA biodegradable internal bone fixation devices [64].

A PCL polymer together with a polycationic non biodegradable acrylic polymer was shown to preserve insulin's biological activity in an oral formulation given to diabetic rats [65]. Furthermore, encapsulating insulin in alginate/chitosan nanoparticles showed enhanced intestinal absorption after it was administered orally [66].

Several studies have been conducted on the first line anti-tuberculosis drugs. For example INH, RIF and pyrazinamide were incorporated into SLN's and administered

to TB infected guinea-pigs. The drugs maintained detectable levels for over 10 days in the lung, spleen and liver [50]. Silva and co-workers produced micelle forming carrier-drug conjugates of the anti-tuberculosis agents INH, RIF and pyrazinamide. The results indicated stable micelles *in vitro* with extended release times as well as better anti-mycobacterial activity compared to the original drugs [67].

A number of research groups have turned their focus to making use of nanotechnology platforms for targeted delivery to the lungs, as TB manifests itself mainly in the respiratory system [68]. PLGA containing RIF particles, incorporated into mannitol by a spray drying technique for inhalation therapy, effected improved uptake by alveolar macrophages [69]. RIF was also incorporated into nanoemulsions in another study using excipients such as Sefsol, Tween and saline. The *in vitro* studies showed an initial burst effect with more moderate drug release afterwards [16]. Even niosomes could be used to enhance the effect of RIF, as it was shown to have an increased accumulation in the lymphatic system compared to free drug following intraperitoneal administration [49]. In a study done with RIF loaded mannosylated dendrimers, where the RIF was bound inside the dendritic crevices, the haemolytic effect of RIF was reduced and the drug release was prolonged [70].

Therapeutic compounds against *Mycobacterium avium* (*M. avium*) were also improved by encapsulation. A nanocrystalline suspension of the drug clofazimine was produced and was shown to have reduced toxicity and increased solubility [71]. Liposomal formulations of ciprofloxacin and azithromycin indicated an increase in potency against the bacteria *in vitro* compared to the free drugs [72].

1.3.6 PLGA as preferred nanoencapsulation approach for anti-TB drugs

PLGA is a synthetic copolymer that is biodegradable and biocompatible. The polymer has slow drug release characteristics *in vivo*, is not significantly immunogenic and has the capacity to encapsulate hydrophobic and hydrophilic agents [34, 54, 55]. PLGA particles are easy to prepare with high stability in biological environments [63]. This polymer has lower toxicity compared to other polymers such as PAC, and is more stable than liposomes or SLNs in biological environments [56]. As mentioned

previously, PLGA particles are taken up into macrophages and dendritic cells [61], which comprise the main target cells for delivery of anti-TB drugs [32, 51]. Another advantage of PLGA is that the degradation rate of the particle can be altered by changing the monomer composition and thereby the molecular weight of the polymer [58]. For the purpose of our study, we investigated PLGA as a nanocarrier molecule for the anti-TB agent, INH.

1.4 Targeting of nanoencapsulated anti-TB drugs to the sites of infection

Nanoencapsulation of drugs for delivery allow the opportunity to incorporate targeting strategies to further enhance drug efficiency and limit systemic toxic side-effects to the patient. This demands an intricate knowledge of the cellular and molecular aspects of the disease in order to identify suitable ligands that can be incorporated into the polymeric shell of the nanoparticle. These ligands should bind to disease specific receptors with an affinity high enough to effect a higher local concentration of the encapsulated drug at the site of infection rather than remaining in circulation. Any toxic side-effects that the drug may have will then mainly manifest in the vicinity of the infected tissue, while the mycobactericidal drug dose level is maintained there for longer periods than in the rest of the body.

For infectious diseases a first consideration for drug targeting would be to identify the receptors on the host cell that is used for entry of the pathogen. Nanoencapsulated drugs can then use a ligand that follows the pathogen into the host cell using the same selective mechanism of entry. Another approach would be to identify surrogate markers of infection that characterize the disease at the site where the pathogen is localized in the host tissues. If a non-toxic ligand can be identified that recognizes such surrogate marker receptors, then it can be incorporated into nanoparticle for targeting the drugs.

1.4.1 Macrophage receptor(s) for entry of *M. tuberculosis*

Infection in humans occurs through inhalation of the tuberculosis bacilli, which is taken up by alveolar macrophages in the lungs. When the *M.tb* is inside the phagocyte, the bacteria prevent fusion with acidic lysosomal compartments to circumvent destruction. Granuloma formation then occurs. The granuloma can either contain the infection that could lead to sterilization or localized caseation and necrosis can take place that will lead to the release of infectious bacteria into the airways [73].

Mycobacteria enter macrophages by various receptors such as complement, mannose, Fc and scavenger receptors. Selective receptor blockade studies done by Zimmerli and co-workers indicated that the mycobacteria were able to survive and replicate in human macrophages regardless of the receptors used for binding and entry into the cell. The authors discovered that class A scavenger receptors accounted for the most significant amount of interaction and uptake of *M.tb* into macrophages. Scavenger receptors have the ability to bind and mediate the endocytosis of polyanionic macromolecules and particles such as low density lipoproteins, as well as interact with lipopolysaccharide of gram negative bacteria and lipoteichoic acids of gram positive bacteria [74-76]. Scavenger receptors have been implicated to play a role in cholesterol deposition in atherosclerosis, due to uptake of modified low density lipoproteins, which contain cholesterol, triacylglycerides and phospholipids [77].

1.4.2 Localized tissue markers of TB infection

Receptor mediated drug delivery can be achieved by linking a ligand to the drug-containing nanoparticle to interact with specific receptors, such as scavenger receptors or mannose receptors at the site of infection [78]. For example, mannosylated liposomes were used to target infected alveolar macrophages *in vivo* more efficiently than unmodified liposomes could [79].

Cholesterol may also be considered as a surrogate marker due to its accumulation at the sites of infection [80, 81]. Furthermore, infection of macrophages with mycobacteria results in the accumulation of cholesterol at the entry site. The latter

indicated that cholesterol has a direct role in uptake of mycobacteria by the macrophages as the binding of the mycobacteria to the cell surface required sufficient amounts of cholesterol in the plasma membrane. Entry of *M.tb* could be hindered by prior cholesterol depletion of the macrophage membrane [81-83]. However, these conclusions made by the early studies of Gatfield and Pieters were not as simple as they first thought.

Cholesterol plays an important role in the structural and functional aspects in macrophages [84]. Lipid bodies are observed in macrophages from the very beginning of infection and may play a role in immunomodulation [85] as well as being a nutrient rich reservoir for tubercle bacilli [82].

Peyron *et al.* (2000) argued that the resistance to uptake of tuberculous bacilli in membrane-cholesterol depleted cells is because of perturbed receptor signalling rather than inhibition of binding of the bacilli directly to membrane cholesterol as entry mechanism. Using the human neutrophil model as host and *M. kansasii* as mycobacterial pathogen, they suggested complement receptor type 3 (CR3) as the main entry receptor, which is associated with GPI- anchored proteins localized in cholesterol rich microdomains (lipid rafts) [86, 87]. Without cholesterol in the membrane, the CR3 remains outside the cholesterol-rich lipid raft domains and do not activate the cell to take up the mycobacteria.

Ferrari *et al.* identified a phagosome coat protein (Figure 1.6) termed TACO (tryptophane aspartate containing coat protein), coronin 1 or P57 that was retained at the cytoplasmic face of the phagosomes carrying the viable mycobacteria [88]. This protein is associated with the microtubule network and is present in cells of the lymphoid/myeloid lineage. It is not an integral protein, but is bound to the phagosomal membrane via a steroid moiety, cholesterol. The attraction of TACO protein to the phagosome membranes occurs in a cholesterol dependent way [81]. Viable mycobacteria were shown to maintain the TACO protein on the phagosome thereby hindering lysosome fusion, whereas heat killed bacteria caused a release of the protein resulting in lysosome fusion. In addition, macrophages that did not have TACO (example in Kupffer cells) destroyed mycobacteria after being taken up, suggesting that the protein is involved in the intracellular survival of mycobacteria

[88]. In a review by Pieters and Gatfield they speculated that the coat protein, TACO, could possibly mimic the plasma membrane thereby avoiding lysosomal delivery [89]. It was more recently shown that TACO is responsible for activating the calcium (Ca^{2+}) dependent phosphatase calcineurin, that leads to the inhibition of lysosomal delivery [90].

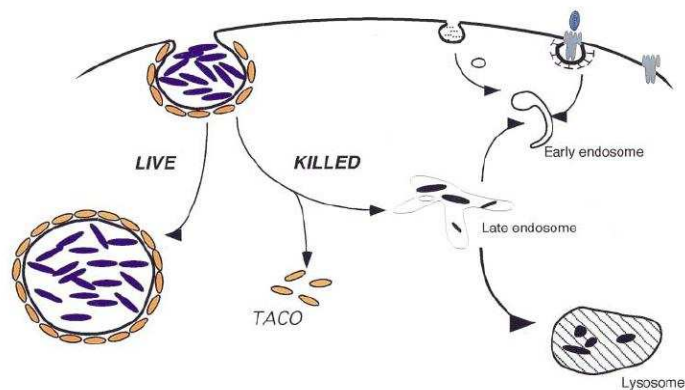


Figure 1.6 Survival mechanisms of the mycobacteria, in the macrophage host. Phagocytosis of mycobacteria (blue) into the macrophages triggers the recruitment of TACO (yellow) around the emerging phagosome. The TACO coat must be removed in order for the mycobacteria in the phagosome to be delivered to the lysosome where the contents of the phagosome are degraded. Living mycobacteria in contrast to heat killed *M.tb* are able to retain TACO at the phagosomal membrane, preventing the delivery to the lysosome so that the bacteria can survive within the phagosome [91].

In addition a human cholesterol specific receptor – C_k like molecule was found that could possibly interact with the cholesterol rich domains on the macrophage surface, forming a synaptic-junction that facilitates signalling events such as the association to the TACO protein [92, 93].

Pathogenic mycobacteria are able to survive within the phagosomes by interfering with the phagosome maturation and therefore do not fuse with lysosomes [94]. A number of different mechanisms have been shown to play a role in the maturation block [87]. Work done by De Chastelier and co-workers derived from morphological observations that a close apposition of the phagosome membrane with the whole mycobacterial surface was necessary for a maturation block [95]. During phagocytic

uptake of mycobacteria plasma membrane cholesterol dependence was observed [81, 86]. De Chastelier and her colleagues then investigated the effect of cholesterol depletion on the close interaction between the internalized bacterium's cell wall and the phagosome membrane. When the cholesterol was depleted, the mycobacterial surface was not closely associated with the phagosome membrane anymore and lysosomal fusion followed, pointing towards an important role for cholesterol in the maturation block. Interestingly, when cholesterol was replenished again, the mycobacteria were able to restore themselves in phagosomes [96].

In conclusion, cholesterol may be considered as a marker of localised TB infection due to its accumulation at the site of mycobacterial entry [81]. It could, however, be quite a challenge to find a non-toxic ligand to cholesterol to facilitate drug delivery. The cholesterol-binding drugs Amphotericin B or cyclodextrins are too toxic to include into the nano-encapsulated anti-TB drug particles.

1.4.3 Mycolic acid ligands for drug targeting

The cell wall envelope of *M.tb*, as depicted in figure 1.7, consists of a cytoplasmic membrane and an outer capsule comprising peptidoglycan and arabinogalactan complexes as well as mycolic acids with intercalated free standing lipids, glycolipids and proteins. This provides an extremely robust and impermeable envelope with high resistance to host-derived and therapeutic anti-bacterial agents [97, 98]. Other predominant components include the lipopolysaccharides, lipoarabinomannan (LAM) and phosphatidylinositides anchored in the plasmamembrane [99].

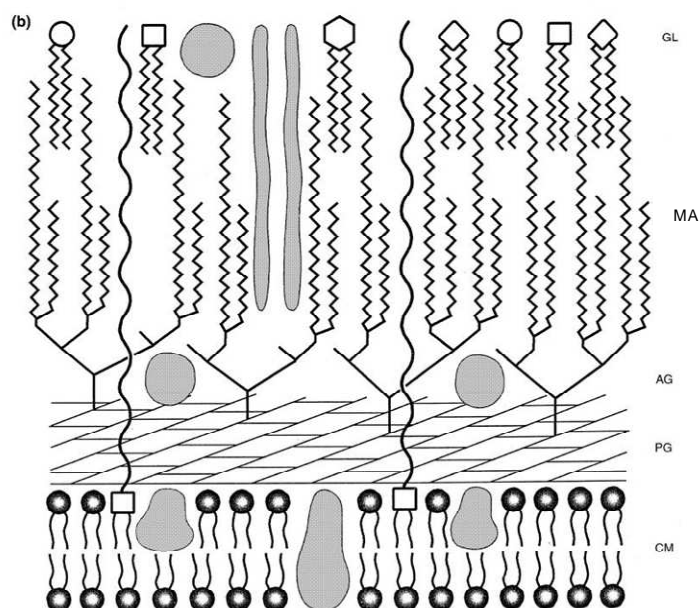


Figure 1.7 Schematic representation of a mycobacterial cell wall PG: peptidoglycan, CM: cytoplasmic membrane, GL: glycolipids, MA: mycolic acids, AG: arabinogalactan, the shaded areas represent different proteins present in the membranes[100].

The most abundant high molecular weight lipids present in the envelope are mycolic acids (MA), an extended family of long 2-alkyl 3-hydroxyl fatty acids, typically 70-90 carbon atoms in length. The members of the mycobacterium complex i.e *M.tb*, *Mycobacterium africanum*, *Mycobacterium bovis* and *Mycobacterium microti* are pathogenic and produce α -, keto- and methoxy- MA. Two moieties could be distinguished in the MA structure, the meromycolate moiety and the mycolic motif (Figure 1.8). The mycolic motif is similar for all mycolic acids with a few minor variations in chain length in the α position. The meromycolate moiety defines the subtypes of MA. These sections can be differently substituted with carboxyl, methyl, carbonyl, epoxy groups, double bonds or cyclopropanes in the proximal and distal positions [101]. A variety of MA patterns occur other than the α -, keto- and methoxy-MA found in *M.tb*. Amongst other different mycobacterial species carboxymycolates are found in *M. avium* and epoxy mycolates are produced in *Mycobacterium fortuitum* and *Mycobacterium smegmatis* [99, 101].

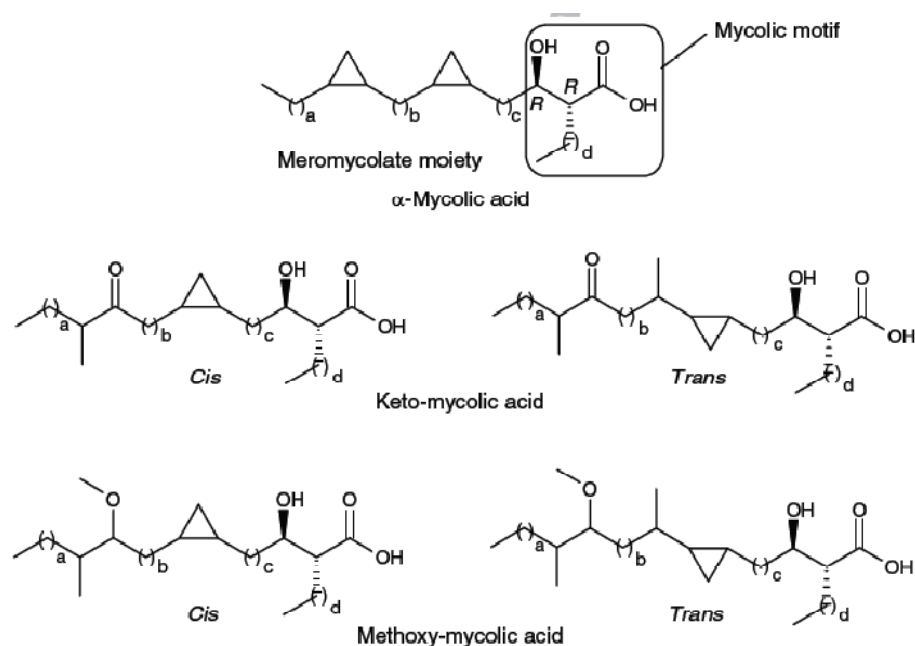


Figure 1.8 Structures of mycolic acids from *M.tb* [97].

MA are predominantly found in the bound form. The MA can either be linked to arabinogalactan polysaccharide via ester linkages, which is linked to peptidoglycan of the cell wall, some MA exist as trehalose monomycolate (TMM) and dimycolates (TDM) or be loosely associated with the insoluble matrix [99]. The folding of the MA molecules differs for each subtype depending on the functional groups present. Langmuir trough studies showed that keto MA tended more towards a W-shaped configuration with exceptional rigidity in monolayers, whereas methoxy- and alpha-MA exhibited a more flexible conformation towards variation of experimental parameters [102, 103]. The precise conformation of the MA within the cell wall structure is complicated to determine as the MA are present in different subclass mixtures with different carbon chain lengths within each group [97].

The biosynthesis of MA is a unique system as it employs the fatty acid synthetases (FAS) type I and II for synthesis. The FAS I and II are also NADH/NADPH dependent for their respective reactions. FAS type II is especially important for drug development and targeting as this synthetase is found in prokaryotic organisms and plants but not in mammalian cells. FAS type I is involved in the *de novo* synthesis of C₁₆₋₁₈ and C₂₄₋₂₆ fatty acids which is then subsequently used in the FAS type II process for further elongation and insertion of functional groups. The formation of the MA occurs through repetitive cycles of condensation, keto reduction, dehydration and

enoyl reduction in the fatty acid synthesis process, each product of the completed cycle is used as the substrate for the next cycle until the specific chain length is acquired. Several enzymes are involved to catalyse the reactions, β -ketoacyl synthase, β -ketoacyl reductase, β -hydroxyacyl dehydrase and enoyl reductase. For the formation of the functional groups the fatty acids undergo desaturation and cyclopropanation that is all part of the FAS type II pathway [104-106]. Cyclopropanation occurs via the S-adenosylmethionine dependent methyl transferases not found in other bacteria. The next step is the Claisen-type condensation to join the meromycolate to the mycolic motif [99]. In the last step the mycolic acids are esterified with the arabinogalactan complex or with free glycolipids to form trehalose dimycolate (TDM) by the antigen 85 complex [107].

1.4.3.1 MA structure-function relationship

The various subtypes of MA have been shown to date to play a role in the virulence of the pathogen [108, 109]. In a study done by Dubnau and co-workers, they synthesized a mutant strain of *M.tb* that did not produce oxygenated (methoxy- and keto-) MA. This strain was shown to have a decrease in membrane permeability and thus confirmed that the fluidity of the cell wall greatly depends on the type of mycolate produced [101, 110]. The results also showed that the bacteria were attenuated in mice, thus the oxygenated MA playing a role in virulence of the bacteria [108].

An array of mycobacterial cell wall components have been considered as surrogate markers for TB in the past [111, 112]. Antigenic activity of mycolic acids and the glycolipid derivatives such as the lipid extractable trehalose mono- or dimycolates, TMM or TDM respectively (cord factors) have been previously described [97, 109, 113]. Of all the antigens prevalent in the cell wall of the mycobacteria that may be considered for use in TB serodiagnosis, MA provide a special opportunity due to their variability among different species of Mycobacterium and the unique way that they communicate their presence to the immune response of the host [97, 114, 115]. Their ability to elicit CD4, CD8 double negative T cells by means of their presentation on CD1b lipid presentation proteins on dendritic cells [116] may well be the reason that

the antibody titers to mycolic acids in AIDS patients with even very low CD4 T cell counts are maintained, relative to other patients that are not infected with HIV, or have normal CD4 T cell counts [117, 118].

Using mycolic acids as surrogate markers for TB diagnosis was shown to be successful in an ELISA assay [117-119]. Pan *et al.* have shown that the most antigenic part of the cord factor antigen was the mycolic acid [97, 118, 119]. This was also shown in a study done by a group in Japan that the anti-cord factor IgG produced from rabbits, recognized specifically the MA subclasses [112]. Due to the low specificity achieved, this was not the ideal solution

A biosensor approach showed improved accuracy to a level that may be seriously considered for the possibility of commercialization, when using free mycolic acids in liposomes as antigens in a competitive binding assay [117, 120]. This test, subsequently dubbed the MARTI-test (for Mycolic acids Antibody Real-Time Inhibition), can diagnose TB within four hours of sampling by analyzing the serum sample for the presence of anti-mycolic acid antibodies as immune surrogate markers for active TB that is has an accuracy of 84% [120].

The structure of MA showed significant characteristics as was previously investigated by our group. A biosensor study was done which showed that amphotericin B interacted with MA and cholesterol, and that MA associated with cholesterol. This lead to the conclusion that MA exhibit a structural similarity to a sterol such as cholesterol [121].

The contribution that MA makes in the host pathogen interaction has been an area of interest for the past decade. In a study done by Korf *et al.* where they measured the cellular responses in peritoneal and alveolar macrophages when injected with MA, these authors observed the induction of foamy macrophages (intracellular lipid accumulation in macrophages) as well as MA being able to induce an inflammatory response of IL-12 and IFN- γ [14] as was also shown with TDM except TDM also induced TNF- α response whereas MA did not [122, 123]. Therefore, cytokine inducers such as TDM have good potential to be used as adjuvants and immunomodulators [124].

This mycobacterial induced host response for foamy macrophage formation is probably for active lipid import that the bacteria can utilise as metabolic substrates for survival and replication [14]. This was confirmed when it was shown that *M.tb* could utilise cholesterol as an energy and carbon source [125].

Foamy macrophages arise from the onset of infection by the accumulation of lipid bodies as indicated by *M.tb* infected mice and guinea pig studies done by Caceres *et al.* 2009 [85]. Peyron and co-workers illustrated in an *in vitro* human tuberculous granuloma model that virulent mycobacteria (*M.tb*, *M. avium*) and not the saprophytic type (*M. smegmatis*) induce foamy macrophages. The *M.tb* resides within the foamy macrophages singularly in phagosomes in a non-replicative state. A very interesting observation the group made was that a number of the bacteria were in close apposition to the lipid bodies present in the foamy macrophages. The role that MA plays in the induction of the foamy macrophages was shown to be through the oxygenated mycolic acids, and are thus virulence factors enabling the bacteria to persist in the macrophage over a long time [82].

The MA elicited responses points towards a macrophage steering of T regulatory immune responses. This was illustrated when Korf *et al.* used a mouse model of asthma by treating ovalbumin sensitized mice with MA. The airways of the mice were tolerant to a secondary exposure to the ovalbumin indicating that MA suppressed Th2 reactivity [126]. MA might also serve as a liver X receptor (LXR) ligand, which plays a role in macrophage cholesterol, fatty acid and glucose homeostasis [127]. These functions in effect have an influence on the inflammatory status of the macrophage.

Mycobacteria have been shown to have conserved molecular products (pathogen associated molecular patterns (PAMP) including the glycolipid lipoarabinomannan, lipopeptides and soluble tuberculosis factor recognised by Toll-like receptors (TLR) [128, 129], but MA was excluded being recognised by TLR2 and TLR4 [14]. TDM is an immunogenic lipid associated with pro-inflammatory responses, recognition to TLR2 was shown to be mediated by the macrophage scavenger receptor MARCO and CD14 [130].

1.4.3.2 MA as virulence factors

Infection occurs when inhaled bacilli are phagocytosed by alveolar macrophages. Macrophages that are infected with *M.tb* are the initiators of granulomas, which consist out of lymphocytes, extra cellular matrix components, calcifications and caseous necrotic tissue [73, 82]. Interactions of the bacteria with other leukocytes include dendritic cells, the professional antigen presenting cells. However, experimental work done by Tailleux and colleagues indicated that the bacteria do not grow within dendritocytes, but infected dendritocytes do accumulate in the regional lymph node, adding to the immune response. Within the phagocyte of the macrophage on the other hand the bacteria prevents the fusion with acidic compartments, enabling it to replicate within the macrophages [73, 131].

Pioneering work of Armstrong and D’Arcy Hart showed that *M.tb*-containing phagosomes do not fuse with lysosomes [132]. When mycobacteria enter the macrophages via phagocytosis, they reside and multiply within phagosomes, the process of fusion with lysosomes is inhibited by the mycobacteria to form phagolysosomes [94, 132]. Mycobacterial lipids such as phosphatidylinositol-mannoside (PIM) [133] and TDM [123, 134] have been implicated to slow down the maturation of the phagosomes into phagolysosomes. Mannose-capped lipoarabinomannan (ManLAM) [135] was shown to play a role in the maturation block but more recent findings point to opposite results [136]. Beatty and co-workers found that mycobacterial lipids were released from the mycobacterial phagosome and that these microvesicles entered a secretory pathway (possibly lysosomal like organelles) and then could be phagocytosed by bystander macrophages [137, 138].

A single *M. avium* per phagosome was shown to require a close apposition between the mycobacterial surface and the enclosing phagosome membrane to inhibit phagolysosome formation, when more than one bacteria was present within the phagosome the close apposition was not maintained and the phagosomes fuse with lysosomes [95, 96, 135, 139]. In a study done by De Chastellier in 2009 it was shown that in the event of phagolysosome formation, *M. avium* was able to rescue itself and reside again in immature phagosomes [140]. Similarly Armstrong and D’Arcy Hart

observed that *M.tb* were able to grow even when phagosome lysosome fusion occurred [132].

1.4.3.3 Mycolic acids as surrogate marker antigen in TB

Ojha and colleagues demonstrated in an *in vitro* study that *M.tb* was capable of biofilm formation in the slow turn over, persistent stage of the *M.tb* life cycle. The formation of these biofilms was found to be dependent of iron and zinc metal-ions, as well as gaseous exchange of CO₂. The films were shown to provide resistance to anti-TB drugs, i.e. the bacteria were able to survive in the presence of these drugs *in vitro*. The findings that were most relevant to this were the presence of abundant free MA in these biofilms. The major MAs that were detected with NMR and MS studies turned out to be the methoxy MA and some α mycolates [141]. From observations with *M. smegmatis*, a TDM specific serine esterase is utilized to hydrolyze TDM to form the free MA. It was suggested that *M.tb* could also form free MA from TDM by an esterase. The free MA could then be excreted to form the biofilm matrix [142].

MA incorporated into nanoparticles may interact with the anti-mycolic acid antibodies that should be present in higher concentrations at the infected areas. In this way, targeting may be achieved by an accumulation of the nanoparticles in immune complexes at the site of infection. Alternatively MA could also serve as a ligand for cholesterol-rich areas, due to the cholesteroid nature of MA and the fact that MA is attracted to cholesterol [121].

1.5 Aim of the project

The ultimate aim is to provide a nano-encapsulated anti-TB drug delivery vehicle which will overcome the difficulty of daily supervision of drug-taking by patients and possibly shorten the regime of anti-TB treatment. For this study, MA structure-function properties and the practical feasibility of encapsulating MA into PLGA

Chapter 1: General introduction

nanoparticles as targeting ligand was investigated as well as the product's toxicity to and efficiency of uptake in host macrophages.

In chapter 2 the cholesterol nature of MA was investigated by testing the tolerance of structural changes of natural mixed MA for recognition by Amphotericin B. In addition, the structure of synthetic mycolic acids in relation to their antigenicity in tuberculosis was determined.

Chapter 3 describes how the MA containing nanoparticles were synthesized and assembled, characterized for their ability to be internalized and processed into macrophage cell lines and what degree they may be toxic to host cells. In addition, the effect that MA may have on the mycobactericidal properties of co-encapsulated isoniazid was explored *in vitro* in *M.tb* infected macrophages.

The potential impact of the results from the experimental chapters on TB treatment in future is discussed in chapter 4.

Chapter 2: The cholesteroid nature of MA as a tool for targeting

2.1 Introduction

Upon inhalation of *M.tb*, the bacteria enter the lungs and are phagocytosed by alveolar macrophages. This causes a proinflammatory response that leads to the recruitment of mononuclear cells. These cells cluster at the site of infection to form granulomas which contain the *M.tb*. Within granulomas a variety of cells are found which include differentiated macrophages, highly vacuolated macrophages and lipid rich foamy macrophages [143]. These *M.tb* infected macrophages induce an accumulation of cholesterol esters that could be a major component of foamy macrophages [144]. Foamy macrophages present in the outer ring of the granuloma were shown to accumulate during the chronic phase of infection in mouse experimental models [85, 145]. Experiments with radio-labelled lipids have shown that the presence of *Mycobacterium leprae* (*M.leprae*) in tissues was associated with increased intracellular levels of cholesterol-esters, which may be responsible for conversion of macrophages into foam cells [84]. In tuberculosis, the foam cells are surrounded by lymphocytes and later fibroblasts [146]. Active disease only comes about when necrosis and cavity formation occur in the lungs, in which massive numbers of bacteria are produced. This occurs concomitantly with changes in the immune status of the host [140].

In order for *M.tb* to survive in a heterogeneous and continually changing macrophage environment, they need to adapt their nutrient sources. Cholesterol is a major sterol in eukaryotic organisms. It is involved in membrane stabilization and plays a role in cell signalling pathways [147]. It can also be used as a carbon and energy source for various microorganisms [80]. Previous papers suggested that pathogenic bacteria use lecithin instead of cholesterol as carbon source [144], but more recent evidence points

to the pathogenic mycobacteria being able to accumulate [80] and consume cholesterol as major nutrient in the persistent stage of the disease [125, 148]. The genomic sequence of *M.tb* revealed the full repertoire of sterol biosynthetic and cholesterol degradation enzymes [149]. Av-Gay and colleagues have suggested that cholesterol could play a role in the prevention of phagosomal maturation of mycobacterially infected macrophages and that soluble cholesterol may accumulate into the cell wall surface of mycobacteria [80].

Brzostek *et al.* 2009 found that *M.tb* can both accumulate and utilize cholesterol. They showed that cholesterol, as primary source of carbon, was degraded via the 4-androstene-3,17-dione/1,4androstadiene-3,17-dione pathway (AD/ADD) together with an intact KstD enzyme. Cholesterol was also shown to accumulate in the free lipid zone of the cell walls of the bacteria and that the accumulation affected cell wall permeability [148]. Whether cholesterol as a carbon source could support long term persistence of tubercle bacilli is not yet known.

It was shown that during the chronic phase of murine infection and in IFN- γ activated macrophages *in vitro* the Mce4 transporter is necessary for cholesterol import into the bacterium and that the bacteria can indeed degrade cholesterol as primary source for carbon and energy [125, 150]. The cholesterol degradation was measured by detecting the no. 4- and no. 26-carbons of the molecule, with C-26 being incorporated into the cell membrane lipids and the C-4 part converted to CO₂ (g) [125]. The study showed that the Mce4 mutant was not able to convert cholesterol. Mce4 was also not required for replication of *M.tb* in resting macrophages. In another study it was shown that the acquisition of cholesterol was dependent on a cholesterol oxidase [151].

Genes that are required for the survival of *M.tb* in the hostile environment of the macrophage were shown with transposon site hybridization (TraSH) using a microarray based technique. Genes that seemed to be critical for survival within macrophages included those involved in lipid transport and degradation as well as those involved in phosphate transport [152]. The TraSH technique was also used to study the *mce4* locus. It suggested that a group of genes were involved in lipid metabolism, including the operon Rv3540-5c [150]. The operon was later called *igr* (intracellular growth) and was required for growth in THP-1 cells and in a tissue

culture model of infection [153]. It was also shown that mutants thereof were attenuated for growth *in vivo* [154]. In an *M.tb* related actinomycete *Rhodococcus sp.* a 51-gene cluster was identified whose transcription was induced specifically in the presence of cholesterol. The cholesterol catabolic pathway investigated was also shown to be conserved in related species such as *M.tb*, where the matching gene cluster included the *igr* operon and the *mce4* transport system [155]. Miner *et al.* 2009, showed that an *igr* deletion mutant could not grow in the presence of cholesterol, whereas the *mce4* mutant was only attenuated in mice in late stages, pointing to the notion that cholesterol metabolism was only required in the chronic infection stage [154].

Dynamic interactions between host and mycobacterial factors may play an important role in mycobacterial survival [140]. Mycobacterial cell wall components include phosphoinositol mannosides (PIMs) interacting with cholesterol-enriched microdomains of the host [156], ManLAM induces reorganisation of lipid membranes, preventing vesicle fusion, thereby inhibiting phagosome maturation [157]. Phthiocerol dimycocerosates (DIM) have been shown to be involved in the prevention of phagosomal acidification, which precedes phagolysosomal fusion and eventual destruction of internalized mycobacteria. DIM is also involved in receptor dependent phagocytosis (rather than macropinocytosis) into macrophages that are dependent on an intact actin filament network. This is done by a possible mechanism of targeting of lipids and disturbing their organisation in the host membrane [83]. Interestingly it has been shown that *M.tb* forms biofilms that is distinct from planktonic growth and that free mycolic acids were present in the extracellular matrix of these films [141].

Host membrane cholesterol seems to play a role in at least one route of entry and survival of mycobacteria in macrophages, also facilitating the phagosomal association of TACO on mycobacteria-containing phagosomes. TACO inhibits lysosomal delivery of the mycobacteria by activating a Ca^{2+} dependent phosphatase calcineurin [90]. The TACO protein is associated with the prevention of phagosome-lysosome fusion [81, 96, 154]. In *M. avium* infected mouse bone marrow macrophages, phagosome maturation and lysosome fusion occurred when the macrophages were

depleted of cholesterol. Cholesterol replenishment showed that mycobacterium could rescue itself from phagolysosomes [96]. It was shown that in *M.tb* a compound with epitopes similar to the human cholesterol specific receptor – C_k like molecule was found that has an affinity for cholesterol, and that it was responsible for entry into macrophages as well as the mediation of phagosomal association with Coronin-1A, which inhibits endosomal/lysosomal fusion [92, 93].

The rationale for using free mycolic acids as targeting agent in nanodrug delivery is due to their cholesteroid nature [121] and their attraction to cholesterol. It may therefore target cholesterol enriched mycobacterially infected areas. Further investigation into the characteristics of mycolic acids was done in order to establish how structural changes affect the cholesteroid nature of the MA.

To measure the interaction between Amphotericin B and MA as indicative of the cholesteroid function of MA, an ESPRIT SPR biosensor was used. The principle of the SPR biosensor is based on the change in refractive index on a modified thin gold film surface when mass is accumulated onto an immobilized ligand [158]. This interaction is measured in real time. An important advantage that this technique has above the conventional methods is that no labeling is required and that low affinity specific binding can be detected. The instrument was also used to determine the effect of labelling of MA on its manifestation of the cholesteroid nature, the binding interaction between amphotericin B and either cholesterol-, MA-, or fluorescein-labeled MA-containing immobilized liposomes. In addition to the amphotericin B affinity experiments on the SPR biosensor, the antibody recognition of modified MA was tested in an ELISA based experiment. Thereafter the relationship between the structure and the cholesteroid nature of MA was investigated by testing different stereo-controlled synthetic MA to antibodies in TB patient serum.

2.2 Hypothesis

The cholesteroid nature of MA derives from a specific folding of the mero-chain that is stabilized by hydrogen bonding to the carboxylic acid.

2.3 Aims of study

- Comparing the ability of cholesterol, fluorescein-MA and MA to associate with AmB
- Investigating the tolerance of structural changes of natural mixed mycolic acids for human antibody recognition.
- How structure of synthetic mycolic acids relates to antigenicity in tuberculosis

2.4 Materials

2.4.1 Consumables

Amber vials	Separations Pty Ltd, Randburg, RSA
Amphotericin B	Sigma-Aldrich, Steinheim, Germany (isolated from <i>Streptomyces</i> to 80% purity, identified by HPLC)
5-Bromomethyl fluorescein	Molecular Probes, Leiden, The Netherlands
Chloroform	Merck, Darmstadt, Germany
18-crown-6 ether	Sigma-Aldrich, Steinheim, Germany

Dimethyl formamide	Merck, Darmstadt, Germany
Ethanol	BDH, Gauteng, RSA, Analytical grade
Hydrochloric acid	Saarchem, Gauteng, RSA
Methanol	Merck, Darmstadt, Germany
Molybdato-phosphoric acid	Merck, Darmstadt, Germany
Mycolic acids	Sigma Chemical Co., St Louis, USA
Octadecanethiol	Sigma Chemical Co., St Louis, USA
Phosphatidyl choline pure)	Sigma Chemical Co., St Louis, USA, (99 %
Potassium chloride	Merck, Darmstadt, Germany
Potassium dihydrogen phosphate	Merck, Darmstadt, Germany
Potassium hydrogen carbonate	Merck, Darmstadt, Germany
Potassium hydroxide	Saarchem, Gauteng, RSA
Silica plate	ALUGRAM SIL G/UV, layer: 0.2mm silica gel 60 with fluorescent indicator UV254, Düren, Germany
Sodium azide	Sigma Chemical Co., St Louis, USA
Sodium chloride	Saarchem, Gauteng, RSA
di-Sodium hydrogen phosphate	Merck, Darmstadt, Germany
Ethylenediaminetetraacetic acid salt	Merck, Darmstadt, Germany

2.4.2 Buffers

PBS-Azide EDTA buffer (PBS/AE): 8.0 g NaCl, 0.2 g KCl, 0.2 g KH₂PO₄ and 1.05 g Na₂HPO₄ per 1 L double distilled, deionized water with 1 mM EDTA and 0.025% (m/v) sodium azide, adjusted to pH 7.4

2.4.3 Instrumentation

For the measurement of the binding properties of mycolic acids and derivatives thereof to other low molecular weight ligands an ESPRIT biosensor from Metrohm Autolab B.V., Utrecht, the Netherlands was used. For preparation of liposomes a Virsonic sonifier, (Virtis, Gardiner, N.Y.) was used. Well Wash4 ELISA washer (Labsystems, Helsinki, Finland) was used for ELISA plates wash steps. Absorbancies were measured with a SLT 340 ATC photometer (SLT Labinstruments, Austria) at 450 nm.

2.5 Methods

2.5.1 Fluorescent labelling of mycolic acids

MA was fluorescently labelled by derivatization with 5-bromomethyl fluorescein (5-BMF) as described by Korf *et al.*, according to a general protocol first described by [159]. The first step in the methodology involves re-saponification of the MA. Briefly, reagent A (1 ml of potassium hydroxide, KOH 25%, i.e. 5 g in ddd H₂O, 10 ml, and methanol 10 ml) was added to MA (1 mg, 8.3×10^{-7} mol, 1 eq), and the capped solution was heated for an hour. Following cooling, 1 ml of reagent B (50% aqueous dilution of concentrated Hydrochloric acid (32%)) was added and the solution vortexed. Chloroform (1 ml) was added, the organic layer removed and the aqueous phase washed three times with chloroform. After evaporation of the organic solvent on a heat block with N₂ (g), reagent C, 800 µl (Potassium hydrogen carbonate

KHCO₃, 0.01 mol in ddd H₂O, 25 ml and methanol, 25 ml) was added and heated for 1.5 hours at 86 °C. The saponified MA product was dried and the solvent evaporated with heat under an N₂ (g) atmosphere. Chloroform (500 µl) was added to the dried, saponified MA and mixed, before 18-crown-6 ether (1.1 mg, 4.16 x 10⁻⁶ mol, 5 eq), dissolved in chloroform, was added and vortexed. The reaction was incubated for 30 min and 5-BMF (712.5 µg, 1.67 x 10⁻⁶ mol, 2 eq dissolved in 95 µl DMF) was added to the solution, vortexed and heated at 86 °C for one hour. The solution was left overnight at room temperature. The unbound fluorescence was removed by washing with 1ml chloroform saturated reagent E (reagent B mixed 1:1 with methanol). The washing with concomitant vortexing and phase separation was repeated 17 times. Each chloroform phase wash was monitored by measuring absorbance at 450 nm with 690 nm as reference filter. The organic layer was collected and dried under N₂ (g) after five final washes with CHCl₃ saturated HCl:H₂O.

Quality control was performed using TLC on a silica gel thin layer plate. Chromatography was performed in two dimensions, with chloroform:methanol:water as the mobile phase in the first dimension, and 100% methanol as the mobile phase in the second dimension. For visualisation, the TLC was stained with 5% molybdato-phosphoric acid solution. Fluorescently labelled MA was incorporated into liposomes for assessment by the biosensor.

2.5.2 Biosensor experiments

2.5.2.1 Preparation of mycolic acids, labelled mycolic acids or cholesterol-containing liposomes

For the preparation of the different liposomes, phosphatidyl choline stock solution (90 μ l, 100 mg/ml chloroform) was added to an amber glass vial containing either mycolic acid (1 mg) or an equimolar amount of 5-BMF labeled mycolic acid (1.35 mg). For the preparation of cholesterol containing liposomes, phosphatidyl choline stock solution (60 μ l, 100 mg/ml chloroform) was added to a cholesterol solution (30 μ l, 100 mg/ml chloroform). The samples were mixed well until dissolved, then dried under a stream of N₂ (g) at 85 °C. Saline (2 ml) was then added and the sample was heated on a heat block for 20 min. at 85 °C. The sample was then vortexed for 1 min, sonicated with a Virsonic probe sonicator until a clear solution formed to indicate vesicle formation, aliquoted at 0.2 ml per vial, lyophilized and stored at -70 °C until use. Before use, lyophilized liposomes were reconstituted with PBS buffer (2 ml). The liposomes were placed on a heat block for 30 min. at 85 °C. Following incubation, the solution was vortexed for 2 min, then sonified briefly and a final liposome stock concentration of 500 μ g lipid/ml was used for experiments.

2.5.2.2 Measuring the affinity between Amphotericin B and either mycolic acids, labelled mycolic acids or cholesterol

The binding interaction between Amphotericin B and either cholesterol, MA or fluorescein labelled MA immobilized liposomes were tested on an ESPRIT biosensor. The gold coated sensor disk used for immobilizing the lipids on, was first incubated with 10 mM octadecanethiol (ODT), dissolved in absolute ethanol for 16 hours. An automated software program sequence was created to control the addition of all the samples and liquids into the cuvette [117]. Filtered PBS/AE was used as buffer, and

He (g) was used to degas the buffer when needed. The sequence included flushing the cuvette with 500 μ l ethanol (96%) using the automatic dispenser with simultaneous draining, followed by brief washing with PBS/AE. SPR 'dips' were continuously measured to ensure the quality of the surface for surface plasmon resonance. Cleaning of the ODT coated surface was done with 96% ethanol and a mixture of isopropanol and 50 mM sodium hydroxide (2:3, v/v) before the start of the experiment. The samples were transferred from a 384 multi-well plate (Bibby Sterilin Ltd, Stone, UK) to the cuvette surface by an auto pipettor. The baseline of the ESPRIT biosensor was formed with 10 μ l PBS/AE, followed by addition of 50 μ l test liposomes on the disc for 20 min. Washing was done 5 times with 100 μ l non-degassed PBS/AE with mixing to obtain a baseline. Amphotericin B (1×10^{-4} M) was added to the liposome layer and the direct binding interaction was recorded for 10 min., after which the disk was washed 5 times with non-degassed PBS/AE, and left for 5 min.

2.5.3 Enzyme-linked immunosorbent assay (ELISA) to test the antigenicity of MA derivatives

For coatings done in PBS, methylester MA (ME-MA) or free MA (250 μ g) was dissolved in 1 x PBS (4 ml, pH= 7.4) by heating at 90° C for 20 min on a heat block. PBS (4 ml) served as control. The solutions were vortexed for 30 s before sonifying for 2 min. using the Virsonic sonifier at output of 2. The warm solutions were subsequently loaded onto the ELISA plates (50 μ l per well) and the presence of oily drops viewed under a light microscope. The plates were kept at 4 °C overnight in plastic bags. For the coatings done using hexane as coating solution, the lipid samples (250 μ g) were dissolved in hexane (4 ml, distilled) and vortexed for 30 s. Hexane (4 ml) served as control. Solutions were coated using a Hamilton syringe (50 μ l per well) and the liquid was loaded in the centre of the wells. Lipid was visible as a circular waxy layer after 2 hours of evaporation of the hexane at room temperature. The plates were then stored in plastic bags at 4 °C overnight [160].

The rest of the ELISA experiment and the experiment done with the fluorescein-MA were carried out as described below.

2.5.4 Enzyme-linked immunosorbent assay (ELISA) of synthetic MA

In the ELISA experiments, pooled TB positive and TB negative sera for active disease were used. Both groups were HIV negative. The sera dated from the year 2000 and was initially collected for another study [118]. To coat the ELISA plates with the different synthetic mycolic acid subclasses, natural mycolic acids or modified mycolic acids, the lipids were dissolved in hexane (3 $\mu\text{g}/$ 50 μl) and vortexed one minute, heated (at ~ 85 $^{\circ}\text{C}$) for a minute and allowed to stand at room temperature for 15 minutes. Hexane coating as such served as a control. The ELISA plates were coated with the different mycolic acids at 50 μl per well using Hamilton syringes. The lipids were visible as a waxy coating after 2 hours of evaporation at RT. Plates were stored in a plastic bag at 4 $^{\circ}\text{C}$ overnight.

The following day the plates were blocked with 400 μl of 0.5% Casein / PBS pH 7.4 for 2 hours. The blocking buffer was removed and the wells were aspirated to dryness under vacuum and then coated with 50 μl per well of serum (1:20 dilution in 0.5% Casein / PBS pH7.4) for an hour. The plate was washed 3 times (Well Wash 4 ELISA washer) with 0.5% Casein / PBS pH 7.4. The plates were then coated with the goat anti-human Immunoglobulin G (H + L) peroxidase conjugate (50 μl / well) for 30 min. at RT. After the incubation the wells were washed three times with 0.5% Casein / PBS pH 7.4, then coated with 50 μl per well of the substrate solution consisting of 10 mg of OPD plus 8 mg of Urea- H_2O_2 in 10 ml of citrate buffer to measure the peroxidase activity. After 30 min. incubation at RT the plate was read with a SLT 340 ATC photometer at 450 nm with a reference filter at 690 nm. Background binding of the serum to the plate was corrected for by subtracting the average binding signal of serum to MA from that registered for the hexane coated wells. The results obtained were analysed by the making use of the Student's t test for statistical significance.

2.6 Results

2.6.1 Fluorescent labeling of MA

In order to study the binding of modified MA to AmB on the biosensor, the mycolic acids were labeled with 5-Bromomethylfluorescein (5- BMF) [161], the product formed tested on TLC and the R_f value determined for labeled MA (R_f = 0.89 in CHCl₃:MeOH:H₂O, 30:14:2). 5-BMF is a sensitive fluorescent reagent that is used for derivatization via carboxylic acids [159]. The reaction mechanism involves the conversion of the free acid to a salt and then reacting with the 5-BMF, using crown ether as the phase transfer catalyst to form the conjugated product [159].

By making use of thin layer chromatography (TLC), the coupling of the fluorescein to the MA was assessed. A reconstruction of the two dimensional TLC results are as shown in figure 2.1 and table 2.1. The Fluorescein-MA sample migrated in the 1st dimension, whereas a slight streak was visible in the 2nd dimension indicating a small fraction of label not linked to the MA. The 5BMF alone migrated in the 1st and 2nd dimension. Repeated washes (16 times) with acid water were used to remove any unbound fluorescent label from the Fluorescein-MA. The washed, labelled MA product was incorporated into liposomes for the biosensor studies.

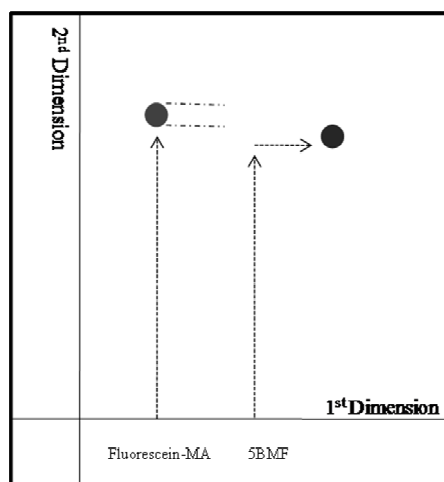


Table 2.1

	1 st Dimension Rf value	2 nd Dimension Rf value
Fluorescein-MA	0.89	0
5BMF	0.86	0.93

Figure 2.1 Reconstruction of the two dimensional TLC. The Fluorescein-MA represent the coupled MA to 5BMF and the 5BMF the fluorescent label alone. The 1st dimension had a mobile phase of $CHCl_3:MeOH:H_2O$, 30:14:2 and the 2nd dimension had a mobile phase of methanol. Table 2.1 gives the Rf values obtained. The plates were visualized by staining with 5% molybdato-phosphoric acid solution.

2.6.2 Comparative Amphotericin B recognition of MA, labelled MA or cholesterol

A structural relationship and attraction between free MA and cholesterol was shown in our laboratories in a previous study [121]. This was demonstrated on the IAsys biosensor system, where the interaction between MA and Amphotericin B - an antifungal macrolide agent known to bind to cholesterol [162] - was shown. On the ESPRIT biosensor, the same principle was confirmed (Figure 2.2). In an attempt to determine what the effect of labelling of MA would be on its manifestation of cholesteroid nature, the binding interaction between Amphotericin B and either cholesterol-, MA-, or fluorescein labeled MA-containing immobilized liposomes were tested. The results confirmed the ability of the ESPRIT biosensor (SPR) to demonstrate that Amphotericin B recognizes both cholesterol and MA and shows for the first time how altering the structure of MA by adding a bulky label on its carboxylic acid group affects the binding to Amphotericin B (Figure 2.2).

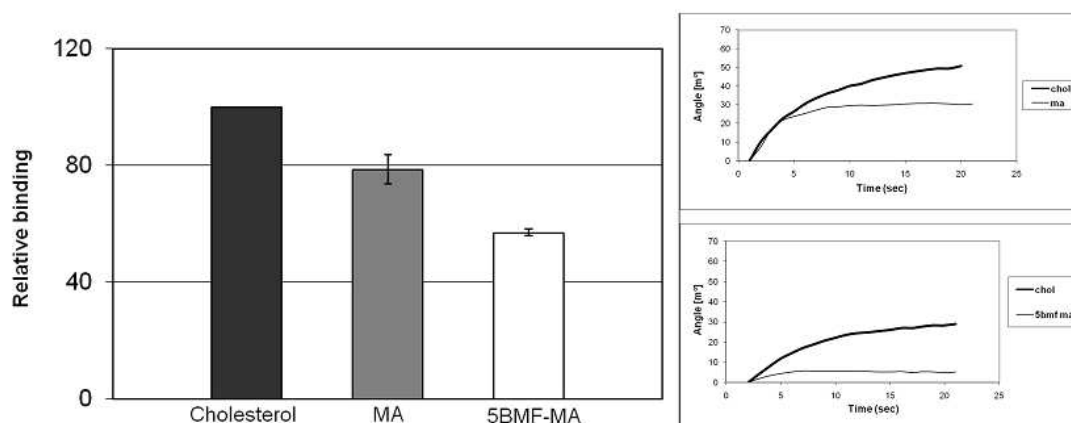


Figure 2.2 Normalised AmB binding capacity (left) on immobilized lipid antigens: cholesterol, MA and Fluorescein-MA. Typical AmB binding curves (right) on immobilized MA or Fluorescein-MA compared to cholesterol. The error bars indicate the standard deviation, $n = 3$ for each set.

A reduction in the relative binding for the labelled MA was observed, compared to the binding of MA and cholesterol. From these findings it could not be unequivocally established whether the fluorescent label on the MA destroyed, or merely affected the biological activity, as it is difficult to define the point of zero-activity with this application of the evanescent field biosensor. The ELISA experiments that follow were designed to shed more light on the matter.

2.6.3 Effect of a modified carboxylic group of MA on antibody binding and recognition

The cholesteroid nature of modified MA was implied in 2.6.2 by its ability to bind with AmB in an SPR biosensor. It was not clear whether derivatization of the carboxylic acid destroyed, or merely weakened its recognition by Amphotericin B, i.e. the cholesteroid nature of MA. To shed more light on this, the antibody recognition of modified MA was tested in an ELISA experiment. Pan *et al.* (1999) reported that methylesters of mycolic acids were recognised by TB positive patient sera in an ELISA assay [119]. Previously, our group showed that free mycolic acids were antigenic [118]. Here we tested the antigenicity of both the methyl- and Fluorescein-esters of MA to determine what the role of the carboxylic acid is in maintaining an

antigenic conformation. The ELISA plates were coated with the three different lipid antigens and TB patient sera were allowed to bind to it. The binding was measured at 450 nm with an indirect ELISA. Coating the antigens from hexane solution gave better results than when coating was done from hot PBS, but both methods served the purpose (Figure 2.4). When the carboxylic acid of MA was derivatised with 5- BMF (Figure 2.3), the TB positive and TB negative patient serum antibodies were still able to bind and recognise the molecule (Figure 2.4). This could be due to the carboxyl and hydroxyl group present on the fluorescein molecule that could substitute for the role of the carboxyl group of MA to stabilise the functionally active conformation by hydrogen bonding [102, 103, 121]. The methylated MA showed negligible binding compared to the labelled MA, despite the fact that both modifications entailed esterification of the carboxylic acid of the molecule. The results suggest that the binding of antibodies to mycolic acid relies on the availability of a free carboxylic acid in the vicinity of the mycolic motif. TB negative pooled sera also gave strong antibody binding signals to the natural MA as well as the Fluorescein-MA, possibly due to cholesterol cross-reactivity with mycolic acids as suggested previously [117, 118, 121].

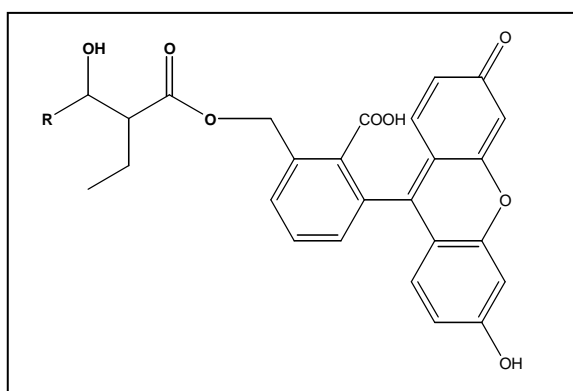


Figure 2.3 Chemical structure of fluorescein labelled MA.

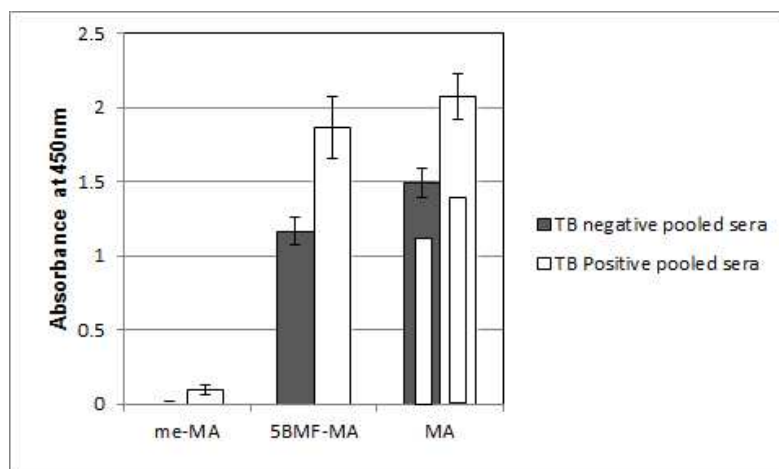


Figure 2.4 Comparison of antibody recognition to MA, ME-MA [160] and Fluorescein-MA. The ELISA signals of pooled TB positive and pooled TB negative sera was measured at an absorbance of 450 nm to the whole fraction of MA, Fluorescein-MA and ME-MA [160] antigens coated onto ELISA plates from hexane. Inner bars indicated within the MA mix bars indicate the signals when coating was done from hot PBS instead of hexane. The error bars indicate the standard deviation.

2.6.4 Response of patient sera to natural and synthetic mycolic acids

Mycolic acids in *M.tb* contain a mycolic motif, which is an α -alkyl, β -hydroxy acid. Stereochemically, the α and β positions relative to the carboxylic group present in all mycolic acids have been shown to be in the R-configuration. The main branch, known as the meromycolate moiety, contains two functionalities, which are differently substituted around the distal and proximal positions [97]. The proximal position is usually either a cis- or an alpha-methyl-trans-cyclopropane, while the distal functionality is usually a cis-cyclopropane or one of several oxygenated functional groups including hydroxyl-, methoxy- and alpha-methyl-keto- groups.

The relationship between the structure and the cholesteroid nature of MA was investigated by testing different stereo-controlled synthetic MA to antibodies in TB patient serum. The difference in binding to TB negative and TB positive patient sera was examined as well as the extent of binding that could be achieved with every synthetic MA with both types of sera. The hypothesis tested here was that a specific

synthetic MA structure can be found that represents the cholesteroid nature and that another synthetic MA structure manifests as the stronger antigen for antibody binding in TB positive patient sera.

The binding signals of TB positive and TB negative pooled sera towards the different synthetic MA subclasses were compared to that obtained towards natural free MA in ELISA. The importance of the stereochemistry of the merochains of mycolic acids for antigenic activity was studied by using different isomers of stereo-controlled chemically synthesized methoxy-, keto-, alpha- and hydroxy-MAs as antigens. Hexane was used as solvent to coat the plates with the MAs, similar to the approach of Pan *et al.* (1999) [119]. The four major subclasses of mycolic acids produced different results indicating the importance of the main functional groups on the merochain (Figure 2.5). Methoxy-MA bound strongest, followed in descending order by hydroxy-, keto- and alpha-MA. The exact stereochemistry of each subtype, i.e. the precise spatial arrangement of the functional groups, also appeared to be important.

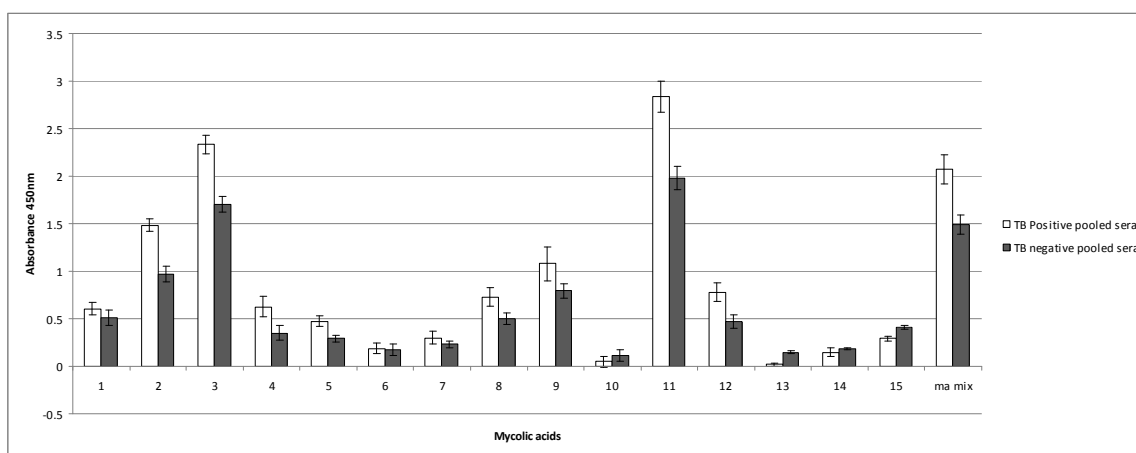


Figure 2.5 ELISA signals of antibody binding in TB positive and TB negative pooled patient sera to synthetic (1 – 14), natural alpha- (15) and the natural mixture mycolic acids (ma mix). Methoxy-MAs: 1-4, 11; Hydroxy-MAs: 5, 7-9; Keto-MAs: 6, 10, 12; Alpha-MAs: 13-15. The error bars indicate the standard deviation. The 2.5 d rule was applied to remove outliers. $n = \min 7, \max 16$.

The natural MA mixture as well as several of the synthetic MAs showed antibody binding with both TB positive and TB negative patient sera, while some MAs

appeared to have little or no antigenic activity. Strikingly, however, was the fact that the ratio of binding signal between TB positive and TB negative patient sera remained comparable among all the various types and isomers of MA. Although TB positive patient sera always gave better binding to the antigenic mycolic acids than TB negative patient sera, there generally was, in fact, no single antigenic mycolic acid that was significantly better able to differentiate between TB positive and TB negative patient sera than the natural mixture of mycolic acids could. This could in principle mean that if a MA is antigenic, then it assumes the cholesteroid functional structure that cross-reacts with anti-cholesterol antibodies. The question of whether a particular MA structure assumes a cholesteroid functional character then simply reduces to whether the particular MA is antigenic or not. The fact that TB positive patient sera statistically score higher than TB negative patient sera in recognition of MA in ELISA may then be explained simply by a higher concentration of the reactive antibodies in TB patient sera. Whether a single antibody would be able to recognize both cholesterol and MA, or whether cross-reactivity is due to the presence of a mixture of anti-cholesterol and anti-MA antibodies remains unanswered at this stage, although the observation that Amphotericin B can bind both cholesterol and MA (Figure 2.2) argues in favour of the former.

Each subtype's ELISA antibody binding signal (antigenicity) was subsequently compared to that obtained from the natural MA mixture and analyzed for its significance in defining the structure function relationship of MA.

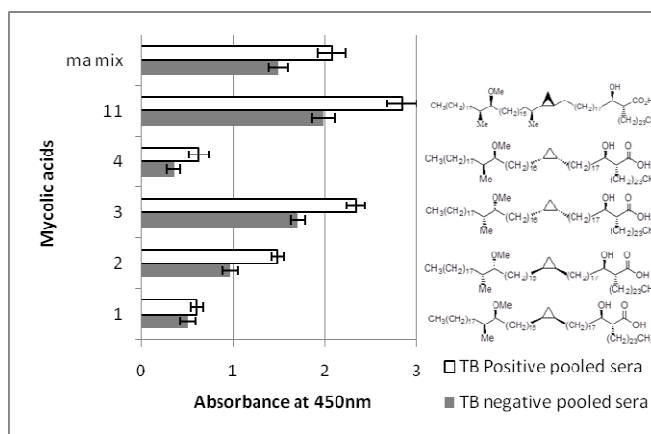


Figure 2.6 ELISA antibody binding signals of TB positive and TB negative patient sera to synthetic methoxy mycolic acids. The error bars indicate the standard deviation. The 2.5 σ rule was applied to remove outliers. $n = \min 14, \max 16$.

Chemically synthetic MA derivatives were made that were representative of four MA subclasses, namely methoxy-MA, hydroxy-MA, keto-MA and alpha-MA. The synthetic methoxy MA subclass had the highest binding to the antibodies from the four synthetic subclasses tested, followed by hydroxy-, keto- and alpha MA (Figure 2.6). The stereochemistry of the methoxy group is important for the recognition by antibodies in the sera. Even small changes in the stereochemical arrangement of the groups influenced the amount of binding observed. As seen from figure 2.6 the antibody binding signal of RR-cis-cyclopropane, RS-methoxy MA configuration (no 3) most closely resembles the response towards the natural mixture of MA. A change of the stereochemistry of either the cyclopropane (no 2) to SR-cis, or the methoxy-group (no 4) to SS reduced the binding signal by approximately half. If the weaker SR-cis configuration of the cyclopropane is combined with the weaker SS-methoxy configuration (no 1), the signal is once again halved, as may be expected. However, when the cyclopropane group assumed the methyl-trans configuration (no 11), an antigenicity signal was obtained that was even higher than that obtained for the natural MA mixture, despite its association with the weaker SS configuration around the methoxy-group ($P < 0.01$). This proves beyond a doubt that the stereochemical configuration of the two functional groups on the mero-chain of the most antigenic methoxy-MA influences the way in which they are recognised by patient antibodies.

If the assumption holds that antigenicity and the cholesteroid configuration are one and the same functional property, then a synthetic methoxy MA with a methyl-trans cyclopropane configuration would provide the strongest targeting ligand to steer towards cholesterol-rich TB infection foci, at least when the methoxy group is in the SS-configuration. It remains to be determined whether the RS-configuration of the methoxy group combined with the methyl-trans cyclopropane will provide an even more antigenic/cholesteroid MA.

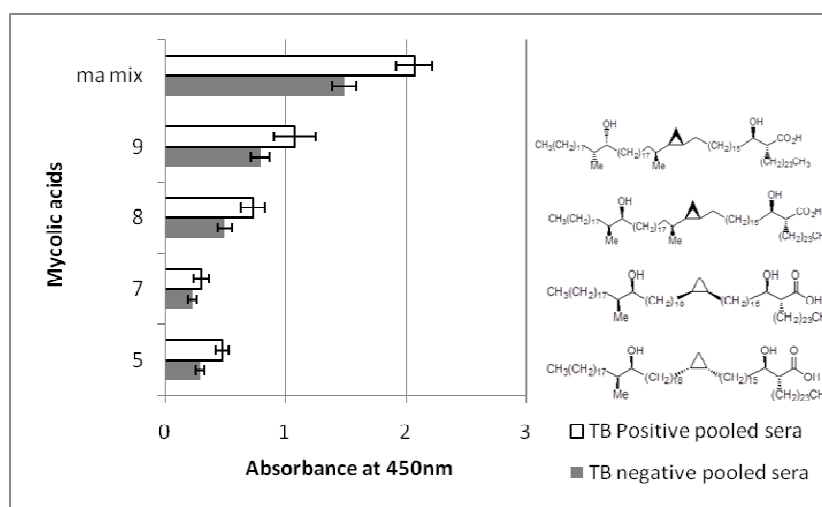


Figure 2.7 ELISA antibody binding signals of TB positive and TB negative patient sera to synthetic hydroxyl mycolic acids. The error bars indicate the standard deviation. The 2.5 σ rule was applied to remove outliers. $n = \min 15, \max 16$.

The synthetic hydroxy mycolates (Figure 2.7), which are the likely precursors of both methoxy- and keto-mycolates [106, 115, 163] all attracted weaker antibody binding compared to the natural MA mixture. The methyl-trans configuration of the proximal cyclopropane group appears to be a pre-requisite for antigenicity of the hydroxyl MAs (no.8 and 9, compared to the RS-, or SR-cis-cyclopropaned no 5 and 7). The hydroxyl group in the RR conformation (no 9) is preferred over the SS configuration (no 8) with statistical significance, $P < 0.01$.

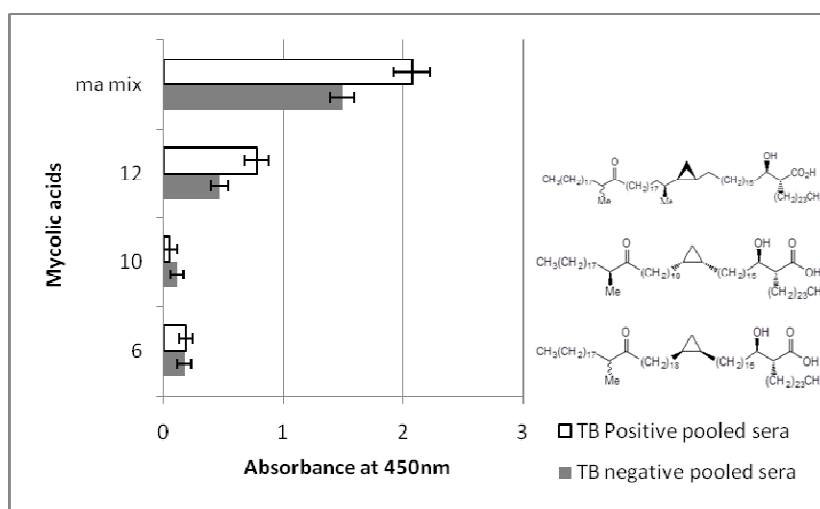


Figure 2.8 ELISA antibody binding of TB positive and TB negative patient sera to synthetic keto mycolic acids. The error bars indicate the standard deviation. The 2.5 d rule was applied to remove outliers. $n = \min 15, \max 16$.

Similar to the hydroxy-MAs, keto-MAs also require a proximal cyclopropane in the methyl-trans configuration (no 12, Figure 2. 8) to be antigenic, compared to the two (RS- and SR-) cis-cyclopropane configurations (no 10 and 6, Figure 2.8) that did not show any significant antigenic activity. In all the oxygenated MAs (i.e. methoxy-, hydroxyl- and keto-MA), the methyl-trans cyclopropane configuration provides for the best antigenic/cholesteroid functionality.

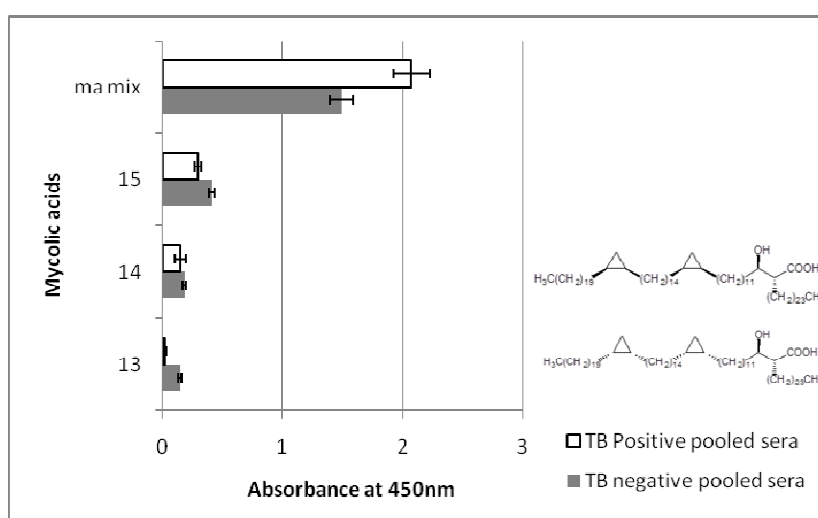


Figure 2.9 ELISA antibody binding signals of TB positive and TB negative sera to synthetic alpha mycolic acids. The error bars indicate the standard deviation. The 2.5 d rule was applied to remove outliers. $n = \min 8, \max 16$.

Two synthetic alpha MAs (no.13 and 14) were compared to natural alpha-MA (no.15) and the natural MA mix to determine their relative antigenicity. The antibody binding signal to either the natural, or the synthetic alpha MA failed to distinguish between TB positive and TB negative patient sera compared to the natural MA mix. The synthetic MA gave such low antibody binding signals, that nothing could be learned from the variations in the stereochemistries of the distal and proximal cyclopropanes on the antigenicity of alpha-MA. It could well be that the natural alpha MA gains its higher antigenicity from the presence of methyl-trans alpha MAs in the isolated mixture.

For the first time it is demonstrated here that synthetic, stereochemically and diastereomerically pure mycolic acids show differential biological activity in terms of recognition by TB positive patient serum. The results seem to favour methoxy mycolic acid of *M.tb* as the best cholesteroid functional entity or antigen to use in TB serodiagnostic devices, while a proximal methyl-trans cyclopropane enhances these functionalities.

2.7 Discussion

An antibody binding cross-reactivity between cholesterol and MA was first suggested by Schleicher *et al.*, (2002) [118] and subsequently shown to exist [121]. AmB is an antifungal macrolide that is able to bind cholesterol [162] through hydrogen bond formation between the amine or hydroxyl group of the mycosamine moiety of AmB and the hydroxyl group of the sterol [164, 165], as well as hydrophobic interactions [162]. It was shown also to bind to immobilized mycolic acids by means of a wave-guide evanescent field biosensor [121], thereby giving the first clue to a cholesteroid functionality of MAs. The same principle was applied and confirmed in the more popularly used surface plasmon resonance (SPR) variation of an evanescent field biosensor [117]. The antibody binding to mycolic acids with TB negative patient sera was most likely due to anti-cholesterol antibodies that are known to exist in all

humans [166, 167]. The cholesteroid nature of MA was previously shown to manifest also as an attraction between cholesterol and MA [168].

The structure-function relationship study of MAs was initiated by determining the role of the carboxylic acid. Methyl-esterification destroyed all functional activity, but esterification with fluorescein merely decreased the affinity towards AmB and antibody somewhat. The structure of fluorescein reveals that it has a free carboxylic acid that may remain available for hydrogen bonding to oxygenated functional groups in the mero-chain, probably to support a fold that determines antigenicity or a cholesteroid functional nature. Methyl-esterification of MA destroys a carboxylic acid that seems to be essential for hydrogen bonded stabilization of a functional oxygenated MA. Oxygenated (at least methoxy- and keto-) mycolic acids play a major role in the pathogenesis of the bacteria [108, 109]. Methoxy MA is the major free mycolic acid present in mycobacterial biofilms [141] that may be associated with the dormant stage of TB to create a cholesterol rich environment that may be utilized as a source of carbon nutrient. The attraction of cholesterol to MA that was previously demonstrated by our group [121] would fit well in such a hypothesis of nutrient provision to the dormant TB bacilli in an unvascularized tuberculous lesion. Cholesterol is able to cross bilayer membrane barriers by diffusion, independently of receptor mediated transport [169].

Mycolic acids might be attracted to cholesterol by means of their hydrophobic nature (Van der Waals forces) or through a more specific hydrogen bonding by the structural features of both molecules [121]. By Langmuir monolayer studies it was shown that a structural fold of the mycolic acids present itself in a “W” or a “Z” conformation giving a hydrophobic surface that could resemble a shape of cholesterol [97, 103]. The packing of mycolic acids in a Langmuir monolayer has previously been shown to differ among alpha-, keto- and methoxy-MA subclasses. Keto MA tended more towards a W-shaped configuration with exceptional rigidity in monolayers, whereas methoxy- and alpha-MA exhibited a more flexible conformation towards variation of experimental parameters [102, 103]. Thus, the packing of MA appears to be influenced by the orientation of the functional groups, and thus assumes different conformations for interaction with antibodies in sera.

For the first time it was demonstrated here that synthetic, stereochemically and diastereomerically pure mycolic acids show differential biological activity in terms of recognition by TB positive patient serum. The results seem to favour methoxymycolic acid of *Mycobacterium tuberculosis* as the best cholesteroid antigen for cholesterol attraction, based on its binding response with the TB negative patient sera. The results do not suggest with certainty what the stereochemical specifications are for the naturally produced mycobacterial mycolic acids found in the cell walls of *M.tb*. The best antigenicity seen in synthetic MA does not necessarily indicate the most likely structure of the mycolic acid antigen(s) in nature. In particular, it seems unlikely that a particular MA molecule can constitute an antibody binding site filling antigen or hapten. Rather, the surface created by packed mycolic acids is likely to be the structure that is recognized by antibodies, similar to the case of monoclonal antibody recognition of cholesterol [170]. Different from cholesterol, which is homogeneous of structure, MA exists as a mixture in *Mycobacterium tuberculosis*. It may well be that mycolic acid folding and packing is influenced by the presence of different types of MA subclasses and variants thereof together, such that the natural mycolic acid antigen(s) may never be recreated synthetically by the use of a single species of pure synthetic mycolic acid. Exact specifications for an optimal mycolic acid mixture to assume cholesteroid nature and be attracted to cholesterol may in future be determined by mixing various ratios of different MA subclasses as coating antigen in ELISA, or as cholesterol capturing entity in evanescent field biosensing. In summary then, the hypothesis that one particular mycolic acid class represents cholesteroid nature, while another is more antigenic in TB positive patient sera is hereby rejected. Antigenicity and cholesteroid nature appears to correlate with one another in mycolic acid structure.

Chapter 3: Synthesis and characterization of mycolic acid containing nanoparticles

3.1 Introduction

As described in chapter 1 and 2, MA is a constituent of *M.tb* which forms the major part of the cell wall of the bacteria. MA consists of an extended family of long chain 2-alkyl 3-hydroxyl fatty acids, typically 70-90 carbon atoms in length. The reason why MA was considered as targeting agent is twofold: Firstly as an antigen that forms immune-complexes with anti-MA antibodies, which universally occur in all TB patients [120] and may facilitate opsonisation of the nanoparticles for macrophage uptake mainly at the site of antigen production; and secondly, because of the cholesteroid nature of the MA molecules [121]. By its property of attraction of cholesterol, it may in effect be attracted to the cholesterol rich site of *M.tb* infection. Due to the extremely hydrophobic nature of mycolic acids, a suitable vehicle was needed to introduce them into the body and guide them to their presumed targets of infection. The synthetic PLGA polymer was ideally suited to encapsulate both the MA and the drug into nanoparticles, as they can harbour both hydrophilic as well as hydrophobic molecules.

Nanoparticles are generally prepared with natural or synthetic polymers using various techniques including emulsification, nanoprecipitation and salting out procedures to yield particles ranging in size between 10-1000 nm [29, 35, 36]. These particles were first developed by Birrenbach and Speiser in the 1970's [171]. Nanoparticles, spheres or capsules can be made, depending on the method used and the specific characteristics needed from the particle. Improved efficacy, fewer dosages to be administered due to sustained release properties, reduced toxicity and delivery of therapeutic agents to the site of infection are some of the benefits of nano-encapsulated drugs as discussed in more detail in chapter 1. An additional advantage

of nanocarriers for treatment of intracellular infections such as *M. tb* is their intracellular uptake and accumulation in macrophages, which is also the target of infection of *M.tb* [45, 172].

Nanoparticles have the advantage over other drug carriers such as liposomes or micelles [173] by their increased stability and slow release of drugs. This makes them better to control compared to liposomes, which are generally leaky and with limited shelf life [34]. The sub-micron size of nanoparticles effects a higher cellular uptake and ability to penetrate deep into tissue, therefore being able to target a wider variety of biological components within cells of choice than larger microparticles could [51]. By functionalizing the surface of the particles with a targeting ligand, higher bioavailability is generated at the site of infection and therefore the dose and side effects of the drug may be minimized [51].

For this study it was decided that PLGA nanoparticles will be used as the nanocarrier for the MA and INH drug for reasons explained in Chapter 1. The PLGA nanoparticle carrier was designed to encapsulate MA together with an anti-TB drug, INH, in an attempt to increase the drug's efficacy. The developed formulation was tested on *M.tb* infected macrophages, after the MA containing nanoparticle drug was assembled and tested *in vitro* for uptake by macrophages and cytotoxicity.

A double emulsion solvent evaporation technique was used for formation of the particles. They were characterized for Zeta potential, a measure of surface charge, dynamic light scattering, i.e. size analysis and size distribution, and surface morphology. The latter was investigated by means of scanning electron microscopy (SEM). The drug and lipid encapsulation efficiency was measured spectrophotometrically. For effective therapy and usefulness of the polymer drug construct the intracellular uptake and trafficking *in vitro* of the particles were investigated. The THP-1 and U937 monocyte-macrophage-like cell lines were used. Cellular uptake of fluorescently labelled nanoparticles was assessed with confocal laser scanning microscopy. The cytotoxicity of the nanoparticles was investigated by the WST and MTT technologies, i.e. cell proliferation assays.

Alexa fluor 633:

Goat anti-mouse IgG (H+L) Invitrogen, Oregon USA

Alexa Fluor 633:

Rabbit anti-mouse IgG (H+L) Invitrogen, Oregon USA

BACTEC 460 culture media Becton Dickinson International, Belgium

Basic fuchsin Fluka, Sigma-Aldrich, Steinheim, Germany

5-Bromomethyl fluorescein Molecular Probes, Leiden, The Netherlands

Calcium chloride Merck, Darmstadt, Germany

Chloroform Merck, Darmstadt, Germany

Cytochalasin D Sigma Chemical Co., St Louis, USA

Dakocytomation fluorescent

mounting medium oil Dako Cytomation, Carpinteria, CA, USA

Dextran Alexa Fluor 647,

10 000 MW, anionic, fixable Invitrogen, Oregon, USA

Dichloromethane Merck, Darmstadt, Germany

Dimethyl sulfoxide Sigma Chemical Co., St Louis, USA

3(4,5-dimethylthiazol-2)-2,5-diphenyl

tetrazolium bromide (MTT) ICN Biomedicals, Ohio, USA

DMEM culture media Highveld biologicals, RSA

Dynasore Sigma Chemical Co., St Louis, USA

Ethanol BDH, Gauteng, RSA (Analytical grade)

5-N-ethyl-N-isopropylamiloride

(EIPA)	Sigma Chemical Co., St Louis, USA
Foetal calf serum	Highveld biologicals, RSA
Ferrous oxide nanoparticles	Gift from prof. Walter Focke, University of Pretoria, SA
Hexane	Merck, Darmstadt, Germany
Isoniazid, 99% purity	Sigma Aldrich, Steinheim, Germany
Magnesium chloride	Merck, Darmstadt, Germany
Methyl- β -cyclodextran	Sigma Chemical Co., St Louis, USA
Monoclonal anti- α -Tubulin antibody produced in mouse	Sigma Chemical Co., St Louis, USA
Mycolic acids	Sigma Chemical Co., St Louis, USA
Nocodazole	Sigma Chemical Co., St Louis, USA
Paraformaldehyde	Merck, Darmstadt, Germany
Penicillin/Streptomycin	Highveld biologicals, RSA
Phalloidin-Tetramethyl rhodamine B	
Isothiocyanate	Sigma Chemical Co., St Louis, USA
Phenol	BDH, Gauteng, RSA
Phorbol 12-myristate 13-acetate	Sigma Chemical Co., St Louis, USA
Poly, DL, lactic-co-glycolic acid, 50:50 (Mw: 45000-75000)	Sigma Chemical Co., St Louis, USA
Polyvinyl alcohol (PVA) MW: 13000-23000,	

partially hydrolysed (87-89)	Sigma Chemical Co., St Louis, USA
Sodium chloride	Saarchem, Gauteng, RSA
di-Sodium hydrogen phosphate	Merck, Darmstadt, Germany
Potassium chloride	Merck, Darmstadt, Germany
Potassium dihydrogen phosphate	Merck, Darmstadt, Germany
RPMI-1640 culture media (with L-glutamine)	Gibco, Invitrogen, Paisley, UK
Silica Oxide (amorphous)	Gift from prof. Walter Focke, University of Pretoria, SA
Sodium dodecyl sulphate	Sigma Chemical Co., St Louis, USA
Transferrin Alexa Fluor 633	Invitrogen, Oregon, USA
Triton X-100	Sigma Chemical Co., St Louis, USA
Trypan blue	Sigma Chemical Co., St Louis, USA
Trypsin/ Versene	Highveld biologicals, RSA
Wortmannin	Sigma Chemical Co., St Louis, USA
Zinc oxide nanopowder	Sigma Chemical Co., St Louis, USA

3.4.2 Buffers

PBS buffer (PBS): 8.0 g NaCl, 0.2 g KCl, 0.2 g KH₂PO₄ and 1.05 g Na₂HPO₄ per 1 L double distilled, deionized water, adjusted to pH 7.4

Buffer A: PBS containing 1mM CaCl₂ and 1mM MgCl₂

3.4.3 Instrumentation

Size and zeta potential measurements: Zetasizer nano-zs, Malvern instruments, Worcestershire, UK.

Confocal microscopy: Leica TCS SP5 confocal microscope, Mannheim, Germany.

Morphology of particles was investigated on a LEO 1525 Field Emission SEM.

For particles synthesis and characterization: Silverson L4R homogenizer, UK,

Virtis Benchtop freeze dryer, USA.

Absorbancies were measured with a SLT 340 ATC photometer.

FACS analysis: Becton Dickinson FACS ARIA Cell Sorter, USA.

In vitro mycobacterial growth experiments: BACTEC 460 radiometric apparatus, Becton Dickinson, Johnston Laboratories, USA.

3.5 Methods

3.5.1 Preparation of INH containing nanoparticles with labelled MA

To prepare nanoparticles, the double emulsion solvent evaporation freeze drying technique was used as previously described in literature with modifications [174]. Poly DL, lactic-co-glycolic acid (PLGA) 50:50 (MW: 45000-75000) was dissolved in 6 ml of dichloromethane (DCM) at a concentration of 1.25% weight/volume (w/v). Partially labelled MA (1:1 w/w, with 5-Bromomethylfluorescein (5BMF) labelled MA total of 2 mg, 1.7 μmol) was dissolved in 2 ml dichloromethane and added whilst stirring. For the first water in oil (w/o) emulsion, aqueous phosphate buffer saline (PBS, pH 7.4, 2 ml) was added to the mixture and homogenization was done at 5000 rpm for 3 min. For nanoparticles containing INH, the INH (100 mg, 729 μmol) was

dissolved in the PBS and then added to the mixture. The emulsion formed was subsequently transferred to an aqueous solution of 1% w/v of the polyvinyl alcohol (PVA, MW: 13000-23000 and partially hydrolysed (87-89%)) as a stabilizer. The second water in oil in water (w/o/w) emulsion was formed by homogenization at 8000 rpm for 3 min. The second emulsion formed was stirred at 500 rpm overnight at atmospheric pressure to evaporate the organic solvent. The PLGA nanoparticles were recovered by centrifugation at 19000 rpm for 15 min. The resulting particles were dried by lyophilization in a Vitrus Benchtop freeze dryer.

3.5.2 Nanoparticle characterization

The nanoparticles collected after lyophilization was subjected to size distribution, polydispersity and surface potential measurements by means of a zetasizer. The samples were diluted with PBS and manually shaken to disperse the particles into solution before measurement at a temperature of 25 °C. The surface morphology of the particles was investigated by scanning electron microscopy done by the Nano Centre department at the CSIR. The gold sputtering technique was used to prepare the samples for visualization by fixing the NPs to aluminum sample stubs with double-sided carbon tape and sputter coating with gold for viewing by scanning electron microscopy. Drug and lipid loading was analyzed as described in the subsequent sections.

3.5.2.1 Quantification of INH in nanoparticles

Quantification of the INH encapsulated in the nanoparticles was performed via an indirect method. The supernatant left after particle centrifugation was tested for the amount of free INH present in the supernatant measured with absorbance at 260 nm. The amount of drug was calculated by the formula:

Equation 1:

$$\text{Encapsulation efficiency (EE)} = \frac{\text{Amount of drug initially used} - \text{amount of drug in the supernatant}}{\text{Amount of drug initially used}} \times 100$$

3.5.2.2 Quantification of MA in nanoparticles

For the MA-containing nanoparticles, carbol fuchsin dye (basic fuchsin 0.3 g, ethanol (95%) 10.0 ml, phenol 5.0 ml, ddd H₂O 95 ml) was used to quantify the amount of MA present in the nanoparticles. The MA containing nanoparticles (20 mg) were dissolved in chloroform (10 ml) and stirred overnight. Hexane was added to precipitate the PLGA, and stirred vigorously for an hour. The precipitate was recovered by filtration through a 0.45 µm organic solvent resistant filter (Pall Acrodisk, PSF, GXF/GHP) and washed with hexane 2 to 3 times. The mother liquor was evaporated with N₂ (g). The MA left in the vial was re-dissolved in hexane followed by the addition of an equal amount of carbol fuchsin dye. To prepare the standards, MA was dissolved in hexane and added to the Carbol fuchsin (1:1 v/v). The Carbol fuchsin forms a lower pink aqueous layer and MA in hexane forms the upper transparent layer. After thorough mixing the upper layer turned pink due to the complex formation between MA and Carbol fuchsin. The absorbance of the hexane layer was measured at 492 nm in an absorbance plate reader and a standard curve was compiled.

3.5.3 In vitro cell viability assay

Caco-2 cells (human colorectal carcinoma) and U937 (histiocytic lymphoma) cells were purchased from Highveld Biologicals, RSA. The cells were grown and maintained at a confluency of $0.5 - 5 \times 10^6$ cells/ml, in DMEM media for Caco-2 and RPMI-1640 for U937 cells, both supplemented with penicillin (50 μ g/ml), streptomycin (50 μ g/ml) and 10% heat inactivated foetal calf serum (FCS). The cells were incubated at 37 °C in a 5% CO₂ (g) humidified incubator and passaged 2-3 times a week. Cell viability was determined by making use of the trypan blue exclusion test.

Cells were seeded in 96 well plates at a density of $0.5 - 1 \times 10^6$ cells/ml at 100 μ l per well and incubated for 24 hours before treatment. U937 cells were differentiated as described in 3.5.4.2. Cells were incubated with different concentrations of empty PLGA nanoparticles, MA nanoparticles or Fluorescein-MA containing nanoparticles of an average size of ~ 500 nm. Ferrous oxide (Fe₂O₃) [175, 176] and amorphous silica oxide (SiO₂) were used as negative controls [177] and zinc oxide (ZnO) nanopowder with known toxicity [178] was used as positive control in the studies in order to determine cell viability after exposure. The WST assay (Quick Cell Proliferation Assay Kit II, Biovision, USA) was performed as per manufacturer's procedures for the Caco-2 cells. The assay is based on the reduction of the tetrazolium salt, WST to water-soluble orange formazan by cellular mitochondrial dehydrogenase present in viable cells. The amount of formazan dye formed is determined colourimetrically at 450 nm with a reference wavelength at 630 nm. It is directly proportional to the number of living cells. The MTT assay was performed for the U937 cells by adding the MTT dissolved in PBS pH 7.4 (100 μ g/well) to the cells and incubated for 5 hours at 37 °C. The untransformed MTT was removed by careful aspiration and the formazan crystals formed, were dissolved in 100 μ l dimethyl sulfoxide. The absorbance was read at 550 nm. Percentage viability was calculated by the absorbance intensity of the cells incubated with the particles as a function of that of the untreated cells.

3.5.4 Uptake of nanoparticles by macrophages

In order to elucidate the feasibility of these nanoparticles for intracellular delivery of drugs, nanoparticle uptake into macrophage cells *in vitro* was analysed by fluorescence activated cell sorting (FACS).

3.5.4.1 Cell culture maintenance

To determine particle uptake flow cytometry experiments were conducted as follows. For cell growth the THP-1 monocytes were grown in RPMI-1640 medium with L-glutamine, supplemented with penicillin (50 µg/ml), streptomycin (50 µg/ml) and 10% heat inactivated FCS and maintained as described in 3.5.3.

3.5.4.2 Differentiating cells

To differentiate the THP-1 cells into adherent macrophages, 50 nM Phorbol 12-myristate 13-acetate (PMA) was added to the wells containing 1×10^6 cells/ml with total volume of 2 ml per well and incubated for 48 hours [172, 179]. Thereafter the medium was replaced with complete RPMI-1640 media for another 24 hours. The formation of adherent macrophages was confirmed via microscopy.

3.5.4.3 Flow cytometry

Differentiated THP-1 cells were washed twice with PBS at room temperature (RT). Thereafter the cells were incubated for 2 hours at 37 °C in incomplete RPMI containing different concentrations of Fluorescein-MA or Rhodamine containing nanoparticles, which were similar in size. The plates containing the cells were subsequently placed on ice and the cells were washed twice with ice cold PBS. Ice cold acid wash (NaCl 1.15 g and Acetic acid 1.14 ml /100 ml) was included and the plates were incubated for 1min. on ice. The cells were then washed twice with PBS at

RT and trypsinized at RT with 600 μ l trypsin/versene (0.25 % Trypsin + 0.05 % EDTA). To inhibit the trypsin reaction, 600 μ l ice cold PBS was added. The cells were washed twice with ice cold PBS, centrifuged at 900 rcf for 3 min. and resuspended in trypan blue stain to minimize background fluorescence [180, 181]. The cells were washed once more and resuspended in ice cold PBS. The fluorescence of 10 000 viable cells was acquired via the fluorometer.

Chemical uptake inhibitors were used to investigate the mechanism of uptake. The differentiated cells were incubated in incomplete RPMI for 15 min. at 37 °C containing either 150 nM wortmannin, 5 mM methyl- β -cyclodextran, 75 μ M dynasore, 10 μ M nocodazole, 10 μ M 5-N-ethyl-N-isopropylamiloride (EIPA), 50 μ M cytochalasin D. Fluorescein-MA or Rhodamine containing nanoparticles were subsequently added and incubated for a total of 2 hours in the continued presence of the inhibitors. The cells were then prepared for FACS analysis as describe above. The specific inhibitors used were wortmannin – affects macropinocytosis and phagocytosis by inhibiting PI(3)kinase, methyl- β -cyclodextran – extracts cholesterol and affects lipid rafts, dynasore is a dynamin GTPase inhibitor, nocodazole depolymerises the microtubule network, 5-N-ethyl-N-isopropylamiloride (EIPA) is used to inhibit macropinocytosis and cytochalasin D depolymerises the actin network [140, 182, 183].

3.5.5 Nanoparticle uptake and localization by confocal microscopy

To determine where the NP's localize within the cells, live and fixed cell imaging was conducted.

3.5.5.1 Cell culture maintenance

For cell growth of the suspension cultures, the THP-1 monocytes and the human monocyte-macrophage like cell line U937 were grown and maintained in RPMI-1640

medium with L-glutamine, supplemented with penicillin (50 µg/ml), streptomycin (50 µg/ml) and 10% heat inactivated foetal calf serum (FCS) and maintained as described in 3.5.3.

3.5.5.2 Differentiating cells

To differentiate the cells into adherent macrophages, THP-1 (1×10^6 cells/ml) was exposed to 50 nM PMA whereas the U937 (1×10^6 cells/ml) cell line was exposed to 8 nM PMA for 48 hours [179, 184]. Thereafter the medium was replaced with complete RPMI-1640 medium for another 24 hours and the formation of adherent macrophages was confirmed via microscopy. The differentiated cells were treated for live cell imaging or fixed for immunostaining.

3.5.5.3 Nanoparticle uptake in U937 and THP-1 macrophages

In order to determine the uptake of the particles in the macrophage cells, the cells were incubated for an hour with Fluorescein-MA containing PLGA nanoparticles (0.1 mg/ml). The cells were then washed three times with buffer A (PBS containing 1mM CaCl₂ and 1mM MgCl₂) and visualized in 1 ml of clear incomplete RPMI on the Leica confocal microscope equipped with a temperature stage set at 37 °C.

3.5.5.4 Nanoparticle, transferrin and dextran uptake in U937 and THP-1 macrophage cells

In order to determine the accumulation point of molecules within intracellular compartments a pulse/chase study was conducted. A pulse/chase analysis allows for the determination of the endocytic route of the particles by successively exposing the cells to the labeled particles and/or endosomal marker (pulse) thereafter removing the

excess particles followed by an incubation step (chase) [185]. The study was performed with the nanoparticles together with transferrin, which is a marker of early endosomes and the late endosome marker, dextran. For the THP-1 and U937 macrophages, the media was removed and replaced with incomplete RPMI for 10 min. at 37 °C. The nanoparticle solutions (0.1 mg/ml) suspended in incomplete RPMI were then added to the cells (pulse step), and incubated for 4 hours [186]. Thereafter the cells were washed 3 times with buffer A at 37 °C. Buffer A was replaced with complete RPMI and the cells were incubated for a further 3.5 hours and another 0.5 hours in incomplete RPMI (chase step). To the cells, 100 nM transferrin 633 (final concentration of 0.008 mg/ml) was added and incubated as indicated in table 3.3. The cells were washed 3 times with buffer A at 37°C. Incomplete, clear RPMI (1 ml) was added at 37 °C. The cells were visualized via confocal microscopy equipped with a temperature stage set at 37 °C. Alternatively, instead of transferrin 633, the pulse/chase study was performed with dextran alexa fluor 647 (0.125 mg/ml).

3.5.5.5 Nanoparticle treatment and fixation of macrophage cells

Nanoparticle (0.2 mg/ml in incomplete RPMI) treatment of the cells consisted of a 3 hour incubation followed by washing the cells 3 times in buffer A at room temperature (RT). The fixation medium, 3% PFA (paraformaldehyde) in PBS was added to cover the cells and left for 20 min. The wells were then washed 3 times with buffer A and dipped once in distilled H₂O. The excess water was drained and the coverslip mounted on a glass slide face down together with a drop of Dakocytomation fluorescent mounting medium oil. Subsequently the coverslip was sealed with clear nail polish. Confocal microscopy was then conducted as needed.

3.5.5.6 Immunofluorescence staining of U937 and THP-1 fixed macrophages

To determine the uptake of the nanoparticles by the cells, the cells were treated with Fluorescein-MA PLGA nanoparticles (0.1 mg/ml in incomplete RPMI) for 4 hours at 37 °C. Thereafter the cells were fixed and stained for α -tubulin with serial antibody treatment. Alternatively cells were incubated for 15 min. with the actin depolymerising agent, Cytochalasin D (5 μ M) or the microtubule polymerization disrupting agent, Nocodazole (10 μ M) at 37 °C in incomplete RPMI. The media was removed and the cells were either washed 3 times with PBS and treated with nanoparticles, or the cells were not washed, but treated with nanoparticles. Another set was treated with Cytochalasin D (5 μ M) or Nocodazole (10 μ M) at 37 °C for a total of 4 hours. Cytochalasin D treated and untreated cells were then stained for actin as described in 3.5.5.6.2. Nocodazole treated and untreated cells were then stained for α -tubulin as described in 3.5.5.6.1.

3.5.5.6.1 Immunostaining for α -tubulin

The medium was removed and the cells washed once with ice cold PBS. Methanol (100%) at -20 °C was quickly added (to maintain microtubule integrity) and incubated for 5 min. The rest of the method was done at RT. The cells were washed 3 times in PBS and then a blocking solution (10% FCS in PBS) was added for 30 min. The primary α -tubulin mouse antibody (25 μ l of 1:500 dilution in blocking buffer) was added to the cells and incubated for 30 min. at RT. The cells were washed 3 times in 0.2% Triton/PBS and once in PBS only at RT. The secondary anti-mouse antibody (25 μ l of 1:400 dilution in blocking buffer) was added and incubated for 45 min. at RT in a humidified atmosphere in the dark. The cells were then washed 3 times in 0.2% Triton/PBS and once in PBS at RT. The cells were washed twice in buffer A at RT and prepared for confocal imaging.

3.5.5.6.2. Rhodamine staining for actin

The cells were fixed with 3% PFA as described in 3.5.5.5 and incubated with Phalloidin-Tetramethyl rhodamine B isothiocyanate (2 µg/ml) for 10 min. at RT. The cells were then washed 4 times with buffer A at RT and prepared for confocal viewing.

3.5.6 In vitro drug testing in *Mycobacterium tuberculosis* H37Rv infected THP-1 macrophages

In order to determine what the antimicrobial effect will be on intracellular bacteria, the *M.tb* H37Rv strain was used for drug susceptibility testing in THP-1 macrophages by making use of the radiometric CO₂ (g) - release BACTEC 460 apparatus.

3.5.6.1 Cell culture maintenance

For cell growth THP-1 monocytes (kind gift from Dr. B. Baker from University of Stellenbosch, SA) were grown and maintained as described in 3.5.4.1 but without the addition of antibiotics through out the entire duration of the experiments.

3.5.6.2 Differentiating cells

All the experiments were conducted in the differentiated macrophage state of the cells unless otherwise stated. To differentiate the cells into adherent macrophages, THP-1 (1 x 10⁶ cells/ml) were treated with 100 nM PMA in RPMI/FCS [179, 184]. To ensure monolayer formation the plate was tilted for 1 minute per side and repeated several times. The cells were incubated at 37 °C in a 5% CO₂ (g) atmosphere for 24 hours. Thereafter the cells were washed twice with RPMI/FCS media and left for another 24 hours. The formation of adherent macrophages was confirmed with microscopy.

3.5.6.3 Macrophage infection with *M.tb* H37Rv

A frozen aliquot of *M.tb* H37Rv was thawed (2.3×10^8 CFU/ml) and passaged 30 times up and down with a 1 ml insulin syringe. The amount required (5:1 multiplicities of infection (MOI), thus 5×10^6 mycobacteria per well) was centrifuged (520 μ l per 24 well plate) at 13 000 rpm for 20 min. The supernatant was removed and 1.2 ml medium (RPMI/ FCS) was added. The bacteria were resuspended in the media by passaging 30 times up and down with 1 ml insulin syringe. To each well of 1×10^6 cells, 50 μ l of *M.tb* H37Rv was added for infection. The plate was incubated for 4 hours and then washed to remove non-internalized *M.tb* H37Rv, before incubation overnight.

3.5.6.4 Nanoparticle drug treatment

Nanoparticles containing INH and partially labelled MA were prepared in RPMI/FCS medium at a final concentration of 0.2 μ g/ml and 2 μ g/ml of free INH. After the medium was removed from the wells, 1 ml of the prepared nanoparticle suspensions was added to the cells, and incubated for 5 hrs, 1 day or 2 days with additional 2 day incubation after removing the particles not taken up by the cells [172].

3.5.6.5 Harvesting TB bacilli from macrophages

After the nanoparticle treatment the cells were washed 3 times with RPMI/FCS to remove non-phagocytosed TB bacteria and un-ingested particles. Cells were harvested by removing 1 ml of medium and adding 100 μ l 0.25% SDS to each tube, at a final concentration of 0.025%. To the wells 1 ml of 0.025% SDS was added to lyse the adherent macrophages or alternatively 0.1% Triton X-100 was used for this purpose.

The cells were physically removed by gentle pipetting. The suspension of cells was removed and added to tubes. Centrifugation at 13 000 rpm for 20 min. was done to pellet the bacteria. The pellet was passaged 10 times up and down with a 1 ml insulin syringe in 100 µl Bactec 460 media and added to the Bactec vials.

For the controls, drug free vials consisted of bacterial inocula only. Negative control vials contained media without any bacteria or drugs to monitor if any contamination occurred. All the vials were read and flushed with 5% CO₂ (g) daily until the growth index (GI) of the bacterial control reached 999.

3.6 Results

3.6.1 Characterization of MA / INH encapsulated particles

The freeze dried particles, recovered after the encapsulation of INH and MA in the double emulsion evaporation technique [174], were used in all experiments without further purification. The particles were subsequently subjected to size and zeta potential analysis with a Zetasizer. Knowing the zeta potential, the stability of the nanoparticles in terms of aggregation in different media may be predicted. Charged nanoparticles have a lesser tendency to aggregate than neutral nanoparticles. Table 3.1 describes the physical characteristics obtained for the nanoparticles.

Table 3.1. Mean diameter and zeta potential of nanoparticles prepared by the solvent evaporation freeze drying method

Sample	Average particle size (nm)	Polydispersity index (PDI)	Zeta potential (mV) in PBS pH 7.4
PLGA NP	412 (\pm 82)	0.43	-9.2 (\pm 0.7)
Fluorescein-MA PLGA	508 (\pm 101)	0.48	- 5.32 (\pm 1.8)
50% Fluorescein-MA/MA/ INH/ PLGA	555 (\pm 86)	0.51	- 6.68 (\pm 0.2)
INH/PLGA	419 (\pm 92)	0.47	- 8.39 (\pm 1.6)

nm = nanometer, mV = milli-volts

The technique reproducibly yielded drug-free nanoparticles of 412 (\pm 82) nm diameter as well as nanoparticles loaded with MA and INH of 555 (\pm 86.4) nm, as analyzed by dynamic light scattering. The nanoparticle suspension stability was examined by

measuring the zeta potential. Theoretically, the more positive or negative the values are, the less the possibility for aggregation. PLGA has a negative zeta potential due to the presence of uncapped end carboxyl groups. The values indicated that the MA lipid molecules reduced the negative values to some extent. The change in zeta potential could be an indication that some of the MA molecules may be located on the external surface of the PLGA nanoparticles.

Spectrophotometric determination of the concentration of INH was determined indirectly, by measuring the amount of INH (measured at 260 nm) present in the supernatant after collection and washing of the nanoparticles. The amount of drug encapsulated in the nanoparticles is given in table 3.2.

Table 3.2. Concentration of the INH in the sample

Sample	Starting mass of INH (mg)	Encapsulation efficiency (EE)	Yield (mg)	Loading (%)	Amount of drug in sample (mg)
INH/PLGA	96	0.1201	79.4	14.52091	11.5296
50% Fluorescein-MA /MA /INH PLGA	107	0.1135	86.7	14.0075	12.1445

Thus the amount of drug in the sample is approximately 14% of particle mass. The encapsulation efficiency (EE) was determined by using equation 1 from section 3.5.2.1. The encapsulation efficiency indicates the final amount of drug incorporated into the system compared to the original amount of drug used, whereas the percentage drug loading in the sample is the amount of drug in the whole formulation of the nanoparticle samples.

The surface morphology of the formed nanoparticles was characterized via SEM. The SEM was used to study the external morphology of the PLGA nanoparticles. Figure 3.1 shows a micrograph of nanoparticles containing fluorescein-MA NPs magnified 50 000 times. The image shows coalescent, spherical particles with a smooth surface containing no observable pores and a large size distribution as also indicated by the PDI in table 3.1. A variation in size would possibly lead to the individual particles having different release profiles of the drug which is a function of polymer degradation where the smaller particles could degrade faster. The results showed that the external morphology of the particles had a smooth spherical surface which will facilitate more uniform particle degradation. Thus by making use of the double emulsion evaporation freeze drying technique, successful formation of MA containing PLGA nanoparticles was achieved together with the anti-TB drug INH.

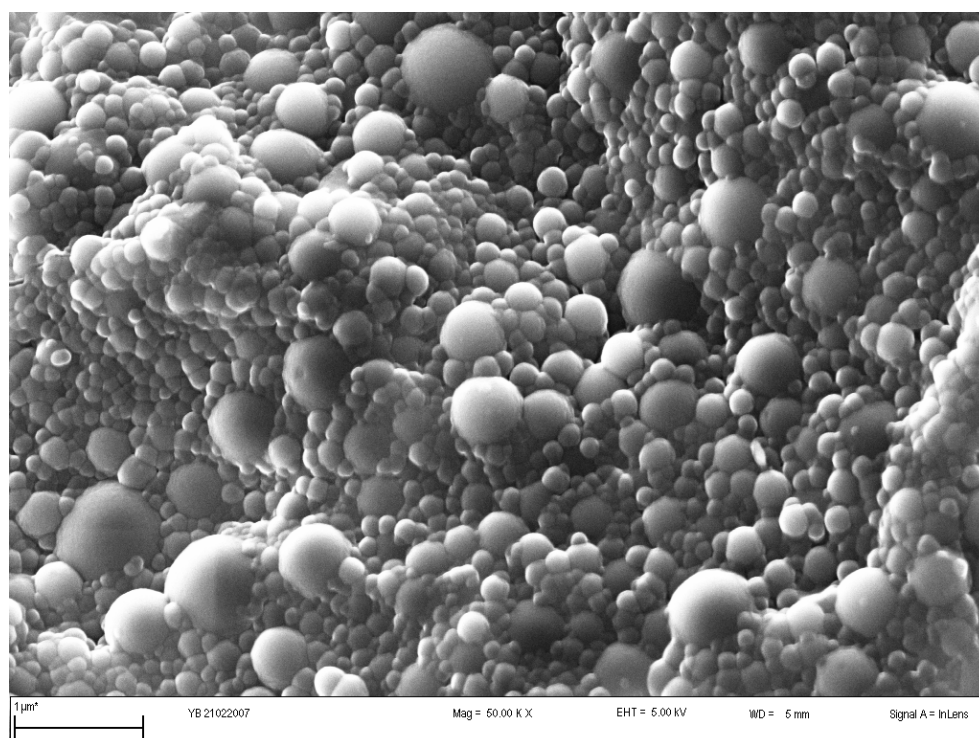


Figure 3.1 Representative SEM image of the surface of PLGA nanoparticles with Fluorescein labelled MA.

3.6.2 Quantification of MA containing nanoparticles

MA are long chain 2-alkyl 3-hydroxyl fatty acids comprising typically of 70-90 carbon atoms making it a very hydrophobic molecule with limited solubility in commonly used solvents. Different methods could be employed to determine the encapsulation efficiency into nanoparticles. However, the hydrophobicity of MA limits the techniques that can be used. In literature, HPLC analysis is used for the detection of mycobacterium species through their different mycolic acid profiles [187-190], applying primarily a photodiode array detector. Because mycolic acids do not contain suitable chromophores for UV detection, derivatization is needed for spectrophotometric detection. Another method of quantification is by colorimetric methods. According to a patent by Khanuja S *et al.* published in 2003 [191], mycolic acids could be quantified by making use of a carbol fuchsin dye indicated in Figure 3.2. This dye interacts with the MA in a concentration dependent way, producing a coloured complex that could be measured at 492 nm.

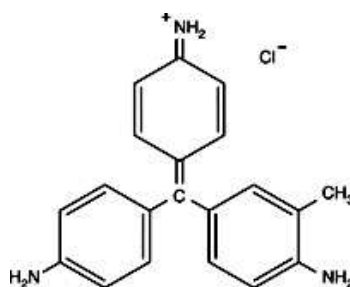


Figure 3.2 Basic fuchsin that will associate with mycolic acids of *M.tb* [191].

From the standard curve prepared, the amount of MA in the sample could be determined. Thus, by making use of the equation obtained for the standard curve (Figure 3.3) for the Fluorescein-MA PLGA particles: 0.5 mg Fluorescein -MA in 73 mg NP sample with an encapsulation efficiency of 26% was observed. PLGA was also tested alone as a control.

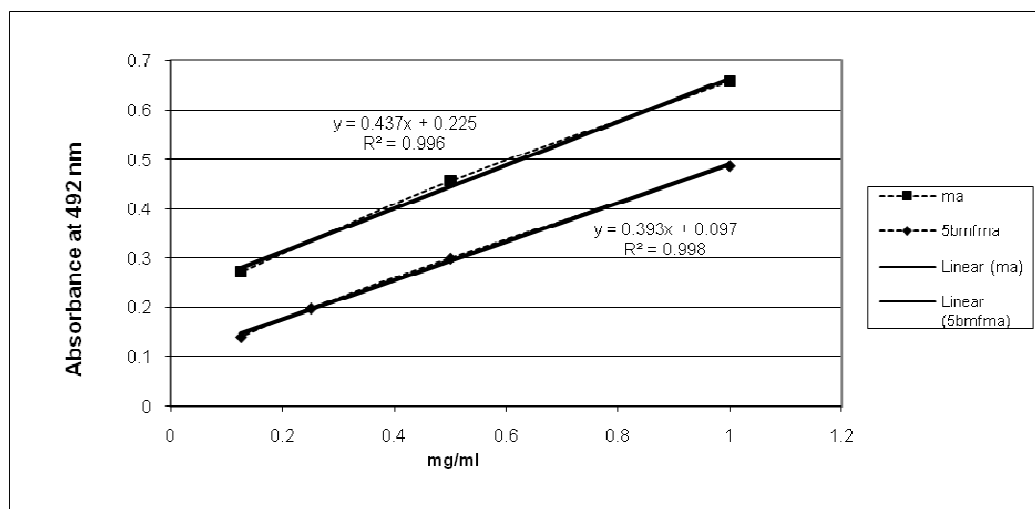


Figure 3.3 Standard curve obtained for MA and Fluorescein-MA by making use of the Carbol fuchsin dye.

3.6.3 In vitro cell viability assay

In order to elucidate the effect of the nanoparticles on the viability of cells, non-radiometric assays were used to determine *in vitro* the cell viability after treatment with the specific MA containing nanoparticles. By making use of the WST assay, the *in vitro* cytotoxicity of MA containing nanoparticles were compared to PLGA nanoparticles, amorphous SiO₂, Fe₂O₃ particles and ZnO nanopowder at concentrations of 0.1, 0.01 and 0.001 mg/ml. The adherent Caco-2 cells were exposed for 3.5 hours to the different compounds and incubated for a further 20.5 hours. The cells were then washed and incubated in fresh complete media. The results in figure 3.4 indicated that compared to untreated cells (control), the Caco-2 cell lines showed more than 75% viability when treated with various concentrations of PLGA nanoparticles, SiO₂ and Fe₂O₃ particles. Therefore the PLGA nanoparticles compared well to the controls and did not show any adverse effects on the cells. This result illustrates the safety of this drug delivery system. MA containing nanoparticles caused no more than 25% cell death in the Caco-2 cells. MA containing nanoparticles showed lower % viability with statistical significance ($P < 0.01$) compared to PLGA only nanoparticles, whereas the Fluorescein-MA containing nanoparticles compared to PLGA did not differ with significance. The MA containing nanoparticles differed

from the % viability with statistical significance ($P < 0.01$) compared to Fluorescein-MA nanoparticles. One possible reason for this is that the percentage MA in the Fluorescein-MA is less than for the MA alone. The MA (0.01 mg/ml) but not the Fluorescein-MA containing nanoparticles statistically were not significantly more toxic compared to the control, ZnO, but this might be attributed to the large standard deviation obtained for the ZnO. A longer incubation time up to 48 hour and 72 hours study was also done, but because of the fast growth rate of the Caco-2 cells even after treatment, the nanoparticles did not show any significant toxicity in comparison to the controls.

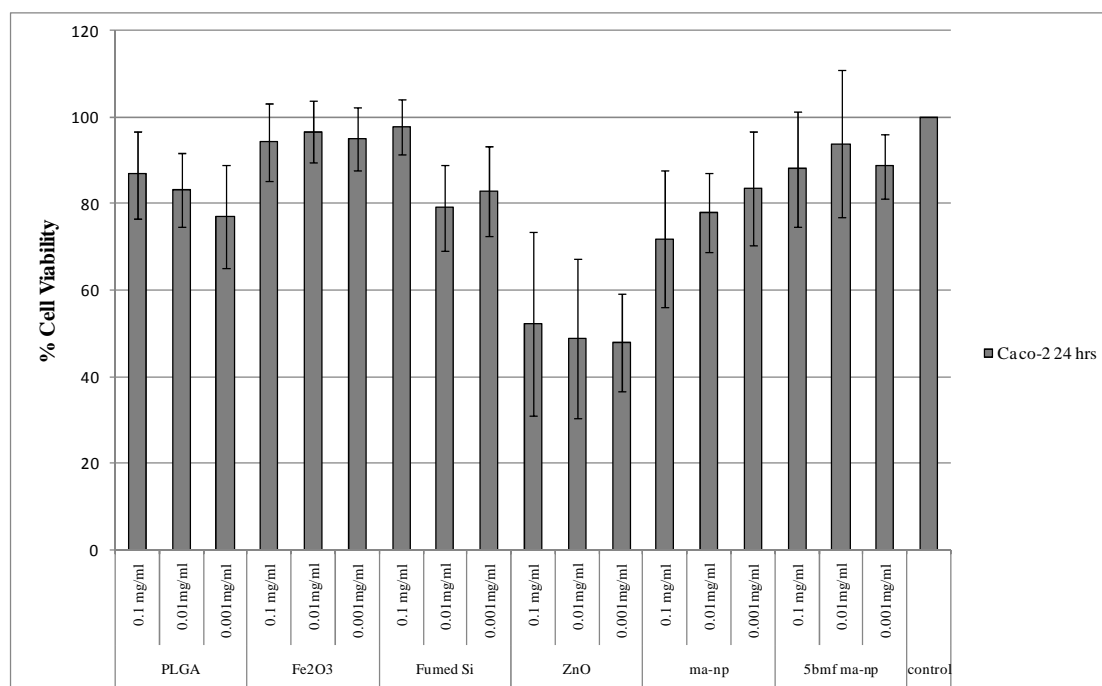


Figure 3.4 Effects of PLGA, ferrous oxide, fumed silica, zinc oxide and MA containing particles on viability of the Caco-2 cell line after 24 hours as done by a WST assay. The data are representative of two repeats of $n = 6$ and the error bars indicate standard deviation.

An initial viability study on differentiated U937 macrophage cells was also done by means of a non-radiometric MTT assay [192, 193]. The formazan crystals formed were dissolved and the absorbance of the dye measured as an indication of the number

of live cells per well. MA containing nanoparticles showed more than 80% viability in the U937 cells as shown in figure 3.5. Because the MTT assay was not repeated statistical significance was not determined. But these initial studies do indicate that the MA containing nanoparticles have a small negative effect on the cell growth albeit a bit more toxic compared to PLGA nanoparticles alone.

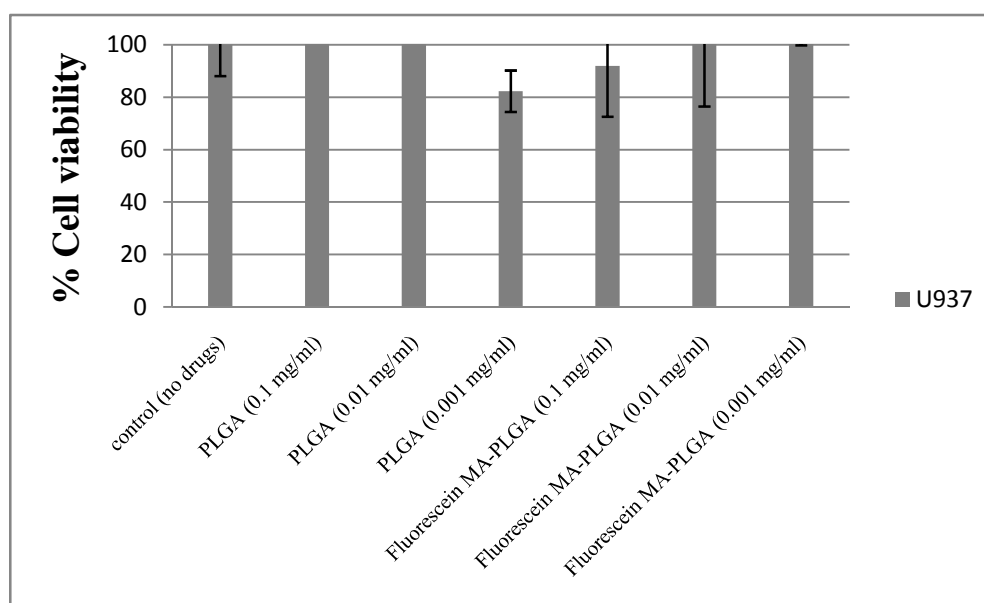


Figure 3.5 Effects of PLGA and MA containing particles on viability of the U937 cell line after 24 hours as done by a MTT assay. The data are representative of one experiment of $n = 4$ and the error bars indicate standard deviation.

3.6.4 Flow cytometric measurement of uptake of nanoparticles by macrophages

The THP-1 cells were used in their chemically differentiated state. Uptake of labelled nanoparticles by macrophages was measured by flow cytometry. The instrument was set for each sample to collect 10 000 events. Fluorescein and rhodamine have excitation wavelengths of 488 nm and 526 nm respectively and were detected at their respective emission wavelengths of 520 nm and 555 nm. The data consisted of side scatter, forward scatter and fluorescence emission centered at 520 nm (P1, for Fluorescein) and 555 nm (P2, for rhodamine). Labelled and unlabelled samples were

used to set the respective gates, where the unlabelled cells would be eliminated from the analyzed population. The Fluorescein-MA and Rhodamine containing nanoparticles of a similar size range were used for this study. In addition cells were washed with a trypan blue solution before analysis to quench extracellular fluorescence, therefore measuring only the fluorescent particles that were internalized [180].

The results shown in figure 3.6 for both of the nanoparticle groups indicate a concentration dependent uptake in macrophage cells. The graphs indicated that no additional fluorescence peaks were observed when the cells were exposed to higher concentrations of MA or rhodamine containing nanoparticles. Thus it could be assumed that only the number of cells that take up the particles are increased and that all cells take up similar amounts of particles. Thus MA seems not to interfere with the thermodynamics of the nanoparticle uptake. For the confocal studies a concentration of 0.1 mg/ml was used, so that the macrophages were not saturated with nanoparticles.

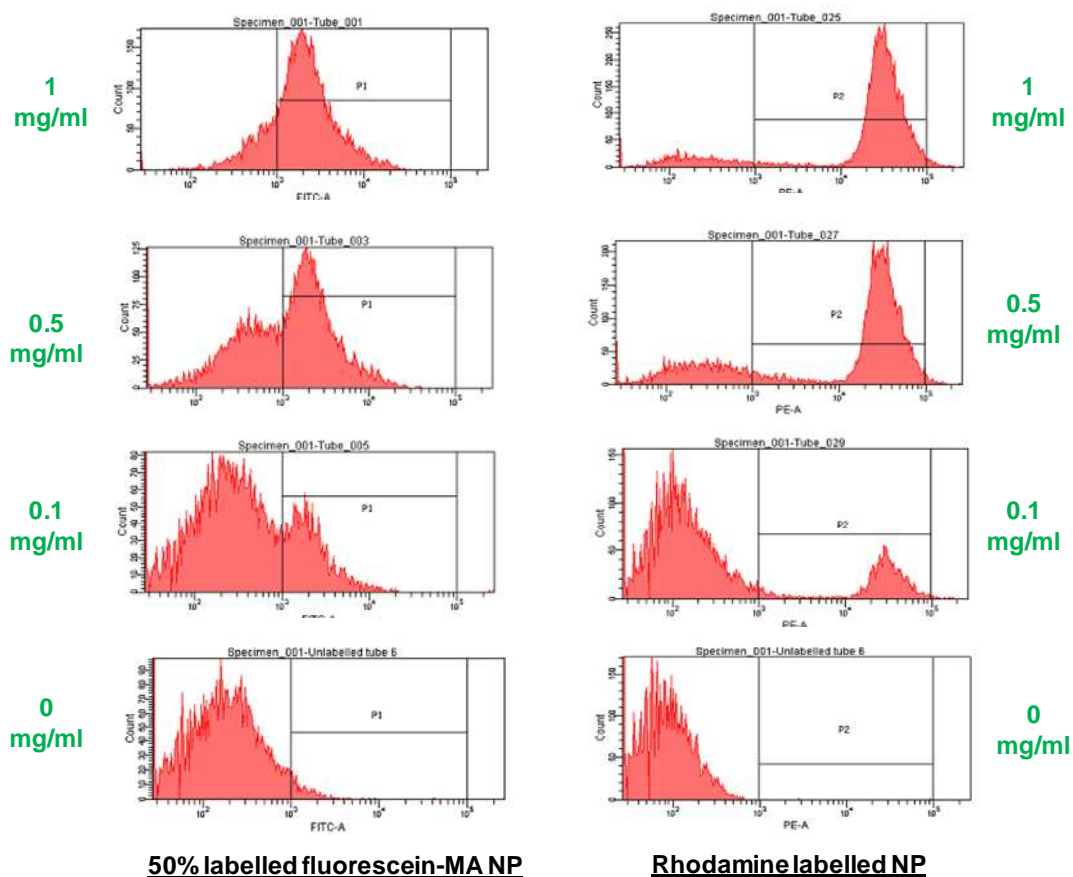


Figure 3.6 Flow cytometry of nanoparticle uptake in THP-1 cell culture at increasing concentrations of Fluorescein -MA and rhodamine containing nanoparticles.

When flow cytometry of nanoparticle uptake was measured on the macrophage cells pre-incubated individually with chemical inhibitors of endocytic pathways no inhibition was observed for any of the inhibitors used. Uptake was observed of the NPs similar to where no inhibitors were used. The specific inhibitors used were as described in section 3.5.4.3. No conclusion could therefore be drawn with flow cytometry regarding the mechanism of uptake of the nanoparticles.

3.6.5 Cell culture

The results obtained for the live and fixed cell imaging on the uptake of Fluorescein-MA NP studies was done to provide visual assessment of the uptake process and kinetics.

3.6.5.1 Nanoparticle uptake in U937 and THP-1 macrophages

All the results that are presented here are those of cells in their chemically differentiated state, which was achieved via treatment with PMA. Phorbol esters, such as PMA were reported to induce macrophage like differentiation in myelomonocytic and histiocytic leukaemic cell lines (e.g. THP-1 and U937) [179, 194].

The capability of macrophages to take up and accumulate the nanoparticles was investigated via confocal microscopy. The data as presented in figure 3.7 A and B illustrated that after treating the cells for an hour with 0.1 mg/ml Fluorescein-MA PLGA- or coumarin-PLGA-nanoparticles, the particles were visible within the cells and were thus successfully taken up into both the THP-1 and U937 macrophage cell lines, corroborating the flow cytometry results. Therefore including the MA into the nanoparticles did not affect the uptake into the macrophages negatively.

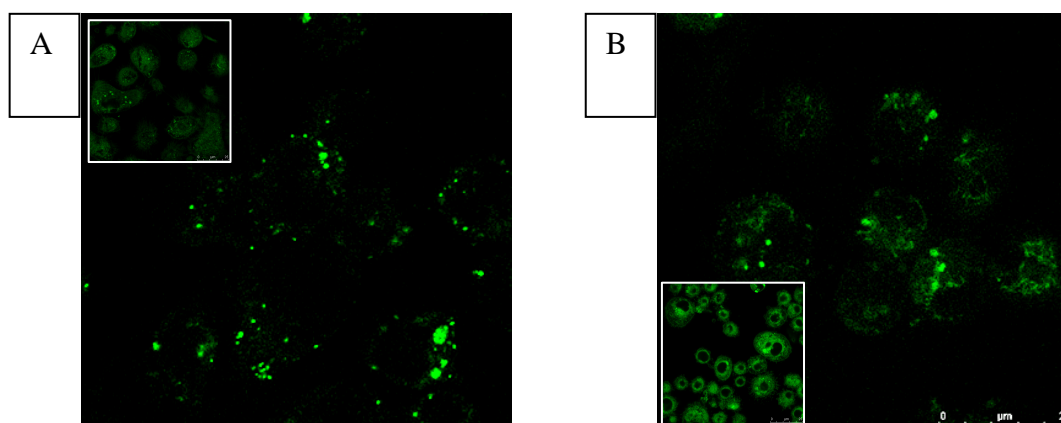


Figure 3.7 Live cell images of Fluorescein-MA PLGA nanoparticles taken up by a) THP-1 and b) U937 macrophages. Inserts are controls i.e. coumarin labelled PLGA nanoparticles.

For the effective design of clinically useful therapeutic molecules, it is necessary to understand the intracellular trafficking and fate of the molecules. To determine whether the nanoparticles reside within the early endosomes, initial co-incubation studies with Fluorescein-MA containing PLGA nanoparticles (green) and transferrin (red), with the transferrin representing early and recycling endosomes, was done for half an hour in the two different macrophage cell lines. The results (not shown) did not indicate co-localization. Whether the particles already moved through early endosomes or not could therefore not be concluded. To resolve this, pulse/chase studies were undertaken.

Interestingly, the coumarin PLGA particles were observed to affect the morphology of the macrophages. Light microscopy images (Figure 3.8) of THP-1 macrophages incubated either with unlabeled PLGA or coumarin labeled PLGA nanoparticles indicated that the coumarin PLGA treated cells (Figure 3.8A) yielded more flattened / less dense cells than the PLGA unlabeled treated cells. Whether coumarin PLGA serves as a good representative control as was used in literature is a point of contention [29]. It may be that in macrophage like cell lines the dye appears to be toxic whereas in other cell lines it is not [29]. It was decided not to use the coumarin labelled PLGA in the co-localization studies due to the coumarin most probably interfering with the metabolism of the cells.

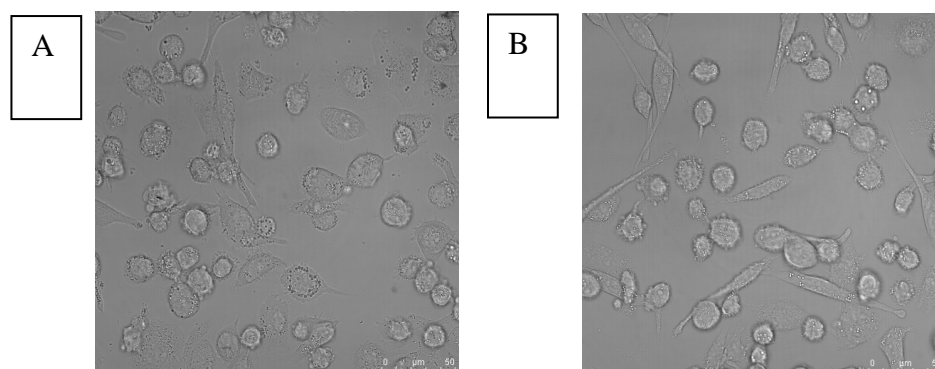


Figure 3.8 Bright field confocal images of cell morphology of THP-1 macrophages after uptake of nanoparticles A) Coumarin PLGA B) unlabeled PLGA nanoparticles.

Pulse/chase studies allow the determination of the path and end location of the nanoparticles within the cells after uptake. The endocytic probes (Figure 3.9) that were used were transferrin 633 or transferrin 488 and dextran alexa fluor 647, to represent early/recycling endosomes and late endosomes/lysosomes respectively. Dextran follows the route of early endosomes, through late endosomes reaching lysosomes [182]. Previous groups have shown that late endosomes and lysosomes are accessible to molecules in the plasma within 10-30 min. after uptake, with the half-life delivery of a fluid phase marker between 90 and 120 min. [182, 185, 195, 196].

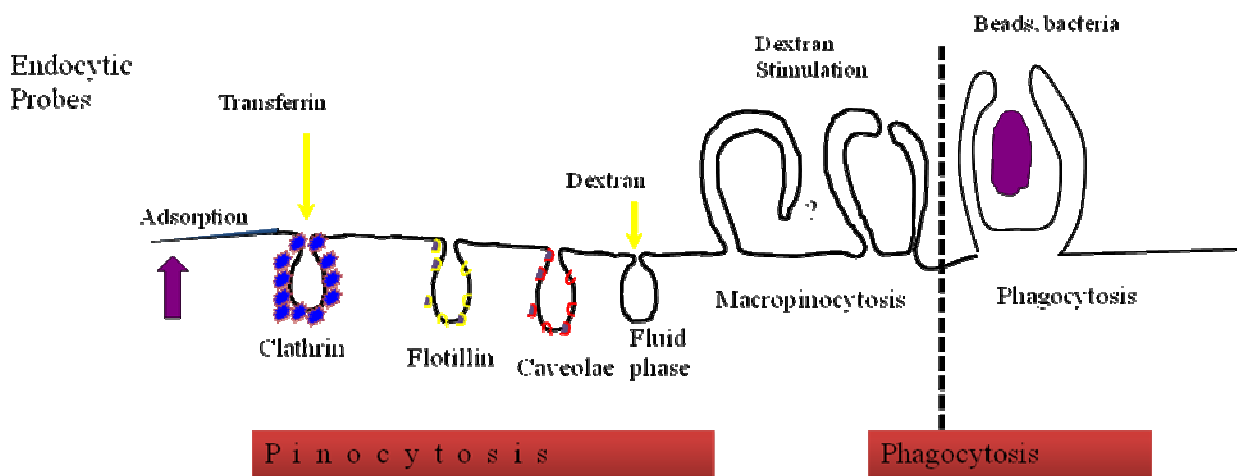


Figure 3.9 Endocytic probes used for representation of endocytic pathways (Courtesy Dr. Arwyn T. Jones, Cardiff University, UK).

In figure 3.10, the control experiment was done to show that the dextran positive compartments (late endosomes/lysosomes) were distinct from the early/recycling endosomes represented by transferrin-labelling. Z-stack imaging confirmed no-colocalization in areas where possible yellow spots were observed. The cells were treated with the nanoparticles at different time points as well as incubated with dextran or transferrin as indicated in figure 3.10

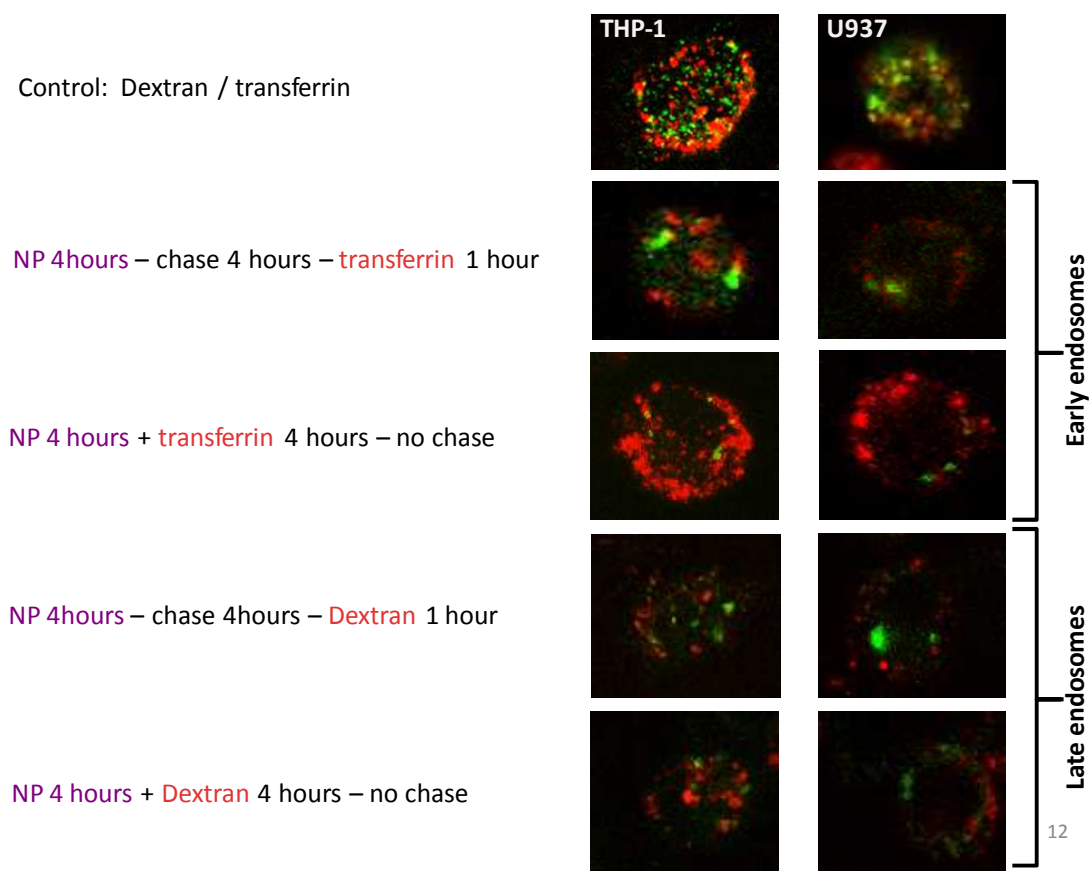


Figure 3.10 Confocal images of intracellular processing of Fluorescein-MA using single sections through the macrophage cells of the pulse/chase experiments. The red stained regions represent either transferrin 633 or dextran alexa fluor 647. The green colours in the figures represent Fluorescein-MA PLGA nanoparticles. Yellow colours are indicative of co-localization.

A summary for the transferrin 633 and the dextran alexa fluor 647 pulse/chase experiments with the nanoparticles is presented in the table 3.3

Table 3.3 Summary of figure 3.9 of pulse/chase studies that was conducted

	Observation:
Control:	
Dextran (red) 1 hour – chase – transferrin (green) 1 hour	No colocalization
Particles and transferrin:	
1. NP 4 hours – chase 4 hours – transferrin (red) 10 min	No colocalization
2. NP 4 hours – chase 4 hours – transferrin (red) 1 hour	No colocalization
3. NP + transferrin (red) 4 hours – no chase	Few areas of colocalization
Particles and Dextran:	
4. NP 4 hours – chase 4 hours – dextran (red) 1 hour	No colocalization
5. NP + dextran (red) 4 hours – chase 4 hours	No colocalization
6. NP + dextran (red) 4 hours – no chase 4 hours	No colocalization
7. Dextran (red)1 hour – chase 4 hours – NP 4 hours	No colocalization

The main reason why these pulse/chase experiments were done was to determine the endpoint location of the nanoparticles, and therefore without a chase step the nanoparticles could be at different stages of uptake (Figure 3.10 and table 3.3). When the study was done with the nanoparticles and transferrin, the only colocalization that was observed was when the nanoparticles and the transferrin were incubated together for 4 hours without a chase incubation step in between. This result could indicate that some of the particles might move through the recycling endosomes given the long incubation time of the transferrin, but no colocalization was observed in the early

endosomes by using this approach indicating that the nanoparticles have moved beyond the compartments which are represented by transferrin. It might be that the particles already passed through the early endosomes during the course of the longer incubation times used. The different pulse/chase studies with the nanoparticles and dextran did not show any colocalization indicating that the nanoparticles and the dextran are not localized in the same compartments of the cell. No co-localization was observed in these pulse/chase studies under the conditions used and it might be that the particles are already localized within the cytoplasm or other compartments.

3.6.5.2 Immunofluorescence staining of fixed macrophages

Because no conclusive results were obtained from the pulse/chase studies regarding the intracellular processing of the MA containing NPs after uptake, another approach was taken. The cells were treated with Fluorescein-MA PLGA nanoparticles for three hours, fixed and immunostained with different primary antibodies directed to specific cell organelles. As shown in figure 3.11, the early endosome antigen 1 marker (red) was used but did not show co-localization with the fluorescein-MA PLGA nanoparticles. The particles (green) in the image were confirmed to be present within the cells by z-stack imaging. The results correlate with that of figure 3.10, where with live cell imaging, co-localization with the early endosomes could also not be observed.

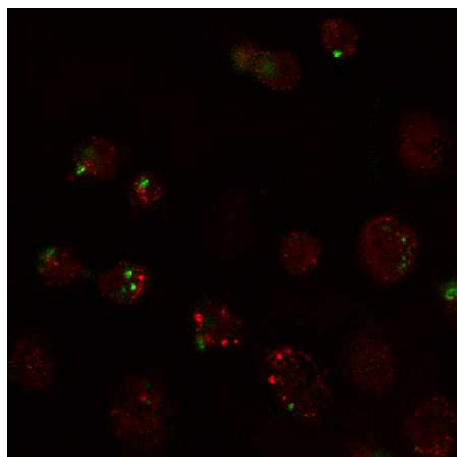


Figure 3.11 Confocal imaging of possible colocalization of Fluorescein-MA PLGA (green) with primary antibody EEA1 (red) labelled organelles in THP-1 macrophage cells. Alexa fluor 633 secondary antibody stain was used to visualize the labelled organelles.

Microscopic imaging was used to investigate two cytoskeletal inhibitors. Cytochalasin D was used to disrupt actin dependent pathways and nocodazole to disrupt the microtubule network. Attempts made with flow cytometry as discussed in section 3.6.4, showed that uptake took place regardless of several inhibitors used. Here confocal results indicated (figure 3.12) that Cytochalasin D treatment decreased uptake of the particles in both the THP-1 (shown) and U937 (not shown) cell lines. This suggests dependency of MA nanoparticles uptake on actin (red) and therefore microfilaments, at least in these cell lines. The illustration in figure 3.11A indicates intact actin networks and nanoparticles (green) within the cells, whereas in figure 3.11B a disrupted actin network (red) together with particles present on the outside of the cell is visible. Nocodazole, which disrupts microtubules, treatment (not shown) did not have an effect on MA nanoparticle uptake in both the THP-1 and U937 cell lines.

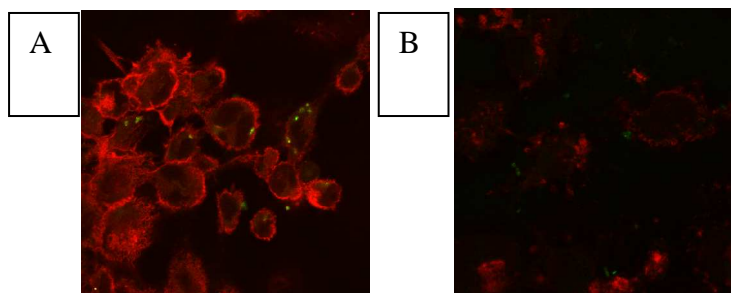


Figure 3.12 Actin involvement in the uptake of Fluorescein-MA PLGA in THP-1 macrophage cells stained with rhodamine phalloidin for actin, a) No Cytochalasin D treatment, b) Treatment with Cytochalasin D.

3.6.6 In vitro drug testing in *M.tb* H37Rv infected THP-1 macrophages

To determine the mycobactericidal activity of the INH containing nanoparticles compared to free INH, i.e. whether the drug is released from the nanoparticle, an *in vitro* infection study was performed where THP-1 macrophage cells were infected with *M.tb* H37Rv and used in the radiometric experiments as described in Methods [172]. A second aim was to determine whether the MA in the particles influences the efficiency of the *M.tb* inhibition. The radiometric experiments with the NPs containing INH and the free INH, were conducted at the same concentrations as for free INH (0.2 $\mu\text{g/ml}$ and 2 $\mu\text{g/ml}$) so that the concentration of INH in the NP is the same as for the free INH.

The uptake of the particles was observed in THP-1 macrophage cells with previous confocal studies as discussed in section 3.6.5.1. The presumed advantage that the particles hold compared to the free drug is that due to its nanosize, intracellular uptake of the drugs will improve the availability of the drug to the intracellular bacteria. This was tested here. The effect of the inclusion into the nanoparticle of MA as targeting agent was tested here as well. The targeting advantage that may be gained by MA

inclusion was not tested, due to the absence of natural host anti-MA antibodies in the *in vitro* experimental design.

Infected macrophages were exposed to free INH and encapsulated INH with or without MA at different concentrations over 3 time points (5 hour, 1 day and 2 day exposures followed by an additional 2 day incubation time after washing the cells to remove particles and/or drugs that have not been taken up into the cells). After treatment with the different drugs and two days of incubation, the bacterial growth index (GI) was determined by means of the radiometric BACTEC 460 system. The bacteria were harvested for BACTEC by lysing macrophage cells with 0.1% Triton X-100. The results (figure 3.13) indicated the expected dose dependent effect of the drug on the inhibition of the growth of the bacteria. For the 5 hour treatment the standard deviations were too large to draw conclusions between the different test groups (results not shown). The 1 day and 2 day incubation time did show better growth inhibition compared to the 5 hour study compared to the nanoencapsulated INH, but was still not as effective as the free drug alone. The 2 $\mu\text{g/ml}$ concentration of the nanoparticles was already out of range and showed just as good efficiency in the 1 and 2 day study as for the free drug alone.

It can be concluded from the results that the nanoencapsulation of INH results in a delay in drug release, possibly as a function of the polymer that slowly degrades in the macrophage. After 1 and 2 day exposure to the nanoencapsulated INH, significantly more inhibition was observed, but with reduced toxicity/efficiency compared to free INH. The effect of free INH on bacterial growth inhibition could be matched by using the higher concentration of 2 $\mu\text{g/ml}$ of the nanoencapsulated INH with or without MA.

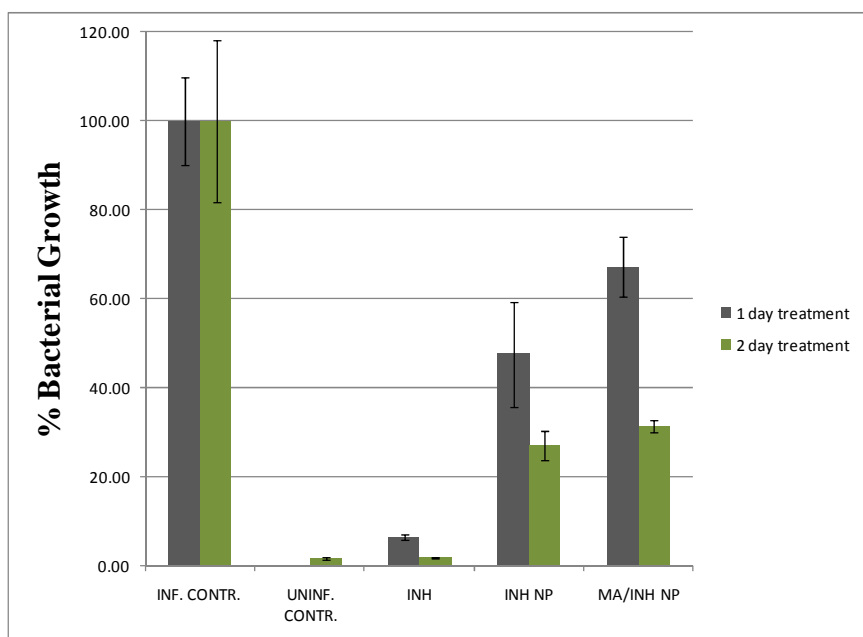


Figure 3.13 The effect of nano-encapsulation of INH on its efficiency to suppress growth of *M.tb* in infected THP-1 macrophages using BACTEC. The results represent the average of triplicate values. Concentration for INH shown was 0.2 μ g/ml for free and encapsulated drug. The study with 2 μ g/ml INH was out of range. INF.CONTR = infected control, UNINF.CONTR = uninfected control, INH = isoniazid, INH NP = isoniazid containing nanoparticles, MA/INH NP = mycolic acid and isoniazid containing nanoparticles.

In the *in vitro* model, the inclusion of MA in the INH nanoencapsulated particle did not show significant enhanced efficiency of delivery or toxicity of the INH drug in the macrophage. As the target for MA is represented by host antibodies to MA or concentrated spots of cholesterol, which were not present in the test, no significant difference in INH mycobactericidal efficiency was expected by the inclusion of MA in the nanoparticles. What was interesting to note was the fact that between the INH containing nanoparticles with and without MA incorporated, there was a statistical significant difference for both days ($P < 0.01$) where the INH in the MA NP had a lower efficiency compared to the INH in the NP without MA. It appeared as if the MA actually worked against INH in killing the *M.tb* in the macrophages. The observation that the MA inclusion actually worked against INH's bacterial inhibition, came as quite a surprise. This observation could be explained by the notion that the

MA might serve as an external source of the MA cell wall component, overcoming the bottleneck in cell wall synthesis during the proliferation cycle of *M.tb*.

The data further illustrates that INH was not incapacitated by the process of encapsulation, i.e. the double emulsion solvent evaporation freeze-drying technique, which involves shear forces and low temperatures. It further firmly confirmed that the nanoparticles are taken up by the macrophages and that INH is released from the particles, at the expected slower rate of release compared to the free drug.

3.7 Discussion

In the search for new or improved treatment against TB, nanoencapsulation of a known anti-TB drug was investigated here, including the use of a potential targeter to increase the efficiency of drug delivery to the site of infection. As mentioned before, controlled drug delivery devices such as nano and microparticles have numerous advantages compared to conventional dosage forms. Poly lactide-co-glycolide (PLGA) co-polymer, is a biodegradable and biocompatible polymer, that has often been used for controlled drug delivery systems, especially because of its non-immunogenic properties and having the capacity to encapsulate hydrophobic and hydrophilic agents [54]. As targeting agent, the mycobacterial cell wall component, MA from *M.tb* was investigated. MA has interesting biological activities, including foam cell formation and immune steering towards Th1 cellular responses [14, 126], as well as cholesterol like properties [121]. The MA being present on the external surface of the nanoparticles may interact with anti-MA antibodies in the vicinity of the sites of infection to cause a localized immune complex that may enhance uptake of the NPs in the infected and surrounding uninfected macrophages. MA could also target cholesterol that is presumed to be concentrated around the sites of infection [81, 148] by means of its attraction to cholesterol [121]. By combining the possible targeting effect of MA to the infected cells and the slow release of the polymer, this approach was hypothesized to lead to effective TB treatment where the TB infected cells could be targeted and high intracellular concentrations of INH could be achieved.

The double emulsion-solvent evaporation freeze drying technique [55, 174] can be used for hydrophilic and hydrophobic drugs to be encapsulated in a polymer matrix [32, 60]. This method was applied to formulate nanoparticles of MA and INH into PLGA, a biocompatible and biodegradable polymer [34, 51, 55]. Successful encapsulation of 14% INH together with MA was achieved with the technique used, resulting in a negative zeta potential that may prevent unwanted agglomeration [32,

33]. The percentages of the INH and MA inside of the nanoparticles were not optimised for the purpose of these experiments.

The PLGA and MA-PLGA particles were found to be non-toxic to the mammalian host macrophage cells, compared to industrial nanoparticles [197]. This result supports literature indicating that amorphous silica, as was used in this study, is not toxic to cells [177] as well as Fe₂O₃ [175, 176]. The ZnO nanopowder which is toxic to cells, resulted in a significant reduction in cell viability as also described in literature [178].

The therapeutic effect of the drug loaded MA PLGA nanoparticles will greatly depend on the internalization and sustained retention in diseased cells. Although an *in vitro* system does not even remotely represent a highly evolved biological system, some preliminary data could be obtained to indicate the behaviour of the particles with the cells. THP-1 and U937 monocyte-macrophage like cell lines, which are often used in nanoparticle uptake studies [179, 198], were used to determine whether the labelled MA nanoparticles would be taken up by the cells. The data illustrated that labelled MA nanoparticles were successfully taken up into the two different macrophage cell lines which represent the target cells in the host. The results also indicated that the nanoparticles with an average size of 500 nm, a slightly negative zeta potential and a smooth external surface were appropriate for uptake by macrophage cell lines. This demonstrated that nanoparticles may serve as a suitable carrier for MA to reach their target sites.

These results of using PLGA in the formulation corroborate with examples in literature. PLGA microparticles were reported to be taken up specifically by macrophages of peritoneal exudate cells [32]. Hasegawa *et al.* also showed that RIF containing PLGA microparticles were phagocytosed in alveolar macrophages [186].

In another *in vivo* study it was also shown that PLGA microspheres containing trehalose dimycolate (TDM) were taken up by phagocytic cells [199].

The endocytic and intracellular trafficking routes are intricate and highly regulated to help mediate cellular homeostasis [185]. Knowledge of these complex systems could be used to better design and use nanoparticles for effective chemotherapy. After endocytic uptake, drug delivery systems could go into early sorting endosomes and recycling endosomes. Thereafter from early endosomes transported to late endosomes and finally to lysosomes [185]. In order to identify the intracellular compartments that the nanoparticles traverse, different endocytic markers were used. For live cell imaging transferrin was used to represent early / recycling endosomes. Transferrin binds to the transferrin receptor and is taken up by clathrin coated endocytosis, which then goes through the early and recycling endosomes, returning to the plasma membrane [182]. Dextran was used to represent late endosomes / lysosomal compartments because the molecule is taken up by fluid phase and then moves through early to late endosomes and finally to lysosomes [182].

In the pulse / chase experiments that determine the compartments the particles would occupy, it was observed that the nanoparticles only co-localized to a small extent with transferrin and not with dextran. From these results it was also observed that the endpoint of the nanoparticles was not the lysosomes. Whether they do pass through the lysosomes, remain to be determined. Live cell imaging, using short time intervals and different chase times are warranted to further elucidate particle trafficking. These results correlate with an *in vitro* uptake study done by Trombone and co-workers in peritoneal macrophages. They showed that no colocalization was observed with the marker dextran for PLGA microspheres containing TDM [199] even after 15 days of administration.

Another possibility is that the nanoparticles containing the MA reside within the cytoplasmic compartments of the cell as was previously illustrated for PLGA nanoparticles in human arterial smooth muscle cells (HASMC) by confocal and transmission electron microscopy experiments. The *in vitro* studies of Panyam *et al.* showed that endo-lysosomal escape occurred within 10 minutes through a process of surface cationization, where the particles associated with the wall of the endocytic vesicles before being released into the cytoplasm. Due to the acidic environment of the endo-lysosomes the particles had a cationic potential associating with the negatively charged membrane, leading to the particles' escape. The experiments also showed that the lysosomal vesicles stayed intact, possibly because of localized destabilisation and extrusion of the particles at the point of contact with the membrane [29]. If this applies to the present study as well, it might be that the MA containing nanoparticles can enter the cytoplasmic compartment of the cell soon after uptake. This property will be beneficial in drug delivery as the drug load in the particles will not be retained in the degradative environment of the lysosomal compartments in the cell but will rather be in the cytoplasmic compartment. MA incorporated into the PLGA nanoparticles could also contribute to the endocytic route that the nanoparticles might follow. As the coumarin labelled PLGA nanoparticles influenced the metabolism of the cells, no comparative studies were done to determine the effect the MAs would have on the nanoparticles localization within the cells. Another fluorescent label will be investigated in the future for comparative studies.

There are a number of obstacles in fluorescence microscopy when investigating endocytic trafficking. Live cell imaging does not allow for immuno-staining of intracellular structures and therefore fluorescent probes are used that also poses the challenge of concentration and pH dependent quenching that could be released from the carrier leading to misinterpretation of results. Traditional fixation methods could cause permeabilization of intracellular membranes allowing material to diffuse out leading to deceptive results. Both approaches are therefore applied to eliminate the possibility of fixation artefacts [185]. Here, fixation of the cells were done together with EEA1 (early endosomal antigen 1) antibody staining for early endocytic

structures. The Fluorescein-MA PLGA nanoparticles did not co-localize with EEA1, representing early endosomes, similar to the results obtained in the pulse/chase study with transferrin. One possibility could be that the particles might move through these compartments at a much faster rate as was intervalled for measurements in the actual experiments.

Preincubation of the cells with cytoskeletal inhibitors, before nanoparticle treatment, indicated an actin dependent uptake that could be inhibited by cytochalasin D. Nocodazole, which disrupts polymerization of microtubules and numerous endocytic processes [182, 200], did not have an effect on MA PLGA nanoparticle uptake. These results differ from a study done by Panyam and co-workers where the PLGA nanoparticles in HASMC cells were reported to be affected by Nocodazole and not by cytochalasin D [29]. But this could be due to the difference in size, as our particles are around 500 nm whereas the particles in the study of Panyam was around 70 nm in size, which also plays a role in the route of uptake. This could also point towards a difference in the reaction to chemical inhibitors [201] by the different cell lines used, or by the inclusion of MA that may affect the route of uptake and processing of the NPs. The main challenge here is that for every type of cell line the different inhibitors should be optimized and tested. The effect of uptake and processing inhibitors depends on the specific cell line used, as was shown in a report by Vercauteren *et al.* [201]. The authors showed that even poor specificity was observed in some cell lines. Thus the optimized concentrations obtained in literature [140, 182, 183] can only be used as a guideline. Optimization of inhibitor concentrations for the specific cell lines used in this study, with rigorous controls in place, may yield more data on the mechanism of uptake and processing of MA containing NPs.

The efficacy of the free vs encapsulated drugs were tested with *M.tb* infected macrophage cells over a period of 4 days. A 5 hour incubation of nanoparticles was less effective compared to the 1 and 2 day exposures to kill the mycobacteria as was to be expected due to the slow degradation rate [58] of the nanoparticles and the

probability that the INH remains associated to the polymer during the degradation. The indication of a reduction in the bacterial growth in the NP-INH-MA treated macrophages confirmed uptake of the nanoparticles into the TB infected cells and the subsequent release of the drug from the polymer.

Although the encapsulated INH appeared to be less effective compared to the free drug, it might be that the INH is still associated with the polymer in an environment where the polymer is not degraded as efficiently as would be the case in a physiological environment. Comparing the rate of degradation of PLGA microspheres in an *in vivo* vs an *in vitro* environment in literature, it was shown that the *in vivo* degradation was much faster (1.7-2.6 times) than that *in vitro*, in buffer at physiological pH and temperature, regardless of the end group or molecular weight of the PLGA. The faster degradation might be due to several factors, such as free radical formation and acid or enzymatic products formed by the host's immune cells that could enhance the degradation process that is not present in an *in vitro* environment [58]. As mentioned previously, PLGA microparticles have been shown to be taken up by macrophage cells even without targeting ligands. Therefore it is envisioned that the effective dose required *in vivo* would be much less than the free drug that is able to traverse to different areas in the host in contrast to what was observed in the *in vitro* experiments.

A number of research groups are currently investigating the use of nanodrug delivery vehicles to enhance the efficacy of anti-TB drugs. The research group of Khuller and co-workers have been analysing a number of different delivery vehicles to enhance the efficiency of existing anti-TB drugs. They tested the use of solid lipid inhalable particles for the first line anti-TB drugs, where they could reduce the number of administrations required by more than 6-fold [50]. The group also showed that inhalable alginate nanoparticles were detectable for up to 15 days in organs [202-204], and that PLGA microparticles have a sustained release over several days [205]. The frequency of dose administration could also be reduced by making use of carrier

systems. In a guinea pig model it was shown that the treatment frequency could be reduced 9-fold by encapsulating RIF or INH into PLGA nanoparticles due to the sustained slow release of the drugs from the carrier vehicle [206]. The results shown in literature, as mentioned above for PLGA polymers as carrier vehicle, support sustained release and the possibility of enhanced uptake in the macrophages without the use of targeting ligands. The contribution that our research is able to make is in the region of specific targeting. The uptake of drugs by infected macrophages would not only be enhanced by the synthetic PLGA polymer carrier vehicle but also by the presence of MA that may facilitate opsonisation of the nanoparticles for macrophage uptake mainly at the site of MA antigen production. In addition, the cholesterol nature of MA and its ability to bind cholesterol could also cause a physical attraction to the cholesterol rich sites of persistent *M.tb* infection.

This study is the first to report encapsulation of MA into solid matrix PLGA nanoparticles together with anti-TB drugs. *In vitro* experiments did show successful uptake into macrophages. The localization fate of the NPs within the cells still needs to be confirmed. Because the studies done by Panyam *et al.* did indicate that the PLGA particles ended up within the cytoplasm, the predictions are that our PLGA nanoparticles will also preferentially occupy the cytoplasm [29]. The inclusion of the MA into the PLGA nanoparticles did not reduce the efficiency of uptake into the macrophage cells, as indicated with flow cytometry and confocal imaging, although the mechanism of uptake and processing in the cells could not be concluded with the results obtained. A requirement for the actin cytoskeleton was observed when the cells were treated with cytochalasin D and visualized with confocal microscopy. Actin plays a role in various different uptake mechanisms such as clathrin dependent endocytosis and macropinocytosis [51, 207].

The BACTEC experiments confirmed a slow release of the anti-TB drug from the polymer. The inclusion of MA into the nanoparticles seemed harmless to the host macrophages, but decreased the mycobactericidal efficiency of INH somewhat, an observation that may possibly be attributed to INH inhibiting the natural MA

biosynthesis of the pathogen, while inclusion of MA in the NP adds an external source of this metabolite to the pharmacologically stressed *M.tb*.

The system is now ready to be tested *in vivo*, where the efficiency of MA as a targeting agent may be assessed. It is envisaged that the MA will firstly serve as an antigen that forms immune-complexes with anti-MA antibodies, which universally occur in all TB patients [120]. This may facilitate opsonisation of the nanoparticles for macrophage uptake mainly at the site of infection, where the mycolic acid antigen is naturally produced and released. Secondly, because of the cholesterol and cholesterophilic nature of MA [121], it may in effect be attracted to the anticipated cholesterol rich sites of *M.tb* infection.

Chapter 4: Conclusion

Tuberculosis can be classified as a new disease since HIV/TB co-infection became such a prominent problem in especially third world countries [1]. South Africa currently has the highest incidence of TB per 100 000 (358 per 100 000) people in the world. In 2007 alone 112 000 people died of TB in South Africa, of which 94 000 (72%) were co-infected with HIV [1]. Sputum smear microscopy for detection of acid fast bacilli is still the primary tool for diagnosis of TB especially in resource poor countries [1]. This detection method has low sensitivity particularly in an HIV burdened population [22]. A need for a more rapid diagnostic test is highly desirable [1]. Studies from a gold mine community in South Africa showed that due to the diagnosis delay and inappropriate therapy, drug resistance and disease transmission increased in the HIV co-infected population [9]. Standard first line chemotherapy is not effective for individuals that have MDR-TB and there is practically no cure for XDR-TB. The failure to complete lengthy drug regimens and the pathogens becoming resistant to especially the two first line drugs INH and RIF through mutations are increasingly detected in persons who have been previously treated for TB [16, 18-20]. The approach to control this disease now is to discover new chemotherapies effective against *M.tb*, as well as to enhance the potential of existing drugs to treat MDR-TB [21].

As discussed in chapter 1, effective chemotherapies do exist for TB treatment for more than 50 years but due to the persistence of the bacteria in the human host for several months despite treatment, curing patients becomes quite a challenge. Failure to complete therapy due to non compliance is associated with increased infectious time, relapse and drug resistance [19]. Due to the treatment period for drug susceptible TB of up to 9 months, toxic side effects of the combination therapy asks for special consideration, such that the decision for treatment cannot be taken lightly.

Another drawback of the combination therapy against TB is the low solubility of the drugs, their short half life and rapid clearance from the biological system [16]. One approach in development of more efficient anti-TB drugs is to nanoencapsulate the drugs and to design systems capable of targeting the drug to the site of infection at relatively low drug concentrations in the blood to prevent systemic toxic side effects. There are different approaches that could be followed in order to focus the drug towards its target. The way our group decided on was to investigate targeted nanotechnology based drug delivery systems with slow release capabilities. The long term aim is to reduce the concentrations and frequency of dosing, hoping also for a reduced treatment period earned from more efficient and compliant treatment.

In developing countries patient non-compliance turned out to be a major cause of treatment failure and the development of drug resistance [16]. To address this particular issue a DOTs (Directly Observed Treatment) programme was introduced by the WHO, where a trained person directly observes the medication being swallowed daily by the TB patient [10]. This programme is human resource intensive. The cost of this service could be reduced by developing a nano-encapsulated anti-TB drug delivery vehicle, which can be taken weekly instead of daily due to the slow release properties of the nanoparticles.

In the TB strategic plan for 2007 to 2011, as set out by the South African Department of Health, the role that the scientific community should play is in the development of new drugs, diagnostics and vaccines for the prevention and control of TB. The CSIR (Council for Scientific and Industrial Research) embarked on a national health strategy since 2008, which includes research towards the development of novel solutions and pharmaceutical products that could treat diseases such as malaria, HIV/AIDS, and tuberculosis. The CSIR annual report of 2008/2009 announced our group's contribution to this strategy in focusing on slow-release nanomedicines against tuberculosis. Instead of new therapeutic compounds, our group focused on improved uptake and delivery of existing drugs by exploring the practical feasibility

of encapsulating drugs into PLGA nanoparticles. In addition, this study focused on MA as targeting ligand to be included in the nanoparticle together with the anti-TB drugs. The product's toxicity to and efficiency of uptake in host macrophages was investigated, to prepare for animal studies and eventual clinical trials in humans.

Nanotechnology can be used to overcome the main technological obstacles of therapeutic agents. By making use of polymeric nanoparticles such as PLGA based nanoparticles, the efficacy of the drugs could be enhanced by targeting the molecules to the site of infection and thereby reducing the dose needed for treatment [16]. Because the degradability of the nanoparticles could be controlled, the advantage of slow release of the therapeutics could be achieved [37]. As described in chapter 1, there is a wide array of nano-carrier vehicles to choose from. PLGA was the polymer of choice mainly because of its non-immunogenic properties, biodegradability and having the capacity to encapsulate hydrophobic and hydrophilic agents [34, 54, 55]. An additional advantage that PLGA is reported to have over other drug delivery vehicles is that the particles are selectively taken up into macrophages and dendritic cells [61], the main target for infection of *M. tuberculosis* [32, 51], [45, 172]. The results shown in literature, as mentioned above for PLGA polymers as carrier vehicle, support sustained release and the possibility of enhanced uptake in the macrophages without the use of targeting ligands. Several literature references show research done on PLGA nanocarriers in the field of TB. One such group is lead by G.K. Khuller, who showed that PLGA drug carrier microparticles released antitubercular INH and RIF over several days [205]. The frequency of dose administration could also be reduced by making use of carrier systems. In a guinea pig model it was shown that the treatment frequency could be reduced 9-fold by encapsulating RIF or INH into PLGA nanoparticles due to the sustained release of the drugs from the carrier vehicle [206]. Another laboratory showed that PLGA particles containing RIF and mannitol by using a four-fluid nozzle spray drying technique, led to improved uptake by alveolar macrophages in rats [69].

The discovery of the structural relationship between cholesterol and MA in our group [121] provided an excellent opportunity for specific drug targeting. The initial observation was made in an ELISA assay to detect antibodies to MA in human patient sera. Cross-reactivity between cholesterol and MA by antibodies from tuberculosis patients was so strong that the cholesterol could equally well suit as a substitute for MA as antigen in the ELISA, without affecting the outcome significantly [118]. Thereafter the cholesterol nature of MA was more directly demonstrated by showing the strong interaction between MA and Amphotericin B - an antifungal macrolide agent known for its binding to cholesterol [162] - on a wave-guide evanescent field biosensor system. The structural specificity of this attraction was demonstrated by showing that the methylester of MA was unable to bind Amphotericin B [121]. The same principle was confirmed with a surface plasmon resonance biosensor in a follow-up study [117], in which it was shown what the effect of chemical modification of MA would be on the manifestation of its cholesterol nature, i.e. its propensity for binding to Amphotericin B. Mycolic acids were shown to attract cholesterol from liposomes in an evanescent field biosensor [121]. In another study by a member of our group, evidence of a more circumstantial nature was found: Cholesterol was shown to hinder the efficacy of INH to eradicate *M.tb* in radiometric culture experiments [208]. One important target of INH is the enzyme called InhA, which catalyzes the final stage of the mycolic acid biosynthesis pathway. This enzyme is known to be related to the steroid dehydrogenase family of enzymes, suggesting the possibility that cholesterol could compete with the synthesized MA for binding to the substrate binding site of the enzyme, thereby competing with INH for binding into the active centre. Competitive inhibition between MA and cholesterol for binding to an enzyme's active site would further support the notion of a structural mimicry between MA and cholesterol.

Mycobacterial MAs are immunogenic. Stimulation of human CD4⁺, CD8⁺ T-lymphocytes to proliferate is done by MA upon CD1b presentation [116, 209]. Anti-MA antibodies generally occur in human TB positive patient serum [119, 137]. In one targeting scenario, MA incorporated into nanoparticles may interact with the anti-

mycolic acid antibodies that are anticipated to be present in higher concentrations at the infected areas. In this way, targeting may be achieved by an accumulation of the nanoparticles in immune complexes at the site of infection.

Furthermore, free MA is likely to play a role in the drug tolerant persistence of *M.tb* infection in the extracellular caseous lesions of a tubercle [141, 142]. Free MA has been reported to being pumped out of the bacilli for the specific purpose to form a biofilm. It cannot be excluded that mycolic acids simultaneously fulfils the role of attracting cholesterol to the biofilm as a carbon source for the slow growing, persistent mycobacteria. Cholesterol has been shown to be present in foamy macrophages surrounding the granulomas [14, 126] and can accumulate around the bacteria [148]. In this way, it is anticipated that foci of high cholesterol concentration is associated with late stage persistent TB infection in the lungs and other affected organs. Therefore, in another targeting scenario, the MA incorporated into nanoparticles could also serve as a ligand for cholesterol-rich areas, due to the cholesterol nature of MA and the fact that MA is attracted to cholesterol [121].

Cholesterol is also immunogenic, but only at high concentrations, when their homogenous existence with phospholipids is no longer possible and cholesterol separates out to form islands of high cholesterol concentration in liposomes or membranes. Such foci of high cholesterol concentration in natural eukaryotic cell membranes are known as lipid rafts. At lower than 40% cholesterol concentration in the liposomes, antibodies tend not to locate the cholesterol as it is hidden in the phospholipids [166, 167, 210]. Monoclonal IgG and IgM antibodies to cholesterol have been developed by immunizing animals with high cholesterol concentrations in liposomes [166, 167]. Such antibodies have the ability to recognize and bind to areas of high cholesterol concentration, such as the lipid rafts of immune cells and even lipoproteins [166]. Rather than binding to single cholesterol molecules, these antibodies tend to bind to cholesterol clusters [170]. Antibodies to cholesterol have been reported to exist in all human beings, but their role in the body has not been

unequivocally determined to date. Proposals of the auto-antibodies to cholesterol playing a role in activation of complement and/ or the phagocytic system in order to remove dead cells and viruses to assist in pathological conditions seems very likely [166]. Antibodies to cholesterol become elevated during HIV-progression to AIDS, but decrease when the patient is put on anti-retrovirals. As with TB, HIV also relies on cholesterol for infection of host cells. Measles and influenza viruses are other examples where cholesterol plays a role in the progression of disease: they rely on lipid rafts for budding [210]. It could well be that the dependence on cholesterol for pathogenicity increases the immunogenicity of host cholesterol. In all these cases, targeting of nano-encapsulated drugs to cholesterol-rich foci may be beneficial for treatment. MA may therefore be a useful targeting agent in more applications than TB.

From the discussions above the specific role that anti-cholesterol and anti-MA antibodies play in TB infected individuals may be contemplated. It was reported that anti-cholesterol antibodies bind to human lipoproteins with a possible role in opsonisation and removal by scavenger macrophages [211]. From the observation that persons infected with TB have hypocholesterolemia [212], it may be concurred that anti-cholesterol antibodies may aid in the uptake of cholesterol containing lipoproteins in macrophages. A question that could be investigated in the future is whether the anti-MA antibodies assist in this process. This could be a possible mechanism in which the *M.tb* bacteria use the host in order to accumulate cholesterol in the macrophages that it infected. Thus, in order to understand the strategy of MA targeting, it may be necessary to take a look into how the pathogen uses the lipid metabolism to create a cholesterol rich environment that enables the survival of *M. tb* in the persistent state.

Cholesterol was recently shown to play a very important role in *M.tb* infection as it can be utilised as a carbon and energy source for the mycobacteria. The bacteria need to adapt to their nutrient environment during the cycle of infection, persistence and

spread. In nutrient poor conditions the mycobacteria are able to convert their nutrient dependence towards the use of mainly cholesterol [125, 148, 155]. Another benefit to the pathogen that is gained from cholesterol, is its incorporation into the free lipid zone of the cell wall of *M.tb*, to affect cell wall permeability. In this way, uptake of antagonist compounds such as RIF is inhibited [148]. This may especially be important to gain a competitive advantage over other antibiotic-producing microorganisms that may compete for infecting the ailing host.

Lipids from the host play an important role in mycobacterial pathogenesis. In one study it was shown that when the *M.tb* infection reached the chronic phase, the bacteria produce intracellular lipophilic inclusions [85]. Bacteria in general and *M.tb* in particular, make use of the complexity of the host lipidome in order to escape the immune system [213]. In the case of *M.tb* a number of genes code for production of enzymes involved in lipogenesis and lipolysis [149]. The lipids of the host are not only used as a source of carbon but are also manipulated to enable the survival and replication of the bacteria. Inhibition of phagosome lysosome formation is an important mechanism that *M.tb* uses to be able to survive within the macrophages. Various mechanisms have been identified that contribute to the inhibition of phagolysosome formation that have been described in a recent review of Van der Meer-Jansen *et al.* [213]. The feature that interested our group was where host cholesterol plays a role in the virulence of the bacteria.

Cholesterol could influence the interaction between the pathogen and its host in the membrane-trafficking pathways. Host cholesterol mediates the binding of TACO, an actin binding protein [214], on live mycobacteria-containing phagosomes in order to prevent lysosomal degradation of the mycobacteria [81, 96, 154]. TACO is not only retained by cholesterol from the host but is also actively retained on the phagosomes by the mycobacterial protein, coronin interacting protein (CIP)50 or later identified as lipoamide dehydrogenase C (LpdC) [215]. LpdC is the E3 component of the pyruvate dehydrogenase complex. Cholesterol depletion of the phagosome membrane inhibited

the TACO – LpdC interaction showing the cholesterol dependence of the association [215]. TACO is responsible for activating the Ca^{2+} dependent phosphatase calcineurin. This leads to the inhibition of lysosomal delivery [90, 213, 216]. In previous studies it was shown that upon cholesterol depletion of pre-existing phagosomes, the close apposition between the phagosome membrane and the mycobacterial surface is loosened and fusion with lysosomes occur [96]. Thus from the observations from literature it can be expected that cholesterol will not only concentrate around the granulomas of the infected macrophages but also within the macrophages on the phagosome membrane of active *M.tb* [14, 80, 81, 96, 126, 151]. Cholesterol was also shown to accumulate in the free lipid zone of the cell walls of the bacteria and that the accumulation affected cell wall permeability [148]. Therefore there is an accumulation of cholesterol from the outside of the granuloma to the inside of the macrophage, up to the bacterial cell wall.

In this study it was shown that no individual synthetic MA subclass was responsible for the cholesterol nature of the MA. All the antigenic synthetic MA subclasses contribute to the cholesterol nature, whether tested separately or as a mixture as it exists in the natural MA. The importance of antigenic configuration of MA, stabilized through hydrogen bonding at the carboxylic acid moiety of the MA, was indicated by the effect that carboxylic acid modification had on the biological activity of the MA molecule. Furthermore a structure-function relationship between the stereochemistry and the antigenicity/cholesterol nature of the synthetic mycolic acids were observed. Recent ELISA evidence from monoclonal antibody scFv fragments generated from a chicken antibody gene library against MA's indicated that one antibody cross-reacted with cholesterol and the other not, indicating a mixture of anti-cholesterol and anti-MA antibodies in human patient serum or a single antibody with cross-reactive specificity [217].

In this thesis, the structure of synthetic mycolic acids in relation to their antigenicity in tuberculosis was determined. The attraction of MA to cholesterol might be due to their hydrophobic nature (Van der Waals forces) or through a more specific hydrogen

bonding by the structural features of both molecules [121]. Keto MA exhibited a W-shaped configuration with exceptional rigidity in Langmuir monolayers, whereas methoxy- and alpha-MA exhibited a more flexible conformation towards variation of experimental parameters [102, 103]. Therefore the packing of MA appears to be influenced by the orientation of the functional groups. MA appears to assume different conformations for interaction with antibodies in sera. The results obtained showed that the methoxy MA of *M.tb* had the strongest functional antigenicity. This property is so specific, that even the stereochemistry on the functional groups on the mero chain influenced the binding activity. However, the functional groups or their chemical modifications on the distal position did not hold the key to differentiate between antigenicity or the cholesterol nature of MA. TB negative serum also bound best to that synthetic MA homologue that was recognised best by TB positive patient serum. If the antibody cross-reactivity to cholesterol [118] is taken into consideration, the argument can be made that the methoxy MA also has the highest cholesterol cross-reactivity. This may imply that methoxy MA may also be the strongest cholesterol attractor. It is likely that a surface created by packed mycolic acids is likely to be the structure that is recognized by antibodies, similar to the case of monoclonal antibody recognition of cholesterol [170]. MA subclasses are present in mixtures in *M.tb* and it may well be that different types and variations of MA subclasses form part of an overall structure, such that the natural mycolic acid antigen(s) may never be re-made synthetically by the use of a single species of pure synthetic mycolic acid homologue.

The contribution that our research is able to make is to specifically target PLGA nano-encapsulated anti-TB drugs to TB infected macrophages. The uptake of drugs by infected macrophages would not only be enhanced by the synthetic PLGA polymer carrier vehicle but also by the presence of MA that may facilitate opsonisation of the nanoparticles for macrophage uptake mainly at the site of MA antigen production. In addition, the cholesterol nature of MA and its ability to bind cholesterol could also cause a physical attraction to the cholesterol rich sites of persistent *M.tb* infection.

The objective in this study was to determine the feasibility of encapsulating anti-TB chemotherapies into nanoparticles together with MA that will be taken up by macrophages with little or no toxicity to the host. Successful encapsulation of 14% INH together with MA was achieved with the double emulsion-solvent evaporation freeze drying technique used, resulting in a negative zeta potential that may prevent unwanted agglomeration [32, 33]. The percentages of the INH and MA inside of the nanoparticles were not optimised for the purpose of this study. It was shown that the particles were taken up into macrophages with little toxicity to the cells. The results reported here corroborate those of others who have demonstrated the uptake of various formulations of PLGA drug carriers by macrophage cell lines [32, 186, 199].

Endocytic traffic studies indicated that the endpoint of the MA containing nanoparticles was not the lysosomes, but it is not yet confirmed whether the particles actually end up in the cytoplasm or not. We speculate that the particles may probably escape into the cytoplasm, in accordance with a report that showed that endo-lysosomal escape of PLGA nanoparticles was possible by a mechanism of surface cationization [29]. It would be favourable for our particles to reside in the cytoplasm and not be degraded in the lysosomes, as the nanoparticle should preferably be slowly degraded to result in a sustained therapeutic effect. Additional experiments are warranted to further elucidate particle trafficking. For instance, it would be interesting to learn if the MA present in the cytoplasm of the macrophage could interfere with the LpdC–TACO association. With MA and cholesterol having an affinity to one another, they could compete for binding to the LpdC protein that may affect the way that phagolysosome formation is avoided.

The BACTEC studies that were conducted, aimed at determining the efficiency of the nanoencapsulated INH to kill and suppress the growth of *M.tb* in the infected macrophage. It also determined how this may be influenced by the simultaneous inclusion of MA in the nanocapsules. Targeting efficiency of the MA was not tested, as the required physiological conditions were not observed *in vitro*. These include the

presence of antibodies to MA and cholesterol in the patient, as well as the establishment of cholesterol-rich foci around tubercles in the persistent phase of tuberculosis. Experiments to determine the efficiency of the MA as targeting ligand fell beyond the scope of this thesis at this stage. The experimental work was done to illustrate the plausibility to encapsulate the MA into the nanoparticles without negatively affecting uptake or toxicity of the particles. It prepares the way for an investigation to determine whether targeting of the anti-TB drug containing nanoparticles to the sites of infection can be effected with MA inclusion.

In this study the cholesteroid nature of MA was confirmed. It was demonstrated how this related to the fine structure of the MA and how dependent the cholesteroid nature of MA was to structural changes of natural mixed MA. This was done by measuring its recognition by Amphotericin B after chemical modification. In particular, it demonstrated that MA could be made fluorescent by esterification to fluorescein via the MA carboxylic acid, without significantly changing its cholesteroid nature. This prepares the way to use fluorescein labelled MA in extracellular and intracellular trafficking studies in future. In addition, the structure of synthetic mycolic acids in relation to their antigenicity in tuberculosis was determined showing that methoxy MA associated the most with antibodies in both TB positive and TB negative patient serum. MA containing nanoparticles were synthesized and assembled successfully and were shown *in vitro* to be taken up in macrophage cell lines, without the MA hindering the uptake of the particles. The toxicity of the MA containing nanoparticles was only slightly worse than that of the nanoparticles alone. This investigation into the feasibility of forming MA containing nanoparticles therefore paves the way for testing MA as a ligand to target anti-TB drugs to mycobacterially infected macrophages in human TB patients.

This MA project forms part of a collaborative programme between the CSIR and the University of Pretoria. Animal studies investigating the immunogenicity of MA and the nanoparticle carrier compared to other carrier vehicles for MA is underway. The

contribution that this programme makes in the larger health strategy of the CSIR is in the investigation of MA and its ability to be used as a ligand for targeted drug delivery. Continuation of this project aims to address the issue of persistence of TB infection that is the major cause of long term therapy. When properly understood, the ideal of shortening the anti-TB therapy regime may eventually be realised. It is not excluded that MA may play a crucial role in the persistence of TB, the understanding of which may provide new direction towards efficient TB therapy by making use of targeted drug delivery.

References

1. WHO, *Global tuberculosis control: epidemiology, strategy, financing : WHO report*. WHO/HTM/TB/2009.411, 2009.
2. Crubezy, E., Ludes, B., Poveda, J., Clayton, J., Crouau-Roy, B., Montagnon D., *Identification of Mycobacterium DNA in an Egyptian Pott's disease of 5 400 years old*. C. R. Acad. Sci. Paris, Sciences de la vie / Life Sciences, 1998. **321**: p. 941-951.
3. Donoghue, H.D., Lee, O.Y-C., Minnikin, D.E., Besra, G.S., Taylor, J.H., Spigelman, M., *Tuberculosis in Dr Granville's mummy: a molecular re-examination of the earliest known Egyptian mummy to be scientifically examined and given a medical diagnosis*. Proc R Soc B, 2010. **277**: p. 51-56.
4. Koch, R., *Die Aetiologie der Tuberkulose*. Berliner Klinischen Wochenschrift, 1882. **15**: p. 221-230.
5. Tuberculosis, *In Encyclopædia Britannica*. 2010, www.britannica.com/EBchecked/topic/608235/tuberculosis/253299/Tuberculosis-through-history.
6. Mccarthy, O.R., *The key to the sanatoria*. J R Soc Med, 2001. **94**: p. 413-417.
7. Andrews, J., Basu, S., Scales, D., Smith-Rohrberg Maru, D., *XDR-TB in South Africa*. PLOS Medicine, 2007. **4**: p. 770-771.
8. Wise, J., *Southern Africa is moving swiftly to combat the threat of XDR-TB*. Bull World Health Organ, 2006. **84**: p. 924-925.
9. Calver, A.D., Falmer, A.A., Murray, M., Strauss, O.J., Streicher, E.M., Hanekom, M., Liversage, T., Masibi, M., van Helden, P.D., Warren, R.M., Victor, T.C., *Emergence of increased resistance and extensively drug-resistant tuberculosis despite treatment adherence, South Africa*. Emerg Infect Dis, 2010. **16**(2): p. 264-271.
10. Department of Health. *The South African national tuberculosis control programme practical guidelines*. 2004.
11. Dick, T., *Dormant tubercle bacilli: the key to more effective TB chemotherapy?* J Antimicrob Chemother, 2001. **47**: p. 117-118.
12. Parrish, N.M., Dick, J.D., Bishai, W.R., *Mechanisms of latency in Mycobacterium tuberculosis*. Trends Microbiol, 1998. **6**: p. 107-112.
13. Barry 3rd, C.E., Boshoff, H.I., Dartois, V., Dick, T., Ehrt, S., Flynn, J., Schnappinger, D., Wilkinson, R.J., Young, D., *The spectrum of latent tuberculosis: rethinking the biology and intervention strategies*. Nature Rev, 2009. **7**: p. 845-855.
14. Korf, J., Stoltz, A., Verschoor, J.A., De Baetselier, P., Grooten, J., *The Mycobacterium tuberculosis cell wall component mycolic acid elicits pathogen-associated host innate immune responses*. Eur J Immunol, 2005. **35**: p. 890-900.
15. Cardona, P.J., *RUTI: A new chance to shorten the treatment of latent tuberculosis infection*. Tuberculosis, 2006. **86**: p. 272-289.
16. Sosnik, A., Carcaboso, A.M., Glisoni, R.J., Moretton, M.A., Chiappetta, D.A., *New old challenges in tuberculosis: Potentially effective nanotechnologies in drug delivery*. Adv Drug Deliv Rev, 2009. **62**: p. 547-559.
17. Nardell, E.A., *The Merck Manual Online*. 2009, www.merck.com/mmpe/sec14/ch179/ch179b.html.

References

18. Dye, C., *Global epidemiology of tuberculosis*. Lancet, 2006. **367**: p. 938-940.
19. Zignol, M., Hosseini, M.S., Wright, A., Lambregts-van Weezenbeek, C., Nunn, P., Watt, C.J., Williams, B.G., Dye, C., *Global incidence of multidrug-resistant tuberculosis*. J Infect Dis, 2006. **194**: p. 479-485.
20. McIlleron, H., Meintjes, G., Burman, W.J., Maartens, G., *Complications of antiretroviral therapy in patients with tuberculosis: Drug interactions, toxicity, and immune reconstitution inflammatory syndrome*. J Infect Dis, 2007. **196**: p. S63-75.
21. Rastogi, N., Goh, K.S., Horgen, L., Barrow W.W., *Synergistic activities of antituberculosis drugs with cerulenin and trans-cinnamic acid against Mycobacterium tuberculosis*. FEMS Immunol Med Microbiol, 1998. **21**: p. 149-157.
22. Maartens, G., Wilkinson, R.J., *Tuberculosis*. Lancet, 2010. **370**: p. 2030-43.
23. Barry 3rd, C.E., *New horizons in the treatment of tuberculosis*. Biochem Pharmacol, 1997. **54**(11): p. 1165-1172.
24. Ramsden, J.J., *What is nanotechnology?* . Nanotechnology Perceptions, 2005. **1**: p. 3-17.
25. Wagner, V., Dullaart, A., Bock, A.,Zweck, A., *The emerging nanomedicine landscape*. Nat Biotechnol, 2006. **10**: p. 1211-1217.
26. Bangham, A.D., Standish, M.M., Watkins, J.C., *Diffusion of univalent ions across the lamellae of swollen phospholipids*. J Mol Biol, 1965. **13**: p. 238-252.
27. Langer, R., Folkman, J., *Polymers for the sustained release of proteins and other macromolecules*. Nature, 1976. **263**: p. 797-800.
28. Farokhzad, O.C., Langer, R., *Impact of nanotechnology on drug delivery*. ACSNANO, 2009. **3**: p. 16-20.
29. Panyam, J., Zhou, W., Prabha, S., Sahoo, S.K., Labhasetwar, V., *Rapid endo-lysosomal escape of poly(DL-lactide-coglycolide) nanoparticles: implications for drug and gene delivery*. FASEB J, 2002. **16**: p. 1217-1226.
30. Alexis, F., Pridgen, E., Molnar, L.K., Farokhzad, O.C., *Factors Affecting the Clearance and Biodistribution of Polymeric Nanoparticles*. Mol Pharmaceutics, 2008. **5**: p. 505-515.
31. Storm, G., Belliot, S.O., Daemen, T., Lasic, D.D., *Surface modification of nanoparticles to oppose uptake by the mononuclear phagocytic system*. Adv Drug Deliv Rev, 1995. **17**: p. 31-48.
32. Gomes, A.J., Faustino, A.S., Machado, A.E., Zaniquelli, M.E., de Paula Rigoletto, T., Lunardi, C.N., Lunardi, L.O., *Characterization of PLGA microparticles as a drug carrier for 3-ethoxycarbonyl-2h-benzofuro[3,2-f]-1-benzopyran-2-one. Ultrastructural study of cellular uptake and intracellular distribution*. Drug Deliv, 2006. **13**: p. 447-54.
33. Ravi Kumar, M.N.V., Bakowsky, U., Lehr, C.M., *Preparation and characterization of cationic PLGA nanospheres as DNA carriers*. Biomaterials, 2004. **25**: p. 1771-1777.
34. Soppimath, K.S., Aminabhavi, T. M., Kulkarni, A. R., Rudzinski, W. E., *Biodegradable polymeric nanoparticles as drug delivery devices*. J Control Release, 2001. **70**: p. 1-20.
35. Kumari, A., Yadav, S.K., Yadav, S.C., *Biodegradable polymeric nanoparticles based drug delivery systems*. Colloid Surface B, 2010. **75**: p. 1-18.

References

36. Mohanraj, V.J., Chen, Y., *Nanoparticles - A review*. Trop J Pharm Res, 2006. **5**: p. 561-573.
37. Look, M., Bandyopadhyay, A., Blum, J.S., Fahmy, T.M., *Application of nanotechnologies for improved immune response against infectious diseases in the developing world*. Adv Drug Deliv Rev, 2009. **62**: p. 378-393.
38. Constantinides, P.P., Chaubal, M.V., Shorr, R., *Advances in lipid nanodispersions for parenteral drug delivery and targeting*. Adv Drug Deliv Rev, 2008. **60**: p. 757-767.
39. Cheng, J., Teply, B.A., Sherifi, I., Sung, J., Luther, G., Gu, F.X., Levy-Nissenbaum, E., Radovic-Moreno, A.F., Langer, R., Farokhzad, O.C., *Formulation of functionalized PLGA-PEG nanoparticles for in vivo targeted drug delivery*. Biomaterials, 2007. **28**: p. 869-876.
40. Montet, X., Weissleder, R., Josephson, L., *Imaging pancreatic cancer with a peptide-nanoparticle conjugate targeted to normal pancreas*. Bioconjugate Chem, 2006. **17**: p. 905-911.
41. Shamsipour, F., Zarnani, A.H., Ghods, R., Chamankhah, M., Forouzesh, F., Vafaei, S., Bayat, A.A., Akhondi, M.M., Oghabian, M.A., Jeddi-Tehrani, M., *Conjugation of monoclonal antibodies to super paramagnetic iron oxide nanoparticles for detection of her2/neu antigen on breast cancer cell lines*. Avicenna J Med Biotech, 2009. **1**(1): p. 27-31.
42. Leroux, J., Allemann, E., De Jaeghere, F., Doelker, E. Gurny, R., *Biodegradable nanoparticles from sustained release formulations to improved site specific drug delivery*. J Control Release, 1996. **39**: p. 339-350.
43. Owens, D.E., Peppas, N.A., *Opsonization, biodistribution, and pharmacokinetics of polymeric nanoparticles*. Int J Pharm, 2006. **307**: p. 93-102.
44. Shenoy, D.B., Amiji, M.M., *Poly(ethylene oxide)-modified poly(ε-caprolactone) nanoparticles for targeted delivery of tamoxifen in breast cancer*. Int J Pharm, 2005. **293**: p. 261-270.
45. Gulyaev, A.E., Gelperina, S.E., Skidam, I.N., Antropov, S., Kivman, G.Y., Kreuter, J., *Significant transport of doxorubicin into the brain with polysorbate 80 - coated nanoparticles*. Pharm Res, 1999. **16**: p. 1564-1569.
46. Nayar, R., Fidler, I.J., *The systemic activation of macrophages by liposomes containing immunomodulators*. Springer Semin Immunopathol, 1985. **8**: p. 412-428.
47. Raz, A., Bucana, C., Fogler, W.E., Poste, G., Fidler, I., *Biochemical, morphological, and ultrastructural studies on the uptake of liposomes by murine macrophages*. Cancer res, 1981. **41**: p. 487-494.
48. Tomalia, D.A., *Birth of a new macromolecular architecture: dendrimers as quantized building blocks for nanoscale synthetic polymer chemistry*. Prog Polym Sci, 2005. **30**: p. 294-324.
49. Jain, C.P., Vyas, S.P., Dixit, V.K., *Niosomal system for delivery of rifampicin to lymphatics*. Indian J Pharm Sci 2006. **68**: p. 575-578.
50. Pandey, R., Khuller, G.K., *Solid lipid particle based inhalable sustained drug delivery system against experimental tuberculosis*. Tuberculosis, 2005. **85**: p. 227-234.
51. Panyam, J., Labhasetwar, V., *Biodegradable nanoparticles for drug and gene delivery to cells and tissue*. Adv Drug Deliv Rev, 2003. **55**: p. 329-47.
52. Sahoo, S.K., Labhasetwar, V., *Nanotech approaches to drug delivery and imaging*. Drug Discov Today, 2003. **8**: p. 1112-1120.

References

53. Artursson, P., Lindmark, T., Davis, S.S., Illum, L., *Effect of chitosan on the permeability of monolayers of intestinal epithelial cells*. *Pharm Res*, 1994. **11**: p. 1358-1361.
54. Tsung, M.J., Burgess, D. J., *Preparation and characterization of gelatin surface modified PLGA microspheres*. *AAPS Pharm Sci*, 2001. **3**: p. E11.
55. Jain, R.A., *The manufacturing techniques of various drug loaded biodegradable poly(lactide-co-glycolide) (PLGA) devices*. *Biomaterials*, 2000. **21**: p. 2475-90.
56. Derakhshandeh, K., Erfan, M., Dadashzadeh, S., *Encapsulation of 9-nitrocamptothecin, a novel anticancer drug, in biodegradable nanoparticles: Factorial design, characterization and release kinetics*. *Eur J Pharm Biopharm*, 2007. **66**: p. 34-41.
57. Sahoo, S.K., Panyam, J., Prabha, S., Labhasetwar, V., *Residual polyvinyl alcohol associated with poly (D,L-lactide-co-glycolide) nanoparticles affects their physical properties and cellular uptake*. *J Control Release*, 2002. **82**: p. 105-114.
58. Tracy, M.A., Ward, K.L., Firouzabadian, L., Wang, Y., Dong, N., Qian, R., Zhang, Y., *Factors affecting the degradation rate of poly(lactide-co-glycolide) microspheres in vivo and in vitro*. *Biomaterials*, 1999. **20**: p. 1057-1062.
59. Labhasetwar, V., Song, C., Humphrey, W., Shebuski, R., Levy, R. J., *Arterial uptake of biodegradable nanoparticles: effect of surface modifications*. *J Pharm Sci*, 1998. **87**: p. 1229-34.
60. Song, C.X., Labhasetwar, V., Murphy, H., Qu, X., Humphrey, W.R., Shebuski, R.J., Levy, R.J., *Formulation and characterization of biodegradable nanoparticles for intravascular local drug delivery*. *J Control Release*, 1997. **43**: p. 197-212.
61. Thapa, P., Zhang, G., Xia, C., Gelbard, A., Overwijk, W.W., Liu, C., Hwu, P., Chang, D.Z., Courtney, A., Sastry, J.K., Wang, P.G., Li, C., Zhou, D., *Nanoparticle formulated alpha-galactosylceramide activates NKT cells without inducing anergy*. *Vaccine*, 2009. **27**: p. 3484-3488.
62. Arias-Negrete, S., Keller, K., Chadee, K., *Proinflammatory cytokines regulate cyclooxygenase-2 mRNA expression in human macrophages*. *Biochem Biophys Res Commun*, 1995. **208**: p. 582-9.
63. Fonseca, C., Simoes, S., Gaspar, R., *Paclitaxel-loaded PLGA nanoparticles: preparation, physicochemical characterization and in vitro anti-tumoral activity*. *J Control Release*, 2002. **83**: p. 273-286.
64. Di Toro, R., Betti, V., Spampinato, S., *Biocompatibility and integrin-mediated adhesion of human osteoblasts to poly(DL-lactide-co-glycolide) copolymers*. *Eur J Pharm Sci*, 2004. **21**: p. 161-169.
65. Damgé, C., Maincent, P., Ubrich, N., *Oral delivery of insulin associated to polymeric nanoparticles in diabetic rats*. *J Control Release*, 2007. **117**: p. 163-170.
66. Sarmiento, B., Ribeiro, A., Veiga, F., Sampaio, P., Neufeld, R., Ferreira, D., *Alginate/Chitosan Nanoparticles are Effective for Oral Insulin Delivery*. *Pharm Res*, 2007. **24**: p. 2198-2206.
67. Silva, M., Ferreira, E.I., Leite, C.Q.F., Sato, D.N., *Preparation of Polymeric Micelles for Use as Carriers of Tuberculostatic Drugs*. *Trp J Pharm Res*, 2007. **6**: p. 815-824.
68. Azarmi, S., Roa, W.H., Löbenberg, R., *Targeted delivery of nanoparticles for the treatment of lung diseases*. *Adv Drug Deliv Rev*, 2008. **60**: p. 863-875.

References

69. Ohashi, K., Kabasawa, T., Ozeki, T., Okada, H., *One-step preparation of rifampicin/poly(lactic-co-glycolic acid) nanoparticle-containing mannitol microspheres using a four-fluid nozzle spray drier for inhalation therapy of tuberculosis*. J Control Release, 2009. **135**: p. 19-24.
70. Kumar, P.V., Asthana, A., Dutta, T., Jain, N.K., *Intracellular macrophage uptake of rifampicin loaded mannosylated dendrimers*. J Drug Target, 2006. **14**: p. 546-556.
71. Peters, K., Leitzke, S., Diederichs, J.E., Borner, K., Hahn, H., Muller, R.H., Ehlers, S., *Preparation of a clofazimine nanosuspension for intravenous use and evaluation of its therapeutic efficacy in murine Mycobacterium avium infection*. J Antimicrob Chemother, 2000. **45**: p. 77-83.
72. Oh, Y., Nix, D.E., Straubinger, R.M., *Formulation and efficacy of liposome-encapsulated antibiotics for therapy of intracellular Mycobacterium avium infection*. Antimicrob Agents Chemother, 1995. **39**: p. 2104-2111.
73. Russell, D.G., Cardona, P., Kim, M., Allain, S., Altare, F., *Foamy macrophages and the progression of the human tuberculosis granuloma*. Nat Immunol, 2009. **10**: p. 943-948.
74. Ernst, J.D., *Macrophage receptors for Mycobacterium tuberculosis*. Infect Immun, 1998. **66**: p. 1277-1281.
75. Zimmerli, S., Edwards, S., Ernst, J.D., *Selective receptor blockade during phagocytosis does not alter the survival and growth of Mycobacterium tuberculosis in human macrophages*. Am J Respir Cell Mol Biol, 1996. **15**: p. 760-770.
76. Yamaguchi, Y., Kunitomo, M., Haginaka, J., *Assay methods of modified lipoproteins in plasma*. J Chromatogr B 2002. **781**: p. 313-330.
77. Suzuki, H., Kurihara, Y., Takeya, M., Kamada, N., Kataoka, M., Jishage, K., Ueda, O., Sakaguchi, H., Higashi, T., Suzuki, T., Takashima, Y., Kawabe, Y., Cynshi, O., Wada, Y., Honda, M., Kurihara, H., Aburatani, H., Doi, T., Matsumoto, A., Azuma, S., Noda, T., Toyoda, Y., Itakura, H., Yazaki, Y., Horiuchi, S., Takahashi, K., Kruijt, J.K., van Berkel, T.J.C., Steinbreger, U.P., Ishibashi, S., Maeda, N., Gordon, S., Kodama, T., *A role for macrophage scavenger receptors in atherosclerosis and susceptibility to infection*. Nature, 1997. **386**: p. 292-296.
78. Majumdar, S., Basu, S.K., *Killing of intracellular Mycobacterium tuberculosis by receptor-mediated drug delivery*. Antimicrob Agents Chemother, 1991. **35**: p. 135-140.
79. Chono, S., Tanino, T., Seki, T., Morimoto, K., *Efficient drug targeting to rat alveolar macrophages by pulmonary administration of ciprofloxacin incorporated into mannosylated liposomes for treatment of respiratory intracellular parasitic infections*. J Control Release, 2008. **127**: p. 50-58.
80. Av-Gay, Y., Sobouti, R., *Cholesterol is accumulated by mycobacteria but its degradation is limited to non-pathogenic fast-growing mycobacteria*. Can J Microbiol, 2000. **46**: p. 826-831.
81. Gatfield, J., Pieters, J., *Essential role for cholesterol in entry of mycobacteria into macrophages*. Science, 2000. **288**: p. 1647-1650.
82. Peyron, P., Vaubourgeix, J., Poquet, Y., Levillain, F., Botanch, C., Bardou, F., Daffe, M., Emile, J., Marchou, B., Cardona, P., de Chastellier, C., Altare, F., *Foamy macrophages from tuberculous patients granulomas constitute a nutrient-rich reservoir for M.tuberculosis persistence*. PLOS Pathogens, 2008. **4**: p. e1000204.

References

83. Astarie-Dequeker, C., Le Guyader, L., Malaga, W., Seaphanh, F., Chalut, C., Lopez, A., Guilhot, C., *Phthiocerol Dimycocerosates of M. tuberculosis participate in macrophage invasion by inducing changes in the organization of plasma membrane lipids*. PLOS Pathogens, 2009. **5**: p. e1000289.
84. Kurup, I.G., Mahadevan, P.R., *Cholesterol metabolism of macrophages in relation to the presence of Mycobacterium leprae*. J Biosci, 1982. **4**: p. 307–316.
85. Caceres, N., Tapia, G., Ojanguren, I., Altare, F., Gil, O., Pinto, S., Vilaplana, C., Cardona, P., *Evolution of foamy macrophages in the pulmonary granulomas of experimental tuberculosis models*. Tuberculosis, 2009. **89**: p. 175-182.
86. Peyron, P., Bordier, C., N'Diaye, E., Maridonneau-Parini, I., *Nonopsonic phagocytosis of mycobacterium kansasii by human neutrophils depends on cholesterol and is mediated by CR3 associated with glycosylphosphatidylinositol-anchored proteins*. J Immunol, 2000. **165**: p. 5186–5191.
87. Russell, D.G., Mwandumba, H.C., Rhoades, E.E., *Mycobacterium and the coat of many lipids*. J Cell Biol, 2002. **158**: p. 421–426.
88. Ferrari, G., Langen, H., Naito, M., Pieters, J., *A coat protein on phagosomes involved in the intracellular survival of mycobacteria*. Cell, 1999. **97**: p. 435-447.
89. Pieters, J., Gatfield, J., *Hijacking the host: survival of pathogenic mycobacteria inside macrophages*. Trends Microbiol, 2002. **10**: p. 142-146.
90. Jayachandran, R., Sundaramurthy, V., Combaluzier, B., Mueller, P., Korf, H., Huygen, K., Miyazaki, T., Albrecht, I., Massner, J., Pieters, J., *Survival of mycobacteria in macrophages is mediated by coronin 1-dependent activation of calcineurin*. Cell, 2007. **130**: p. 37–50.
91. Pieters, J., *Evasion of host cell defense mechanisms by pathogenic bacteria*. Curr Opin Immunol, 2001. **13**: p. 37-44.
92. Kaul, D., Anand, P.K., Verma, I., *Cholesterol-sensor initiates M. tuberculosis entry into human macrophages*. Mol Cell Biochem, 2004. **258**: p. 219–222.
93. Kaul, D., *Coronin-1A epigenomics governs mycobacterial persistence in tuberculosis*. FEMS Microbiol Lett, 2008. **278**: p. 10-14.
94. De Chastellier, C., Lang, T., Thilo, L., *Phagocytic processing of the macrophage endoparasite, Mycobacterium avium, in comparison to phagosomes which contain Bacillus subtilis or latex beads*. Eur J Cell Biol, 1995. **68**: p. 167-182.
95. De Chastellier, C., Thilo, L., *Phagosome maturation and fusion with lysosomes in relation to surface property and size of the phagocytic particle*. Eur J Cell Biol, 1997. **74**: p. 49-62.
96. De Chastellier, C., Thilo, L., *Cholesterol depletion in Mycobacterium avium - infected macrophages overcome the block in phagosome maturation and leads to the reversible sequestration of viable mycobacteria in phagolysosome derived autophagic vacuoles*. Cell Microbiol, 2006. **8**: p. 242-256.
97. Sekanka, G., Baird, M., Minnikin, D., Grooten, J., *Mycolic acids for the control of tuberculosis*. Expert Opin Ther Patents, 2007. **17**: p. 315-331.
98. Berg, S., Kaur, D., Jackson, M., Brennan, P.J., *The glycosyltransferases of Mycobacterium tuberculosis—roles in the synthesis of arabinogalactan, lipoarabinomannan, and other glycoconjugates*. Glycobiology, 2007. **17**: p. 35R–56R.

References

99. Minnikin, D.E., Kremer, L., Dover, L.G., Besra, *The methyl-branched fortifications of Mycobacterium tuberculosis*. Chem Biol, 2002. **9**: p. 545-553.
100. Lambert, P.A., *Cellular impermeability and uptake of biocides and antibiotics in Gram-positive bacteria and mycobacteria*. J Appl Microbiol, 2002. **92**(Suppl): p. 46S-54S.
101. Minnikin, D.E., Minnikin, S.M., Parlett, J.H., Goodfellow, M., Magnusson, M., *Mycolic acid patterns of some species of Mycobacterium*. Arch Microbiol, 1984. **139**: p. 225-231.
102. Villeneuve, M., Kawai, M., Kanashima, H., Watanabe, M., Minnikin, D.E., Nakahara, H., *Temperature dependence of the Langmuir monolayer packing of mycolic acids from Mycobacterium tuberculosis*. Biochim Biophys Acta, 2005. **1715**: p. 71-80.
103. Villeneuve, M., Kawai, M., Watanabe, M., Aoyagi, Y., Hitotsuyanagi, Y., Takeya, K., Gouda, H., Hirono, S., Minnikin, D.E., Nakahara, H., *Conformational behavior of oxygenated mycobacterial mycolic acids from Mycobacterium bovis BCG*. Biochim Biophys Acta, 2007. **1768** p. 1717–1726.
104. Takayama, K., Wang, C., Besra, G.S., *Pathway to synthesis and processing of mycolic acids in Mycobacterium tuberculosis*. Clin Microbiol Rev, 2005. **18**: p. 81-101.
105. Barry 3rd, C.E., Lee, R.E., Mdluli, K., Sampson, A.E., Schroeder, B.G., Slayden, R.A., Yuan, Y. *Mycolic acids: structure, biosynthesis and physiological functions*. Prog Lipid Res, 1998. **37**: p. 143-179.
106. Asselineau, C., Asselineau, J., Laneelle, G., Laneelle, M.A., *The biosynthesis of mycolic acids by mycobacteria: current and alternative hypotheses*. Prog Lipid Res, 2002. **41**: p. 501-523.
107. Belisle, J.T., Vissa, V.D., Sievert, T., Takayama, K., Brennan, P.J., Besra, G.S., *Role of the major antigen of Mycobacterium tuberculosis in cell wall biogenesis*. Science, 1997. **276**: p. 1420-1422.
108. Dubnau, E., Chan, J., Raynaud, C., Mohan, V. P., Laneelle, M.A., Yu, K., Quemard, A., Smith, I., Daffe, M., *Oxygenated mycolic acids are necessary for virulence of Mycobacterium tuberculosis in mice*. Mol Microbiol, 2000. **36**: p. 630-637.
109. Fujita, Y., Okamoto, Y., Uenishib, Y., Sunagawab, M., Uchiyamac, T., Yano, I., *Molecular and supra-molecular structure related differences in toxicity and granulomatogenic activity of mycobacterial cord factor in mice*. Microb Pathog, 2007. **43**: p. 10-21.
110. Liu, J., Barry 3rd, C.E., Besra, G.S., Nikaido, H., *Mycolic acid structure determines the fluidity of the mycobacterial cell wall*. J Biol Chem, 1996. **271**: p. 29545-29551.
111. Lyashchenko, K., Colangeli, R., Houde, M., Al Jahdali, H., Menzies, D., Gennaro, M.L., *Heterogeneous antibody responses in tuberculosis*. Infect Immun, 1998. **66**: p. 3936–3940.
112. Fujiwara, N., Pan, J., Enomoto, K., Terano, Y., Honda, T., Yano, I., *Production and partial characterization of anti-cord factor (trehalose-6,6P-dimycolate) IgG antibody in rabbits recognizing mycolic acid subclasses of Mycobacterium tuberculosis or Mycobacterium avium*. FEMS Immunol Med Microbiol, 1999. **24**: p. 141-149.
113. Fujita, Y., Naka, T., McNeil, M.R., Yano, I., *Intact molecular characterization of cord factor (trehalose 6,69-dimycolate) from nine species*

References

- of mycobacteria by MALDI-TOF mass spectrometry. *Microbiology*, 2005. **151**: p. 3403–3416.
114. Shui, G., Bendt, A.K., Pethe, K., Dick, T., Wenk, M.R., *Sensitive profiling of chemically diverse bioactive lipids*. *J Lipid Res*, 2007. **48**: p. 1976–1984.
115. Yuan, Y., Crane, D.C., Musser, J.M., Sreevatsan, S., Barry 3rd, C.E., *MMAAS-1, the branch point between cis- and trans-cyclopropane containing oxygenated mycolates in Mycobacterium tuberculosis*. *J Biol Chem*, 1997. **272**: p. 10041–10049.
116. Beckman, E.V., Porcelli, S.A., Morita, C.T., Behar, S.M., Furlong, S.T., Brenner, M.B., *Recognition of a lipid antigen by CDI-restricted $\alpha\beta^+$ T cells*. *Nature*, 1994. **372**: p. 691 – 694.
117. Lemmer, Y., Thanyani, S.T., Vrey, P.J., Driver, C.H.S., Venter, L., van Wyngaardt, S., ten Bokum, A.M.C., Ozoemena, K.I., Pilcher, L.A., Fernig, D.G., Stoltz, A.C., Swai, H.S., Verschoor, J.A., *Detection of Antimycolic Acid Antibodies by Liposomal Biosensors*. *Methods Enzymol*, 2009. **464**: p. 80-102.
118. Schleicher, G.K., Feldman, C., Vermaak, Y., Verschoor, J.A., *Prevalence of anti-mycolic acid antibodies in patients with pulmonary tuberculosis co-infected with HIV*. *Clin Chem Lab Med*, 2002. **40**: p. 882-887.
119. Pan, J., Fujiwara, N., Oka, S., Maekura, R., Ogura, T., and Yano, L., *Anti-Cord Factor (Trehalose 6,6'-Dimycolate) IgG antibody in tuberculosis patients recognizes mycolic acid subclasses*. *Microbiol Immunol*, 1999. **43**: p. 863 – 869.
120. Thanyani, S.T., Roberts, V., Siko, D.G., Vrey, P., Verschoor, J.A., *A novel application of affinity biosensor technology to detect antibodies to mycolic acid in tuberculosis patients*. *J Immunol Methods*, 2008. **332**: p. 61-72.
121. Benadie, Y., Deysel, M., Siko, D. G., Roberts, V. V., Van Wyngaardt, S., Thanyani, S. T., Sekanka, G., Ten Bokum, A. M., Collett, L. A., Grooten, J., Baird, M. S., Verschoor, J. A., *Cholesteroid nature of free mycolic acids from M. tuberculosis*. *Chem Phys Lipids*, 2008. **152**: p. 95-103.
122. Indrigo, J., Hunter, R.L., Actor, J.K., *Influence of trehalose 6,6H-dimycolate (TDM) during mycobacterial infection of bone marrow macrophages*. *Microbiology*, 2002. **148**: p. 1991–1998.
123. Indrigo, J., Hunter, R.L., Actor, J.K., *Cord factor trehalose 6,69-dimycolate (TDM) mediates trafficking events during mycobacterial infection of murine macrophages*. *Microbiology* 2003. **149**: p. 2049–2059.
124. Lima, V.M.F., Bonato, V.L.D., Lima, K.M., Dos Santos, S.A., Dos Santos, R.R., Goncalves, E.D.C., Faccioli, L.H., Branda, I.T., Rodrigues, J.M., Silva, C.L., *Role of trehalose dimycolate in recruitment of cells and modulation of production of cytokines and NO in tuberculosis*. *Infect Immun*, 2001. **69**: p. 5305–5312.
125. Pandey, A.K., Sasseti, C.M., *Mycobacterial persistence requires the utilization of host cholesterol*. *P Natl Acad Sci USA*, 2008. **105**: p. 4376–4380.
126. Korf, J.E., Pynaert, G., Tournoy, K., Boonefaes, T., van Oosterhout, A., Ginneberge, D., Haegeman, A., Verschoor, J.A., De Baetseller, P., Grooten, J., *Macrophage reprogramming by mycolic acids promotes a tolerogenic response in experimental asthma*. *Am J Resp Crit Care*, 2006. **174**: p. 152 - 160.
127. Korf, H., Van der Beken, S., Romano, M., Steffensen, K.R., Stijlemans, B., Gustafsson, J., Grooten, J., Huygen, K., *Liver X receptors contribute to the*

References

- protective immune response against Mycobacterium tuberculosis in mice.* J Clin Invest 2009. **119**: p. 1626-1637.
128. Means, T.K., Lien, E., Yoshimura, A., Wang, S., Golenbock, D.T., Fenton, M.J., *The CD14 ligands of lipoarabinomannan and lipopolysaccharide differ in their requirement for Toll-like receptors.* J Immunol 1999. **163**: p. 6748-6755.
129. Means, T.K., Wang, S., Lien, E., Yoshimura, A., Golenbock, D.T., Fenton, M.J., *Human toll-like receptors mediate cellular activation by Mycobacterium tuberculosis.* J Immunol 1999. **163**: p. 3920-3927.
130. Bowdish, D.M.E., Sakamoto, K., Kim, M., Kroos, M., Mukhopadhyay, S., Leifer, C.A., Tryggvason, K., Gordon, S., Russell, D.G., *MARCO, TLR2, and CD14 are required for macrophage cytokine responses to mycobacterial trehalose dimycolate and Mycobacterium tuberculosis.* PLOS Pathogens, 2009. **5**: p. e1000474.
131. Tailleux, L., Neyrolles, O., Honore´-Bouakline, S., Perret, E., Sanchez, F., Abastado, J., Lagrange, P.H., Gluckman, J., Rosenzweig, M., Herrmann, J., *Constrained intracellular survival of Mycobacterium tuberculosis in human dendritic cells.* J Immunol, 2003. **170**: p. 1939–1948.
132. Armstrong, J.A., D'arcy Hart, P., *Phagosome-lysosome interactions in cultured macrophages infected with virulent tubercle bacilli.* J Exp Med, 1975. **142**: p. 1-15.
133. Vergne, I., Fratti, R.A., Hill, P.J., Chua, J., Belisle, J., Deretic, V., *Mycobacterium tuberculosis phagosome maturation arrest: Mycobacterial phosphatidylinositol analog phosphatidylinositol mannoside stimulates early endosomal fusion.* Mol Biol Cell, 2004. **15**: p. 751-760.
134. Axelrod, S., Oschkinat, H., Enders, J., Schlegel, B., Brinkmann, V., Kaufmann, S.H.E., Haas, H. Schaible, U.E., *Delay of phagosome maturation by a mycobacterial lipid is reversed by nitric oxide.* Cell Microbiol, 2008. **10**: p. 1530–1545.
135. Hmama, Z., Sendide, K., Talal, A., Garcia, R., Dobos, K., Reiner, N.E., *Quantitative analysis of phagolysosome fusion in intact cells: inhibition by mycobacterial lipoarabinomannan and rescue by an 1a,25-dihydroxyvitamin D3–phosphoinositide 3-kinase pathway.* J Cell Sci, 2004. **117**: p. 2131-2139.
136. Appelmelk, B.J., den Dunnen, J., Driessen, N.N., Ummels, R., Pak, M., Nigou, J., Larrouy-Maumus, G., Gurcha, S.S., Movahedzadeh, F., Geurtsen, J., Brown, E.J., Eysink Smeets, M.M., Besra, G.S., Willemsen, P.T.J., Lowary, T.L., van Kooyk, Y., Maaskant, J.J., Stoker, N.G., van der Ley, P., Puzo, G., Vandenbroucke-Grauls, C.M.J.E., Wieland, C.W., van der Poll, T., Geijtenbeek, T.B.H., van der Sar, A.M., Bitter, W., *The mannose cap of mycobacterial lipoarabinomannan does not dominate the Mycobacterium–host interaction.* Cell Microbiol, 2008. **10**: p. 930–944.
137. Beatty, W.L., Rhoades, E.R., Ullrich, H.J., Chatterjee, D., Heuser, J.E., Russell, D.G., *Trafficking and release of Mycobacterial lipids from infected macrophages* Traffic, 2000. **1**: p. 235 - 247.
138. Beatty, W.L., Ullrich, H-J., Russell, D.G., *Mycobacterial surface moieties are released from infected macrophages by a constitutive exocytic event.* Eur J Cell Biol, 2001. **80**: p. 31-40.
139. Pietersen, R., Thilo, L., de Chastellier, C., *Mycobacterium tuberculosis and Mycobacterium avium modify the composition of the phagosomal membrane*

References

- in infected macrophages by selective depletion of cell surface derived glycoconjugates.* Eur J Cell Biol, 2004. **83**: p. 153-158.
140. De Chastellier, C., *The many niches and strategies used by pathogenic mycobacteria for survival within host macrophages.* Immunobiol, 2009. **214**: p. 526–542.
 141. Ojha, A.K., Baughn, A.D., Sambandan, D., Hsu, T., Trivelli, X., Guerardel, Y., Alahari, A., Kremer, L., Jacobs Jr, W.R., Hatfull, G.F., *Growth of Mycobacterium tuberculosis biofilms containing free mycolic acids and harbouring drug-tolerant bacteria.* Mol Microbiol, 2008. **69**: p. 164–174.
 142. Ojha, A.J., Trivelli, X., Guerardel, Y., Kremer, L., Hatfull, G.F., *Enzymatic hydrolysis of trehalose dimycolate releases free mycolic acids during mycobacterial growth in biofilms.* J Biol Chem, 2010: p. doi/10.1074/jbc.M110.112813.
 143. Cardona, P.J., Llatjos, R., Gordillo, S., Diaz, J., Ojanguren, I., Ariza, A., Ausina, V., *Evolution of Granulomas in Lungs of Mice Infected Aerogenically with Mycobacterium tuberculosis.* Scand J Immunol, 2000. **52**: p. 156-163.
 144. Kondo, E., Kanai, K., *Accumulation of cholesterol esters in macrophages incubated with mycobacteria in vitro.* Jpn J Med Sci Biol, 1976 (b). **29**: p. 123-137.
 145. Cardona, P.J., Gordillo, S., Diaz, J., Tapia, G., Amat, I., Pallares, A., Vilaplana, C., Ariza, A., Ausina, V., *Widespread bronchogenic dissemination makes DBA/2 mice more susceptible than C57BL/6 mice to experimental aerosol infection with Mycobacterium tuberculosis.* Infect Immun, 2003. **71**: p. 5845-5854.
 146. Saunders, B.M., Cooper, A.M., *Restraining mycobacteria: Role of granulomas in mycobacterial infections.* Immunol Cell Biol, 2000. **78**: p. 334–341.
 147. Lamb, D.C., Kelly, D. E., Manning, N. J., Kelly, S. L., *A sterol biosynthetic pathway in Mycobacterium.* FEBS Lett, 1998. **437**: p. 142-144.
 148. Brzostek, A., Pawelczyk, J., Rumijowska-Galewicz, A., Dziadek, B., Dziadek, J., *Mycobacterium tuberculosis is able to accumulate and utilize cholesterol.* J Bacteriol, 2009. **191**: p. 6584–6591.
 149. Cole, S.T., Brosch, R., Parkhill, J., Garnier, T., Churcher, C., Harris, D., Gordon, S.V., Eiglmeier, K., Gas, S., Barry 3rd, C.E., Tekaia, F., Badcock, K., Basham, D., Brown, D., Chillingworth, T., Connor, R., Davies, R., Devlin, K., Feltwell, T., Gentles, S., Hamlin, N., Holroyd, S., Hornsby, T., Jagels, K., Barrell, B.G., *Deciphering the biology of Mycobacterium tuberculosis from the complete genome sequence.* Nature, 1998. **393**: p. 537-544.
 150. Joshi, S.M., Pandey, A.K., Capite, N., Fortune, S.M., Rubin, E.J., Sasseti, C.M., *Characterization of mycobacterial virulence genes through genetic interaction mapping.* PNAS, 2006. **103**: p. 11760–11765.
 151. Brzostek, A., Dziadek, B., Rumijowska-Galewicz, A., Pawelczyk, J., Dziadek, J., *Cholesterol oxidase is required for virulence of Mycobacterium tuberculosis.* FEMS Microbiol Lett, 2007. **275**: p. 106–112.
 152. Rengarajan, J., Bloom, B.R., Rubin, E.J., *Genome-wide requirements for Mycobacterium tuberculosis adaptation and survival in macrophages.* P Natl Acad Sci USA, 2005. **102**: p. 8327–8332.
 153. Chang, J.C., Harik, N.S., Liao, R.P., Sherman, D.R., *Identification of Mycobacterial Genes That Alter Growth and Pathology in Macrophages and in Mice.* J Infect Dis, 2007. **196**: p. 788-795.

References

154. Miner, M.D., Chang, J.C., Pandey, A.K., Sassetti, C.M., Sherman, D.R., *Role of cholesterol in Mycobacterium tuberculosis infection*. Indian J Exp Biol, 2009. **47**: p. 407-411.
155. Van der Geize, R., Yam, K., Heuser, T., Wilbrink, M.H., Hara, H., Anderton, M.C., Sim, E., Dijkhuizen, L., Davies, J.E., Mohn, W.W., Eltis, L.D., *A gene cluster encoding cholesterol catabolism in a soil actinomycete provides insight into Mycobacterium tuberculosis survival in macrophages*. P Natl Acad Sci USA, 2007. **104**: p. 1947–1952.
156. Maldonado-Garcia, G., Chico-Ortiz, M., Lopez-Mariny, L.M., Sanchez-Garcia, F.J., *High-polarity Mycobacterium avium-derived lipids interact with murine macrophage lipid rafts*. Scand J Immunol, 2004. **60**: p. 463–470.
157. Hayakawa, E., Tokumasu, F., Nardone, G.A., Jin, A.J., Hackley, V.A., Dvorak, J.A., *A Mycobacterium tuberculosis-derived lipid inhibits membrane fusion by modulating lipid membrane domains*. Biophys J, 2007. **93**: p. 4018–4030.
158. Lee, J.W., Sim, S.J., Cho, S.M., Lee, J., *Characterization of a self-assembled monolayer of thiol on a gold surface and the fabrication of a biosensor chip based on surface plasmon resonance for detecting anti-GAD antibody*. Biosens Bioelectron, 2005. **20**: p. 1422–1427.
159. Mukherjee, P.S. and H.T. Karnes, *Ultraviolet and fluorescence derivatization reagents for carboxylic acids suitable for high performance liquid chromatography: a review*. Biomed Chromatogr, 1996. **10**: p. 193-204.
160. Roberts, V.V., *Immunochemical analysis of Mycolic acid antigens in Tuberculosis*. MSc Dissertation, in Department of Biochemistry, Faculty of Natural and Agricultural Sciences. 2008, University of Pretoria: Pretoria.
161. Butler, W.R., Kilburn, J. O., *High-performance liquid chromatography patterns of mycolic acids as criteria for identification of Mycobacterium chelonae, Mycobacterium fortuitum, and Mycobacterium smegmatis*. J Clin Microbiol, 1990. **28**: p. 2094-8.
162. Baginski, M., Resat, H., Borowski, E., *Comparative molecular dynamics simulations of amphotericin B-cholesterol/ergosterol membrane channels*. Biochim Biophys Acta, 2002. **1567**: p. 63-78.
163. Yuan, y., Barry III, C.E., *A common mechanism for the biosynthesis of methoxy and cyclopropyl mycolic acids in Mycobacterium tuberculosis*. P Natl Acad Sci USA, 1996. **93**: p. 12828–12833.
164. Hervé, M., Debouzy, J.C., Borowski, E., Cybulska, B., Gary-Bobo, C.M., *The role of the carboxyl and amino groups of polyene macrolides in their interactions with sterols and their selective toxicity. A ³¹P-NMR study*. Biochim Biophys Acta, 1989. **980**: p. 261-272.
165. Matsumori, N., Umegawa, Y., Oishi, T., Murata, M., *Bioactive fluorinated derivative of amphotericin B*. Bioorg Med Chem Lett, 2005. **15**: p. 3565–3567.
166. Biro, A., Cervenak, L., Balogh, A., Lorincz, A., Uray, K., Horvath, A., Romics, L., Matko, J., Fust, G., Laszlo, G., *Novel anti-cholesterol monoclonal immunoglobulin G antibodies as probes and potential modulators of membrane raft-dependent immune functions*. J Lipid Res, 2007. **48**: p. 19-29.
167. Swartz, G.M., Gentry, M.K., Amendeo, L.M., Blanchette-Mackie. E.J., Alving, C.R., *Antibodies to cholesterol*. P Natl Acad Sci USA, 1988. **85**: p. 1902-1906.
168. Siko, D.G.R., *Mycobacterial mycolic acids as immunoregulatory lipid antigens in the resistance to tuberculosis*. PhD thesis, in Department of

References

- Biochemistry. Faculty of Natural and Agricultural Sciences* 2002, University of Pretoria: Pretoria.
169. Fielding, C.J., Fielding, P.E., *Cellular cholesterol efflux*. *Biochim Biophys Acta*, 2001. **1533**: p. 175-189.
 170. Kruth, H.S., Ifrim, I., Chang, J., Addadi, L., Perl-Treves, D., Zhang, W., *Monoclonal antibody detection of plasma membrane cholesterol microdomains responsive to cholesterol trafficking*. *J Lipid Res*, 2001. **42**: p. 1492–1500.
 171. Bogunia-Kubik, K., Sugisaka, M., *From molecular biology to nanotechnology and nanomedicine*. *Biosystems*, 2002. **65**: p. 123-38.
 172. Kisich, K.O., Gelperina, S., Higgins, M.P., Wilson, S., Shipulo, E., Oganesyanyan, E., Heifets, L., *Encapsulation of moxifloxacin within poly(butyl cyanoacrylate) nanoparticles enhances efficacy against intracellular Mycobacterium tuberculosis*. *Int J Pharm*, 2007. **345**: p. 154–162.
 173. Torchilin, V.P., *Structure and design of polymeric surfactant-based drug delivery systems*. *J Control Release*, 2001. **73**: p. 137–172.
 174. Lamprecht, A., Ubrich, N., Hombreiro Perez, M., Lehr, C-M., Hoffman, M., Maincent, P., *Biodegradable monodispersed nanoparticles prepared by pressure homogenization-emulsification*. *Int J Pharm*, 1999. **184**: p. 97-105.
 175. Brunner, T.J., Wick, P., Manser, P., Spohn, P., Grass, R.N., Limbach, L.K., Brunnink, A., Stark, W.J., *In vitro cytotoxicity of oxide nanoparticles: comparison to asbestos, silica, and the effect of particle solubility*. *Environ Sci Technol*, 2006. **40**: p. 4374-4381.
 176. Choi, J.Y., Lee, S.H., Na, H.B., An, K., Hyeon, T., Seo, T.S., *In vitro cytotoxicity screening of water-dispersible metal oxide nanoparticles in human cell lines*. *Bioproc Biosyst Eng*, 2010. **33**: p. 21-30.
 177. Merget, R., Bauer, T., Küpper, H.U., Philippou, S., Bauer, H.D., Breitstadt, R., Bruening, T., *Health hazards due to the inhalation of amorphous silica*. *Arch Toxicol* 2002. **75**: p. 625-634.
 178. Sharma, V., Shukla, R.K., Saxena, N., Parmar, D., Das, M., Dhawan, A., *DNA damaging potential of zinc oxide nanoparticles in human epidermal cells*. *Toxicol Lett*, 2009. **185**: p. 211-218.
 179. Spano, A., Monaco, G., Barni, S., Sciola, L., *Expression of cell kinetics and death during monocyte-macrophage differentiation: effects of Actinomycin D and Vinblastine treatments*. *Histochem Cell Biol*, 2007. **127**: p. 79-94.
 180. Rejman, J., Oberle, V., Zuhorn, I.S., Hoekstra, D., *Size-dependent internalization of particles via the pathways of clathrin and caveolae-mediated endocytosis*. *Biochem J*, 2004. **377**: p. 159-169.
 181. Mosiman, V.L., Patterson, B.K., Canterero, L., Goolsby, C.L., *Reducing cellular autofluorescence in flow cytometry: an in situ method*. *Cytometry (Communications in Clinical Cytometry)*, 1997. **30**: p. 151-156.
 182. Al-Taei, S., Penning, N.A., Simpson, J.C., Futaki, S., Takeuchi, T., Nakase, I., Jones*, A.T., *Intracellular Traffic and Fate of Protein Transduction Domains HIV-1 TAT Peptide and Octaarginine. Implications for Their Utilization as Drug Delivery Vectors*. *Bioconjugate Chem*, 2006. **17**: p. 90-100.
 183. Tsai, C., Lin, C., Wang, T., Chou, A., Chou, M., Lee, C., Peng, I., Liao, J., Chen, Y., Pan, C., *Dynasore inhibits rapid endocytosis in bovine chromaffin cells*. *Am J Physiol-Cell Ph*, 2009. **297**: p. C397–C406.

References

184. Fukunaga, M. and K. Tsuruda, *Actinobacillus actinomycetemcomitans induces lethal effects on the macrophage-like human cell line U937*. Oral Microbiol Immunol, 2001. **16**: p. 284-9.
185. Richardson, S.C.W., Wallom, K., Ferguson, E.L., Deacon, S.P.E., Davies, M.W., Powell, A.J., Piper, R.C., Duncan, R., *The use of fluorescence microscopy to define polymer localisation to the late endocytic compartments in cells that are targets for drug delivery*. J Control Release, 2008. **127**: p. 1-11.
186. Hasegawa, T., Hirota, K., Tomoda, K., Ito, F., Inagawa, H., Kochi, C., Soma, G., Makino, K., Terada, H., *Phagocytic activity of alveolar macrophages toward polystyrene latex microspheres and PLGA microspheres loaded with anti-tuberculosis agent*. Colloid surface B, 2007. **60**: p. 221-228.
187. Butler, W.R., Guthertz, L.S., *Mycolic acid analysis by high-performance liquid chromatography for identification of Mycobacterium species*. Clin Microbiol Rev, 2001. **14**: p. 704-726.
188. Duffey, P.S., Guthertz, L.S., Evans, G.C., *Improved rapid identification of mycobacteria by combining solid-phase extraction with high-performance liquid chromatography analysis of BACTEC cultures*. J Clin Microbiol, 1996. **34**: p. 1939-43.
189. Kellogg, J.A., Bankert, D.A., Withers, G.S., Sweimler, W., Kiehn, T.E., Pfyffer, G.E., *Application of the Sherlock Mycobacteria Identification System using high-performance liquid chromatography in a clinical laboratory*. J Clin Microbiol, 2001. **39**: p. 964-70.
190. Hagen, S.R. and J.D. Thompson, *Analysis of mycolic acids by high-performance liquid chromatography and fluorimetric detection. Implications for the identification of mycobacteria in clinical samples*. J Chromatogr A, 1995. **692**: p. 167-72.
191. Khanuja, S.P.S., Srivastava, S., Kumar, T.R.S., Shasany, A.K., Darokar, M.P., Awasthi, S., *PCT WO 03/080860. A quick and sensitive method of quantifying mycolic acid*, W.I.P. Organisation, Editor. 2003.
192. Young, F.M., Phungtamdet, W., Sanderson, B.J.S., *Modification of MTT assay conditions to examine the cytotoxic effects of amitrax on the human lymphoblastoid cell line, WIL2NS*. Toxicol In Vitro, 2005. **19**: p. 1051-1059.
193. Sinha, D., Bhattacharya, D.K., Mandal, C., *A colorimetric assay to evaluate the chemotherapeutic response of children with acute lymphoblastic leukemia (ALL) employing AchatininH: a 9-O-acetyl sialic acid binding lectin*. Leuk Res, 1999. **23**: p. 803-809.
194. Kohro, T., Tanaka, T., Murakami, T., Wada, Y., Aburatani, H., Hamakubo, T., Kodama, T., *A comparison of differences in the gene expression profiles phorbol-12-myristate 13-acetate differentiated THP-1 cells and human monocyte derived macrophage*. J Atheroscler Thromb, 2004. **11**: p. 88-97.
195. Grifliths, G., Back, R., Marsh, M., *A quantitative analysis of the endocytic pathway in baby hamster kidney cells*. J Cell Biol, 1989. **109**: p. 2703-2720.
196. Green, S.A., Zimmer, K., Grifliths, G., Mellman, I., *Kinetics of intracellular transport and sorting of lysosomal membrane and plasma membrane proteins*. J Cell Biol, 1987. **105**: p. 1227-1240.
197. Semete, B., Booysen, L., Lemmer, Y., Kalombo, L., Katata, L., Verschoor, J., Swai, H.S., *In vivo evaluation of the biodistribution and safety of PLGA nanoparticles as drug delivery systems*. Nanomedicine, 2010. **6**(5): p. 662-671.

References

198. Sun, E.Y., Josephson, L., Kelly, K.A., Weissleder, R., *Development of Nanoparticle Libraries for Biosensing*. *Bioconjugate Chem*, 2006. **17**: p. 109-113.
199. Trombone, A.P.F., Silva, C.L., Almeida, L.P., Rosada, R.S., Lima, K.M., Oliver, C., Jamur, M.C., Coelho-Castelo, A.A.M., *Tissue distribution of DNA-Hsp65/TDM-loaded PLGA microspheres and uptake by phagocytic cells*. *Genet Vaccines Ther*, 2007. **5**: p. 9.
200. Murray, J.W., Wolkoff, A.W., *Roles of the cytoskeleton and motor proteins in endocytic sorting*. *Adv Drug Deliv Rev*, 2003. **55**: p. 1385-1403.
201. Vercauteren, D., Vandenbroucke, R.E., Jones, A.T., Rejman, J., Demeester, J., De Smedt, S.C., Sanders, N.N., Braeckmans, K., *The use of inhibitors to study endocytic pathways of gene carriers: optimization and pitfalls*. *Molecular Therapy*, 2009. **18**: p. 561-569.
202. Zahoor, A., Sharma, S., Khuller, G.K., *Inhalable alginate nanoparticles as antitubercular drug carriers against experimental tuberculosis*. *Int J Antimicrob Agents*, 2005. **26**: p. 298-303.
203. Zahoor, A., Pandey, R., Sharma, S., Khuller, G.K., *Pharmacokinetic and pharmacodynamic behaviour of antitubercular drugs encapsulated in alginate nanoparticles at two doses*. *Int J Antimicrob Agents*, 2006. **27**: p. 409-416.
204. Zahoor, A., Sharma, S., Khuller, G.K., *Chemotherapeutic evaluation of alginate nanoparticle-encapsulated azole antifungal and antitubercular drugs against murine tuberculosis*. *Nanomedicine*, 2007. **3**: p. 239-243.
205. Dutt, M., Khuller, G. K., *Liposomes and PLG microparticles as sustained release antitubercular drug carriers - an in vitro-in vivo study*. *Int J Antimicrob Agents*, 2001. **18**: p. 245-52.
206. Johnson, C.M., Pandey, R., Sharma, S., Khuller, G.K., Basaraba, R.J., Orme, I.M., Lenaerts, A.J., *Oral therapy using nanoparticle-encapsulated antituberculosis drugs in guinea pigs infected with Mycobacterium tuberculosis*. *Antimicrob Agents Chemother*, 2003. **49**: p. 4335-4338.
207. Jones, A.T., *Macropinocytosis: searching for an endocytic identity and a role in the uptake of cell penetrating peptides*. *J Cell Mol Med*, 2007. **11**: p. 670-684.
208. Sebattjane, S.I., *Anti-tuberculosis drug design based on a possible mimicry between host and pathogen lipids*. *MSc Dissertation*, in *Department of Biochemistry. Faculty of Natural and Agricultural Sciences* 2003, University of Pretoria: Pretoria.
209. Goodrum, M.A., Siko, D.G.R., Niehues, T., Eichelbauer, D., Verschoor, J.A., *Mycolic acids from Mycobacterium tuberculosis: Purification by countercurrent distribution and T cell stimulation*. *Microbios*, 2001. **106**: p. 55-67.
210. Biro, A., Horvath, A., Varga, L., Nemesanszky, E., Csepregi, A., David, K., Tolvaj, G., Ibranyi, E., Telegdy, L., Par, A., Romics, L., Karadi, I., Horanyi, M., Gervain, J., Ribiczey, P., Csondes, M., Fust, G., *Serum anti-cholesterol antibodies in chronic hepatitis-C patients during IFN- α -2b treatment*. *Immunobiol*, 2003. **207**: p. 161-168.
211. Horvath, A., Fustab, G., Horvath, I., Vallus, G., Duba, J., Harcos, P., Prohaszka, Z., Rajnavolgyi, E., Janoskuti, L., Kovacs, M., Csaszar, A., Romics, L., Karadi, I., *Anti-cholesterol antibodies (ACHA) in patients with different atherosclerotic vascular diseases and healthy individuals. Characterization of human ACHA*. *Atherosclerosis*, 2001. **156**: p. 185-192.

References

212. Perez-Guzman, C., Vargas, M.H., *Hypocholesterolemia: A major risk factor for developing pulmonary tuberculosis?* Med Hypotheses, 2006. **66**: p. 1227–1230.
213. Van der Meer-Janssen, Y.P.M., van Galen, J., Batenburg, J.J., Helms, J.B., *Lipids in host–pathogen interactions: Pathogens exploit the complexity of the host cell lipidome.* Prog Lipid Res, 2009. **49**: p. 1-26.
214. De Hostos, E.L., *The coronin family of actin-associated proteins.* Trends Cell Biol, 1999. **9**: p. 345-349.
215. Deghmane, A., Soualhine, H., Bach, H., Sendide, K., Itoh, S., Tam, A., Noubir, S., Talal, A., Lo, R., Toyoshima, S., Av-Gay, Y., Hmama, Z., *Lipoamide dehydrogenase mediates retention of coronin-1 on BCG vacuoles, leading to arrest in phagosome maturation.* J Cell Sci, 2007. **120**: p. 2796-2806.
216. Trimble, W.S., Grinstein, S., *TB or not TB: Calcium regulation in mycobacterial survival.* Cell, 2007. **130**: p. 12-14.
217. Beukes, M., Lemmer, Y., Deysel, M., Al Dulayymi, J.R., Baird, M., Koza, G., Iglesias, M.M., Rowles, R.R., Theunissen, C., Grooten, J., Toschi, G., Roberts, V.V., Pilcher, L., Van Wyngaardt, S., Mathebula, N., Balogun, M., Stoltz, A.C., Verschoor, J.A., *Structure-function relationships of the antigenicity of mycolic acids in tuberculosis patients.* Chem Phys Lipids, 2010: p. doi:10.1016/j.chemphyslip.2010.09.006.

Appendix

Articles that this thesis contributed towards

1. Appendix A (p130-155):

Lemmer, Y., Thanyani, S.T., Vrey, P.J., Driver, C.H.S., Venter, L., van Wyngaardt, S., ten Bokum, A.M.C., Ozoemena, K.I., Pilcher, L.A., Fernig, D.G., Stoltz, A.C., Swai, H.S., Verschoor, J.A., *Detection of Antimycolic Acid Antibodies by Liposomal Biosensors*. *Methods Enzymol*, 2009. **464**: p. 80-102.

2. Appendix B (p156-165):

Semete, B., Booysen, L., Lemmer, Y., Kalombo, L., Katata, L., Verschoor, J., Swai, H.S., *In vivo evaluation of the biodistribution and safety of PLGA nanoparticles as drug delivery systems*. *Nanomedicine*, 2010. **6**(5): p. 662-671.

3. Appendix C (p166-174):

Beukes, M., Lemmer, Y., Deysel, M., Al Dulayymi, J.R., Baird, M., Koza, G., Iglesias, M.M., Rowles, R.R., Theunissen, C., Grooten, J., Toschi, G., Roberts, V.V., Pilcher, L., Van Wyngaardt, S., Mathebula, N., Balogun, M., Stoltz, A.C., Verschoor, J.A., *Structure-function relationships of the antigenicity of mycolic acids in tuberculosis patients*. *Chem Phys Lipids*, 2010. **doi:10.1016/j.chemphyslip.2010.09.006**.

CHAPTER FIVE

DETECTION OF ANTIMYCOLIC ACID ANTIBODIES BY LIPOSOMAL BIOSENSORS

Y. Lemmer,^{*,‡} S. T. Thanyani,^{*} P. J. Vrey,^{*} C. H. S. Driver,[†]
L. Venter,^{*} S. van Wyngaardt,^{*} A. M. C. ten Bokum,^{*}
K. I. Ozoemena,[†] L. A. Pilcher,[†] D. G. Fernig,[¶] A. C. Stoltz,^{*,§}
H. S. Swai,[‡] and J. A. Verschoor^{*}

Contents

1. Introduction	80
2. Experimental	81
2.1. Purification of mycobacterial MA	81
2.2. Fluorescent labeling of MA	82
2.3. Determination of MA carrying capacity of liposomes	82
2.4. MA liposome size is influenced by cholesterol and MA content, but not by pH	84
2.5. MA liposome immobilization on IAsys biosensor cuvettes	86
2.6. Technology transfer from the IAsys waveguide to the ESPRIT SPR biosensor	89
2.7. The cholesterol nature of MA demonstrated on the ESPRIT biosensor	100
3. Conclusion	102
Acknowledgments	102
References	102

Abstract

Antibodies to mycolic acid (MA) antigens can be detected as surrogate markers of active tuberculosis (TB) with evanescent field biosensors where the lipid antigens are encapsulated in liposomes. Standard immunoassay such as ELISA, where the lipid antigen is not encapsulated, but directly adsorbed to the well-bottoms of microtiter plates, does not yield the required sensitivity and

* Department of Biochemistry, University of Pretoria, Pretoria, South Africa

† Department of Chemistry, University of Pretoria, Pretoria, South Africa

‡ Materials Science and Manufacturing, CSIR, Pretoria, South Africa

§ Department of Infectious Diseases, University of Pretoria, Pretoria, South Africa

¶ School of Biological Sciences, University of Liverpool, United Kingdom

specificity for accurate diagnosis of TB. One reason for this is the cross-reactivity of natural anticholesterol antibodies with MAs. MAs are the major cell wall lipids of mycobacteria. Mycobacterial MA has immunomodulatory properties and elicits specific antibodies in TB patients. Liposomes were optimized for their use as carriers both for the presentation of immobilized purified mycobacterial MA on sensor surfaces, and as a soluble inhibitor of antibody binding in inhibition assays. By using an inhibition assay in the biosensor, the interference by anticholesterol antibodies is reduced. Here, we describe the MA carrying capacity of liposomes with and without cholesterol as a stabilizing agent, optimized concentration and size of liposomes for use in the biosensor assay, comparison of the methods for wave-guide and surface plasmon resonance biosensors and how the cholesterol nature of MA can be demonstrated by the biosensor when Amphotericin B is allowed to bind to MA in liposomes.

1. INTRODUCTION

As a result of the development of drug-resistant strains of *Mycobacterium tuberculosis* and the breakdown of the immune system of its host by HIV, tuberculosis (TB) is no longer a “controlled” disease and has become a major health problem in both developed and developing countries (Houghton *et al.*, 2002). Diagnosis of TB is no longer 100% reliable due to AIDS, and was never adequate for determining extrapulmonary and child TB. HIV coinfection and drug resistance appears to shorten the lifetime of a TB patient considerably, such that it becomes a matter of life and death to be able to diagnose TB within 24 h of sampling. The decision toward treatment cannot be taken lightly, as the treatment regime has to be maintained for at least 6 months to clear all the latent TB from the body. The current drive toward new tools for TB diagnosis arose from these facts, and that the mycobacterial pathogen isolated from sputum samples is slow growing, thereby requiring several weeks to become visible during *in vitro* growth (Reischl, 1996; Samanich *et al.*, 2000). Although DNA-amplifying technology has reduced the period from sampling to TB diagnosis to within days, it still uses mainly samples obtained from the lungs. Therefore, fast, affordable, and reliable diagnosis of TB has become a high priority in public health (Chan *et al.*, 2000), and is currently actively pursued in several laboratories. Mycolic acids (MAs) appeared to be promising antigens for the design of fast immuno-diagnostics for TB (Verschoor and Onyebujoh, 1999).

The major cell wall lipids of mycobacteria are the MAs, which are long chain (C60–C90) α -branched, β -hydroxy fatty acids. Mycobacterial MAs are immunogenic. MA was the first nonprotein antigen shown to stimulate the proliferation of human CD4⁺, CD8⁺, and CD4⁺ T-lymphocytes upon CD1 presentation (Beckman *et al.*, 1994; Goodrum *et al.*, 2001). In addition, anti-MA antibodies could be detected in the serum of patients with active

pulmonary TB (Pan *et al.*, 1999) using the standard ELISA procedure, indicating that free MAs are present in the circulation during active TB disease (Beatty *et al.*, 2000). The prevalence of anti-MA antibodies appeared to be independent of the degree to which a person was suffering from AIDS (Schleicher *et al.*, 2002). Whereas ELISA did not detect anti-MA antibodies well enough to be considered as a basis for a diagnostic test of active TB, biosensor analysis did (Thanyani *et al.*, 2008). It could achieve the required specificity and sensitivity to be regarded seriously as a solution to the current dilemma of standard TB diagnosis taking several weeks after sampling to produce a result. Even the highly sensitive PCR detection of mycobacterial DNA in patient sputum samples still takes a few days to deliver a diagnostic outcome.

MAs are soluble in extremely nonpolar organic solvents such as chloroform, dichloromethane, and hexane. Alternatively, they can be “solubilized” in boiling water or aqueous buffers. For the detection of anti-MA antibodies by means of ELISA, MA was either coated from hexane solutions (Pan *et al.*, 1999) or from boiling phosphate-buffered saline (PBS) (Schleicher *et al.*, 2002). This presentation of MA is clearly not physiological. Presentation of MA in liposomal environments more closely resembles the way in which MA is encountered in the body of the patient. Indeed, when encapsulated into liposomes and injected into mice, MA was shown to behave as a typical pathogen-associated molecular pattern (Korf *et al.*, 2005). It could also act as an immunomodulatory compound that suppresses experimental asthma through Treg cell intervention (Korf *et al.*, 2006). It was only logical to derive that diagnosis of TB by detection of surrogate marker antibodies against MA should perform better when MA antigen was presented in liposomes. This was demonstrated by Thanyani *et al.* (2008) by making use of biosensors. Here, we describe how liposomes are optimized for their use as carriers of MA for immobilization as antigens on sensor surfaces, and as soluble inhibitors of antibody binding in inhibition assays in a TB diagnostic assay. It is dubbed the MARTI-test, as an acronym of Mycolic acid Antibody Real-Time Inhibition. Whereas the original MARTI-test is described for a wave-guide biosensor (Thanyani *et al.*, 2008), we show here how the method is adjusted to also suit the more popularly used surface plasmon resonance (SPR) biosensors. Finally, we demonstrate the cholesterol nature of MA with the biosensor by measuring the binding of Amphotericin B to MA in liposomes.

2. EXPERIMENTAL

2.1. Purification of mycobacterial MA

MAs are isolated and purified from *M. tuberculosis* H37Rv ATTC 27294 purchased from the American Type Culture Collection (ATTC, Baltimore, MD, USA) as described by Goodrum *et al.* (2001). The MA is dissolved in

chloroform (HPLC grade; Merck; Darmstadt, Germany) and aliquotted into glass vials. The chloroform is evaporated under nitrogen gas and the dried MA is stored at 4 °C until use. The purified MAs are checked for LPS contamination using the kinetic-QCL Limulus amoebocyte test kit (Sigma, St. Louis, MO). In the experiments shown in this chapter, no LPS is detected.

2.2. Fluorescent labeling of MA

MA is fluorescently labeled by derivatization with 5-bromomethyl fluorescein (5-BMF; Molecular Probes, Leiden, The Netherlands), as described by Korf *et al.* (2005). Quality control is performed by TLC on a silica gel GH1 thin layer plate. Chromatography is performed in two dimensions, with chloroform:methanol:water as the mobile phase in the first dimension, and 100% methanol (Merck) as the mobile phase in the second dimension. Iodine vapor is used to visualize the MA. The absence of free 5-BMF, not associated with the MA spot, indicates that the label is covalently bound. Fluorescently labeled 5-BMF-MA is incorporated into liposomes for assessment by the biosensor or flow cytometry.

2.3. Determination of MA carrying capacity of liposomes

MAs are dissolved in chloroform and 100 µg quantities are aliquotted into amber vials and stored at 4 °C. Liposomes are prepared according to the method described by Bangham (1983). This involves the deposition of a thin lipid film from an organic solvent medium on the wall of a container, followed by agitation with an aqueous medium. In short, phosphatidylcholine (PC from egg yolk, 99% pure; Sigma), cholesterol (Sigma), and dried MA are all dissolved separately in chloroform. PC (9 mg) with or without 4.5 mg cholesterol and varying amounts of MA are mixed together in a glass vial. The chloroform is evaporated under nitrogen gas in a chemical hood. PBS (1 ml) is added and the mixture is heated to 80 °C until the lipid film dissociates from the wall of the vial. The hot mixture is then vortexed and sonicated for 5 min using a Branson sonifier for 50 pulses at a 20% output level.

MA-carrier liposomes are extracted using a triphase partition method, modified from Dennison and Lovrein (1997). Briefly, a sample (50–200 µl) of MA-carrier liposome solution is diluted to 600 µl with H₂O and extracted three times with equal volumes of *tert*-butanol and chloroform. The chloroform phases are collected and the chloroform is evaporated under nitrogen gas. MA remaining in the vials due to saturation of the liposomes is collected by chloroform rinses. HPLC of the extracted MA is carried out as described (Butler and Kilburn, 1990), after derivatization with *p*-bromophenacyl bromide. A high molecular weight internal standard

(Ribi ImmunoChem Research Company, Hamilton, MT, USA) is added to each sample to allow quantification of the extracted MA.

Liposomes are made with egg PC, with or without the addition of cholesterol. The maximum amount of MA that can be incorporated reproducibly is about 2 mg/ml for liposomes consisting of phosphatidyl choline and cholesterol, but only about 500 μg MA/ml into liposomes consisting of phosphatidyl choline only (Fig. 5.1). MA not incorporated into the liposomes can in most cases be quantitatively recovered from the wall of the vessel in which the liposomes are prepared (shaded part of the bars). At very high concentrations the recovery is not quantitative, as the MA tends to form clumps which float in the liposome suspension. The MA liposomes

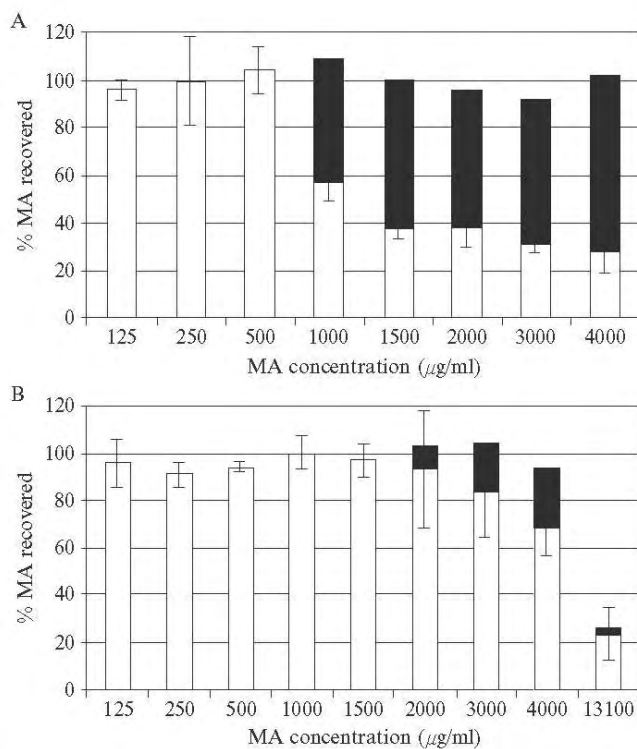


Figure 5.1 Titration of the maximum amount of MA that can be incorporated in liposomes consisting of egg phosphatidylcholine, with or without cholesterol: (A) liposomes consisting of egg phosphatidylcholine (99% pure) only; (B) liposomes consisting of egg phosphatidylcholine (99% pure) and cholesterol. The shaded part of the bars represent the percentage of MA recovered from the wall of the vessel in which the liposomes were prepared. Each bar represents the mean of three samples and the S.D.

can be lyophilized and reconstituted without significant loss of MA content. Heating to 80 °C in the reconstitution process is an important step to ensure full recovery of MA content.

2.4. MA liposome size is influenced by cholesterol and MA content, but not by pH

MA-containing liposomes are prepared with equal amounts of 5-BMF labeled and unlabeled MAs and varying amounts of cholesterol according to Table 5.1.

A liposome stock suspension is obtained by adding PBS (1 ml) to the dried lipid components, dissolving it on a heat block for 60 min after vortexing and sonicating the heated (80 °C) mixture with a Branson Sonifier B30 Cell Disrupter at 20% duty cycle and output control of 2 for 5 min.

Both the size distribution (forward scatter, FS) and the fluorescence (FL-1) of the liposomes are measured on a flow cytometer (a Beckman Coulter Epics Ultra instrument is used to obtain the results in Fig. 5.2). For the analysis, 10 times dilutions of the stock liposomes are prepared using PBS in plastic analyzing tubes covered with foil to prevent the photobleaching of the fluorescent marker. The tubes are kept in a water bath at 37 °C during the experiments. One gate is set on the analyzer to exclude background signals and debris events that have FS values below 10. A constant number of 50,000 events are counted per measurement. Flowset (3.6 μm) fluorospheres measured with each experiment is used to correlate the relative size of the liposomes to that of the beads when varying amounts of cholesterol are added to a constant amount of MA and PC.

The size distribution of the liposomes changes in accordance with a change in the cholesterol concentration (Fig. 5.2A). Two different liposome states can be identified. At the two highest concentrations of cholesterol, the liposomes are 2 log units bigger than the liposomes that contain none or the lowest concentrations of cholesterol. The liposomes obtained with the addition of 11.25 μl of cholesterol stock give an intermittent size of liposomes in between that of the two states. With an increase in the cholesterol concentration and liposome size, the liposomes also show an analogous increase of 2 log units in the amount of fluorescence per liposome that is

Table 5.1 Liposome compositions with various concentrations of cholesterol

Cholesterol (μl from 100 mg/ml stock)	0	5.63	11.25	22.5	45
PC (μl from 100 mg/ml stock)	90	90	90	90	90
5-BMF-MA (μg)	125	125	125	125	125
Unlabeled MA (μg)	125	125	125	125	125

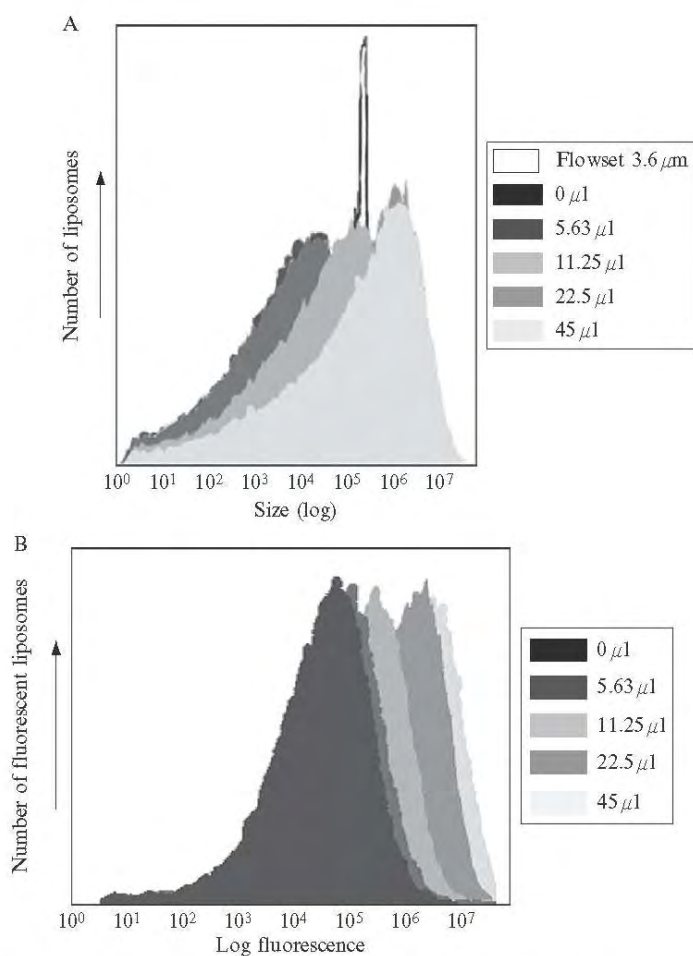


Figure 5.2 Size (A) and fluorescence (B) of MA-containing liposomes containing various amounts of cholesterol according to Table 5.1 as determined with flow fluorometry. Flowset beads (3.6 μm) were used as a marker for the size distribution of the liposomes.

emitted (Fig. 5.2B), indicating that the change from smaller to larger liposomes is not due to swelling with water/PBS, but to an accumulation of more MA-containing material into the bigger liposomes. The results imply that cholesterol content determines two states of liposomes, where higher concentrations of cholesterol induce the disordered state of the bilayer in liposomes that increase their size 100-fold. All cholesterol-containing liposomes used in the biosensor analysis were in the disordered state at the highest concentration of cholesterol shown here.

In Fig. 5.2, the biggest sized liposomes measured around $30\ \mu\text{m}$ and were composed of PC (9 parts), cholesterol (4.5 parts), and MA (0.25 parts). When the phosphatidyl choline is combined with either the MA or the cholesterol, significant changes in the sizes of the liposomes occur. With cholesterol alone the size sharply increases, while with MA alone the size sharply decreases (Fig. 5.3). This effect is not significantly influenced in the pH range between 4 and 10 of the PBS to which the liposomes are exposed, probably due to the unchanged surface charge of phosphatidyl choline liposomes over these pH values. The anionic phosphatidyl residues ($\text{p}K_a \leq 3.5$) only become neutralized below pH 4, while the cationic state of choline ($\text{p}K_a = 13.9$) is maintained over the full pH range measured (Tatulian, 1993). It is therefore expected that the stability of the liposomes described here for use in the biosensor will be quite tolerant to a broad pH window extending to both sides of the typical pH of 7.4 of PBS.

2.5. MA liposome immobilization on IAsys biosensor cuvettes

A number of application notes are available for the adsorption of liposomes to hydrophobic sensor surfaces. These do not stand up as rigorous and reliable for the immobilization of MA antigen-containing liposomes aiming at antibody detection. This motivated the use of nonderivatized sensor cuvettes where the glass-like hafnium oxide surface can be made hydrophobic by treatment with the cationic detergent, cetylpyridinium chloride (CPC). CPC is well known for its use as an antiseptic agent. Its property

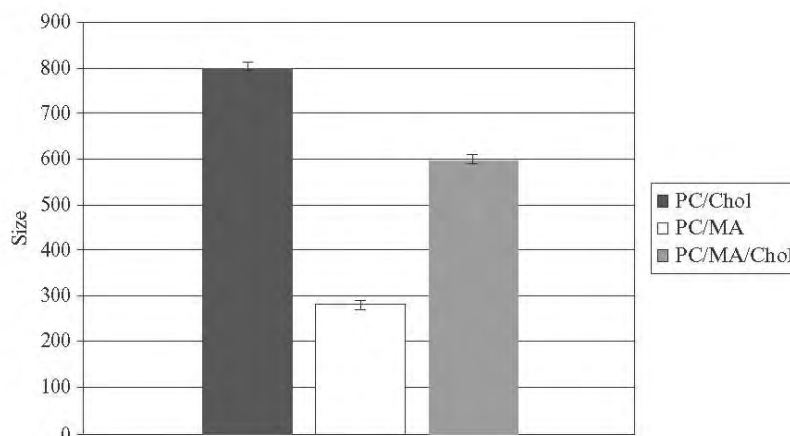


Figure 5.3 Relative sizes of PC/cholesterol and PC/mycolic acid liposomes and a mixture of the two liposomes. All liposome types contained 9 parts of phosphatidyl choline and either 4.5 parts of cholesterol, or 0.25 parts of MA, or both.

of binding to glass when applied at aqueous dilutions below the critical micellar concentration (i.e., <0.1 mg/ml) is long established (Westwell and Anacker, 1959), leaving a “greasy” surface (Hartley and Runnicles, 1938).

PBS/AE buffer consists of 8.0 g NaCl, 0.2 g KCl, 0.2 g KH_2PO_4 , and 1.05 g Na_2HPO_4 per liter of double distilled, deionized water containing 1 mM EDTA and 0.025% (m/v) sodium azide and is adjusted to pH 7.4. CPC (0.02 mg/ml) and saponin (1 mg/ml) are prepared in PBS/AE. The IAsys resonant mirror biosensor system and twin-cell nonderivatized cuvettes are from Affinity Sensors (Farfield Scientific, Crewe, UK). The sensor is set for a data sampling interval of 0.4 s, temperature of 25 °C, and stirring rate of 75% for all experiments. The cells are rinsed three times prior to use with 96% ethanol (Saarchem, South Africa), followed by extensive washing with PBS/AE. A 60 μl volume of PBS/AE is pipetted into each cell of the cuvette to obtain a stable baseline for 1 min. Cuvettes are washed with PBS/AE until a stable baseline could be maintained for at least 5 min. The cells are aspirated and 50 μl of a 20 $\mu\text{g}/\text{ml}$ CPC in PBS/AE solution is added. After 10 min the cells are washed five times with 60 μl PBS/AE. PBS/AE (25 μl) is added until a stable baseline is achieved. Twenty-five microliters of the desired liposome solution are added and the binding response is monitored for 10 min. The MA-containing liposome concentration consisting of 9:3:1 (m/m) phosphatidyl choline:cholesterol:MA is titrated between 0.02 and 10 mg/ml of total lipid concentration. The MA-containing liposome concentration with the optimum binding capacity is found to be 500 μg total lipid/ml (Fig. 5.4). This concentration is used in all subsequent experiments.

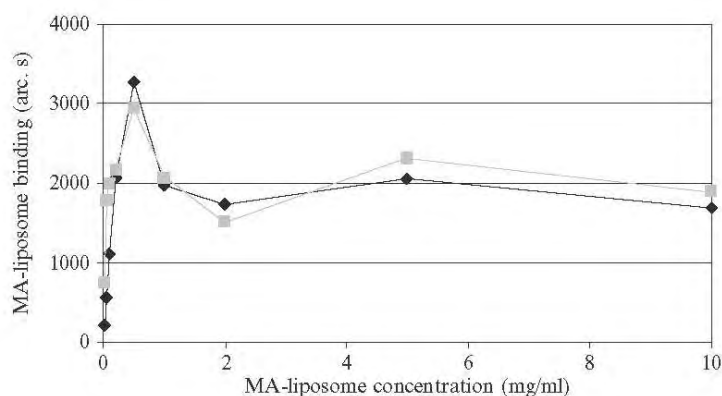


Figure 5.4 Titration of the optimal concentration of MA/cholesterol-containing liposomes for immobilization on a nonderivatized IAsys biosensor cuvette.

After liposome binding, the cells are washed five times with 60 μl PBS/AE and immediately after that, treated five times with 60 μl 1 mg/ml saponin in PBS/AE. Due to response differences among saponin batches, it is necessary to titrate the amount of saponin required each time a new batch of saponin is used. The cells are incubated with saponin for at least 10 min and until a stable baseline is achieved before a final five times wash with 60 μl PBS/AE. Antibody interaction analysis could be continued from this point as described by Thanyani *et al.* (2008). The cells are washed five times with PBS/AE, the content of each cell substituted with 25 μl of PBS/AE and left for about 5–10 min to achieve a stable baseline. Inhibition studies are performed using patient's serum that is first placed at room temperature to thaw completely. After obtaining a stable baseline, a 1/1000 dilution of serum antibodies (10 μl) in PBS/AE is added in each cell, to compare the responses of the two cells over 10 min. A preincubation of 1/500 dilutions of serum with solutions of liposomes-containing MAs and empty liposomes (PC alone) is allowed for 20 min. These are then added (10 μl) for binding inhibition studies in the two cuvette cells, one with MAs liposomes and the other with empty liposomes as a control, and allowed to bind for 10 min. Finally, dissociation of antibodies is effected with three times PBS/AE washing and measurement of the response for 5 min.

Regeneration of the cuvette is effected by three washes with 96% ethanol for 1 min, followed by seven washes with 70 μl PBS/AE for 1 min. The surface is then finally treated with 50 μl potassium hydroxide (12.5 M) for 2 min followed by seven washes with 70 μl PBS/AE for 1 min.

A typical profile of a positive and negative TB test using this method, but applied in the ESPRIT biosensor, is shown in Fig. 5.11. The outcome of the test in the IAsys biosensor scored an overall specificity of 48.4% (15/31) and sensitivity of 86.7% (26/30) with 61 patient sera analyzed (Thanyani *et al.*, 2008). When adjusted for the inadequate performance of the reference culture test in HIV-infected patients, the MARTI-test scored a specificity of 76.9%.

A disadvantage of the IAsys biosensor in this application is the difficulty of aligning the relative basic signal strength of the two cells in a cuvette, which must be identical during the first serum exposure before a patient diagnosis can be derived from the difference of the binding signal during the second liposome-preincubated serum exposure. We experienced an average success rate of around 30% to obtain comparable signals during the first serum exposure. For this reason and due to the fact that the IAsys cuvettes were relatively expensive, we transferred the technology from the wave-guide IAsys biosensor to the more generally used SPR biosensors.

2.6. Technology transfer from the IAsys waveguide to the ESPRIT SPR biosensor

An ESPRIT SPR biosensor (Eco Chemie B.V., Utrecht, The Netherlands) is used in this study to detect antibodies to MA in human patient sera. The principle of the SPR biosensor is based on the change in the refractive index on a thin gold film surface modified with various materials (Lee *et al.*, 2005) to indicate the binding of ligands, in this case anti-MA antibodies. Both IAsys and ESPRIT biosensors use a cuvette system. The light is totally internally reflected from the sensing surface by means of a prism in both biosensors. SPR signals are related to the refractive index close to the sensor surface, and therefore report the amount of macromolecules bound to the sensor surface. An SPR immunosensor is composed of several important components such as a light source, detector, prism with transducer surface and flow system (Shankaran *et al.*, 2007). The transducer surface is usually a gold film (50–100 nm, on which biomolecules, such as antibody or antigen, are immobilized) on a glass slide optically coupled to the glass prism through refractive index matching oil. The resonance conditions are influenced by the biomolecules interacting with their immobilized ligands on the gold layer. When the molecules interact, the change in the interfacial refractive index can be detected as a shift in the resonance angle. These changes are monitored over time and converted into a sensorgram, from which the kinetics and affinity constants of the interaction can be determined.

There has been considerable progress in the development of new methods of immobilizing biological recognition elements onto transducer sensor surfaces (Zhang *et al.*, 2000), a key step in the development of biosensors. The use of self-assembled mono- and multilayers (SAMs) is increasing rapidly in various fields of research, and this applies especially to the construction of biosensors (Zhang *et al.*, 2000, 2008). The uncomplicated procedure for SAM formation and compatibility with metal substrates such as gold for electrochemical measurements enable special benefits for biosensor applications. The term self-assembly involves the spontaneous arrangement of atoms and molecules into an ordered stable form or even aggregate of functional entities (Tecilla *et al.*, 1990). For example, the highly ordered and dense nature of the long-chain alkanethiols of SAMs mimic the cellular microenvironment of lipid bilayer structures, thereby providing novel substrates for immobilized biomolecules (Arya *et al.*, 2006).

The molecular self-assembly of long-chain alkanethiol on gold has drawn considerable attention during the past decade, since self-assembled monolayers (SAMs) have strong adhesion to a substrate, high degree of thermal and chemical stability, and mechanical strength (Kim *et al.*, 2001). The stability of the SAMs of the alkanethiol molecules formed on the gold depends on the strength of Au–S bond and the Van der Waals force between a thiol molecule and its surrounding molecules (Han *et al.*, 2004).

SAMs can be used as interface layers upon which almost all types of biological components, including proteins, enzymes, antibodies, and their receptors can be loaded (Zhang *et al.*, 2000). Here, the preparation of octadecanethiol (ODT) in absolute ethanol to form a SAM is described. It is characterized by cyclic voltammetry (CV) and applied for the measurement of binding, or inhibition of binding of patient serum antibodies to MAs that are immobilized in liposomes onto the alkanethiol coated ESPRIT biosensor surface. The low solubility of ODT in ethanol is preferred to form the SAMs. Kim *et al.* (2001) demonstrated that the adsorption rate of alkanethiol onto clean gold when using a quartz crystal microbalance (QCM) biosensor depends on the thiol concentration, temperature, and solvent used. Here, a full coverage of the underivatized Au surface is observed when 10 mM of ODT is used. This is confirmed by a strongly hindered redox reaction when the surface is characterized with a CV instrument. CV experiments are carried out using an Autolab potentiostat PGSTAT 30 from Eco Chemie (Utrecht, The Netherlands) driven by the General Purpose Electrochemical Systems (GPES) data processing software version 4.9.

Sodium dodecylsulphate (SDS) and absolute ethanol (analytical grade) were obtained from Merck (Gauteng, SA). ODT, ferricyanide [$K_3Fe(CN)_6$], ferrocyanide [$K_4Fe(CN)_6$], potassium chloride (KCl), and urea, all analytical grade, were obtained from Sigma-Aldrich (St. Louis, MO). Acetic acid (analytical grade), sodium hydrogen carbonate ($NaHCO_3$), isopropanol (chemically pure), and sodium hydroxide (NaOH) were obtained from Saarchem (Gauteng, SA). ODT (10 mM) is dissolved in absolute ethanol using a water bath sonifier (Ultrasonic Cleaner, Optima Scientific CC, Model: DC150H) for 30 min. Sodium hydrogen carbonate (0.2 M), SDS (0.5%, w/v), sodium hydroxide (50 mM), 1 mM ferrocyanide/ferricyanide, 1 M KCl, and urea (6 M) are prepared with sterile double distilled water. The coating of the gold disk cannot be monitored in real time, since the ODT is dissolved in absolute ethanol that generates too large refractive index jumps in the sensor signals when alternated with PBS/AE. The underivatized gold disk is incubated for 16 h at room temperature in 10 mM ODT. The ODT-coated gold disk is immersed in a solution of 1 mM ferrocyanide/ferricyanide (used as a redox probe) containing 1 M KCl and scanned at a rate of 25 and 50 mV/s at a potential window of -0.1 to 0.5 V (vs. Ag/AgCl, saturated KCl). The results in Fig. 5.5 show that there is a significant drop in the current response of the ODT-coated disk toward the redox probe in comparison to the uncoated gold disk, indicating the formation of a stable SAM of ODT by S–Au bonds on the surface of the gold disk. The SAM can be maintained after the exposure of the coated surface to several regeneration cycles of absolute ethanol and a mixture of 50 mM NaOH with isopropanol (2:3, v/v).

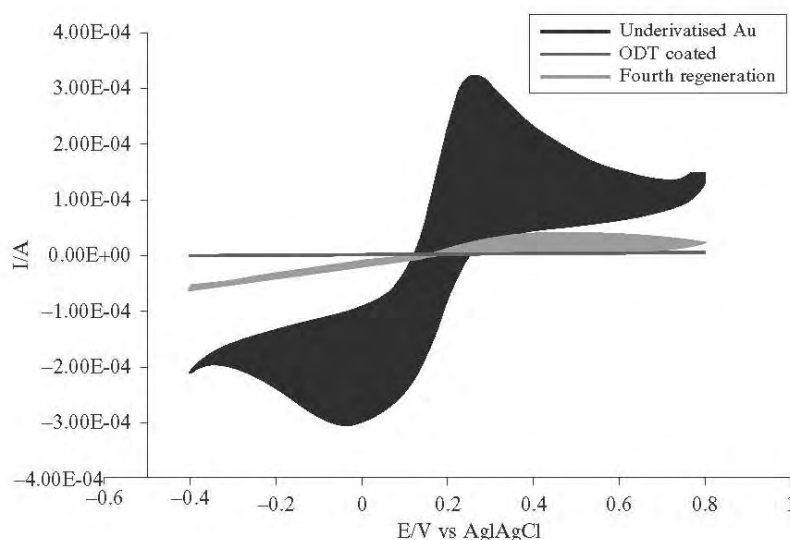


Figure 5.5 Testing of the octadecanethiol-coated ESPRIT biosensor gold surface against sequential times of regeneration with a mixture of isopropanol and 50 mM NaOH (2:3, v/v) using cyclic voltammetry. The voltammograms for the different surfaces are shaded to better identify the one from the other.

Kim *et al.* (2001) reported that partial ODT multilayers on the gold surface could be formed via the formation of disulfides, since thiols are oxidized to disulfides in the presence of oxygen and the solubility of disulfides in ethanol is much less than that of thiols. If a solution of ODT in ethanol is exposed to oxygen and oxidized to disulfide, the oxidized disulfide can be precipitated onto the monolayer. Here, the solution of ODT in absolute ethanol is covered with parafilm to avoid oxygen exposure.

The ODT-coated disk is subsequently inserted into the biosensor on a droplet of special refractive index oil, after wiping the glass bottom surface with lens tissue. The PBS/AE is filtered through a 0.2 μm particle retention membrane and degassed with helium for 30 min before use. Degassing is required whenever a hydrophobic surface is created that is exposed to air before liposome addition to prevent the formation of a “dissolved” air layer onto the hydrophobic surface that prevents SPR to occur. The cuvette is flushed with 500 μl ethanol (96%) using the automatic dispenser with simultaneous draining, followed by brief (~ 60 s) flow-washing with PBS/AE. An automated software program sequence can be created to control the addition of all the samples and liquids into the cuvette. Quality of the surfaces are monitored by determining the SPR dips after cleaning the Au ODT-coated surface with 96% ethanol and a mixture of isopropanol and 50 mM sodium hydroxide (2:3, v/v). The samples are transferred from a

384 multiwell plate (Bibby Sterilin Ltd, Stone, UK) to the cuvette surface by an autopipettor. First, the baseline of the ESPRIT biosensor is set with 10 μ l PBS/AE, followed by addition of 50 μ l MA liposomes on the disk for 20 min. The immobilized liposomes are then finally washed five times with 100 μ l PBS/AE, to prepare for blocking the surface with saponin.

2.6.1. Use of degassed buffers after liposome coating of the sensor surface

A recent study (Eastoe and Ellis, 2007) showed that exposure of lipids to degassed buffers resulted in a detergent effect that destabilized the lipids. The removal of hydrophobic gas by pumping created a limited ability of the degassed water or aqueous buffer to dissolve lipids. To determine whether this will also be the case here where buffers are degassed by bubbling through helium gas, we exposed a liposome-coated surface repeatedly to either degassed or nondegassed buffer. The liposomes-containing MAs are immobilized on ODT-coated gold sensor disks for 20 min. The liposomes are washed five times with degassed or nondegassed PBS/AE, and left for 5 min with mixing to achieve a baseline. This procedure is repeated three times. Figure 5.6A demonstrates how the baseline is affected during movement of degassed PBS/AE over the liposome coat; compared to when buffer is used that is not degassed (Fig. 5.6B). A stable baseline is obtained only when a nondegassed PBS/AE is used. The rest of the procedure in the MARTI-assay that follows after liposome coating is subsequently done with buffer that is not degassed, taking special care that air bubbles do not develop in the fluid lines that could affect the working of the pumps. In several attempts where we test samples with continued use of degassed buffer after liposome coating, we obtain nonreliable results, with the liposome layer often coming apart at the final step of antibody incubation.

2.6.2. Optimization of saponin concentration

Different concentrations of saponin (% m/v) prepared in PBS/AE (0.1%, 0.05%, 0.025%, 0.0125%, and 0.00625%) are tested to block the hydrophobic sites of the MA liposome layer.

The stock saponin concentration is 0.1% and the subsequent dilutions are prepared from this stock solution. From the results obtained (Fig. 5.7A), there is a tendency of an increase in saponin accumulation onto MA liposomes immobilized on an ODT-coated gold surface, as the saponin concentration is increased from 0.00625% to 0.05%. At a saponin concentration of 0.05% there is an amount of net saponin accumulation after PBS/AE buffer wash (Fig. 5.7B). An unstable baseline is also obtained when 0.05% saponin is used. A saponin concentration of 0.0125% is chosen as optimal, because it gives a stable baseline and acceptable variation after PBS/AE wash (Fig. 5.7B) as compared to 0.00625% and 0.025%. The differences in optimal saponin concentration used on the IAsys (0.03%) and current ESPRIT biosensors

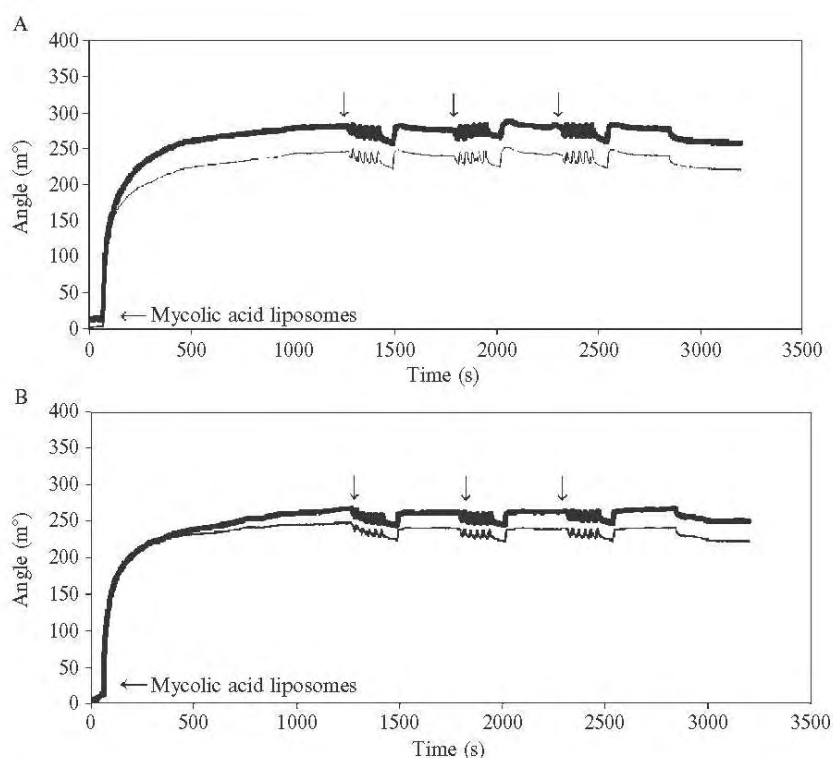


Figure 5.6 Effect of degassed (A) and nondegassed (B) buffer on immobilized mycolic acids liposomes in the ESPRIT biosensor. The arrows indicate where washing cycles with PBS/AE were introduced before allowing a baseline to be reached with mixing before substitution of cell content.

(0.0125%) could be due to different batches of saponin, or that the CPC and ODT activation before immobilization of the MA produces different surface properties.

2.6.3. Optimization of first serum exposure dilution in PBS/AE

After optimization of saponin concentration, the next step is to determine which concentration of serum is optimal for the MARTI-assay in the first exposure to antigen. Chung *et al.* (2005) indicated that serum should be diluted to minimize the nonspecific binding to the biosensor surface. Serum is a complicated protein mixture for direct application to a biosensor surface. The introduction of a first serum exposure at high dilution was previously done on the IAsys biosensor to provide a practical working dilution that did not fully saturate the antigen coat, but was still concentrated enough to give

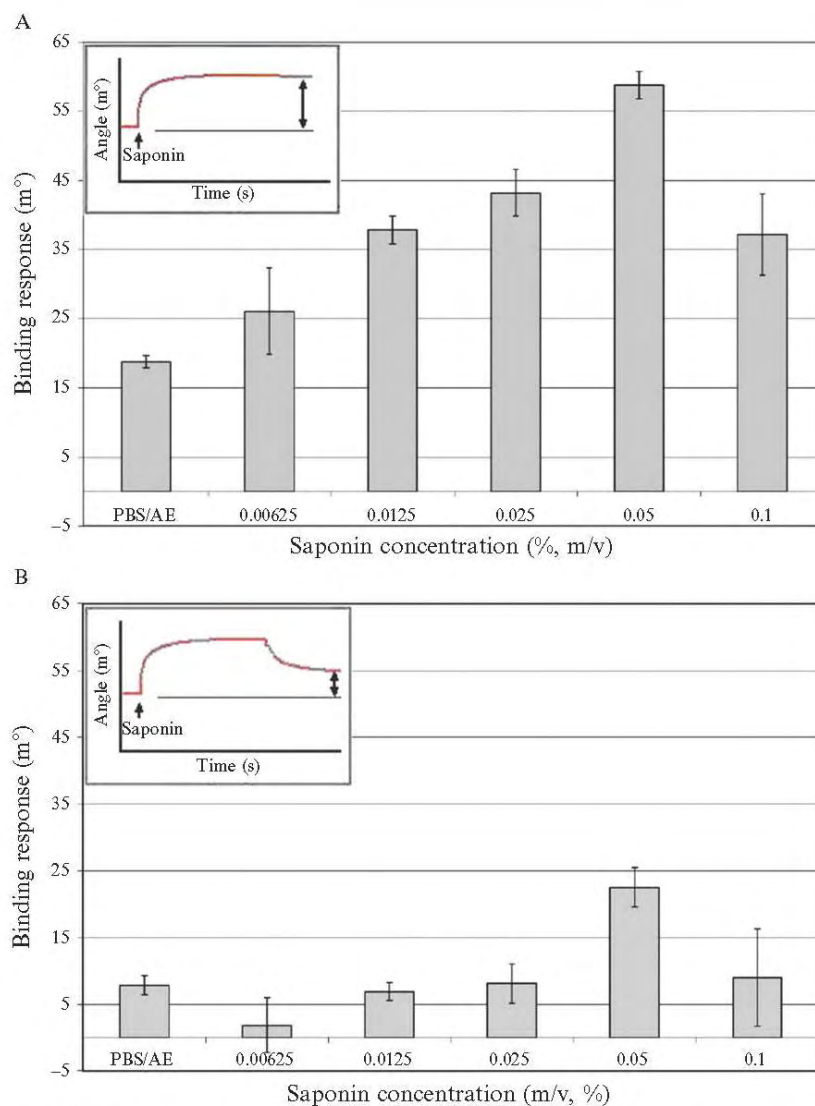


Figure 5.7 Optimization of saponin concentration to avoid nonspecific binding on immobilized mycolic acids on the Au surface coated with octadecanethiol. Accumulation of saponin is performed for 5 min (A) and washed with PBS/AE (B). The error bars indicate the standard error of the mean (S.E.M.) and $n = 3$.

a measurable signal to probe the comparability of the binding signals from the cuvette. This simultaneously blocked off the major nonspecific binding areas and hugely increased the accuracy of the MARTI-test.

Serum samples collected for another study (Schleicher *et al.*, 2002) were used that were obtained from 61 adult patients (aged between 18 and 65 years), who were admitted to the general medical wards of the Helen Joseph Hospital, Johannesburg, South Africa, including a number with active pulmonary TB. The TB-negative patients that were used as controls had medical conditions other than TB and were recruited from the general medical wards.

The liposomes are immobilized as described earlier, the surface blocked with 0.0125% saponin, after which 50 μl of PBS/AE is added and left for 5 min to affect a stable baseline. This is followed by addition of 35 μl of either 1/500, 1/1000, 1/2000, or 1/4000 dilutions of serum in PBS/AE. For the assessment of the optimal dilution of the first serum exposure, a second exposure of serum preincubated in MAs-containing or empty liposomes is kept constant at 1/250 in all the experiments. The results show that the chosen serum dilution range of 1/4000–1/500 responded in an almost linear positive correlation between antibody-binding signal and serum concentration with a slight running out at 1/4000 that indicates that the lower limit of the serum concentration is reached. The results obtained in Fig. 5.8 gave a positive linear correlation with a coefficient (r^2) of 0.9749 between the serum concentrations and their signal binding response over the range measured, which is a requirement for a successful MARTI-assay.

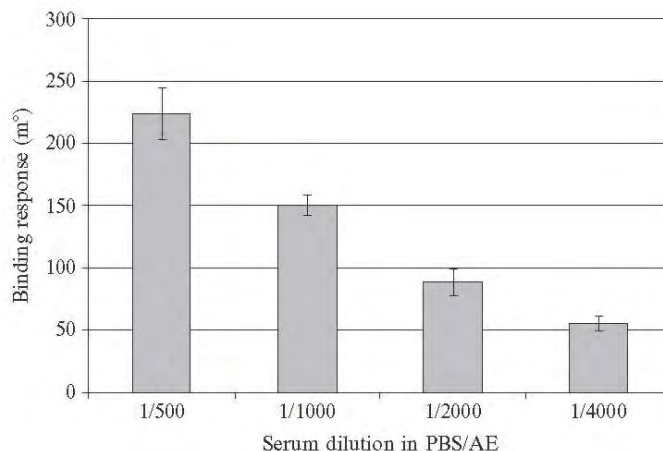


Figure 5.8 Optimization of the dilution of serum (P135) for the first exposure to antigen in the MARTI-assay, after 0.0125% saponin blocking of the mycolic acid liposome coat of the ESPRIT biosensor. The error bars indicate the standard deviation. Correlation coefficient (r^2) = 0.9749, $n \geq 3$.

The 1/4000 and 1/2000 dilutions are adequate for the first serum exposure, leaving enough room for a positive binding event at the second serum exposure.

2.6.4. Second serum exposure with liposome preincubation

P129 (TB-positive) serum was used to optimize the dilution of the second exposure to preincubated serum in MA-containing, or empty liposomes for inhibition studies, following on a first serum exposure to immobilized antigen at a dilution of either 1/4000 or 1/2000. The first exposure should avoid the saturation of antigen with antibody before the addition of preincubated serum. Different dilutions (1/250, 1/500, 1/1000, and 1/2000) of preincubated serum in MA-containing and empty liposomes are applied by 35 μ l addition to either 1/4000 or 1/2000 of first serum exposure in PBS/AE, after 10 min of incubation. This is followed by washing away of the unbound antibody with five times 100 μ l PBS/AE.

The TB-positive patient P129 serum showed a significant decrease of signal when the serum was preincubated in MA-containing liposomes, compared to empty liposomes over a range of 1/250, 1/500, or 1/1000 dilution (Fig. 5.9) after a first serum exposure at 1/4000. There was no inhibition of antibody by MA preincubation observed when 1/2000 dilution of serum was used and binding response signals were also too low.

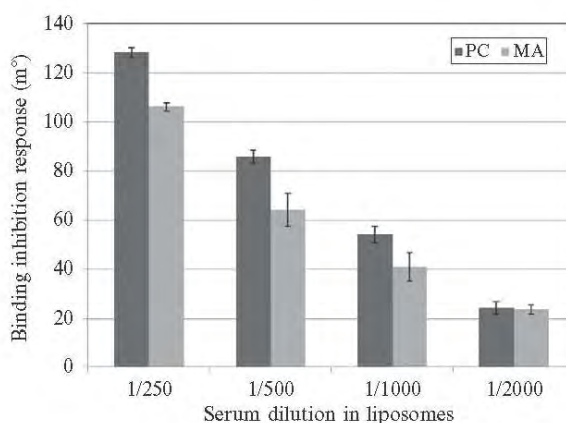


Figure 5.9 MARTI antibody-binding inhibition response of preincubated TB-positive P129 serum dilutions inhibited with mycolic acids (MAs)-containing and empty (PC) liposomes after first serum exposure of 1/4000 on immobilized MAs. The error bars indicate the standard deviation. P129 showed significant MA inhibition signals at 1/250, 1/500, and 1/1000 serum dilutions, with *P*-values of 0.00014, 0.01411, and 0.0393, respectively, but no significant inhibition at 1/2000 serum dilution (*P*-value of 0.7857). A 95% (0.05) confidence limit was used, *n* = 3.

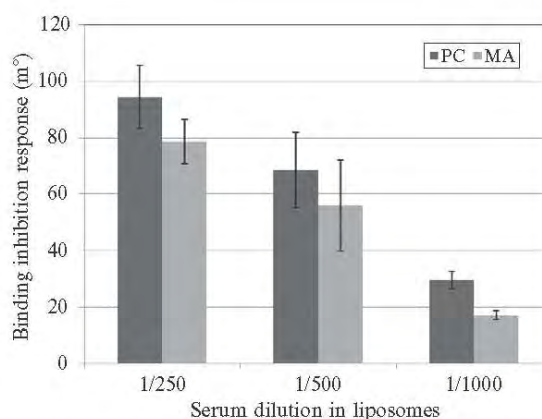


Figure 5.10 MART1-binding inhibition response of various dilutions of preincubated TB-positive patient serum (P129) with mycolic acids (MA)-containing and empty (PC) liposomes after first exposure serum dilution of 1/2000 to surface immobilized MAs. The error bars indicate the standard deviation. No statistical difference (at 95% confidence limit) is obtained at 1/250 and 1/500 dilutions between MA- and PC-inhibited serum, with P -values of 0.116 and 0.356, respectively, while a significant inhibition was observed at 1/1000 (P -value of 0.0086) $n = 3$.

This shows that the lower limit of serum concentration was reached at 1/2000 dilution to measure the inhibition of anti-MA antibody binding.

The results in Fig. 5.10 indicate that inhibition values of 17%, 19%, and 41% were obtained at 1/250, 1/500, and 1/1000 dilutions of serum in liposome solution, respectively, after first serum exposure at 1/2000 dilution. At first sight, it appeared that a better value was obtained by using a first serum exposure of 1/2000 dilution, followed by a second, antigen preincubated serum dilution at 1/1000 dilution (numerical difference: 12.50 millidegrees). However, when looking at the numerical signal difference between MA- and empty liposome-inhibited serum, then the 1/4000 dilution of first serum exposure followed by second serum exposure at 1/500 still gave the best value (numerical difference: 21.53 millidegrees). In addition, the significance of the difference between antibody-binding inhibition with MA liposomes and empty liposomes was significant at 1/250, 1/500, and 1/1000 dilution of serum after first serum exposure at 1/4000 dilution, while only the 1/1000 dilution of inhibited serum produced a significant difference after a first serum exposure of 1/2000 dilution (P -value limit of 0.05). The 1/2000 dilution of first serum exposure appears, therefore, to restrict the workable range of serum dilutions at the second critical serum exposure that provides the inhibition end result. This was confirmed when another TB-positive—HIV-negative serum (P96) was tested and for which a better inhibition response was obtained at the

preferred serum dilutions of 1/4000 and 1/500 for first and second serum exposures, respectively, compared to the result obtained with first exposure at 1/2000. At the preferred serum dilutions of exposure, the TB-negative—HIV-negative serum P94 gave the expected zero inhibition value, with a *P*-value of 0.9863.

2.6.5. Regeneration of the ODT-coated gold disks

After dissociation of the unbound serum antibodies to MAs, the surface is regenerated with 100 μ l mixture of isopropanol and 50 mM NaOH (2:3, v/v) for 2 min and finally washed with 100 μ l of 99% (absolute) ethanol. The surface is washed five times with 100 μ l of PBS/AE after each regeneration step to prepare it for a next round of liposome coating on the stable ODT layer.

2.6.6. Cleaning of cuvette and needles

A flow wash sequence is used to clean the needles after analyzing approximately 30 sample runs. Sequential washes with 0.5% (w/v) SDS, 6 M urea, 1% (v/v) acetic acid, 0.2 M sodium hydrogen carbonate (NaHCO₂), and ddd H₂O are done in order to maintain the quality of the SPR signals during repeated measurements.

2.6.7. The optimized MARTI-assay

With the lesson learnt of avoiding degassed buffers after liposome coating and the conditions optimized for the blocking of the liposome layer with saponin, titrations of the optimal dilutions for first exposures to serum and second exposure to antigen-inhibited serum dilutions were done. It is concluded that best results were obtained with 1:4000 dilution of serum at first exposure and 1:500 dilution of serum at second exposure. In the second exposure, the serum is preincubated with antigen in order to effect an inhibition of binding signal, as graphically demonstrated in Fig. 5.11.

The SPR dips (Fig. 5.11 inserts) between 0% and 10% reflectivity that are associated with the binding profiles proved that the sensor surfaces remained intact and fully activated during the run of the experiments. Using this optimized protocol, four serum samples were selected from the Schleicher *et al.* (2002) collection and assessed for the presence of anti-MA antibodies. In Table 5.2, the MARTI-assay results are presented and compared with that obtained on ELISA by Schleicher *et al.* (2002).

From Table 5.2, P129 and P96 tested false negative on ELISA and true positive on ESPRIT biosensor, while P94 tested equivocally on ELISA and true negative on ESPRIT biosensor, as it was previously shown on the IAsys biosensor (Thanyani *et al.*, 2008). The MARTI-assay on IAsys biosensor was successfully validated to an accuracy of 82% for the serodiagnosis of active pulmonary TB. The IAsys biosensor system applied to the

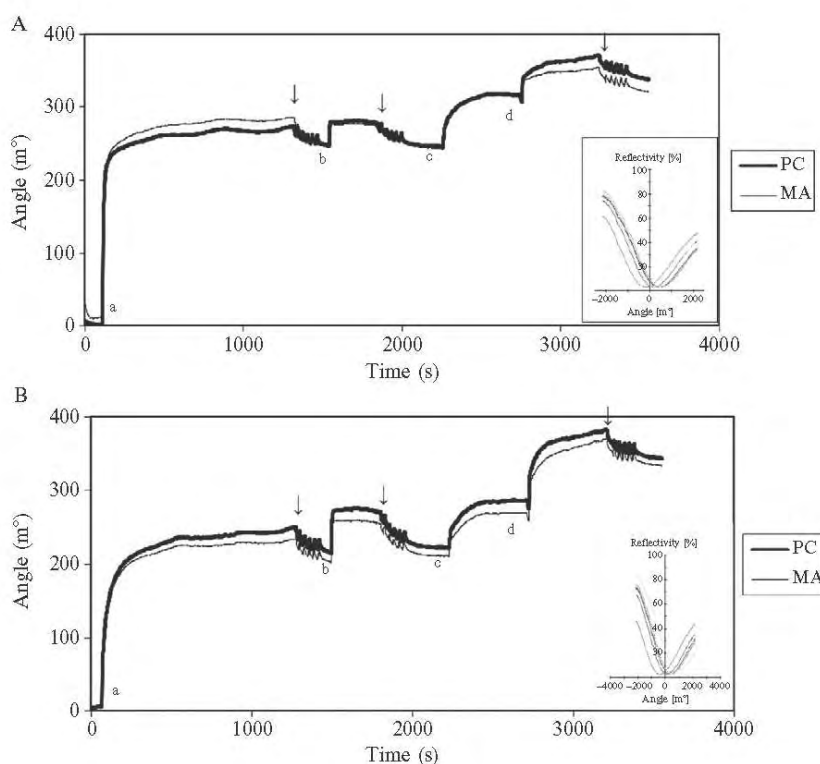


Figure 5.11 Typical sensorgrams summarizing the process of measuring serum antibody (A = TB-positive P129 and B = TB-negative P94) binding, or inhibition of binding by mycolic acid-containing and empty liposomes, on an ESPRIT biosensor with ODT-coated gold surface and immobilized mycolic acid liposomes. Mycolic acids liposomes were immobilized on the ESPRIT biosensor surface (a), blocked with saponin (b), calibrated with a 1/4000 first exposure of serum (c), and applied to measure the binding and dissociation of 1/500 diluted sera inhibited with empty (thick line) or mycolic acid-containing (thin line) liposomes at lesser dilution (d). The arrows indicate washing with PBS/AE.

Table 5.2 MARTI (ESPRIT biosensor) and ELISA analysis compared for their ability to detect antibody to MA in three selected human sera

Patient no.	TB/HIV status	ELISA assay ^a	MARTI-assay ^b
P129	TB ⁺ HIV ⁻	1.59	25.09
P96	TB ⁺ HIV ⁻	1.05	29.53
P94	TB ⁺ HIV ⁻	1.69	-0.23

^a Signal to background value of absorbance at 450 nm. Values higher than 2 are taken as positive.

^b Percentage inhibition of antibody binding to MA liposomes. Values higher than 20% are taken as positive.

MARTI-test has a weakness in that the channels often do not give matching results, while the cuvettes are 10 times more expensive than the gold disks provided for the ESPRIT biosensor. The ESPRIT biosensor is provided with an adjustable laser setting to compensate for differences in the channel readings as well as an automated pipettor system that reduces variance from one sample to the next.

The MARTI-assay as applied in the ESPRIT biosensor has now reached the stage where a result of sample analysis can be guaranteed within 4 h of receipt of the serum. This is the first time that such reliability has been achieved. However, more sera need to be analyzed to confirm the reproducibility of the assay among the HIV-positive population, to prove the value of the MARTI-test against the many studies reported of low sensitivity and specificity with HIV-positive samples using standard techniques of TB diagnosis (Antunes *et al.*, 2002; Hendrickson *et al.*, 2000; Schleicher *et al.*, 2002).

2.7. The cholesterol nature of MA demonstrated on the ESPRIT biosensor

In our previous studies, we have provided evidence for a structural relationship and attraction between free MAs and cholesterol (Benadie *et al.*, 2008). This was supported by demonstrating the interaction between MA and Amphotericin B—an antifungal macrolide agent known to bind to cholesterol (Baginski *et al.*, 2002)—on the IAsys biosensor system. The same principle was confirmed with the ESPRIT biosensor as demonstrated below, in an attempt to determine what the effect of labeling of MA would be on its manifestation of cholesterol nature.

For the preparation of the different liposomes, phosphatidyl choline stock solution (90 μ l, 100 mg/ml chloroform) is added to an amber glass vial containing either MA (1 mg) or an equimolar amount of 5-BMF labeled MA (1.35 mg). For the preparation of cholesterol-containing liposomes, phosphatidyl choline stock solution (60 μ l, 100 mg/ml chloroform) is added to a cholesterol solution (30 μ l, 100 mg/ml chloroform). The samples are mixed well until dissolved, then dried under a stream of N₂ gas at 85 °C. Saline (2 ml) is then added and the sample is heated on a heat block for 20 min at 85 °C. The sample is then vortexed for 1 min, sonicated with a Virsonic probe sonicator until a clear solution forms to indicate vesicle formation, aliquoted at 0.2 ml per vial, lyophilized and stored at -70 °C until use. Before use, lyophilized liposomes are reconstituted with buffer (2 ml). The liposomes are placed on a heat block for 30 min at 85 °C, vortexed for 2 min and sonified. The final liposome concentration comes to 500 μ g lipid/ml.

The binding interaction between Amphotericin B and either cholesterol-, MA-, or 5-BMF labeled MA-containing immobilized liposomes are tested here. An ODT-coated gold disk is mounted in the ESPRIT instrument and the individual liposomes immobilized as described before. The instrument is operated and reagents used at RT. The liposomes are washed five times with nondegassed PBS/AE, and left for 5 min with mixing to obtain a baseline. Amphotericin B ($1 \times 10^{-4} M$) is added to the liposome layer and the direct interaction is recorded for 10 min after which the disk is washed five times with nondegassed PBS/AE, and left for 5 min. The results (Fig. 5.12) confirm the ability of the ESPRIT biosensor to demonstrate that Amphotericin B recognizes both cholesterol and MA, as was previously shown with the IAsys biosensor. In addition, it shows for the first time the intolerance of the system for fettering with the structure of MA by adding a bulky label on its carboxylic acid group.

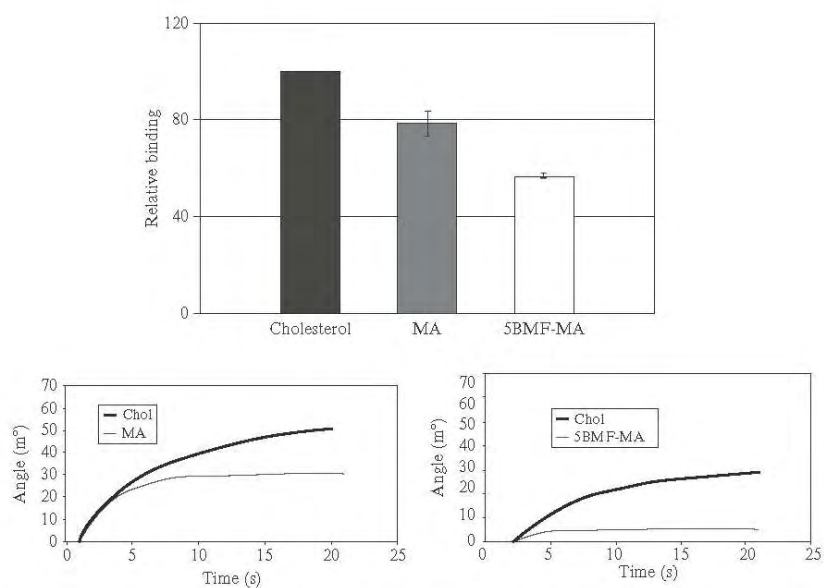


Figure 5.12 Normalized AmB-binding capacity on immobilized lipid antigens cholesterol, MA, and 5BMF-MA and binding curves of MA versus cholesterol and 5BMF-MA versus cholesterol. The error bars indicate the standard deviation, $n = 3$ for each set.

3. CONCLUSION

Antibodies to MA in serum as surrogate markers of active TB can be detected by making use of liposomes as MA antigen carriers in a wave-guide evanescent field biosensor (Thanyani *et al.*, 2008). However, SPR biosensors are more generally in use, more amenable to high-throughput screening, have lower running costs, and provide more comparable binding signals in twin-cell cuvettes. The more preferred technique of SPR biosensor technology, using standard methods to form a hydrophobic surface onto the gold disks on which the MA-containing liposomes can be immobilized, is reported here. This demonstrates the use of liposomes in biosensors to detect large biomolecules such as antibodies. By using Amphotericin B as a small ligand to bind cholesterol and MA in a wave-guide biosensor the cross-reactivity of antibodies to MAs in ELISA can be explained (Benadie *et al.*, 2008). This can also be demonstrated using an SPR biosensor. The biosensor antibody detection approach (MARTI—TB serodiagnostic test) remains unaffected by the antibody cross-reactivity between MA and cholesterol.

ACKNOWLEDGMENTS

This research was supported by a Marie-Curie Early Stage Training Fellowship (Molfun) to Y. Lemmer, the Cancer and Polio Research Fund and the North West Cancer Research Fund, Adcock Ingram Limited (South Africa), the National Research Foundation of South Africa (Technology and Human Resources for Industry Programme), the European and Developing Countries Clinical Trial Partnership Grant No. 2004.1.R.d1, and the Medical Research Council of South Africa. Dr. ten Bokum held a Claude Leon Harris Foundation postdoctoral fellowship.

REFERENCES

- Antunes, A., Nina, J., and David, S. (2002). Serological screening for tuberculosis in the community: An evaluation of the Mycodot procedure in an African population with high HIV-2 prevalence (Republic of Guinea-Bissau). *Res. Microbiol.* **153**, 301–305.
- Arya, S. K., Solanki, P. R., Singh, R. P., Pandey, M. K., Datta, M., and Malhotra, B. D. (2006). Application of octadecanethiol self-assembled monolayer to cholesterol biosensor based on surface plasmon resonance technique. *Talanta* **69**, 918–926.
- Baginski, M., Resat, H., and Borowski, E. (2002). Comparative molecular dynamics simulations of amphotericin B-cholesterol/ergosterol membrane channels. *Biochim. Biophys. Acta* **1567**, 63–78.
- Bangham, A. D. (1983). *Liposomes: An Historical Perspective*. Marcel Dekker, New York.
- Beatty, W. L., Rhoades, E. R., Ullrich, H. J., Chatterjee, D., Heuser, J. E., and Russell, D. G. (2000). Trafficking and release of mycobacterial lipids from infected macrophages. *Traffic* **1**, 235–247.

- Beckman, E. V., Porcelli, S. A., Morita, C. T., Behar, S. M., Furlong, S. T., and Brenner, M. B. (1994). Recognition of a lipid antigen by CD1-restricted $\alpha\beta$ + T cells. *Nature* **372**, 691–694.
- Benadie, Y., Deysel, M., Siko, D. G., Roberts, V. V., Van Wyngaardt, S., Thanyani, S. T., Sekanka, G., Ten Bokum, A. M., Collett, L. A., Grooten, J., Baird, M. S., and Verschoor, J. A. (2008). Cholesteroid nature of free mycolic acids from *M. tuberculosis*. *Chem. Phys. Lipids* **152**, 95–103.
- Butler, W. R., and Kilburn, J. O. (1990). High-performance liquid chromatography patterns of mycolic acids as criteria for identification of *Mycobacterium chelonae*, *Mycobacterium fortuitum*, and *Mycobacterium smegmatis*. *J. Clin. Microbiol.* **28**, 2094–2098.
- Chan, E. D., Reeves, R., Belisje, J. T., Brennan, P. J., and Hahn, W. E. (2000). Diagnosis of tuberculosis by a visually detectable immunoassay for lipoarabinomannan. *Respir. Crit. Care Med.* **161**, 1713–1719.
- Chung, J. W., Kim, D. S., Bernhardt, R., and Pyun, J. C. (2005). Application of SPR biosensor for medical diagnostics of human hepatitis B virus (hHBV). *Sens. Actuator B* **111**, 416–422.
- Dennison, C., and Lovrein, R. (1997). Three-phase partitioning: Concentration and purification of proteins. *Protein Exp. Purif.* **11**, 149–161.
- Eastoe, J., and Ellis, C. (2007). De-gassed water and surfactant-free emulsions: History, controversy, and possible applications. *Adv. Colloid Interface Sci.* **134**, 89–95.
- Goodrum, M. A., Siko, D. G. R., Niehues, T., Eichelbauer, D., and Verschoor, J. A. (2001). Mycolic acids from *Mycobacterium tuberculosis*: Purification by countercurrent distribution and T cell stimulation. *Microbios* **106**, 55–67.
- Han, J., Wang, X., and Kwok, D. L. (2004). Structure and stability of self-assembled monolayer for octadecanethiol adsorbed on flame annealing gold substrate and its potential application to microfluidics. *ICMENS* **4**, 1–4.
- Hartley, G. S., and Runnicles, D. F. (1938). The determination of the size of paraffin-chain salt micelles from diffusion measurements. *Proc. Roy. Soc. London: Math. Phys. Sci.* **168**, 420–440.
- Hendrickson, R. C., Douglass, J. F., Reynold, L. D., McNeill, P. D., Carter, D., Reed, S. G., and Houghton, R. (2000). Mass spectrometric identification of Mtb81, a novel serological marker for tuberculosis. *J. Clin. Microbiol.* **38**, 2354–2361.
- Houghton, R. L., Lodes, M. J., Dillon, D. C., Reynolds, L. D., Day, C. H., McNeill, P. D., Hendrickson, R. C., Skeiky, Y. A. W., Sampaio, D. P., Badaro, R., Lyashchenko, K. P., and Reed, S. G. (2002). Use of multiepitope polyproteins in serodiagnosis of active tuberculosis. *Clin. Diagn. Lab. Immunol.* **9**, 883–891.
- Kim, H. D., Noh, J., Hara, M., and Lee, H. (2001). An adsorption process study on the self-assembled monolayer formation of octadecanethiol chemisorbed on gold surface. *Bull. Korean Chem. Soc.* **22**, 276–280.
- Korf, J., Stoltz, A., Verschoor, J. A., De Baetselier, P., and Grooten, J. (2005). The *Mycobacterium tuberculosis* cell wall component mycolic acid elicits pathogen-associated host innate immune responses. *Eur. J. Immunol.* **35**, 890–900.
- Korf, J. E., Pynaert, G., Tournoy, K., Boonefaes, T., van Oosterhout, A., Ginneberge, D., Haegeman, A., Verschoor, J. A., De Baetselier, P., and Grooten, J. (2006). Macrophage reprogramming by mycolic acids promotes a tolerogenic response in experimental asthma. *Am. J. Respir. Crit. Care Med.* **174**, 152–160.
- Lee, W. J., Sim, J. S., Cho, M. S., and Lee, J. (2005). Characterization of self-assembled monolayer of thiol on a gold surface and the fabrication of a biosensor chip based on surface plasmon resonance for detecting anti-GAD antibody. *Biosens. Bioelectron.* **20**, 1422–1427.
- Pan, J., Fujiwara, N., Oka, S., Maekura, R., Ogura, T., and Yano, L. (1999). Anti-cord factor (trehalose 6, 6'-dimycolate) IgG antibody in tuberculosis patients recognizes mycolic acid subclasses. *Microbiol. Immunol.* **43**, 863–869.

- Reischl, U. (1996). Application of molecular biology-based methods to the diagnosis of infectious diseases. *Front. Biosci.* **1**, 72–77.
- Samanich, K. M., Keen, M. A., Vissa, V. D., Harder, J. D., Spencer, J. S., Belisle, J. T., Zolla-Pazner, S., and Laal, S. (2000). Serodiagnostic potential of culture filtrate antigens of *Mycobacterium tuberculosis*. *Clin. Diagn. Lab. Immunol.* **7**, 662–668.
- Schleicher, G. K., Feldman, C., Vermaak, Y., and Verschoor, J. A. (2002). Prevalence of anti-mycolic acid antibodies in patients with pulmonary tuberculosis co-infected with HIV. *Clin. Chem. Lab. Med.* **40**, 882–887.
- Shankaran, D. R., Gobi, K. V., and Miura, N. (2007). Recent advancements in surface plasmon resonance immunosensors for detection of small molecules of biomedical, food and environmental interest. *Sens. Actuators B* **121**, 158–177.
- Tatulian, S. (1993). *Phospholipids Handbook*. Marcel Dekker Inc., New York.
- Tecilla, P., Dixon, P. D., Slobodkin, G., Alavi, D. S., Waldeck, D. H., and Hamilton, A. H. (1990). Hydrogen-bonding self-assembly of multichromophore structures. *J. Am. Chem. Soc.* **112**, 9408–9410.
- Thanyani, S. T., Roberts, V., Siko, D. G., Vrey, P., and Verschoor, J. A. (2008). A novel application of affinity biosensor technology to detect antibodies to mycolic acid in tuberculosis patients. *J. Immunol. Methods* **332**, 61–72.
- Verschoor, J. A., and Onyebujoh, P. (1999). The menace of the AIDS-tuberculosis combo: Any solutions? *Bioessays* **21**, 365–366.
- Westwell, A. E., and Anacker, E. W. (1959). Adsorption of cetylpyridinium chloride on glass. *J. Phys. Chem.* **63**, 1022–1024.
- Zhang, S., Wright, G., and Yang, Y. (2000). Materials and techniques for electrochemical biosensor design and construction. *Biosens. Bioelectron.* **15**, 273–282.
- Zhang, Y., Wang, H., Yan, B., Zhang, Y., Li, J., Shen, G., and Yu, R. (2008). A reusable piezoelectric immunosensor using antibody-adsorbed magnetic nanocomposite. *J. Immunol. Methods* **332**, 103–111.



ELSEVIER

BASIC SCIENCE

Nanomedicine: Nanotechnology, Biology, and Medicine 6 (2010) 662–671

nanomedicine

www.nanomedjournal.com

Original Article

In vivo evaluation of the biodistribution and safety of PLGA nanoparticles as drug delivery systems

Boitumelo Semete, PhD^{a,*}, Laetitia Booysen, MSc^{a,b}, Yolandy Lemmer, MSc^{a,c},
Lonji Kalombo, MSc^a, Lebogang Katata, PhD^a, Jan Verschoor, PhD^c, Hulda S. Swai, PhD^d

^aCouncil of Scientific and Industrial Research, Polymers and Bioceramics, Pretoria, South Africa

^bDepartment of Pharmacology, North-West University, Potchefstroom Campus, Potchefstroom, South Africa

^cDepartment of Biochemistry, University of Pretoria, Pretoria, South Africa

Received 14 August 2009; accepted 28 February 2010

Abstract

The remarkable physicochemical properties of particles in the nanometer range have been proven to address many challenges in the field of science. However, the possible toxic effects of these particles have raised some concerns. The aim of this article is to evaluate the effects of poly(lactide-co-glycolide) (PLGA) nanoparticles *in vitro* and *in vivo* compared to industrial nanoparticles of a similar size range such as zinc oxide, ferrous oxide, and fumed silica. An *in vitro* cytotoxicity study was conducted to assess the cell viability following exposure to PLGA nanoparticles. Viability was determined by means of a WST assay, wherein cell viability of greater than 75% was observed for both PLGA and amorphous fumed silica particles and ferrous oxide, but was significantly reduced for zinc oxide particles. *In vivo* toxicity assays were performed via histopathological evaluation, and no specific anatomical pathological changes or tissue damage was observed in the tissues of Balb/C mice. The extent of tissue distribution and retention following oral administration of PLGA particles was analyzed for 7 days. After 7 days, the particles remained detectable in the brain, heart, kidney, liver, lungs, and spleen. The results show that a mean percentage (40.04%) of the particles were localized in the liver, 25.97% in the kidney, and 12.86% in the brain. The lowest percentage was observed in the spleen. Thus, based on these assays, it can be concluded that the toxic effects observed with various industrial nanoparticles will not be observed with particles made of synthetic polymers such as PLGA when applied in the field of nanomedicine. Furthermore, the biodistribution of the particles warrants surface modification of the particles to avoid higher particle localization in the liver.

From the Clinical Editor: The aim of this study was to evaluate the effects of poly(lactide-co-glycolide) (PLGA) nanoparticles *in vitro* and *in vivo* compared to industrial nanoparticles including zinc oxide, ferrous oxide, and fumed silica. The authors concluded that the toxic effects observed with various industrial nanoparticles is unlikely to be observed with particles made of PLGA. The biodistribution of these particles warrants surface modification to avoid particle accumulation in the liver.

© 2010 Elsevier Inc. All rights reserved.

Key words: Nanoparticles; Nanomedicine; PLGA; Biodistribution; Toxicity

Nanotechnology has become one of the critical research endeavors of the 21st century; thus, researchers must intensify their efforts to further understand the potential effects of these materials on biological systems. Materials on a nanometer scale have unique physicochemical properties that are due to their small size, surface area, chemical composition, surface structure, solubility, and shape¹; these properties have thus far been

utilized in various fields including drug and gene delivery, imaging, and diagnostics.^{2–4}

Much work in elucidating the possible effects of nanomaterial has been conducted on metal nanoparticles. This is primarily due to the rapid increase in the production of these materials, fueled by the growing need for the properties that these materials provide. Particle toxicity has been studied over a fair number of years, particularly in lung injury in the case of metal nanoparticles, ambient ultrafine particles, asbestos fibers, and dust particles.^{3,5} Various reports have indicated that these particles induce oxidative injury, inflammation, fibrosis, and cytotoxicity.^{3,6,7} It has been reported that smaller particles (aerodynamic diameter <100 nm) have a greater propensity to lead to pulmonary toxicity owing to their small size, larger

No conflict of interest was reported by the authors of this paper.

*Corresponding author. Council for Scientific and Industrial Research, Polymers and Bioceramics, P.O. Box 395, Pretoria 0001, South Africa.

E-mail address: Bsemete@csir.co.za (B. Semete).

1549-9634/\$ – see front matter © 2010 Elsevier Inc. All rights reserved.
doi:10.1016/j.nano.2010.02.002

Please cite this article as: B. Semete, et al. In vivo evaluation of the biodistribution and safety of PLGA nanoparticles as drug delivery systems. *Nanomedicine: NBM* 2010;6:662–671, doi:10.1016/j.nano.2010.02.002

surface area, and deeper penetration into the lungs than bulkier particles of the same material.³

However, with regard to nanomedicine, the adverse effects of the particles have not been extensively studied, possibly because in nanomedicine, mainly biodegradable, biocompatible, and U.S. Food and Drug Administration–approved materials are used.^{2,8} However, concerns over the effects of the physicochemical properties of nanoparticles such as size, surface area, and molecular weight of the material warrants further investigation.

It has been speculated that the specific surface area of nanoparticles is responsible for the potential adverse effects that nanoparticles could have in drug delivery applications.³ This is because smaller particle size increases the specific surface area, thus exposing more atoms or molecules (and thus more reactive groups of the material) on the surface to molecules that would not have access to larger particles.⁹ This aspect could form the basis of the production of reactive oxygen species, wherein the electron donor or acceptor sites on the nanomaterial interact with molecular oxygen, resulting in the formation of superoxide anion or hydrogen peroxide, which subsequently oxidize other chemical species by an electron transfer mechanism. The production of reactive oxygen species has been reported as the most likely mechanism by which these particles exert a toxic effect.³ Therefore, the specific surface area is an important parameter to consider when elucidating the possible adverse effects of a nanomaterial. For efficient drug delivery, the nanosize range of particles is the “holy grail”, because it can facilitate increased intracellular uptake of the drugs to specific cellular targets—a process that is not very efficient in conventional formulations. This, in turn, improves the bioavailability of therapeutic compounds.^{4,10} As suggested by various studies on ultrafine particles,^{5,7} this beneficial property of nanoparticles’ ability to be taken up intracellularly could also be a source of concern, given that the nanosize range of the particles enables unique interaction with biological materials such as key proteins in the cellular pathways, which could possibly culminate in adverse effects.⁶

With the above-mentioned uncertainties about the potential effects of specific surface area, size, and composition of polymeric nanoparticles in mind, our team focused on elucidating the effect of poly(lactide-co-glycolide) (PLGA) nanoparticles, as well as particles composed of ferrous oxide (Fe₂O₃), zinc oxide (ZnO), and fumed silica (SiO₂) on cell viability. Also studied was the effect of PLGA nanoparticles and ZnO particles on various tissues after oral administration. Various reports have indicated that the oral route of drug delivery is still the preferred route and will dominate the drug delivery market for decades to come.¹¹ Hence, for the purpose of the study we explored the effect of these particles when administered orally to Balb/C mice.

In addition, the nanosize range of nanoparticles has been reported to facilitate the crossing of various biological barriers such as the blood-brain barrier (BBB), the skin, and the tight junctions of various epithelial layers.¹² Thus, we further explored the tissue distribution of PLGA particles after oral administration to determine to which tissues these particles localize.

Methods

Preparation of PLGA particles

Nanoparticles were prepared with poly(dl-lactide-co-glycolide) (PLG) 50:50 (molecular weight 45,000–75,000) (Sigma-Aldrich, Johannesburg, South Africa) using a modified double-emulsion solvent evaporation technique.¹³ Aqueous phosphate-buffered saline pH 7.4 was emulsified for a short period with a solution of 100 mg PLGA dissolved in 8 mL of ethyl acetate (EA), by means of a high-speed homogenizer (Silverson L4R, Silverson Machines Limited, Buckinghamshire, United Kingdom) with a speed varying between 3000 and 5000 rpm. The resulting water-in-oil (w/o) emulsion was transferred into a specific volume of an aqueous solution of 1% (wt/vol) polyvinyl alcohol (molecular weight 13,000–23,000 and partially hydrolyzed: 87–89%) used as an emulsion stabilizer, also purchased from Sigma-Aldrich. The mixture was further emulsified for 5 minutes by homogenization at 8000 rpm. The double emulsion (w/o/w) obtained was directly fed into a benchtop Buchi minispray dryer (Model B-290, BÜCHI Labortechnik AG, Flawil, Switzerland) and spray-dried at a temperature ranging between 95° and 110°C, with an atomizing pressure varying between 5 and 8 bars.

To prepare fluorescently labeled PLGA nanoparticles, Rhodamine-6G (Sigma-Aldrich) was dissolved in 2.5 mL EA (0.5 mg/mL), which was added to the solution of PLGA in EA. In cases wherein the particles were labeled with coumarin (Sigma-Aldrich), it was also dissolved in 2.5 mL EA at 0.5 mg/mL. For the preparation of these fluorescently labeled particles, the w/o/w emulsion was left overnight to allow evaporation of the solvent. The pellet recovered after centrifugation was then lyophilized using the Virtis Benchtop freeze dryer (SP Industries, Gardiner, New York). Spray-drying was also applied. The results presented in this article are from the spray-dried formulation, because this method proved to be easier to scale up for the application of these nanoparticles.

Particle size, zeta potential, and surface morphology

Particle size and size distribution were measured by dynamic laser scattering or photon correlation spectroscopy using a Malvern Zetasizer Nano ZS (Malvern Instruments, Worcester-shire, United Kingdom). For each sample, 1–3 mg of nanoparticles were suspended in distilled water, then vortexed and/or sonicated for a few minutes. Each sample was measured in triplicate. The zeta potential was also determined using the same instrument, in pH 6.8. The morphology of PLGA nanoparticles was analyzed using a scanning electron microscope (LEO 1525 Field Emission scanning electron microscope, Zeiss, Oberkochen, Germany).

Surface area determination

Surface area measurements were carried out according to the conventional BET method,¹⁴ using the Nova 1000e surface area and pore size analyzer (Quantachrome Instruments, Boynton Beach, Florida). The method is based on isothermal adsorption of nitrogen onto the particles at liquid nitrogen temperature and relative pressures (P/P₀) ranging from 0.05 to 0.2. Spray-dried

PLGA particles (50 mg), Fe₂O₃, and SiO₂ (obtained from Walter Focke, University of Pretoria, Department of Chemical Engineering) were degassed by heating under vacuum and used for the measurement. The adsorbed nitrogen volume at 77.3 K was calculated by measuring the pressure change resulting from the adsorption of nitrogen gas onto the surface of particles. The area per molecule value for nitrogen was taken at 162 nm², and using this value, the total surface area of the sample was determined. The specific surface area was calculated by dividing the surface area by the sample weight.

In vitro cell viability assay

Caco-2 cells (human colorectal carcinoma) and HeLa (human epithelial carcinoma) cells were purchased from Highveld Biologicals, Johannesburg, South Africa. The cells were cultured in 25-mL flasks at 37°C in humidified atmosphere (90% humidity), 5% CO₂, Dulbecco's minimal essential medium, 1% (wt/vol) nonessential amino acids, 1% (wt/vol) glutamine, 10% (vol/vol) fetal bovine serum, penicillin, (100 U/mL), and streptomycin (100 µg/mL). Stocks of the cells were prepared in culture medium containing 80% (vol/vol) fetal bovine serum and 10% (vol/vol) dimethyl sulfoxide and kept in liquid nitrogen until further use. The cells were maintained according to routine cell culture procedures. To determine cell viability after exposure of all cell lines to different concentrations of PLGA nanoparticles of an average size of 374 nm incubated for 24 hours, the WST assay (Quick Cell Proliferation Assay Kit II, Mountain view, California) was performed according to manufacturer's instructions. This colorimetric cell proliferation kit allows for easy and reliable colorimetric determination of viable cell numbers with excellent sensitivity and linearity. The kit utilizes the tetrazolium salt WST-1, which is reduced to water-soluble orange formazan by cellular mitochondrial dehydrogenase present in viable cells. The amount of formazan dye, determined by the absorbance at 450 nm with a reference wavelength at 630 nm, is directly proportional to the number of living cells. Fe₂O₃, SiO₂, and ZnO (Sigma) nanoparticles were used as controls.

In vivo studies

Animals

Unchallenged Balb/C female mice weighing between 20 and 25 g were selected and housed under standard-environment conditions at ambient temperature of 25°C. Animals were humanely cared for and supplied with food and water ad libitum. Ethics approval was obtained for this study from the Ethics Committee for Research on Animals (ECRA), Tygerberg, Cape Town, South Africa.

Histopathology assays

Mice were placed into different groups with three mice per group based on the particles they were treated with and the time frame of treatment. The different groups consisted of animals treated separately with 4 mg PLGA particles, 4 mg SiO₂, and 4 mg ZnO nanopowder (purity >99%; Sigma-Aldrich) by mouth. The latter was used as a positive control in this study, as it is known to have toxic effects on tissues.¹⁵ Polystyrene beads (Sigma-Aldrich, 300 nm) were used as negative control. Group 1

was treated for 24 hours, group 2 was treated daily for 5 days, and group 3 was treated daily for 10 days. Mice were euthanized on day 1, 5 and 7 respectively. The study was repeated once, except that the second time mice were overdosed with the particles (i.e., 60 mg of PLGA particles and 60 mg of SiO₂ and polystyrene beads for 24 hours, for 5 days, and for 10 days. Full necropsies were conducted on the mice following humane euthanasia. The brain, heart, kidney, liver, lung, spleen, gonad (female genitalia), large and small intestines, pancreas, stomach, and thymus were collected from each animal. Tissues were fixed with formalin, and tissue sections cut and processed using routine histological methods in an automated system. Sections of 5 µm were prepared after paraffin embedding. The slides obtained were stained with routine hematoxylin and eosin staining method in an automated stainer.

Tissue distribution assays of PLGA nanoparticles

To determine the biodistribution of the nanoparticles, fluorescently labeled particles were orally administered to mice. The mice were grouped with three mice per group, and the study was repeated three times. Group 1 was treated with 4 mg of rhodamine-PLGA nanoparticles in 0.2 mL sterile saline by oral gavage. Group 2 was treated with 4 mg coumarin-labeled PLGA nanoparticles in 0.2 mL sterile saline by oral gavage. The two fluorescent dyes were used to determine if there any differential biodistribution occurred based on the fluorescent dyes. Furthermore, rhodamine and coumarin were spray-dried without encapsulating into PLGA nanoparticles and orally administered to mice.

In addition, 4 mg of fluorescently labeled polystyrene beads were orally administered as a control to group 3. The mice were killed via cervical dislocation. The brain, heart, kidneys, liver, lungs, and spleen as well as plasma were collected. The tissues were homogenized on ice in 2 mL phosphate-buffered saline, and diluted 100 times. The resulting diluted homogenates were analyzed for fluorescent particles on the FLx8000 Biotek plate reader (Biotek, Winooski, Vermont) at excitation and emission wavelengths of 488 nm and 525 nm, respectively. The tissues were further analyzed via confocal microscopy to determine if the fluorescence observed was still in the particulate matter or had been leached out.

Results

Particle size, zeta potential, surface morphology, and specific surface area

Various parameters were optimized to obtain an average particle size ranging between 200 and 350 nm, with an average polydispersity index of 0.1 observed when freeze-drying was used (Figure 1, A). However, the polydispersity index of the spray-dried formulation was higher (0.2 as observed in Figure 1, B) with a size range of 300 nm to 1 µm. The particles had a zeta potential between -10 and -18 mV. The spray-dried particles were characterized by a very smooth surface, similar to the freeze-dried particles as depicted by scanning electron microscopy (images in Figure 1, A and B). However, the

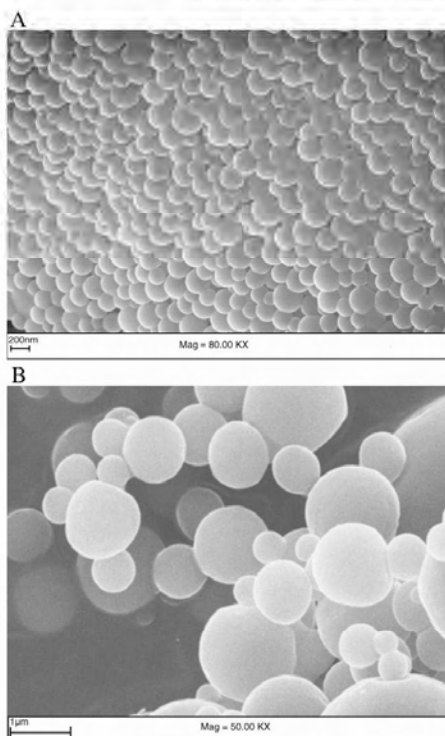


Figure 1. (A) SEM picture of freeze-dried formulation (prepared with 40 mL 1% wt/vol polyvinyl alcohol). Bar = 200 nm. (B) Spray-dried formulation with the same parameters. Bar = 1 μm.

particles were not equivalent in size. The freeze-dried PLGA nanoparticles had a specific surface area ranging between 3 and 10 m²/g, whereas a specific surface area ranging between 15 and 25 m²/g was found for ZnO nanoparticles at a size of 50–150 nm. Fe₂O₃ and SiO₂ had specific surface areas of 11–15 m²/g and 755–1043 m²/g, respectively, and a size range of 100–250 nm. The *in vitro* and *in vivo* data presented in the manuscript are for the freeze-dried PLGA particles.

In vitro cell viability assays

The *in vitro* cytotoxicity of PLGA nanoparticles, SiO₂, Fe₂O₃ particles, and ZnO particles was determined at concentrations of 0.1, 0.01 and 0.001 mg/mL, on Caco-2 cells and Hela cells via the WST assay. The results depicted in Figure 2 indicate that, compared with untreated cells (control), the Hela and Caco-2 cell lines retained more than 75% viability when treated with various concentrations of PLGA nanoparticles, SiO₂, and Fe₂O₃. This result supports literature indicating that amorphous silica, as was used in this study, is not toxic to cells.¹⁵ However, ZnO

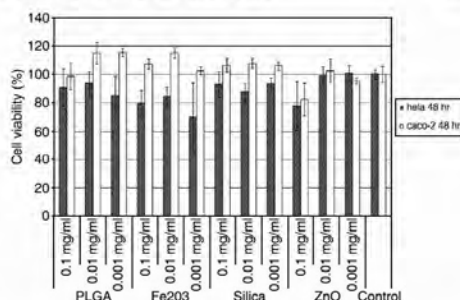


Figure 2. Effects of poly(lactide-co-glycolide), ferrous oxide, and fumed silica particles on percentage viability of Caco-2 and Hela cell lines as shown by a WST assay. The data are representative of two repeats of n = 6; error bars indicate SEM.

nanopowder resulted in a significant reduction in cell viability, as indicated in Figure 2. This result is also in accordance with those of Sharma et al 2009, where it was indicated that ZnO nanoparticles are toxic to cells.

Histopathology assays

Subsequent to oral administration of PLGA particles as well as polystyrene beads for 1, 5, and 10 days, no pathological lesions were detected in the respective groups that could be suggestive of toxicity. (Images of the polystyrene-treated group are not included, as they are similar to those of PLGA particles.) The data were in accordance with those of the saline control group. None of the analyzed tissues exhibited any lesions, even at 60 mg PLGA, as depicted in Table 1. The group treated with amorphous SiO₂ particles showed no noticeable lesion (images not included). The group of mice that were treated with 4 mg ZnO for 24 hours died, and a subset of the mice showed weight loss. Based on these observations, the positive control was not continued for the 5- and 10-day studies. Thus, it can be suggested from these data that PLGA particles at the various concentrations administered do not exhibit any toxicity in mice based on histopathological assays.

Tissue distribution assays

The fluorescently labeled particles were initially not detected in the 5-μm tissue sections via fluorescent microscopy, as a result of the intense autofluorescence of the tissues. Thus, a fluorometer was used to detect fluorescence in the tissue homogenates. The data were normalized with the negative control, which was tissue from mice treated with only saline. The background fluorescence from these tissues was subtracted from the experimental tissue fluorescence readings to exclude the effect of autofluorescence. The percentage particles detected was expressed as the ratio of the fluorescence unit of each tissue relative to the sum of fluorescence units of all tissues analyzed and graphically illustrated in Figure 3 and listed in Table 2 for each tissue. From these data it is evident that most of the particles were detected in the liver at 40.04% ± 8.42%, followed by the

Table 1
 Histopathology and confocal images of different mouse tissues after oral administration of fluorescently labeled PLGA or fumed silica

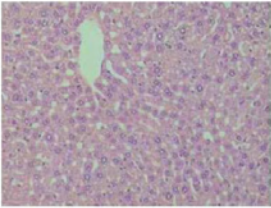
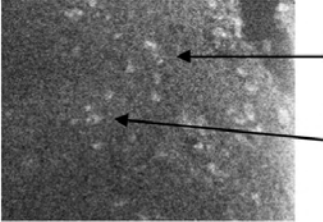
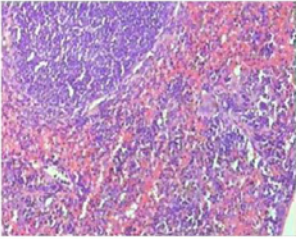
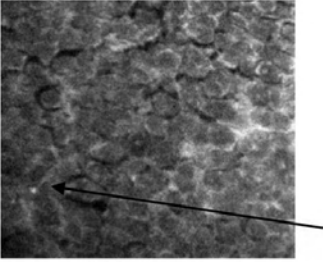
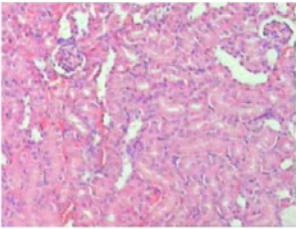
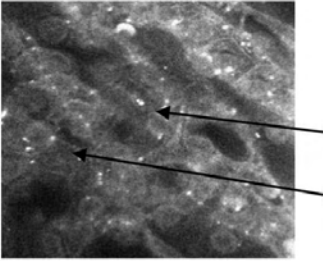
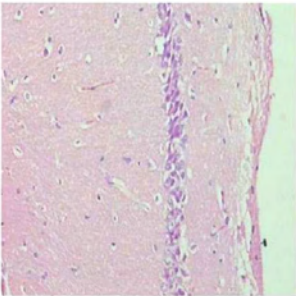
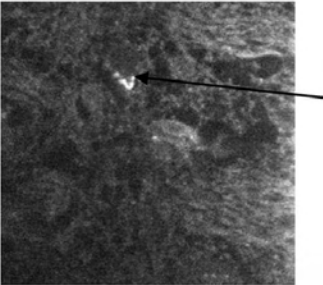
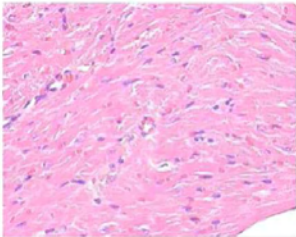
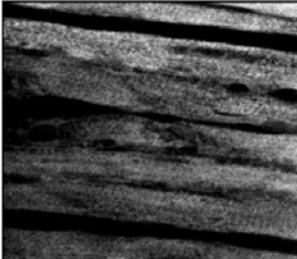
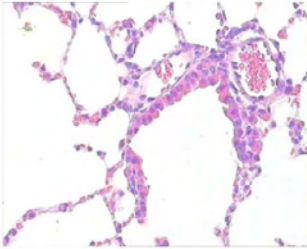
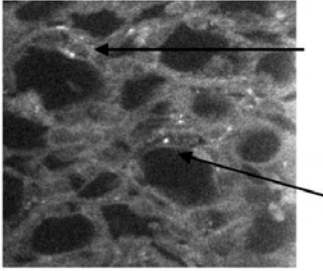
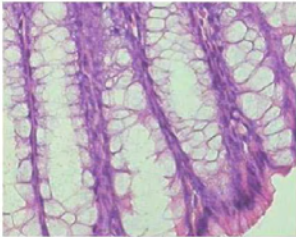
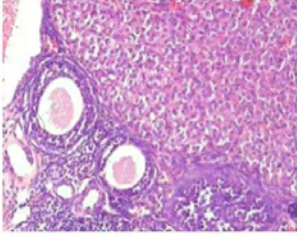
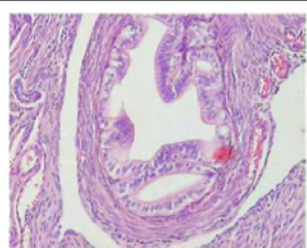
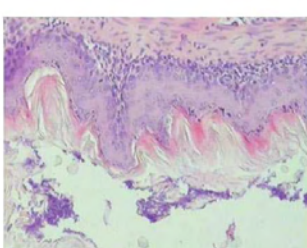
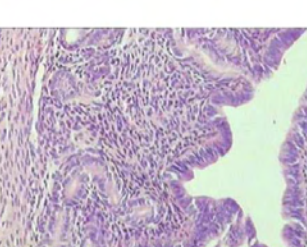

Tissue	Tissues treated with PLGA nanoparticles (fumed SiO ₂ gave results similar to the PLGA particles)	Confocal microscope images (62× magnification) of tissue sections, 1 day after administration of rhodamine-labeled particles
Liver		
Spleen red pulp		
Kidney		
Hippocampus in the cerebrum		

Table 1 (continued)

Tissue	Tissues treated with PLGA nanoparticles (fumed SiO ₂ gave results similar to the PLGA particles)	Confocal microscope images (62× magnification) of tissue sections, 1 day after administration of rhodamine-labeled particles
myocardium		
Terminal bronchiolus and lung		
Large intestines		Not analyzed via confocal microscope
Ovarian follicles and corpus luteum		Not analyzed via confocal microscope

(continued on next page)

Table 1 (continued)

Tissue	Tissues treated with PLGA nanoparticles (fumed SiO ₂ gave results similar to the PLGA particles)	Confocal microscope images (62× magnification) of tissue sections, 1 day after administration of rhodamine-labeled particles
Fallopian duct		Not analyzed via confocal microscope
Glandular gastric mucosa		Not analyzed via confocal microscope
Endometrium of uterine mucosa		Not analyzed via confocal microscope
Thymus lymphoid tissues		Not analyzed via confocal microscope

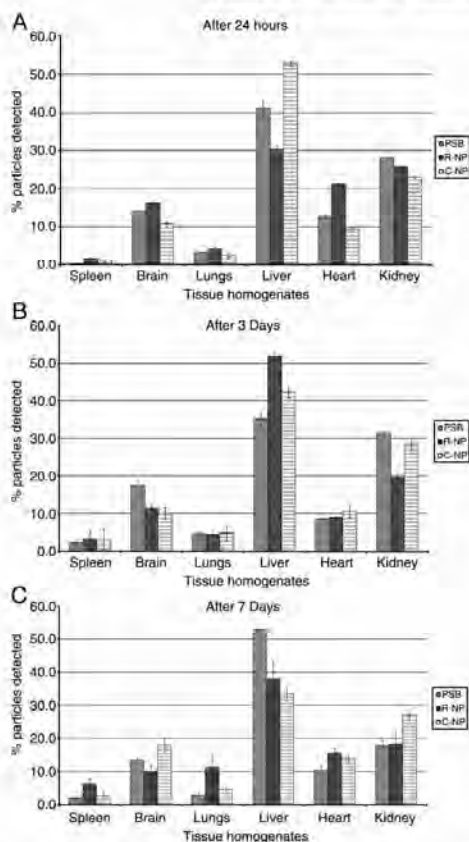


Figure 3. Tissue distribution graphically represented as a measure of percentage of particles detected of the total particles. The data represent three repeats of $n = 6$; error bars indicate SEM. (A) 24 hours, (B) 3 days, (C) 7 days. PSB, polystyrene beads; R-NP, rhodamine nanoparticles; C-NP, coumarin nanoparticles.

kidney ($25.97\% \pm 7.09\%$), heart ($11.92\% \pm 3.16\%$), and brain ($12.86\% \pm 2.82\%$) throughout all 7 days in which the tissues were analyzed. Plasma was also analyzed from day 3 as indicated in Figure 4, but only very small amounts of the particles were detected. Confocal images of the tissues after 1 day of administration of the rhodamine-labeled particles are presented in Table 1, where we have shown, using unstained tissues for comparison, that the fluorescent particles can be detected within the various tissues. It has been reported that rhodamine release from nanoparticles is very slow, and therefore, the detection of fluorescence in the different tissues can be considered to be that of the rhodamine associated with the PLGA nanoparticles.^{16,17} It must be emphasized that the confocal images do not correlate to

Table 2

Percentage particles detected, calculated as a function of total particles

Organ	% Particles detected								
	1 day			3 days			7 days		
	PSB	R-NP	C-NP	PSB	R-NP	C-NP	PSB	R-NP	C-NP
Brain	14.3	16.4	10.8	17.6	11.5	10.2	13.6	10.1	18.1
Heart	12.8	21.3	9.4	8.7	9.1	10.7	10.5	15.7	14
Kidney	28.2	25.9	23.1	31.5	19.7	28.6	18	18.3	27.1
Lung	3.4	4.2	2.7	4.8	4.5	4.9	2.9	11.4	4.7
Liver	41.3	30.5	52.9	35.2	51.9	42.4	55	38.1	33.4
Spleen	0.2	1.7	1.1	2.3	3.3	3.3	2	6.4	2.7

PSB, polystyrene beads; R-NP, rhodamine nanoparticles; C-NP, coumarin nanoparticles.

Data are expressed as a representation of percentage particles detected of total particles; $n = 6$.

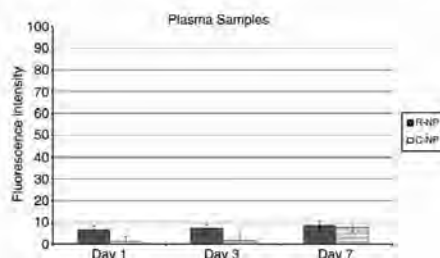


Figure 4. Fluorescence detection in plasma represented as a function of fluorescence intensity. R-NP, rhodamine nanoparticles; C-NP, coumarin nanoparticles.

the quantity of the particles in the tissues, but only indicate the presence of the particles in the respective tissues and also indicate the particulate nature of the fluorescence, suggesting that the observed fluorescence is that of rhodamine in the nanoparticles and not leached rhodamine.

Discussion

The toxicity of nanoparticles involves physiological, physicochemical, and molecular considerations. Extensive studies on industrial nanoparticles investigating these parameters have been conducted, but not much is known about nanoparticles that are used for therapeutic purposes. At present, PLGA is used extensively for drug delivery applications.^{4,18} It is with this in mind that this study focused on elucidating the effect of PLGA nanoparticles in vitro and in vivo. Much controversy still exists regarding the potential adverse effects, so there is a need for reports indicating the safety of these materials. The particles analyzed had specific surface areas within a similar range, except for the amorphous silica, which had a higher specific surface area. Thus, although these PLGA particles had a surface area similar to that of ZnO, which served as a positive control, no toxic effect as presented in the viability

Table 3
Fluorescence units of tissues after oral administration of fluorescently labelled particles or spray dried fluorophores

	Brain	Heart	Kidney	Liver	Lungs	Spleen
RH-NPs day 1	35.9	47.8	53.9	67.1	8.9	3.8
RH day 1	2.5	1	11.8	4	1	1
RH-NPs day 3	36.3	28.4	170.4	63.4	14.4	10.5
RH day 3	4.8	1	4.2	6	1	1
RH NPs day 7	40.3	64.8	156.8	93.2	43.2	29.5
RH day 7	5	1	2	2	1	1
C-NPs day 1	35.4	31.4	75.6	176.3	8.4	3.5
C day 1	1.3	1	4.8	1	14.3	1
C-NPs day 3	50.7	54	171	214.3	27.7	24
C day 3	1	1	5.8	50.3	10.1	1
C-NPs day 7	66.9	53	110.9	140.7	18.9	9.9
C day 7	-0.2	1	8.8	73.3	1	1

RH, Rhodamine; NPs, nanoparticles, C, Coumarin. n = 3.

assays was observed. This suggests that the biodegradability and biocompatibility of PLGA nanoparticles facilitates their safe use in medical applications.

In vitro cytotoxicity of the respective particles was tested in two different cell lines. The PLGA nanoparticles were shown to have no cytotoxic effects on the cells. Although specific surface area has been reported to be causal in some of the observed toxicities in metal nanoparticles,⁶ it is clear from the viability assay that the surface area of PLGA particles did not significantly affect the viability of the cells analyzed. Second, it can be suggested that the chemical composition of the PLGA nanoparticles did not contribute to toxicity. As polyesters in nature, PLGA undergoes hydrolysis and enzymatic degradation upon implantation into the body, forming biologically compatible moieties that can be metabolized (lactic acid and glycolic acid) and are eventually removed from the body by the citric acid cycle.¹⁹ These PLGA biodegradation products are formed at a very slow rate and hence do not affect normal cell function. Although SiO₂ nanopowder and Fe₂O₃ particles had larger specific surface areas as compared with PLGA particles, they did not exhibit any toxicity, thus supporting the observation that surface area is not the main determinant of toxicity in nanoparticulate structures.

Subsequent to oral administration of polystyrene beads, rhodamine-labeled PLGA particles, as well as coumarin-labeled PLGA particles in the respective groups, particles were detected in all tissues evaluated. The highest percentage of particles was detected in the liver, followed by the kidney, the brain, and the heart, as shown in Table 2. To confirm that the fluorescence detected is from the encapsulated fluorophores, Table 3 illustrates the fluorescence measured of the encapsulated fluorophores versus the unencapsulated but spray-dried fluorophores. Thus, from these data it is evident that rhodamine and coumarin are cleared from the tissues within 1 day, and thus low concentrations are detected in comparison with when these fluorophores are encapsulated in PLGA nanoparticles. This result also confirms that these nanoparticles are able to cross cellular barriers such as the BBB and reach hard-to-target tissues—in accordance with work published elsewhere.^{12,20} However, we have also shown that although these particles are detected in various tissues within a 7-day period, these particles do not cause any morphological

pathology in the respective tissues even at high doses (i.e., 60 mg per 25g mice). As demonstrated by the histopathology assays conducted, no lesions or inflammation was observed in the brain. The lowest concentrations were observed in the spleen and lungs. This result could indicate that for oral administration of PLGA particles for drug delivery purposes, these particles will have to be surface-modified with hydrophilic molecules such as polyethylene glycol to minimize opsonization of the particles, thus increasing the circulation time in the blood with the eventual effect of minimizing the amount of particles that reach the liver. Thus far, various hydrophilic surfactants have been used to minimize opsonization.²¹ Poloxamers, poloxamines, and other polymers such as chitosan can also be used for this purpose.²² This will, in turn, minimize first-pass metabolism of the encapsulated drugs. Various groups have also reported modification of the particles with peptides or proteins.¹⁶

Drug delivery systems such as PLGA nanoparticles will provide an ideal carrier system to various tissues that are generally hard to target even with oral administration, as presented in this study as well as other studies.^{18,20} Because of its ability to cross the BBB, this system will present a means of effectively treating neurological and psychiatric disorders,¹⁶ as well as other disseminated diseases such as tuberculosis, by administering the nanoencapsulated drugs orally or via any other noninvasive modes. Furthermore, according to this study, PLGA nanoparticles are safe to use as a drug delivery system, although many concerns still exist regarding the safety of nanomaterials in general.

From this study conducted with biodegradable and biocompatible PLGA nanoparticles, it is clear that these particles are not toxic in cell culture and when orally administered at the mentioned doses to Balb/c mice. More studies need to be conducted with other polymeric nanoscale drug delivery systems, to evaluate their safety. It is clear from the biodistribution data that nanoscale drug delivery systems will be suitable to improve the permeability, and thus the bioavailability of therapeutic compounds. With this approach, delivery of drugs that have poor permeability and solubility can be greatly enhanced with safe and effective drug delivery systems.

Acknowledgments

We thank Kobus Venter at the Medical Research Council for assisting with the mice studies, Robyn Brackin at the Council of Scientific and Industrial Research for assistance with the confocal images, and Dr. Willem Botha of Vetpath Laboratories for assisting with the histopathology assays.

References

- Magenheim B, Benita S. Nanoparticle characterization: a comprehensive physicochemical approach. *S T P Pharm Sci* 1991;1:221–41.
- Duncan R. Nanomedicine gets clinical. *Materials Today* 2005;8:16–7.
- Nel A, Xia T, Madler L, Li N. Toxic potential of materials at the nanolevel. *Science* 2006;311:622–7.
- Panyam J, Labhasetwar V. Biodegradable nanoparticles for drug and gene delivery to cells and tissue. *Adv Drug Deliv Rev* 2003;55:329–47.
- Stone V, Donaldson K. Nanotoxicology: signs of stress. *Nat Nanotechnol* 2006;1:23–4.

6. Li N, Xia T, Nel AE. The role of oxidative stress in ambient particulate matter-induced lung diseases and its implications in the toxicity of engineered nanoparticles. *Free Radic Biol Med* 2008;44:1689–99.
7. Oberdorster G, Maynard A, Donaldson K, Castranova V, Fitzpatrick J, Ausman K, et al. Principles for characterizing the potential human health effects from exposure to nanomaterials: elements of a screening strategy. *Particle Fibre Toxicol* 2005;2:8–43.
8. McNeil SE. Nanotechnology for the biologist. *J Leukocyte Biol* 2005; 78:585–94.
9. Liveridge GG, Cundy KC. Particle size reduction for improvement of oral bioavailability of hydrophobic drugs: I. Absolute oral bioavailability of nanocrystalline dexamethasone in beagle dogs. *Int J Pharm* 1995;125: 91–7.
10. Desai MP, Labhasetwar V, Amidon GL, Levy RJ. Gastrointestinal uptake of biodegradable microparticles: effect of particle size. *Pharm Res* 1996;13:1838–45.
11. Wilkinson JM. Roadmapping medical devices. *Medical Device Link* 2006;6:1-0090 Ref Type: Electronic Citation. Available at: <http://www.devicelink.com/mdt/archive/06/06/014.html>.
12. Koziara JM, Lockman PR, Allen DD, Mumper RJ. In situ blood brain barrier transport of nanoparticles. *Pharm Res* 2003;20:1772–8.
13. Lamprecht A, Ubrich N, Hombreiro Perez M, Lehr CM, Hoffman M, Maincent P. Biodegradable monodispersed nanoparticles prepared by pressure homogenization-emulsification. *Int J Pharm* 1999;184: 97–105.
14. Brunauer S, Emmett PH, Teller E. Adsorption of gases in multimolecular layers. *J Am Chem Soc* 1938;60:309–19.
15. Merget R, Bauer T, Klüpper H, Philippou S, Bauer H, Breitzstadt R, et al. Health hazards due to the inhalation of amorphous silica. *Arch Toxicol* 2002;75:625–34.
16. Vergoni AV, Tosi G, Tacchi R, Vandelli MA, Bertolini A, Costantino L. Nanoparticles as drug delivery agents specific for CNS: in vivo biodistribution. *Nanomed Nanotechnol Biol Med* 2009;5:369–77.
17. Tosi G, Costantino L, Rivasi F, Ruozi B, Leo E, Vergoni AV, et al. Targeting the central nervous system: in vivo experiments with peptide-derivatized nanoparticles loaded with Loperamide and Rhodamine-123. *J Control Release* 2007;122:1–9.
18. Jais RA. The manufacturing techniques of various drug loaded biodegradable poly(lactide-co-glycolide) (PLGA) devices. *Biomaterials* 2000;21:2475–90.
19. Campbell MK. *Biochemistry*. Philadelphia: Saunders College Publishing; 1995. p. 365–84.
20. Lockman PR, Mumper RJ, Khan A, Allen DD. Nanoparticle technology for drug delivery across the blood-brain barrier. *Drug Dev Ind Pharm* 2002;28:1–13.
21. Storm G, Belliot SO, Daemen T, Lasic DD. Surface modification of nanoparticles to oppose uptake by the mononuclear phagocyte system. *Adv Drug Deliv Rev* 1995;17:31–48.
22. Torchilin VP, Trubetskoy VS. Which polymers can make nanoparticulate drug carriers long-circulating? *Adv Drug Deliv Rev* 1995;16:141–55.



ELSEVIER

Contents lists available at ScienceDirect

Chemistry and Physics of Lipids

journal homepage: www.elsevier.com/locate/chemphyslip



Structure–function relationships of the antigenicity of mycolic acids in tuberculosis patients

Beukes Mervyn^{a,1}, Lemmer Yolandy^{a,1}, Deysel Madrey^{a,1}, R. Al Dulayymi Juma'a^d, S. Baird Mark^d, Koza Gani^d, M. Iglesias Maximiliano^d, R. Rowles Richard^d, Theunissen Cornelia^d, Grooten Johan^e, Toschi Gianna^a, V. Roberts Vanessa^a, Pilcher Lynne^b, Sandra Van Wyngaardt^a, Mathebula Nsovo^b, Balogun Mohammed^b, C. Stoltz Anton^c, Jan A. Verschoor^{a,*}

^a Department of Biochemistry, University of Pretoria, South Africa

^b Department of Chemistry, University of Pretoria, South Africa

^c Department of Infectious Diseases, University of Pretoria, South Africa

^d School of Chemistry, University of Wales, Bangor, United Kingdom

^e Department of Molecular Biomedical Research, Molecular Immunology Unit, Gent University, Belgium

ARTICLE INFO

Article history:

Received 16 July 2010

Received in revised form

14 September 2010

Accepted 17 September 2010

Available online xxx

Keywords:

Mycolic acids

Cholesterol

Monoclonal antibodies

Tuberculosis

Diagnostics

Antigenicity

ABSTRACT

Cell wall mycolic acids (MA) from *Mycobacterium tuberculosis* (*M.tb*) are CD1b presented antigens that can be used to detect antibodies as surrogate markers of active TB, even in HIV coinfecting patients. The use of the complex mixtures of natural MA is complicated by an apparent antibody cross-reactivity with cholesterol. Here firstly we report three recombinant monoclonal scFv antibody fragments in the chicken germ-line antibody repertoire, which demonstrate the possibilities for cross-reactivity: the first recognized both cholesterol and mycolic acids, the second mycolic acids but not cholesterol, and the third cholesterol but not mycolic acids. Secondly, MA structure is experimentally interrogated to try to understand the cross-reactivity. Unique synthetic mycolic acids representative of the three main functional classes show varying antigenicity against human TB patient sera, depending on the functional groups present and on their stereochemistry. Oxygenated (methoxy- and keto-) mycolic acid was found to be more antigenic than alpha-mycolic acids. Synthetic methoxy-mycolic acids were the most antigenic, one containing a *trans*-cyclopropane apparently being somewhat more antigenic than the natural mixture. *Trans*-cyclopropane-containing keto- and hydroxy-mycolic acids were also found to be the most antigenic among each of these classes. However, none of the individual synthetic mycolic acids significantly and reproducibly distinguished the pooled serum of TB positive patients from that of TB negative patients better than the natural mixture of MA. This argues against the potential to improve the specificity of serodiagnosis of TB with a defined single synthetic mycolic acid antigen from this set, although sensitivity may be facilitated by using a synthetic methoxy-mycolic acid.

© 2010 Published by Elsevier Ireland Ltd.

1. Introduction

South Africa currently has the highest per capita incidence of TB in the world. In 2007 alone 112,000 people died of TB in South Africa, of whom 94,000 were co-infected with HIV (WHO, 2009). One of the biggest challenges facing clinicians is the time it takes to accurately diagnose TB. Currently, using the conventional methods, it takes on average 4 weeks to diagnose TB, which leads to a delay in treatment of the disease. Two thirds of TB deaths could be prevented by early diagnosis. With fast diagnosis patients could

be put on anti-TB therapy immediately and become non-infective within a few days. With the current methods of diagnosis, patients with persistent symptoms have to remain in quarantine for several weeks while awaiting the results. During this time, they can infect the medical staff, their next of kin or anyone with whom they share a closed area, such as in public transport. With MDR and XDR TB on the increase, this threatens to spread an almost incurable disease among hospital staff and the communities that can be fatal within 2 months. The need for a fast, reliable diagnostic tool for TB is therefore high, especially in high HIV incidence populations (Wood, 2007).

Immunodiagnostic assays detecting pathogen related antibodies in patient sera with active TB disease are an attractive alternative for rapid diagnosis. An array of mycobacterial cell wall components have been considered as antigens for surrogate marker antibodies

Q1 ^{*} Corresponding author. Tel.: +27 124202477; fax: +27 123625302.

E-mail address: Jan.Verschoor@up.ac.za (J.A. Verschoor).

¹ These authors contributed equally towards the article.

for TB (Fujiwara et al., 1999; Lyashchenko et al., 1998; Nabeshima et al., 2005). Antigenic activity of mycolic acids (MA) and their glycolipid derivatives such as the lipid extractable trehalose mono- or dimycolates, TMM or TDM respectively (cord factors) has been reviewed recently (Sekanka et al., 2007). Of all the antigens prevalent in the cell wall of the mycobacteria that may be considered for use in TB serodiagnosis, MAs provide a special opportunity due to their abundance, variability among different species of *Mycobacterium* and the unique way that they communicate their presence to the immune response of the host (Sekanka et al., 2007; Shui et al., 2007; Yuan et al., 1997). The ability of MAs to elicit CD4⁺, CD8⁻ double negative T cells by means of their presentation on CD1b proteins of dendritic cells (Beckman et al., 1994) may well be the reason that antibody binding to MAs in AIDS patients with even very low CD4 T cell counts is maintained, relative to other patients that are not infected with HIV, or have normal CD4 T cell counts (Schleicher et al., 2002). Pan et al. have shown that the most determining antigenic part of the cord factor antigen is the MA (Pan et al., 1999).

The use of MA antigens to detect antibodies as surrogate markers for TB diagnosis was shown to be feasible in ELISA assays (Pan et al., 1999; Schleicher et al., 2002), albeit of limited accuracy. One complication was the apparent cross-reactivity of TB patient serum antibodies between MAs and cholesterol, most likely due to a shared structural feature between cholesterol and a folded form of MA, as both could be liganded by Amphotericin B, a cholesterol binding drug (Benadie et al., 2008). A biosensor approach, the MARTI-test (Mycolic acids Antibody Real-Time Inhibition), using free natural mixtures of MAs in liposomes as antigens in a competitive binding assay showed improved accuracy (Lemmer et al., 2009; Thanyani et al., 2008). This test can diagnose TB within four hours of sampling by detecting anti-MA antibodies as immune surrogate markers for active disease even in HIV infected patients. Although the use of the inhibition of binding of antibodies in a real-time immunoassay seemed to practically solve the problem of cross-reactivity between MAs and cholesterol, it is expected that better resolution between TB positive and TB negative patient sera will be achieved if the nature of the cross-reactivity is better understood. A structure-activity investigation of the antigenicity of MAs and cholesterol may identify an individual synthetic MA which is more selectively antigenic than the natural mixtures.

MAs comprise a large number of various structures within and among *Mycobacterium* species and in a few other genera. In *M. tuberculosis*, they consist mainly of alpha-, keto- and methoxy-MA subclasses, each containing mixtures of homologues of varying chain length and, in some cases different stereochemistry around the functional groups in the main (mero-) chain (Dobson

et al., 1985). They are present either bound to the cell wall as penta-arabinose tetramycolates or as sugar esters (e.g., trehalose dimycolates and trehalose monomycolates). There is increasing evidence of the importance of some natural free MAs (Ojha et al., 2008). Whether all, a few, or one of these MAs is detected as antigens by TB patient antibodies is not clear and is one focus of this report. Pan et al. (1999) indicated that the methyl esters of homologous mixtures of natural methoxy-MAs are more antigenic than those of the keto-MA or the non-oxygenated alpha-MA. A more sensitive and specific diagnostic assay could possibly be developed by making use of specific stereoisomers of single chain lengths of synthetic MA subclasses instead of using natural mixtures of MA. Because different MA subclasses dominate in certain stages of the growth of mycobacteria or stage of disease, it could also be that a specific synthetic MA antigen could provide more reliable data, reveal information on the progress of the disease and be better able to distinguish between TB positive and TB negative patient sera.

The three major classes of MA are exemplified by structures A-C (Fig. 1). In each of these, the stereochemistry of the hydroxy acid part is R,R- and that of the methoxy-methyl fragment in B is reported to be S,S. The alpha-methylketone of C is also apparently of S-stereochemistry, although often in the isolation of such compounds from cells by chemical hydrolysis this centre is epimerized to a mixture of R- and S-forms. The absolute stereochemistry of the cis-cyclopropane remains uncertain, although if a common intermediate is involved in producing methoxy-, hydroxy-, keto- and cyclopropane functionalities, it will be as shown in A-C (see e.g., Koza et al., 2009a). More recently it has become clear that hydroxy-MAs are probably intermediate in the formation of methoxy- and keto-MAs and indeed some examples have been detected directly (Quémard et al., 1997; Dubnau et al., 1997). In a number of cases, the proximal cis-cyclopropane is replaced by an alpha-methyl-trans-cyclopropane as in, for example, D. Generally such compounds will be present together with the corresponding cis-cyclopropane in the complex mixture of different classes and different homologues (chain lengths) of MA extracted from cells. Even when the MA extracted from cells is separated into alpha-, methoxy- and keto-classes, the cis- and trans-cyclopropanes are generally not separated.

The chemical syntheses of MAs representative of various subclasses that appear in the cell wall of *M.tb* and containing both cis-cyclopropanes and alpha-methyl-trans-cyclopropanes have only been reported since 2005 (Al Dulayymi et al., 2005, 2006a,b, 2007; Koza and Baird, 2007; Koza et al., 2009b). Indeed, although there are a number of reports on the biological effects of types of MA isolated from cells, we are unaware of any experiments which distinguish the role of cis- and trans-cyclopropanes directly.

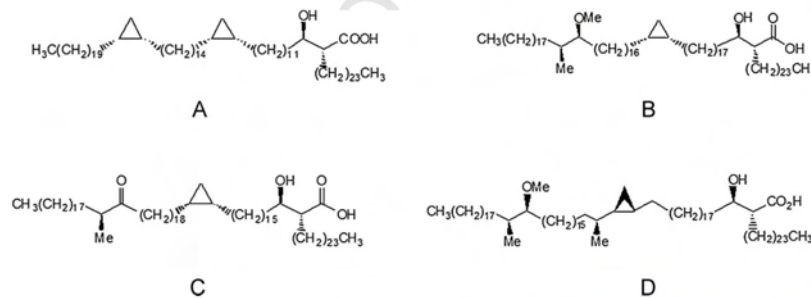


Fig. 1. Structures of the prominent homologues of three main classes of MA of *Mycobacterium tuberculosis*. A: alpha-; B: methoxy-; C: keto-mycolic acid; and D: the alpha-methyl-trans-cyclopropane form of natural methoxy-mycolic acid.

Please cite this article in press as: Mervyn, B., et al., Structure-function relationships of the antigenicity of mycolic acids in tuberculosis patients. Chem. Phys. Lipids (2010), doi:10.1016/j.chemphyslip.2010.09.006

146 The objectives of this study were: (i) to better understand
147 the cross-reactivity of MA antigens with cholesterol by select-
148 ing monoclonal antibody specificities from a recombinant chicken
149 immunoglobulin gene library that might or might not cross-react
150 between these two antigens and (ii) to determine the structural
151 features of MA required for antigenicity using TB positive and TB
152 negative pooled human serum samples in ELISA. This knowledge
153 may be useful to improve TB serodiagnostic tests that are based on
154 the detection of antibodies to MAs as surrogate markers of active
155 TB.

156 2. Materials and methods

157 2.1. Preparation of methyl ester of natural mycolic acid mixture

158 Mycolic acid from the *M. tuberculosis* virulent strain was pur-
159 chased from Sigma–Aldrich, batch M4537. The acid was converted
160 into the corresponding methyl ester. MA (100 mg to 0.1 mmol) was
161 dissolved in a mixture of toluene: methanol (5:1, 18 ml). Thereafter
162 a 2 M solution in n-hexane of trimethylsilyldiazomethane (0.2 ml,
163 0.4 mmol, 4 moleq.) was added. This addition was repeated another
164 3 times, every 45 min (0.1 ml, 0.2 mmol, 2 moleq.). The reaction
165 was monitored by TLC using 4:1 hexane:ethyl acetate solution.
166 After stirring for 72 h, the reaction was quenched by evaporation
167 of the volatiles to give a white residue. This was dissolved in
168 dichloromethane (15 ml) and water (10 ml) was added. The water
169 layer was washed with dichloromethane (2 × 10 ml). The combined
170 organic layers were dried and the solvent evaporated to give the
171 desired MA methyl ester (me-MA). The HNMR and CNMR spectra
172 of this ester were consistent with those reported (Laval et al., 2001).

173 2.2. Fluorescent labelling of natural mycolic acids

174 MAs (Sigma–Aldrich) were esterified to 5-bromomethyl-
175 fluorescein (5BMF) as described by Lemmer et al. (2009).

176 2.3. Preparation of synthetic mycolic acids

177 Mycolic acids representative of the major homologues present
178 in *M.tb* were prepared as previously described (Al Dulayymi et al.,
179 2005, 2006a,b, 2007; Koza and Baird, 2007; Koza et al., 2009b) or
180 by simple variations of those methods. Full details of all the known
181 compounds have been reported already; corresponding details for
182 Q3 the unpublished isomers are provided as supplementary informa-
183 tion.

184 2.4. Generation of recombinant monoclonal scFv

185 2.4.1. Phage display antibody library

186 A naive semi-synthetic chicken phage display library was used
187 (Van Wyngaardt et al., 2004). The library contains recombinant fila-
188 mentous bacteriophages displaying scFv antibody fragments. These
189 fragments were derived from combinatorial pairings of chicken V_H
190 and V_L immunoglobulin domains. V_H and V_L domains are linked
191 by an interpeptide segment consisting of the sequence (GGGG)₃,
192 enabling a fold typical of single variable fragments.

193 2.4.2. Phage display antibody selection

194 A selection of the phages displaying MA reactive scFv's
195 was conducted by several panning rounds. Maxisorp immuno-
196 tubes (Nunc-Immuno Tubes, Nunc, Denmark) were coated with
197 100 µg/ml mycolic acid (Sigma–Aldrich) dissolved in distilled hex-
198 ane, after which the hexane was allowed to evaporate at room
199 temperature. Coated immunotubes were briefly washed with phos-
200 phate buffered saline (PBS, pH 7.4), then blocked with 2% skimmed
201 milk in phosphate buffered saline (2% MPBS) for 60 min. Tubes were

then exposed to 10¹² transforming units of the phage library in 2%
MPBS, 0.1% Tween-20 buffer for 2 h. Unbound phage was removed
by 10 × washing with PBS containing 0.1% Tween-20 followed by
a further 10 × wash with PBS to remove the Tween-20. Bound
phage was eluted with 100 mM triethylamine and neutralized with
1 M Tris, pH 7.4. For enrichment *Escherichia coli* TG1 was infected
with eluted phages, grown at 30 °C in 2 × TYG broth (TY broth
supplemented with 2% glucose) containing 100 µg/ml ampicillin,
and rescued with M13-K07 helper phage (Invitrogen). Panning was
repeated four times.

212 2.4.3. Screening of mycolic acid specific phage clones

213 Following the final panning, individual ampicillin resistant *E. coli*
214 TG1 colonies were selected for further characterization. Colonies
215 were grown in 2 × TYG broth supplemented with 100 µg/ml ampicil-
216 lin in 96-well Microtitre plates at 30 °C. Phages were rescued as
217 described previously (Van Wyngaardt et al., 2004). Phage clones
218 were screened by enzyme-linked immunosorbent assay (ELISA)
219 carried out with MA coated (50 µg/ml) microtitre plates (Maxisorp,
220 Nunc, Denmark). Coating was done by adding 50 µl of 100 µg/ml
221 MA in hexane into each well and evaporating it overnight at room
222 temperature. Wells were briefly washed with PBS, and blocked
223 with 300 µl of 2% MPBS for 60 min. Phage containing supernatants
224 (25 µl) were mixed with blocking solution (25 µl), added to each
225 well, and incubated for 60 min at 30 °C. Wells were washed three
226 times with PBS-0.1% Tween-20. Mouse monoclonal antibody B62-
227 FE2, specific for M13 filamentous phage, in 2% MPBS-0.1% Tween-20
228 (50 µl) was added to each well and further incubated for 60 min
229 at 30 °C. Bound phages were detected using rabbit anti-mouse
230 IgG antibody conjugated with horseradish peroxidase (HRP). Signals
231 were developed with 3,3',5,5'-tetramethylbenzidine using the
232 1-step Ultra TMB ELISA substrate solution according to manufac-
233 turer's instructions. Plates were read using a Multiskan Ascent
234 (Thermo LabSystems) plate reader at a wavelength of 450 nm.

235 2.4.4. Production and purification of mycolic acid reactive scFv

236 Selected anti-MA phage obtained from *E. coli* TG1 clones was
237 used to infect *E. coli* HB2151 to obtain soluble scFv. Single colonies
238 were grown to an OD₆₀₀ of 0.9 in 2 × TYG broth supplemented
239 with 100 µg/ml ampicillin at 37 °C. ScFv expression was induced
240 with isopropyl β-D-thiogalactoside (IPTG; 1 mM) and the culture
241 further incubated at 30 °C overnight, in glucose free media. Solu-
242 ble scFv was extracted with 1 × TES buffer from the periplasm as
243 previously described (Hugo et al., 2002). ScFv was further affini-
244 ty purified using an anti c-myc tag mAb commercially denoted as
245 9E10 IgG. The column was prepared by immobilising 9E10 IgG onto
246 aminoLink Plus gel (Pierce) according to manufacturer's instruc-
247 tions. Periplasmic extracts were applied and after washing with
248 PBS, bound scFv was eluted with 100 mM triethylamine and neu-
249 tralised with 1 M Tris, pH 7.4. Eluted scFv was dialyzed against 1 ×
250 PBS, pH 7.4 at a MW cut-off of 10 kDa. Samples were concentrated
251 using a Macrosep® ultrafiltration device (Pall life sciences, USA)
252 and protein concentrations determined with a BCA protein detec-
253 tion kit (Pierce, USA), according to the manufacturer's instructions.
254 Purified scFv was stored at –20 °C until further use.

255 2.5. Enzyme-linked immunosorbent assay (ELISA)

256 2.5.1. Analysis of the methyl ester and free acid of mycolic acids

257 For coatings done in PBS, methyl MA (me-MA) or free MA
258 (250 µg) was dissolved in 1 × PBS (4 ml, pH 7.4) and placed on the
259 heat block at 90 °C for 20 min. One vial of 1 × PBS (4 ml) served
260 as control. The solutions were vortexed for 30 s before sonifying
261 for 2 min using a Virsonic sonifier at output of 2. The warm solu-
262 tions were subsequently loaded onto the ELISA plates (50 µl per

well) and the presence of oily drops viewed under a light microscope. The plates were kept at 4 °C overnight in plastic bags. For the coatings done using hexane as coating solution, the lipid samples (250 µg) were dissolved in hexane (4 ml, distilled) and vortexed for 30 s. One vial of hexane (4 ml) served as control. Solutions were coated using a Hamilton syringe (50 µl/well) and the liquid was loaded in the centre of the wells. Lipid was visible as a circular waxy layer after 2 h of evaporation of the hexane at room temperature. The plates were then stored in plastic bags at 4 °C overnight. The human sera used for analysis of the methyl ester and free MA samples were a pooled TB positive patient serum and a pooled TB negative patient serum at a 1:20 dilution of serum. The pooled TB pos sample was created by pooling the sera of six patients, three TB positive/HIV positive (TB pos/HIV pos) and three TB positive/HIV negative (TB pos/HIV neg) randomly selected from a collection used for another study (Schleicher et al., 2002) in which it was shown that HIV or its state of progression to AIDS did not affect binding activity of antibodies to natural mycolic acids. TB neg patients were hospitalized for medical conditions other than tuberculosis, but showed no evidence of active tuberculosis. For ELISA the PBS lipid coated plates were aspirated and then blocked with 0.5% Casein/PBS (400 µl/well), while the dry hexane coated plates were directly blocked with 0.5% Casein/PBS (400 µl/well). After 2 h, the blocking buffer was aspirated and serum (1:20 dilution in 0.5% Casein/PBS, pH 7.4) was added to the plate (50 µl/well). After 1 h of serum incubation, the wells were washed three times with a Well Wash4 ELISA washer (Labsystems) and flicked out before adding the goat anti-human Immunoglobulin G (IgG) peroxidase conjugate (whole molecule) for 30 min at room temperature. Subsequently, plates were washed three times and flicked out before adding the OPD substrate solution (50 µl/well). Absorbancies were measured with a SLT 340 ATC photometer at 450 nm with a reference filter at 690 nm at 30 min and 50 min for hexane and PBS coated plates respectively. Background binding of serum to PBS or hexane was corrected for by subtracting each serum response to PBS or hexane from the antibody binding values obtained to the coated lipid antigens. Statistical comparisons of ELISA results were performed using the student *t*-test at a confidence level of 95%.

2.5.2. Analysis of the synthetic mycolic acids

To coat the ELISA plates with the different synthetic mycolic acids subclasses and the natural mycolic acids to which they were compared, the lipids were dissolved in hexane (3 µg/50 µl) and vortexed 1 min, heated (at ~85 °C) for a minute and allowed to stand at room temperature for 15 min. Hexane coating as such served as a control. The ELISA plates were coated with the different mycolic acids at 50 µl per well by application to the well using Hamilton syringes. The lipids were visible as a waxy coating after 2 h of evaporation at RT. Plates were stored in a plastic bag at 4 °C overnight. ELISA was done as described in Section 2.5.1 Background binding of the serum to the plate was corrected for by subtracting the average binding signal of antibody to MA from that registered for the hexane coated wells. The results obtained were analysed by the making use of the Student's *t*-test for statistical significance.

2.5.3. Characterization of scFv's binding specificity of mycolic acids by sandwich ELISA

Purified scFvs were tested for their binding activity using a sandwich ELISA. Maxisorp immunoplates were coated with MA as described above. Plates were blocked with 2% MPBS for 60 min at 30 °C followed by a brief washing step with PBS. ScFv samples (25 µl) were mixed with 2% MPBS (25 µl), added to the wells and incubated for 60 min. Unbound scFv was removed by 3 × washing with PBS-0.1% Tween-20. Anti c-myc monoclonal antibody (AbD serotec, UK) conjugated with HPR was used to detect bound scFv fragments. Signals were developed with 3,3',5,5'-

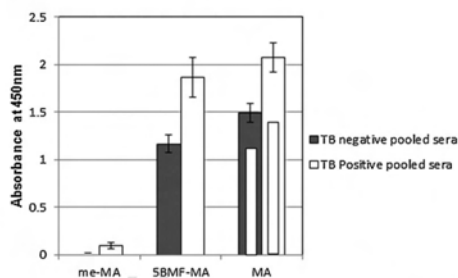
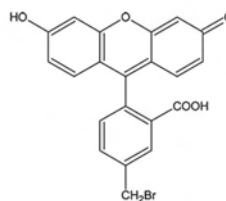


Fig. 2. Human patient antibody recognition of natural Mtb MAs (MA mix), methyl ester of natural MA (me-MA) and natural MA fluorescein ester (5BDMF-MA, prepared from natural MA mix and 5BDMF (structure)) measured with ELISA. Pooled TB positive and pooled TB negative sera were tested on the MA antigen derivatives coated from hexane. Inner bars within the MA mix bars indicate the signals when coating was done from hot PBS instead of hexane. The error bars indicate the standard deviation. The 2.5 *σ* rule was applied to remove outliers. *n* = min 14, max 16.

tetramethylbenzidine using the 1-stepUltra TMB ELISA substrate solution according to manufacturer's instructions. Plates were read using a Multiskan Ascent (Thermo Labsystems) plate reader at a wavelength of 450 nm.

3. Results and discussion

3.1. Antibody recognition of natural mycolic acids and ester derivatives thereof

The strongly hydrophobic nature of MA makes them insoluble in water and water miscible organic solvents. Their recognition by water soluble antibodies in diluted serum is therefore somewhat enigmatic and requires proof that antibody binding is not due to non-specific hydrophobic antibody adsorption to the MA coated surface.

In Fig. 2, the specificity of interaction of TB positive and negative sera with coated MA antigens is demonstrated. Hexane appears to be the better antigen coating solution compared to hot PBS. The MA methyl-ester (me-MA) is not recognized by antibodies, whereas the free MA (MA mix) is recognized by both TB pos and TB neg patient sera, but more strongly with TB pos sera. This supports the hypothesis that the ELISA antibody binding signal is due to recognition of an antigen consisting of one or more MAs, in which the hydroxyl group of the free MA-carboxylic acid probably participates in inter- or intramolecular stabilization of a specific antigen conformation. When the MA is fluoresceinated by esterification of its carboxylic acid, the antibody binding signal is not significantly affected, possibly due to the fact that fluorescein substitutes a free carboxylic acid group in close proximity to where the fluorophore compromises the free carboxylic acid of mycolic acid by ligandation (Fig. 2). These results corroborate those of Lemmer et al. (2009), who reported similar results when MA and fluoresceinated MA were presented

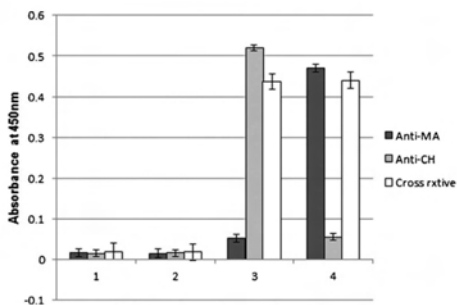


Fig. 3. Chicken scFv antibody fragment recognition of MA (4 - MA mix) and cholesterol (3 - CH) with ELISA. Three scFv specificities were identified, which were denoted Anti-MA (black bars), Anti-CH (grey bars) and Cross rxtive (white bars). MA and cholesterol antigens were coated on hexane, while results on hexane (1 - Hexane) and PBS (2 - PBS) sham coated wells are indicated as well. The error bars indicate the standard deviation of four repeats.

on immobilized liposomes to patient sera in a surface plasmon resonance biosensor.

3.2. Monoclonal scFv antibody fragment recognition of mycolic acid and cholesterol

The high antibody binding signal with human TB negative sera against MA, here again shown in Fig. 2, was previously speculated to be due at least in part to cross-reactivity of the antibodies with cholesterol (Schleicher et al., 2002), an idea that was later supported by showing that both MA and cholesterol were recognized equally well by Amphotericin B in an evanescent field biosensor (Benadie et al., 2008). The cross-reactivity could be due to a mixture of monospecific anti-cholesterol and anti-MA antibodies in the sera, or due to a true cross-reactivity where a particular antibody specificity could recognize both MA and cholesterol. It is known that all humans have anti-cholesterol antibodies in their blood circulation (Swartz et al., 1988), which may at least in part explain the high antibody activity to MAs in TB negative patients. To test what mechanisms are possible for the cross-reactivity, scFv fragments expressed from a chicken antibody gene library were screened for specific binders to cholesterol and MA. Chickens, similar to humans, express a specialized MA-presenting CD1 (chCD1-1) on their antigen presenting cell populations (Dvir et al., 2010). Three different specificities were detected and worked up from the phage display system into monovalent, monoclonal scFv fragments. The monospecific anti-cholesterol scFv was dubbed anti-CH, while two scFv specificities were generated against MA: one monospecific (Anti-MA) and one cross-reactive with cholesterol (Cross rxtive). Fig. 3 shows the characterization of these three scFv's with ELISA. The fact that a single monoclonal, monovalent cross-reactive scFv could be found with binding affinity against both cholesterol and MA corroborates the conclusion reported by Benadie et al. (2008) that cholesterol and MA share some antigenic structural properties and may explain why TB negative sera recognize cholesterol as well as they do MA. On the other hand, the finding that an scFv against MAs could be found that does not cross-react with cholesterol (Anti-MA) and vice versa (Anti-CH), means that anti-MA antibodies may be induced during tuberculosis that are not merely anti-cholesterol antibodies with increased binding activity. This provides a broader perspective on why the results in Fig. 2 show higher antibody binding activity with TB pos patient sera than with TB neg sera as was shown before with larger numbers of human patient sera

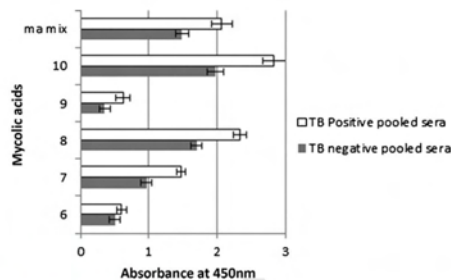


Fig. 4. Comparable ELISA signals of pooled TB positive and TB negative sera to synthetic methoxy mycolic acids. The error bars indicate the standard deviation. The 2.5 σ rule was applied to remove outliers. $n = \min 14, \max 16$.

from the same collection (Schleicher et al., 2002; Thanyani et al., 2008).

3.3. Antibody recognition of synthetic mycolic acids

MAs in *M.tb* contain an R,R - α -alkyl- β -hydroxy acid. The main branch, known as the meromycolate moiety, contains two functionalities at the so called distal and proximal positions (Sekanka et al., 2007). The proximal position is usually either a *cis*- or an α -methyl-*trans*-cyclopropane, while the distal functionality is usually a *cis*-cyclopropane or one of several oxygenated functional groups including β -methyl-hydroxyl-, β -methyl-methoxy- and β -methyl-keto-groups. MA derivatives were chemically synthesised that were representative of four MA subclasses, namely methoxy-MA, hydroxy-MA, keto-MA and α -MA (Table 1). The response of pooled TB positive and TB negative patient sera towards the different synthetic MAs was compared to that obtained towards natural free MA and isolated natural α MA in ELISA. The importance of the stereochemistry of the merochains of MAs for antigenic activity was studied by using different single stereoisomers of chemically synthesised MAs as antigens. Hexane was used as solvent to coat the plates with the MAs.

In general, synthetic methoxy-MA bound most strongly (Fig. 4), followed in descending order by hydroxy-MA (Fig. 5), keto-MA (Fig. 6) and α -MA (Fig. 7). The exact stereochemistry of each sub-type, i.e. the precise spatial arrangement of the functional groups, also appeared to be important. The observation that the oxygenated mycolic acids are more antigenic than the α -MA confirms a previous report by Pan et al. (1999), although they used

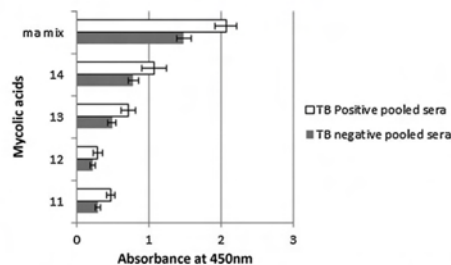


Fig. 5. ELISA antibody binding signals of pooled TB positive and TB negative sera to synthetic hydroxymycolic acids. The error bars indicate the standard deviation. The 2.5 σ rule was applied to remove outliers. $n = \min 15, \max 16$.

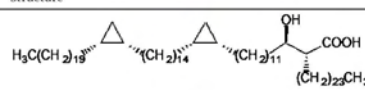
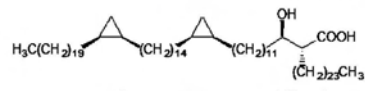
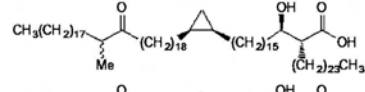
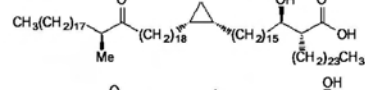
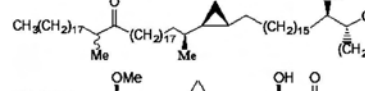
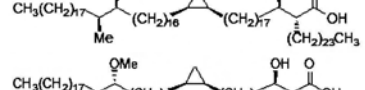
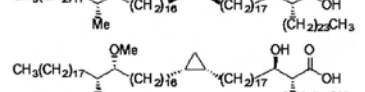
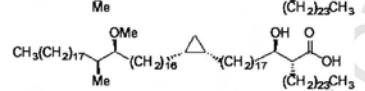
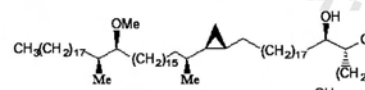
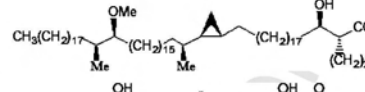
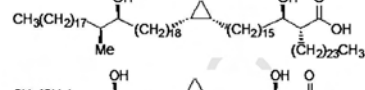
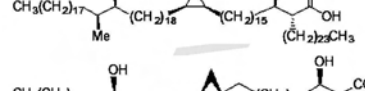
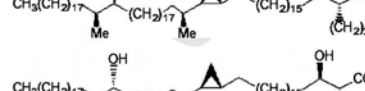
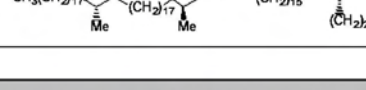
Please cite this article in press as: Mervyn, B., et al., Structure-function relationships of the antigenicity of mycolic acids in tuberculosis patients. Chem. Phys. Lipids (2010), doi:10.1016/j.chemphyslip.2010.09.006

GModel
CPL39471-9
6

ARTICLE IN PRESS

B. Mervyn et al. / Chemistry and Physics of Lipids xxx (2010) xxx-xxx

Table 1
Synthetic MA structures, names and numbers relating to results.

MA subtype	No.	Structure	Source
Alpha	1		Al Dulayymi et al. (2005)
	2		Prepared by the same methods as described in Al Dulayymi et al. (2005), but using the reverse absolute stereochemistry of the cyclopropane intermediates
Keto	3		Koza et al. (2009b)
	4		Koza et al. (2009b)
	5		Prepared from the corresponding protected ketone as in Koza and Baird (2007) using the methods of hydrolysis described in Koza et al. (2009b)
Methoxy	6		Al Dulayymi et al. (2007)
	7		Al Dulayymi et al. (2007)
	8		Al Dulayymi et al. (2007)
	9		Prepared using the same methods as described for the three stereoisomers above (Al Dulayymi et al., 2007)
	10		As for structure 5
Hydroxy	11		Koza et al. (2009b)
	12		Koza et al. (2009b)
	13		As for structure 5
	14		As for structure 5

Please cite this article in press as: Mervyn, B., et al., Structure–function relationships of the antigenicity of mycolic acids in tuberculosis patients. Chem. Phys. Lipids (2010), doi:10.1016/j.chemphyslip.2010.09.006

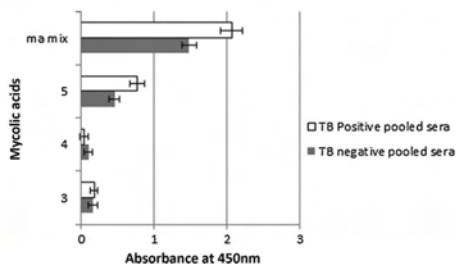


Fig. 6. ELISA antibody binding of pooled TB positive and TB negative sera to synthetic keto-mycolic acids. The error bars indicate the standard deviation. The 2.5 d rule was applied to remove outliers. $n = \text{min } 15, \text{max } 16$.

the methyl esters of the MA subclasses in ELISA, a result which contrasts our finding that the methyl esters are not antigenic (Fig. 2). The packing of mycolic acids in a Langmuir monolayer has previously been shown to differ between alpha-, keto- and methoxy-MA subclasses. Keto-MA tended more towards a W-shaped configuration with exceptional rigidity in monolayers, whereas methoxy- and alpha-MA exhibited a more flexible conformation towards variation of experimental parameters (Villeneuve et al., 2005, 2007). Thus, the packing of MA is influenced by the orientation of the functional groups that induce different conformations for interaction with antibodies in sera. We propose that the antibody binding to mycolic acids with TB negative sera is most likely due to the presence of anti-cholesterol antibodies, known to exist in all humans (Biro et al., 2007; Swartz et al., 1988) that cross-react with MA.

Antibody binding to the natural MA mixture, as well as several of the synthetic MAs was observed with both TB positive and TB negative patient sera, while some synthetic MAs appeared to have little or no antigenic activity. Although TB positive sera generally gave better binding to the antigenic MAs than TB negative sera, no single antigenic MA was significantly better able to differentiate between TB positive and TB negative sera than the natural mixture of MAs could. This could in principle mean that the synthetic MAs tested were antigenic primarily to the antibodies that respond to both MA and cholesterol. The fact that TB positive patient sera statistically score higher than TB negative patient sera in recognition of MA in ELISA could then explained simply by a higher concentra-

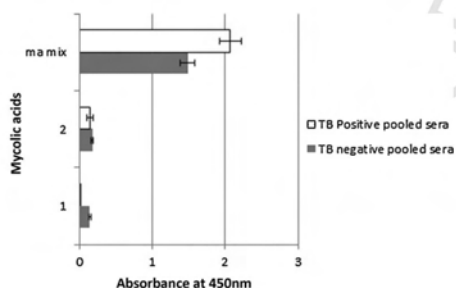


Fig. 7. ELISA antibody binding signals of TB positive and TB negative sera to synthetic alpha mycolic acids. MA-mix – the natural mixture of mycolic acids, 13, 14 – chemically synthetic alpha MA with structures indicated. The error bars indicate the standard deviation. The 2.5 d rule was applied to remove outliers. $n = \text{min } 8, \text{max } 16$.

tion or affinity of the anti-MA/cholesterol antibodies in TB patient sera, even though monospecific antibody activity to mycolic acids has been found to exist at least in the germ-line antibody gene repertoire of chickens (Fig. 3).

The synthetic methoxy-MA subclass had the highest binding to the antibodies of the four synthetic subclasses tested, followed by hydroxy-, keto- and alpha-MA (Figs. 4–7). The stereochemistry of the methoxy group and the cyclopropane is important for the recognition by antibodies in the sera. Even small changes in the stereochemical arrangement of the groups influenced the amount of binding observed. As seen from Fig. 4, the antibody binding signal of *R,R*-methoxy-methyl-*cis*-cyclopropane MA configuration (No. 8) most closely resembles the response towards the natural mixture of MA. A change of the configuration of either the *cis*-cyclopropane (No. 7), or the methoxy-methyl-fragment to *S,S* (No. 9) reduced the binding signal by approximately half. If the more weakly antigenic *S,R*-*cis* configuration of the cyclopropane is combined with the *S,S*-methoxy configuration (No. 6), the signal is once again halved, even though the *S,S*-methoxy configuration is the reported stereochemistry in natural compounds (Al Dulayymi et al., 2007). However, when the cyclopropane group assumed the methyl-*trans*-configuration as in structure No. 10, in this case in association with the reported natural *S,S* configuration around the methoxy-methyl fragment, an antigenicity signal was obtained that was even higher than that obtained for the natural MA mixture ($P < 0.01$). This shows beyond doubt that the stereochemical configuration of the two functional groups on the mero-chain of the methoxy-MA influences the way in which they are recognised by antibodies in human serum. It remains to be determined whether other combinations of absolute configuration of the methoxy-methyl fragment and the methyl-*trans*-cyclopropane will provide an even more antigenic MA.

The synthetic hydroxy-MAs (Fig. 5), which are the likely precursors of both methoxy- and keto-MA (Yuan and Barry, 1996; Yuan et al., 1997; Asselineau et al., 2002) all attracted weaker antibody binding compared to the natural MA mixture. The methyl-*trans* configuration of the proximal cyclopropane group appears to be a pre-requisite for antigenicity of the hydroxy-MAs (Nos. 13 and 14, compared to Nos. 11 and 12, Fig. 5). The hydroxy-methyl fragment in the *R,R* conformation (No. 14) is more antigenic than the supposed natural *S,S* configuration (No. 13) with statistical significance, $P < 0.01$, as was found with the methoxy group stereochemistry (Fig. 4).

Like the hydroxy-MAs, keto-MAs also require a proximal cyclopropane in the methyl-*trans*-cyclopropane configuration (No. 5, Fig. 6) to be antigenic, compared to the two *cis*-cyclopropane configurations (Nos. 4 and 3, Fig. 6) that did not show any significant antigenic activity. In these cases, a mixture of epimers at the chiral centre adjacent to the keto-group was tested; it is possible that *R* and *S*-isomers show different antigenicity. Thus in all the oxygenated MAs (i.e., methoxy-, hydroxy- and keto-MA), the methyl-*trans*-cyclopropane configuration provides for the best antigenic functionality.

Two synthetic alpha MAs (Fig. 7, Nos. 1 and 2) were compared to the natural MA mix to determine their relative antigenicity. The antibody binding signal to the synthetic alpha MA failed to distinguish between TB pos and TB neg patient sera compared to the natural MA mix. The synthetic MA gave such low antibody binding signals, that nothing could be learned from the variations in the stereochemistries of the distal and proximal cyclopropanes on the antigenicity of alpha-MA. It must be noted that the stereochemistry of *cis*-cyclopropanes in alpha-mycolates remains to be proven. However, if a common synthetic intermediate is involved in the production of the different functionalities and this is the same for both proximal and distal substituents, the natural stereochemistry will be as in 1.

Please cite this article in press as: Mervyn, B., et al., Structure–function relationships of the antigenicity of mycolic acids in tuberculosis patients. Chem. Phys. Lipids (2010), doi:10.1016/j.chemphyslip.2010.09.006

518 **4. Conclusion**

519 **Q5** MAs have been shown to play an important role in the virulence
 520 of tuberculosis mycobacteria. Not only do they act as pathogen
 521 associated molecular patterns (PAMP) for induction of murine
 522 **Q6** innate immunity (Korf et al., 2005), but they are also able to repro-
 523 programme murine macrophages to modulate their inflammatory
 524 activity (Korf et al., 2006). That these responses towards free MA
 525 administration may be related to the functional groups expressed
 526 on the merochain is inferred by findings such as that mutants
 527 of *M. tuberculosis* that have no oxygenated mycolic acids are of
 528 reduced virulence in mice (Dubnau et al., 2000), that mutants with-
 529 out the ability to *trans*-cyclopropanate their oxygenated MAs are
 530 hypervirulent (Rao et al., 2006), and that the trehalose dimycolate
 531 (TDM) extracted from such *trans*-cyclopropanase mutants stimu-
 532 lates inflammatory activity of murine macrophages, compared to
 533 TDM extracted from wild-type *M. tuberculosis*. Experiments like
 534 these are not feasible in humans, but the importance of MAs in
 535 human tuberculosis was recently demonstrated by implicating
 536 patient serum antibodies to mycolic acids as surrogate markers
 537 of active TB (Thanyani et al., 2008) using biosensor technology.
 538 With biosensor technology the interference of cross-reactive anti-
 539 bodies against cholesterol could be avoided that was encountered
 540 with the more standard ELISA technology (Schleicher et al., 2002).
 541 Here we determined that the fine structure of MAs is important for
 542 recognition by human TB patient serum antibodies.

543 First, we showed that methyl esters of the natural mycolate
 544 mixture showed no antigenicity, but that it was maintained by
 545 addition of a fluorescein to the MA carboxylate that substituted a
 546 new carboxylic acid functional group close to the ester bond of the
 547 conjugate. This suggested that MA assumes an antigenic configura-
 548 tion that is stabilized by hydrogen bonding to the (undissociated)
 549 carboxylic acid.

550 Two different scFv monoclonal antibody fragments generated
 551 from a chicken antibody gene library that recognized MAs, of which
 552 one cross-reacted with cholesterol and the other not, indicated
 553 that the cross-reactivity of human patient serum between MAs and
 554 cholesterol could either be due to a mixture of anti-cholesterol and
 555 anti-MA antibodies and/or due to a single antibody with cross-
 556 reactive specificity, or both. It also proves that anti-cholesterol
 557 antibodies do not necessarily cross-react with MA. Analysis of the
 558 antigenicity of a range of synthetic MA suggested that the oxygen-
 559 ated mycolic acids were most antigenic. Methoxy-MA repre-
 560 sented the strongest antigen for both TB pos and TB neg patient.
 561 Important, however, was the general observation that the two func-
 562 tional groups on the merochain of single synthetic MAs were both
 563 critically important to determine antigenicity for human serum
 564 antibody recognition.

565 The results seem to favour methoxy MA of *M. tuberculosis* as
 566 the strongest functional entity or antigen to use in TB serodiagnos-
 567 tic devices. A proximal methyl-*trans*-cyclopropane enhances the
 568 antigenicity of these functionalities. The *R,R*-configuration of the
 569 distal methoxy group still remains to be tested in combination with
 570 a *trans*-cyclopropane proximal group to determine antigenicity in
 571 methoxy-MA. The results do not necessarily provide information as
 572 to the stereochemistry of the naturally produced MAs found in the
 573 cell walls of *M. tb*, as the antibody recognition of natural classes may
 574 be due to the complex mixtures of homologues and cyclopropane
 575 stereochemistries present. The best antigenicity seen in synthetic
 576 MA does not therefore necessarily indicate the most likely struc-
 577 ture of the MA antigen(s) in nature. Thus, it seems unlikely that a
 578 particular MA molecule can constitute an antibody binding site fill-
 579 ing antigen or hapten. Rather, the surface created by packed MAs is
 580 likely to be the structure that is recognized by antibodies, similar to
 581 the case of monoclonal antibody recognition of cholesterol (Kruth
 582 et al., 2001). Unlike cholesterol, which has a defined structure, MA

583 exists as a mixture in *M. tuberculosis*. It may well be that MA folding
 584 and packing is influenced by the presence of different types of sub-
 585 classes and variants thereof, such that the natural MA antigen(s)
 586 may never be recreated synthetically by the use of a single species
 587 of pure synthetic MA. It was a disappointment that the cholesterol
 588 cross-reactivity could not be defined to a particular class of MA from
 589 the antigenic mixture as implied by the observation that the TB
 590 positive and TB negative sera were not better resolved with any par-
 591 ticular antigenic MA structure. Nevertheless, the demonstration of
 592 biological antigenic activity of individual stereochemically unique
 593 chemically synthetic MAs to levels that approximate or even exceed
 594 the antigenic activity of the natural mixture of MAs purified from
 595 *M. tuberculosis* bodes well for the possibilities towards improving
 596 the existing assays that aim at detection of anti-MA antibodies as
 597 surrogate markers for TB disease (Schleicher et al., 2002; Thanyani
 598 et al., 2008; Lemmer et al., 2009; Mathebula et al., 2009). It allows
 599 for the first time the possibility of providing exact specifications
 600 for an optimal antigen coated surface and the covalent linkage of
 601 MA to sensor surfaces for easy regeneration and engineering of the
 602 antigen to define the best window of antibody affinity and speci-
 603 ficity.

Uncited references

604 Freund et al. (2002), Fujita et al. (2005, 2007), Goodrum et al.
 605 (2001), and Watanabe et al. (2001).

Acknowledgements

606 MRC travel grant (Deysel), Commonwealth/British Council
 607 research fellowship (Verschoor), Royal Society travel grant (Baird,
 608 Verschoor), NRF research grant (Verschoor), CSIR PhD fellowship
 609 (Lemmer), Wellcome Trust research grant (Al Dulayymi, Baird,
 610 Grooten, Verschoor).

References

- 611 Al Dulayymi, J.R., Baird, M.S., Roberts, E., 2005. The synthesis of a single enantiomer
 612 of a major α -mycolic acid of *M. tuberculosis*. *Tetrahedron* 61, 11939–11951.
 613 Al Dulayymi, J.R., Baird, M.S., Roberts, E., Deysel, M., Verschoor, J., 2007. The first
 614 syntheses of single enantiomers of the major methoxymycolic acid of *Mycobac-*
 615 *terium tuberculosis*. *Tetrahedron* 63, 2571–2592.
 616 Al Dulayymi, J.R., Baird, M.S., Roberts, E., Minnikin, D.E., 2006a. The synthesis of single
 617 enantiomers of meromycolic acids from mycobacterial wax esters. *Tetrahedron*
 618 62, 11867–11880.
 619 Al Dulayymi, J.R., Baird, M.S., Mohammed, H., Roberts, E., Clegg, W., 2006b. The syn-
 620 thesis of one enantiomer of the α -methyl-*trans*-cyclopropane unit of mycolic
 621 acids. *Tetrahedron* 62, 4851–4862.
 622 Asselineau, C., Asselineau, J., Lan elle, G., Lan elle, M.A., 2002. The biosynthesis of
 623 mycolic acids by *Mycobacteria*: current and alternative hypotheses. *Prog. Lipid*
 624 *Res.* 41, 501–523.
 625 Beckman, E.V., Porcelli, S.A., Morita, C.T., Behar, S.M., Furlong, S.T., Brenner, M.B.,
 626 1994. Recognition of a lipid antigen by CD1-restricted $\alpha\beta$ T cells. *Nature* 372,
 627 691–694.
 628 Benadie, Y., Deysel, M., Siko, D.G., Roberts, V.V., Van Wyngaardt, S., Thanyani, S.T.,
 629 Sekanka, G., Ten Bokum, A.M., Collett, L.A., Grooten, J., Baird, M.S., Verschoor,
 630 J.A., 2008. Cholesteroid nature of free mycolic acids from *M. tuberculosis*. *Chem.*
 631 *Phys. Lipids* 152, 95–103.
 632 Biro, A., Arvenak, L., Balogh, A., Lorincz, A., Uray, K., Horvath, A., Romics, L., Marko,
 633 J., Fust, G., Laszlo, G., 2007. Novel anti-cholesterol monoclonal immunoglobulin
 634 G antibodies as probes and potential modulators of membrane raft-dependent
 635 immune functions. *J. Lipid Res.* 48, 19–29.
 636 Dobson, G., Minnikin, D.E., Minnikin, S.M., Parlett, J.H., Goodfellow, M., Ridell, M.,
 637 Magnusson, M., 1985. Systematic analysis of complex mycobacterial lipids. In:
 638 Goodfellow, M., Minnikin, D.E. (Eds.), *Chemical Methods of Bacterial Systemat-*
 639 *ics*. Academic Press, London, pp. 237–265.
 640 Dubnau, E., Lan elle, M.A., Soares, S., Benichou, A., Vaz, T., Prom e, D., Prom e, J.-C.,
 641 Daff e, M., Qu emard, A., 1997. *Mycobacterium bovis* BCG genes involved in the
 642 biosynthesis of cyclopropyl keto- and hydroxymycolic acids. *Mol. Microbiol.* 23,
 643 313–322.
 644 Dubnau, E., Chan, J., Raynaud, C., Mohan, V.P., Lan elle, M.A., Yu, K., Qu emard, A.,
 645 Smith, L., Daff e, M., 2000. Oxygenated mycolic acids are necessary for virulence
 646 of *Mycobacterium tuberculosis* in mice. *Mol. Microbiol.* 36, 630–637.

Please cite this article in press as: Mervyn, B., et al., Structure–function relationships of the antigenicity of mycolic acids in tuberculosis patients. *Chem. Phys. Lipids* (2010), doi:10.1016/j.chemphyslip.2010.09.006

- 550 Dvir, H., Wang, J., Ly, N., Dascher, C.C., Zajonc, D.M., 2010. Structural basis for lipid-
 551 antigen recognition in avian immunity. *J. Immunol.* 184, 2504–2511.
- 552 Freund, Y.R., Dousman, L., Mohagheghpour, A., 2002. Prophylactic clarithromycin
 553 to treat *Mycobacterium avium* in HIV patients receiving zidovudine may signifi-
 554 cantly increase mortality by suppressing lymphopoiesis and hematopoiesis. *Int.*
 555 *Immunopharmacol.* 2, 1465–1475.
- 556 Fujita, Y., Naka, T., McNeil, M.R., Yano, L., 2005. Intact molecular characterization of
 557 cord factor (trehalose 6,6'-dimycolate) from nine species of mycobacteria by
 558 MALDI-TOF mass spectrometry. *Microbiology* 151, 3403–3416.
- 559 Fujita, Y., Okamoto, Y., Uenishi, Y., Sunagawa, M., Uchiyama, T., Yano, L., 2007.
 560 Molecular and supra-molecular structure related differences in toxicity and
 561 granulomatogenic activity of mycobacterial cord factor in mice. *Microb. Pathog.*
 562 43, 10–21.
- 563 Fujiwara, N., Pan, J., Enomoto, K., Terano, Y., Honda, T., Yano, L., 1999. Produc-
 564 tion and partial characterization of anti-cord factor (trehalose-6,6'-dimycolate)
 565 IgG antibody in rabbits recognizing mycolic acid subclasses of *Mycobacterium*
 566 *tuberculosis* or *Mycobacterium avium*. *FEMS Immunol. Med. Microbiol.* 24, 141–
 567 149.
- 568 Goodrum, M.A., Siko, D.G.R., Niehuus, T., Eichelbauer, D., Verschoor, J.A., 2001.
 569 Mycolic acids from *Mycobacterium tuberculosis*: purification by countercurrent
 570 distribution and T-cell stimulation. *Microbios* 100, 55–67.
- 571 Hugo, N., Lafont, V., Beukes, M., Altschuh, D., 2002. Functional aspects of co-variant
 572 surface charges in an antibody fragment. *Protein Sci.* 11, 2697–2705, 2002.
- 573 Korf, J.E., Pynaert, G., Tournay, K., Boonefaes, T., Van Oosterhout, A., Ginneberge, D.,
 574 Haegeman, A., Verschoor, J.A., De Baetselier, P., Grooten, J., 2006. Macrophage
 575 reprogramming by mycolic acid promotes a tolerogenic response in experimen-
 576 tal asthma. *Am. J. Resp. Crit. Care Med.* 174, 152–160.
- 577 Koza, G., Baird, M.S., 2007. The first synthesis of single enantiomers of ketomycolic
 578 acids. *Tetrahedron Lett.* 48, 2165–2169.
- 579 Koza, G., Rowles, R., Theunissen, C., Al Dulayymi, J.R., Baird, M.S., 2009a. The syn-
 580 thesis of single enantiomers of trans-alkene-containing mycolic acids. *Tetrahedron*
 581 *Let.* 50, 7259–7262.
- 582 Koza, G., Theunissen, C., Al Dulayymi, J.R., Baird, M.S., 2009b. The synthesis of single
 583 enantiomers of mycobacterial ketomycolic acids containing cis-cyclopropanes.
 584 *Tetrahedron* 65, 10214–10229.
- 585 Kruth, H.S., Ifrim, L., Chang, J., Addadi, L., Perl-Treves, D., Zhang, W., 2001. Monoclonal
 586 antibody detection of plasma membrane cholesterol microdomains responsive
 587 to cholesterol trafficking. *J. Lipid Res.* 42, 1492–1500.
- 588 Laval, F., Lanéelle, M.A., Déon, A., Monsabat, B., Daffé, M., 2001. Accurate molecular
 589 mass determination of mycolic acids by MALDI-TOF mass spectroscopy. *J. Anal.*
 590 *Chem.* 73, 4537–4544.
- 591 Lemmer, A., Thanyani, S.T., Vrey, P.J., Driver, C.H.S., Venter, L., van Wyngaardt, S., ten
 592 Bokum, A.M.C., Ozoemena, K.I., Pilcher, J.A., Fernig, D.G., Stoltz, A.C., Swai, H.S.,
 593 Verschoor, J.A., 2009. Detection of anti-mycolic acid antibodies by liposomal
 594 biosensors. *Methods Enzymol.* 464, 79–104.
- 595 Lyashchenko, K., Colangelo, R., Hodde, M., Al Jahdali, H., Menzies, D., Gennaro, M.L.,
 596 1998. Heterogeneous antibody responses in tuberculosis. *Infect. Immun.* 66,
 597 3936–3940.
- 598 Mathebula, N., Pillay, J., Toschi, G., Verschoor, J.A., Ozoemena, K.I., 2009. Recogni-
 599 tion of anti-mycolic acid antibody at self-assembled mycolic acid antigens on
 600 gold electrode: a potential impedimetric immunosensing platform for active
 tuberculosis. *Chem. Commun.* 2009, 3345–3347.
- Nabeshima, S., Murata, M., Kashiwagi, K., Fujita, M., Furusyo, N., Hayashi, J., 2005.
 701 Serum antibody response to tuberculosis-associated glycolipid antigen after
 702 BCG vaccination in adults. *J. Infect. Chemother.* 11, 256–258.
- 703 Ojha, A.K., Baughn, A.D., Sambandan, A., Hsu, T., Avelli, X., Guerardel, Y., Alahari,
 704 A., Kremer, L., Jacobs Jr., W.R., Hatfull, G.F., 2008. Growth of *Mycobacterium*
 705 *tuberculosis* biofilms containing free mycolic acids and harbouring drug-tolerant
 706 bacteria. *Mol. Microbiol.* 69, 164–174.
- 707 Pan, J., Fujiwara, A., Oka, S., Maekura, R., Ogura, T., Yano, L., 1999. Anti-Cord Factor
 708 (Trehalose 6,6'-Dimycolate) IgG antibody in tuberculosis patients recognizes
 709 mycolic acid subclasses. *Microbiol. Immunol.* 43, 863–869.
- 710 Quémar, A., Lanéelle, M.A., Marrak, H., Prêtre, D., Daffé, M., 1997. Structure
 711 of a hydroxymycolic acid potentially involved in the synthesis of oxygenated
 712 mycolic acids of the *Mycobacterium tuberculosis* complex. *Eur. J. Biochem.* 250,
 713 758–763.
- 714 Rao, Y., Gao, F., Chen, B., Jacobs, W.R., Glickman, M.S., 2006. Trans-cyclopropanation
 715 of mycolic acids on trehalose dimycolate suppresses *Mycobacterium tuberculo-*
 716 *s* induced inflammation and virulence. *J. Clin. Invest.* 116, 1660–1667.
- 717 Schleicher, G.K., Feldman, C., Vermaak, Y., Verschoor, J.A., 2002. Prevalence of anti-
 718 mycolic acid antibodies in patients with pulmonary tuberculosis co-infected with
 719 HIV. *Clin. Chem. Lab. Med.* 40, 882–887.
- 720 Sekanka, G., Baird, M., Minnion, T., Grooten, J., 2007. Mycolic acids for the control
 721 of tuberculosis. *Expert Opin. Ther. Patents* 7, 315–331.
- 722 Shui, G., Bendt, A.K., Pethe, K., Dick, V., Wenk, M.R., 2007. Sensitive profiling of
 723 chemically diverse bioactive lipids. *J. Lipid Res.* 48, 1976–1984.
- 724 Swartz, G.M., Gentry, M.K., Amendeo, L.M., Blanchette-Mackie, E.J., Alving, C.R., 1988.
 725 Antibodies to cholesterol. *Proc. Natl. Acad. Sci. USA* 85, 1902–1906.
- 726 Thanyani, S.T., Roberts, V., Siko, D.G., Vrey, P., Verschoor, J.A., 2008. A novel appli-
 727 cation of affinity biosensor technology to detect antibodies to mycolic acid in
 728 tuberculosis patients. *J. Immunol. Methods* 332, 61–72.
- 729 Van Wyngaardt, W., Mala, T., Masana, C., Fehrsen, J., Jordaan, F., Miltiadou, D., Du
 730 Plessis, D.H., 2004. A large semi-synthetic single-chain Fv phage display library
 731 based on chicken immunoglobulin genes. *BMC Biotechnol.* 4, 6.
- 732 Villeneuve, M., Kawai, M., Kanashima, H., Watanabe, M., Minnikin, D.E., Nakahara, H.,
 733 2005. Temperature dependence of the Langmuir monolayer packing of mycolic
 734 acids from *Mycobacterium tuberculosis*. *Biochim. Biophys. Acta* 1715, 71–80.
- 735 Villeneuve, M., Kawai, M., Watanabe, M., Aoyagi, H., Hitotsuyanagi, Y., Takeya, K.,
 736 Gouda, H., Hirono, S., Minnikin, D.E., Nakahara, H., 2007. Conformational behav-
 737 ior of oxygenated mycobacterial mycolic acids from *Mycobacterium bovis* BCG.
 738 *Biochim. Biophys. Acta* 1768, 1717–1726.
- 739 Watanabe, M., Aoyagi, Y., Riedell, M., Minnikin, D.E., 2001. Separation and characteri-
 740 zation of individual mycolic acids in representative mycobacteria. *Microbiology*
 741 147, 1825–1833.
- 742 WHO, 2009. Global tuberculosis control: epidemiology, strategy, financing: WHO
 743 report, WHO/HTM/TB 2009, 411.
- 744 Wood, R., 2007. Challenges of TB diagnosis and treatment in South Africa. *South Afr.*
 745 *J. HIV Med.* 27, 44–48.
- 746 Yuan, Y., Barry, C.E., 1996. A common mechanism for the biosynthesis of methoxy
 747 and cyclopropyl mycolic acids in *Mycobacterium tuberculosis*. *Proc. Natl. Acad.*
 748 *Sci. USA* 93, 12828–12833.
- 749 Yuan, Y., Lane, D.C., Musser, J.M., Sreevatsan, S., Barry, C.E., 1997. MMAS-1, the
 750 branch point between cis- and trans-cyclopropane containing oxygenated myco-
 751 lates in *Mycobacterium tuberculosis*. *J. Biol. Chem.* 272, 10041–10049.

Please cite this article in press as: Mervyn, B., et al., Structure–function relationships of the antigenicity of mycolic acids in tuberculosis patients. *Chem. Phys. Lipids* (2010), doi:10.1016/j.chemphyslip.2010.09.006